Fibre and components induced limitations in high capacity optical networks

Peucheret, Christophe; Jeppesen, Palle; Pedersen, Rune S.J.

Publication date:
2003

Document Version
Publisher's PDF, also known as Version of record

Fibre and Components Induced Limitations in High Capacity Optical Networks

Christophe Peucheret

5 June 2003
rev. 1.0 – 1 October 2004

Research Center COM
Technical University of Denmark
Building 345V
DK-2800 Kgs. Lyngby

Contents

Abstract

The design of future all-optical networks relies on the knowledge of the physical layer transport properties. In this thesis, we focus on two types of system impairments: those induced by the non-ideal transfer functions of optical filters to be found in network elements such as optical add-drop multiplexers (OADM) and optical cross-connects (OXC), as well as those due to the interaction of group-velocity dispersion, optical fibre non-linearities and accumulation of amplifier noise in the transmission path.

The dispersion of fibre optics components is shown to limit their cascadability. Dispersion measurement techniques are first reviewed, and the limitations of the commonly used phase-shift technique is discussed. Additionally, an alternative method which enables the direct determination of small dispersion values in the pass-band of optical filters is proposed. Available optical filter technologies are compared with respect to their dispersive properties.

The cascadability of fibre gratings is investigated numerically and experimentally. The conventional Gaussian apodisation profile is shown to result in unwanted dispersion in the pass-band, which will limit its cascadability to less than five devices when a channel spacing of 50 GHz is used at 10 Gbit/s. The use of narrow bandwidth modulation formats such as optical duobinary is suggested in order to improve the detuning tolerance of Gaussian apodised gratings. Alternatively, novel asymmetric apodisation profiles with multiple phase-shifts can be designed to provide reduced dispersion in the pass-band. Large detuning tolerances are demonstrated experimentally for a variety of modulation formats.

A numerical optimisation of pass-band flattened phased-array (PHASAR) multiplexers is performed for use in high spectral efficiency metropolitan area networks at 40 Gbit/s. Even if conventional PHASARs are theoretically dispersion-less devices, the pass-band flattening process is shown to induce unwanted dispersion, which will ultimately limit the device cascadability. A PHASAR based on a parabolic horn input coupler is found to

be the most promising design in order to maximise the spectral efficiency in a four add-drop node ring network.

The concept of "normalised transmission sections" is introduced in order to ease the dimensioning of transparent domains in future all-optical networks. Normalised sections based on standard single-mode fibre (SMF) and dispersion compensating fibre (DCF) are optimised numerically with respect to the positioning of the DCF, the degree of compensation and the input powers to the two fibre types. Experimental validations are performed for 10 Gbit/s non return-to-zero (NRZ) and chirped return-to-zero (CRZ) modulation over 80 km pre-compensated spans. Passive pre-distortion at the transmitter is shown to significantly improve the reach of the systems. Based on the experimental results, transparent domains with a diameter of the order of 1000 km can be realised, thus demonstrating the applicability of the optimisation method to the design of large area networks.

Wavelength division multiplexing (WDM) systems not only require compensation of the dispersion of the transmission fibre, but also of its dispersion slope. The effectiveness of early slope compensating DCFs for broadband compensation of SMF is demonstrated experimentally for 10 Gbit/s NRZ modulation. In particular, transmission in the L-band is achieved over more than 1000 km using a dispersion map optimised for the C-band, removing the need for separate band compensation.

Novel DCFs enabling for the cabled compensation of the dispersion and dispersion slope of SMF (the so-called inverse dispersion fibres, IDF$\times n$, where n is the SMF to DCF length ratio), are compared numerically. For NRZ modulation at 10 Gbit/s, IDF$\times$1 is found to maximise the transmission distance over 50 km spans for single channel, while being prone to cross-phase modulation in WDM systems where IDF$\times$2 or 3 should be preferred. The benefit of using short return-to-zero (RZ) pulses over conventional NRZ modulation in a SMF+IDF$\times$1 link is highlighted. Short pulses disperse faster in the transmission fibre, which is in turn beneficial in terms of optical signal-to-noise ratio, resulting in a twofold increase in transmission distance over NRZ for a 3 dB power penalty criterion.

Resumé

Designet af fremtidens all-optical netværk er baseret på viden om transport egenskaberne ved det fysiske lag. I denne afhandling fokuserer vi på to typer af system forringelser, dem som er introduceret pga. den ikke ideelle overføringsfunktion af optiske filtre der befinder sig i netværkselementer så som optiske add-drop multiplexerer (OADM) og optiske cross-connects (OXC), samt de forringelser som kan tilskrives samspillet mellem group-velocity dispersion, optiske fiber ulinearitetер samt akkumuleret forstærker støj i transmissions vejen.

Det bliver vist at dispersionen i optiske komponenter begrænser muligheden for at kaskadekoble dem. Først bliver dispersions måleteknikker gennemgået, og begrænsningerne i den mest benyttede faseskifts teknik bliver diskuteret. Dernæst, bliver en alternativ teknik foreslået som muliggør en direkte bestemmelse af små dispersionsværdier i optiske filtres båndpas. Eksisterende optiske filter teknologier bliver sammenlignet på baggrund af deres respektive dispersions egenskaber.

Kaskadekoblede fiber gitre bliver undersøgt numerisk og eksperimentelt. Det bliver vist at den konventionelle Gaussiske apodisations profil resulterer i en uønsket dispersion i båndpasset, hvilket begrænser antallet af kaskadekoblede fiber gitre til mindre end 5, når en kanal separationen på 50 GHz bliver benyttet for 10 Gbit/s signaler. Det bliver foreslået at benytte modulationsformater med lille båndbredde, så som optisk dobbelt binær modulation, for at forbedre forskydningstolerancen for Gaussiske apodiserede gitre. Som et alternativ, kan en nyudviklet asymmetrisk apodisation med adskillige fase skift blive designet, således at dispersionen i båndpasset bliver reduceret. Store forskydningstolerancer bliver demonstreret eksperimentelt for modulationsformater.

En numerisk optimering af en flad båndpas phase array (PHASAR) multiplexer bliver foretaget, til brug i et metropolitan netværk ved 40 Gbit/s med en høj spektral udnyttelse. Selvom konventionelle PHASARs teoretisk er dispersions fri komponenter, bliver det vist at processen der indfører

fladt båndpas introducerer uønsket dispersion, som i sidste ende vil begrænse antallet af komponenter som kan kaskadekobles. Det bliver vist at en PHASAR baseret på indgangskoblere formet som parabolisk horn er det mest lovende design, når den spektrale udnyttelsesgrad i et ringnetværk baseret på 4 add-drop netværkselementer skal optimeres.

Konceptet "normaliseret transmissions sektion" er introduceret for at forenkle dimensioneringen af transparente domæner i fremtidens all-optical netværk. Normaliserede sektioner baseret på standard single-mode fibre (SMF) samt dispersions kompenserende fibre (DCF) er optimeret numerisk mht. placeringen af DCF, graden af kompensering samt indgangs effekt til de to typer fiber. Eksperimentel evaluering bliver udført for 10 Gbit/s non return-to-zero (NRZ) samt chirpede return-to-zero (CRZ) modulation over 80 km prækompenseret fiberspand. Passiv forvrængning i senderen bliver vist at forbedre den totale opnåelige transmissionslængde for systemet betydelig. Baseret på de eksperimentelle resultater, kan transparente domæner med en diameter på 1000 km blive realiseret, hvorved anvendeligheden af optimeringsteknikken bliver demonstreret.

Wavelength Division Multiplexing (WDM) systemer kræver ikke kun kompensation af dispersionen af transmissions fibrene, men også af dispersions hældningen. Effektiviteten af de tidligst udviklede DCF med hældnings kompensation til bredbånds kompensation af SMF bliver demonstreret eksperimentelt for 10 Gbit/s NRZ modulation. Specielt er 1000 km transmission i L-båndet opnået, ved at benytte et dispersions kort som er optimeret til C-båndet, hvorved det bliver demonstreret at kompensation af de enkelt separate bånd er unødvendig.

Nyudviklede DCF som muliggør en kabellagt kompensering af dispersionen og dispersions hældningen af SMF (såkaldt inverse dispersion fibre, IDF$\times n$, hvor n er forholdet mellem længderne af SMF og DCF) bliver sammenlignet numerisk. For NRZ modulation ved 10 Gbit/s, bliver det konkluderet at IDF$\times$1 optimere den mulige transmission distance baseret på 50 km spand for en enkelt kanal. Ved WDM systemer, begrænser cross-phase modulation brugen af IDF$\times$1, hvorfor IDF$\times$2 og IDF$\times$3 er at foretrække. Fordelen ved at benytte korte Return-to-Zero (RZ) pulser sammenlignet med NRZ modulation i en SMF+IDF$\times$1 link er fremhævet. Korte pulser forbredder hurtigere i transmissions fibre, hvilket er fordelagtigt mht. optisk signal-støj forhold, idet den opnåelige transmissions distance defineret ved 3 dB power penalty kravet, bliver fordoblet sammenlignet med NRZ.

Ph.D. publications

[1] C. Peucheret, F. Liu, and R. J. S. Pedersen,"Measurement of small dispersion values in optical component", *Electronics Letters*, vol. 35, no. 5, pp. 409-411, 1999.

[2] F. Liu, R. J. S. Pedersen, C. Peucheret, and P. Jeppesen, "Experimental verification of a very low crosstalk wavelength router construction using arrayed-waveguide grating multi/demultiplexers", in *Digest of IEEE/LEOS Summer Topical Meetings 1999*, San Diego, California, U.S.A, paper TuA1.3, pp. 33-34, 1999.

[3] C. Peucheret, I. Muñoz, A. Buxens, F. Liu, and S. N. Knudsen, "L-band transmission over 1000 km using standard and dispersion-compensating fibres in pre-compensation scheme optimised at 1550 nm", *Electronics Letters*, vol. 35, no. 20, pp. 1759-1761, 1999.

[4] C. Caspar, R. Freund, N. Hanik, L. Molle, and C. Peucheret, "Using normalised sections for the design of all optical networks", in A. A. Stavdas (editor) *New Trends in Optical Network Design and Modeling, IFIP TC6 Fourth Working Conference on Optical Network Design and Modeling, ONDM'00, Athens Greece*, Kluwer Academic Publishers, pp. 163–172, 2001.

[5] J. Yu, A. Clausen, H. N. Poulsen, X. Zheng, C. Peucheret, and P. Jeppesen, "40 Gbit/s wavelength conversion in cascade of SOA and NOLM and demonstration of extinction ratio improvement", *Electronics Letters*, vol. 36, no. 11, pp. 963-964, 2000.

[6] J. Yu, X. Zheng, C. Peucheret, A. T. Clausen, H. N. Poulsen, and P. Jeppesen, "40–Gb/s all-optical wavelength conversion based on a nonlinear optical loop mirror", *Journal of Lightwave Technology*, vol. 18, no. 7, pp. 1001-1006, 2000.

[7] J. Yu, X. Zheng, C. Peucheret, A. T. Clausen, H. N. Poulsen, and P. Jeppesen, "All-optical wavelength conversion of short-pulses and NRZ signals based on a nonlinear optical loop mirror", *Journal of Lightwave Technology*, vol. 18, no. 7, pp. 1007-1017, 2000.

[8] J. Yu, X. Zheng, F. Liu, C. Peucheret, A. T. Clausen, H. N. Poulsen, and P. Jeppesen, "8×40 Gb/s 55-km WDM transmission over conventional fiber using a new RZ optical source", *IEEE Photonics Technology Letters*, vol. 12, no. 7, pp. 912-914, 2000.

[9] F. Liu, X. Zheng, C. Peucheret, S. N. Knudsen, R. J. S. Pedersen, and P. Jeppesen, "Chirped return-to-zero source used in 8×10 Gbit/s transmission over 2000 km of standard singlemode fibre", *Electronics Letters*, vol. 36, no. 16, pp. 1399-1400, 2000.

[10] C. Peucheret, N. Hanik, R. Freund, L. Molle, and P. Jeppesen, "Optimisation of pre- and post-dispersion compensation schemes for 10-Gbit/s NRZ links using standard and dispersion compensating fibers", *IEEE Photonics Technology Letters*, vol. 12, no. 8, pp. 992-994, 2000.

[11] H. N. Poulsen, A. T. Clausen, A. Buxens, L. Oxenloewe, C. Peucheret, C. Rasmussen, F. Liu, J. Yu, A. Kloch, T. Fjelde, D. Wolfson, and P. Jeppesen, "Ultra fast all-optical signal processing in semiconductor and fiber based devices", in *Proceedings European Conference on Optical Communication, ECOC'00*, Munich, Germany, paper 7.4.1 (invited), vol. 3, pp. 59-62, 2000.

[12] F. Liu, C. Peucheret, X. Zheng, R. J. S. Pedersen, and P. Jeppesen, "A novel chirped return-to-zero transmitter and transmission experiments", in *Proceedings European Conference on Optical Communication, ECOC'00*, Munich, Germany, paper 8.3.5, vol. 3, pp. 113-114, 2000.

[13] N. Hanik, C. Caspar, F. Schmidt, R. Freund, L. Molle, and C. Peucheret, "Optimised design of transparent optical domains", in *Proceedings European Conference on Optical Communication, ECOC'00*, Munich, Germany, paper P3.5, vol. 3, pp. 195-197, 2000.

[14] A. T. Clausen, L. Oxenloewe, C. Peucheret, S. N. Knudsen, L. Grüner-Nielsen, A. Bjarklev, S. Barkou, H. N. Poulsen, and P. Jeppesen, "Novel single/multiple wavelength RZ pulsesource based on four-wave mixing in newly developed highly non-linear fibre", in *Proceedings European Conference on Optical Communication, ECOC'00*, Munich, Germany, paper P3.14, vol. 3, pp. 221-222, 2000.

[15] A. T. Clausen, L. Oxenløwe, C. Peucheret, H. N. Poulsen, P. Jeppesen, S. N. Knudsen, and L. Grüner-Nielsen, "10-GHz return-to-zero pulse source tunable in wavelength with a single- or multiwavelength output based on four-wave mixing in a newly developed highly nonlinear fiber", *IEEE Photonics Technology Letters*, vol. 13, no. 1, pp. 70–72, 2001.

[16] C. Peucheret, T. Tokle, S. N. Knudsen, C. J. Rasmussen, and P. Jeppesen, "System performance of new types of dispersion compensating fibres", in *Technical Digest Conference on Lasers and Electro-Optics, CLEO'01*, Baltimore, Maryland, U.S.A., paper CFA2, p. 544, 2001.

[17] C. Peucheret, A. Buxens, T. Rasmussen, C. F. Pedersen, and P. Jeppesen, "Cascadability of fibre Bragg gratings for narrow channel spacing systems using NRZ and duobinary modulation", in *Proceedings Opto-Electronics and Communications Conference, OECC'01*, Sydney, Australia, paper TUA3, pp. 92–93, 2001.

[18] T. Tokle, C. Peucheret, J. Seoane, and P. Jeppesen, "Transmission of 1.8 and 4.8 ps RZ signals at 10 Gbit/s over more than 2700 km of a dispersion managed link made of standard and inverse dispersion fibre", in *Proceedings Opto-Electronics and Communications Conference, OECC'01*, Sydney, Australia, paper WA4, pp. 266–267, 2001.

[19] A. T. Clausen, C. Peucheret, L. Oxenløwe, H. N. Poulsen, and P. Jeppesen, "OTDM and WDM systems", *Danish Optical Society, DOPS-NYT*, vol. 16, no. 2, pp. 9–12, 2001.

[20] C. Peucheret, T. Tokle, S. N. Knudsen, J. Seoane, and P. Jeppesen, "Novel schemes for dispersion management in high speed optical communication systems", *Danish Optical Society, DOPS-NYT*, vol. 16, no. 2, pp. 12–16, 2001.

[21] J. M. Gené, R. Nieves, A. Buxens, C. Peucheret, J. Prat and P. Jeppesen, "Reduced driving voltage optical duobinary transmitter and its impact on transmission performance over standard single-mode fiber", *IEEE Photonics Technology Letters*, vol. 14, no. 6, pp. 843–845, 2002.

[22] N. Chi, C. Peucheret, L. Oxenløwe, T. Tokle and P. Jeppesen, "2R all-optical regenerator assessment at 10 Gbit/s over 94 km standard fiber using in-line dispersion-imbalanced loop mirror", in *Proceedings International Conference on Telecommunications, ICT'02*, Beijing, China, pp. 1288–1290, 2002.

[23] L. K. Oxenløwe, A. I. Siahlo, K. S. Berg, A. Tersigni, A. T. Clausen, C. Peucheret, P. Jeppesen, K. P. Hansen and J. R. Jensen, "A photonic crystal fibre used as a 160 to 10 Gb/s demultiplexer", in *Proceedings Opto-Electronics and Communications Conference, OECC'02*, Yokohama, Japan, post-deadline paper PD1-4, 2002.

[24] L. Leick and C. Peucheret, "Dispersion induced penalty for 1×N passive interferometric optical MUX/DEMUXs and its reduction using all-pass filters", in *Proceedings European Conference on Optical Communication, ECOC'02*, Copenhagen, Denmark, paper 1.2.4, vol. 1, 2002.

[25] K. S. Berg, L. K. Oxenløwe, A. Siahlo, A. Tersigni, A. T. Clausen, C. Peucheret, P. Jeppesen, K. P. Hansen and J. R. Jensen, "80 Gb/s transmission over 80 km and demultiplexing using a highly non-linear photonic crystal fibre", in *Proceedings European Conference on Optical Communication, ECOC'02*, Copenhagen, Denmark, paper 2.1.5, vol. 1, 2002.

[26] N. Chi, B. Carlsson, P. V. Holm-Nielsen, C. Peucheret and P. Jeppesen, "Dispersion management for two-level optically labeled signals in IP-over-WDM networks", in *Proceedings European Conference on Optical Communication, ECOC'02*, Copenhagen, Denmark, paper 5.5.1, vol. 2, 2002.

[27] H.-J. Deyerl, N. Plougmann, J. B. D. Jensen, J. El-Bez, H. R. Sørensen, C. Peucheret and M. Kristensen, "Low-dispersion fibre Bragg gratings written using the polarization control method", in *Proceedings European Conference on Optical Communication, ECOC'02*, Copenhagen, Denmark, paper 7.2.7, vol. 3, 2002.

[28] Z. Xu, C. Peucheret, Q. Le and P. Jeppesen, "Short period dispersion management of 160 Gb/s single channel fiber system", in *Proceedings European Conference on Optical Communication, ECOC'02*, Copenhagen, Denmark, paper P3.15, vol. 3, 2002.

[29] N. Chi, B. Carlsson, J. Zhang, P. V. Holm-Nielsen, C. Peucheret and P. Jeppesen, "Transmission performance of all-optically labelled packets using ASK/DPSK orthogonal modulation", in *Technical Digest IEEE Lasers and Electro-Optics Society Annual Meeting, LEOS'02*, Glasgow, Scotland, U.K., paper MF3, vol. 1, pp. 51–52, 2002.

[30] P. A. Andersen, C. Peucheret, P. Jeppesen, K. P. Hansen and J. R. Jensen, "Supercontinuum generation in a photonic crystal fiber around 1550 nm",

in *Book of Abstracts Danish Optical Society (DOPS) Annual Meeting 2002*, Risø National Laboratory, Denmark, 2002.

[31] B. Zsigri, C. Peucheret, H.-J. Deyerl, M. Fujita and M. Kristensen, "Filtering tolerance of optical single-side band modulation for narrow channel spacing wavelength division multiplexing systems", in *Book of Abstracts Danish Optical Society (DOPS) Annual Meeting 2002*, Risø National Laboratory, Denmark, 2002.

[32] N. Chi, B. Carlsson, J. Zhang, P. V. Holm-Nielsen, C. Peucheret and P. Jeppesen, "Transmission properties for two-level optically labeled signals with amplitude-shift keying and differential phase-shift keying orthogonal modulation in IP-over-WDM networks", *Journal of Optical Networking*, vol. 2, no. 2, pp. 46–54, 2003.

[33] J. Zhang, N. Chi, P. V. Holm-Nielsen, C. Peucheret and P. Jeppesen, "A novel optical labeling scheme using a FSK modulated DFB laser integrated with an EA modulator", in *Technical Digest Optical Fiber Communication Conference, OFC'03*, Atlanta, Georgia, U.S.A., paper TuQ5, vol. 1, pp. 279–280, 2003.

[34] J. Zhang, N. Chi, P. V. Holm-Nielsen, C. Peucheret and P. Jeppesen, "A novel method for optical subcarrier label generation", in *Technical Digest Optical Fiber Communication Conference, OFC'03*, Atlanta, Georgia, U.S.A., paper FD5, vol. 2, pp. 653–654, 2003.

[35] N. Chi, L. Xu, L. J. Christiansen, K. Yvind, J. Zhang, P. V. Holm-Nielsen, C. Peucheret, C. Zhang and P. Jeppesen, "Optical label swapping and packet transmission based on ASK/DPSK orthogonal modulation format in IP-over-WDM networks", in *Technical Digest Optical Fiber Communication Conference, OFC'03*, Atlanta, Georgia, U.S.A., paper FS2, vol. 2, pp. 792–794, 2003.

[36] K. P. Hansen, J. R. Folkenberg, C. Peucheret and A. Bjarklev, "Fully dispersion controlled triangular core nonlinear photonic crystal fiber", in *Technical Digest Optical Fiber Communication Conference, OFC'03*, Atlanta, Georgia, U.S.A., post-deadline paper PD2, 2003.

[37] J. Zhang, N. Chi, P. V. Holm-Nielsen, C. Peucheret and P. Jeppesen, "Method for optical subcarrier label generation using carrier suppression technique", *Electronics Letters*, vol. 39, no. 4, pp. 388–389, 2003.

[38] N. Chi, J. Zhang, P. V. Holm-Nielsen, C. Peucheret and P. Jeppesen, "Transmission and transparent wavelength conversion of an optically

labelled signal using ASK/DPSK orthogonal modulation", *IEEE Photonics Technology Letters*, vol. 15, no. 5, pp. 760–762, 2003.

[39] N. Chi, J. Zhang, P. V. Holm-Nielsen, L. Xu, I. T. Monroy, C. Peucheret, K. Yvind, L. J. Christiansen and P. Jeppesen, "Experimental demonstration of cascaded transmission and all-optical label swapping of orthogonal IM/FSK labelled signal", *Electronics Letters*, vol. 39, no. 8, pp. 676–678, 2003.

[40] C. Peucheret, B. Zsigri, P. A. Andersen, K. S. Berg, A. Tersigni, P. Jeppesen, K. P. Hansen and M. D. Nielsen, "Transmission over photonic crystal fiber at 40 Gbit/s using mid-span spectral inversion in a highly nonlinear photonic crystal fiber", in *Technical Digest Conference on Lasers and Electro-Optics, CLEO'03*, Baltimore, Maryland, U.S.A., post-deadline paper CThPDB4, 2003.

[41] B. Zsigri, C. Peucheret, M. D. Nielsen and P. Jeppesen, "Transmission over 5.6 km large effective area and low loss (1.7 dB/km) photonic crystal fibre", *Electronics Letters*, vol. 39, no. 10, pp. 796–798, 2003.

[42] C. Peucheret, B. Zsigri, P. A. Andersen, K. S. Berg, A. Tersigni, P. Jeppesen, K. P. Hansen and M. D. Nielsen, "40 Gbit/s transmission over photonic crystal fibre using mid-span spectral inversion in a highly nonlinear photonic crystal fibre", *Electronics Letters*, vol. 39, no. 12, pp. 919–921, 2003.

[43] P. A. Andersen, C. Peucheret, K. M. Hilligsøe, K. S. Berg, K. P. Hansen and P. Jeppesen, "Supercontinuum generation in a photonic crystal fibre using picosecond pulses at 1550 nm", in *Proceedings International Conference on Transparent Optical Networks / European Symposium on Photonic Crystals, ICTON/ESPC'03*, Warsaw, Poland, paper Mo.C1.6, vol. 1, pp. 66–69, 2003.

[44] J. Zhang, N. Chi, P. V. Holm-Nielsen, C. Peucheret and P. Jeppesen, "An optical FSK transmitter based on an integrated DFB laser/EA modulator and its application in optical labeling", *IEEE Photonics Technology Letters*, vol. 15, no. 7, pp. 984–986, 2003.

[45] A. I. Siahlo, L. K. Oxenløwe, K. S. Berg, A. T. Clausen, P. A. Andersen, C. Peucheret, A. Tersigni, P. Jeppesen, K. P. Hansen and J. R. Folkenberg, "A high-speed demultiplexer based on a nonlinear optical loop mirror with a photonic crystal fiber", *IEEE Photonics Technology Letters*, vol. 15, no. 8, pp. 1147–1149, 2003.

[46] J. Zhang, N. Chi, P. V. Holm-Nielsen, C. Peucheret and P. Jeppesen, "Performance of Manchester-coded payload in an optical FSK labeling scheme", *IEEE Photonics Technology Letters*, vol. 15, no. 8, pp. 1174–1176, 2003.

[47] P. V. Holm-Nielsen, N. Chi, J. Zhang, C. Peucheret, I. Tafur Monroy and P. Jeppesen, "Experimental investigation of transmission properties and all-optical label swapping of orthogonal IM/FSK labeled signals", in *Proceedings Opto-Electronics and Communications Conference, OECC'03*, Shanghai, China, pp. 679–680, 2003.

[48] K. Vlachos, J. Zhang, J. Cheyns, Sulur, N. Chi, E. Van Breusegem, I. Tafur Monroy, J. G. L. Jennen, P. V. Holm-Nielsen, C. Peucheret, R. O'Dowd, P. Demeester and A. M. J. Koonen, "An optical IM/FSK coding technique for the implementation of a label-controlled, arrayed waveguide packet router", *Journal of Lightwave Technology*, vol. 21, no. 11, pp. 2617–2628, 2003.

[49] T. Tokle, C. Peucheret and P. Jeppesen, "System optimisation of dispersion maps using new cabled dispersion compensating fibres", *Journal of Optical Communications*, vol. 25, no. 2, pp. 75–78, 2004.

[50] I. Tafur Monroy, E. J. M. Verdurmen, Sulur, A. M. J. Koonen, H. de Waardt, G. D. Khoe, N. Chi, P. V. Holm-Nielsen, J. Zhang and C. Peucheret, "Performance of a SOA-MZI wavelength converter for label swapping using combined FSK/IM modulation format", *Optical Fiber Technology*, vol. 10, no. 1, pp. 31–49, invited paper, 2004.

Acknowledgements

First of all I would like to thank my supervisors, Palle Jeppesen and Rune J. S. Pedersen for having accepted me in the *"High-speed systems group"* at the Department of Electromagnetic Systems, later incorporated to the *"Systems Competence Area"* at COM, and made this Ph.D. project possible. Their guidance and patience has been much appreciated all over the duration of this project. Our regular progress meetings will be remembered for being both entertaining and a source of inspiration.

During those years at COM, I have been fortunate enough to enjoy the company of two of the best office mates ever. Thanks to Christian Rasmussen and Kim Berg for their patience in tolerating my highly variable mood, as well as the dozens of people knocking on our door everyday.

I am very much indebted to my early colleagues Christian Rasmussen and Fenghai Liu, for initiating me to the art of computer simulations and to laboratory work, respectively. In particular, many of the early results presented in this thesis would not have been made possible without Fenghai's laboratory skills.

The competence and in-depth knowledge of earlier colleagues, combined with their simplicity and modesty have set standards so high that they might be difficult to follow. Many thanks to Rune J. S. Pedersen and Bo Foged Jørgensen for showing me the way to go.

Alvaro Buxens, Anders Clausen, Leif Oxenløwe, Henrik Nørskov Poulsen have constituted for years the hard-core of the *"Systems Competence Area"*. Thanks to all of them for the great spirit and the nice work. I am looking forward to more of both. I am also extremely grateful to Stig Nissen Knudsen for the good collaboration over the years, and for having made the dispersion management studies possible by providing state-of-the-art fibres, as well as to Quang Le for his help on fibre issues.

It has been a pleasure to witness the emergence of a new generation of *"Systems Competence Area"* employees. Many thanks to Beáta Zsigri, Torger Tokle and Jorge Seoane for all the good job done so far, as well as to Kim Berg and Steinar Boge for an unfortunately far too short stay among us. A lot of fascinating challenges are still ahead of us. My hope also is that I did not totally fail in my modest contribution at transmitting the inheritance of the people I have learned so much from.

Past and present colleagues in the *"Systems Competence Area"*, Peter Andreas Andersen, Janne Witt Bengtsen, Lone Bjørnstjerne, Nan Chi, Pablo Holm-Nielsen,

Aline Møller, Andrei Siahlo, Andrea Tersigni, Zhenbo Xu, Jianfeng Zhang are all acknowledged for their help and the friendly atmosphere they contributed to.

One of the purposes of the establishment of COM was to favour cooperation between different disciplines within photonics. Over the years, this has turned out to be rather successful and I would like to thank all my colleagues at COM for making it an exciting place to work. If we sadly have to limit ourselves to the work reported in the following few pages, thanks to Hans-Jürgen Deyerl and Lasse Leick for helping bridging the gap between "components" and "systems" people.

A large part of the work reported in this thesis has been made possible by fruitful external collaborations. In particular I would like to thank Norbert Hanik from T-Systems in Berlin for initiating the work on normalised sections, as well as Lutz Molle and Ronald Freund, then at Virtual Photonics Incorporated, also in Berlin, for a good cooperation on this subject. Thomas Rasmussen from Ibsen Photonics is acknowledged for making some of the experimental investigations on fibre gratings possible by kindly providing a large number of samples. Thanks also to Chretien Herben from Delft University of Technology for sharing his expertise on the design of phased-array devices.

Special thanks go to the many students I was given the chance to supervise over the past few years. They are duly acknowledged for reminding me of my own ignorance, which is the best thing that can happen to a researcher. The successful completion of their projects has been an incredible source for motivation.

Finally, I would also like to have a thought for my own teachers who, through their dedication and enthusiasm share a huge part of responsibilities for me being here today. In particular, thanks to Serge Berretta from Lycée Carnot, Dijon, France, who, in his very personal style has managed to attract my attention towards optics at a time when I was not supposed to enjoy what I was learning. Later on, Pierre Pellat-Finet and Didier Hervé, both from ENST Bretagne, Brest, France, contributed to initiate me to the magic of light, whatever its state of polarisation.

And to the ones I may have forgotten or unfortunately could not find room to mention here, I would like to express my most sincere apologies. Thanks to all of you for the past and future cooperation. Please, keep knocking on my door.

List of acronyms

AM	Amplitude Modulator
ASE	Amplified Spontaneous Emission
ASK	Amplitude Shift Keying
ATM	Asynchronous Transfer Mode
AWG	Arrayed Waveguide Grating
BER	Bit Error Rate
CRZ	Chirped Return-to-Zero
CS-RZ	Carrier-Suppressed Return-to-Zero
CW	Continuous Wave
DCF	Dispersion Compensating Fibre
DFB	Distributed Feed-Back
DSF	Dispersion Shifted Fibre
DUT	Device Under Test
DWDM	Dense Wavelength Division Multiplexing
EDFA	Erbium Doped Fibre Amplifier
EOP	Eye Opening Penalty
FFT	Fast Fourier Transform
FSK	Frequency Shift Keying
FWHM	Full-Width Half-Maximum

FWM Four-Wave Mixing

GVD Group Velocity Dispersion

IDF Inverse Dispersion Fibre

IFWM Intra-channel Four Wave Mixing

IM Intensity Modulation

ISI Inter-Symbol Interference

IWAD Integrated Wavelength Add-Drop

IXPM Intra-channel Cross-Phase Modulation

LSB-RZ Lower Side-Band Return-to-Zero

MI Multilayer Interference

MLFRL Mode-Locked Fibre Ring Laser

MMI Multi-Mode Interference

MZ Mach-Zehnder

NA Network Analyser

NRZ Non Return-to-Zero

NZDSF Non-Zero Dispersion Shifted Fibre

OADM Optical Add-Drop Multiplexer

OBF Optical Band-pass Filter

ONE Optical Network Element

OOK On-Off Keying

OSNR Optical Signal-to-Noise Ratio

OTDM Optical Time Division Multiplexing

OXC Optical Cross-Connect

PCF Photonic Crystal Fibre

PD Photo-Diode

PHASAR Phased Array

PMD Polarisation Mode Dispersion

PRBS Pseudo-Random Binary Sequence

PWM Power Meter

RDF Reverse Dispersion Fibre

RDS Relative Dispersion Slope

RF Radio Frequency

RZ Return-to-Zero

SDH Synchronous Digital Hierarchy

SMF Standard single Mode Fibre

SNR Signal-to-Noise Ratio

SPM Self-Phase Modulation

SRS Stimulated Raman Scattering

TLS Tunable Laser Source

USB-RZ Upper Side-Band Return-to-Zero

WBDCF Wide-band Dispersion Compensating Fibre

WDM Wavelength Division Multiplexing

XPM Cross-Phase Modulation

Foreword

This thesis presents results obtained at the Department of Electromagnetic Systems (EMI), then at COM, following its establishment in 1998, between April 1998 and January 2001. Some of the work on the phase characterisation of optical components had been initiated in 1997 and was used as the starting point for this Ph.D. project.

The present work addresses a number of different issues in optical communication systems. Although all of theses issues are relevant for the design of future optical networks, they might be of interest to different people working in different areas.

The topics covered in this thesis could be tentatively divided in three broad categories:

1. Characterisation of the dispersive properties of optical components to be used in wavelength division multiplexing (WDM) networks

2. Influence of the transfer functions of WDM network elements

3. Dispersion management solutions based on standard single-mode fibre for transparent networks and long-haul applications.

As a consequence, it has been attempted to divide this thesis in self-contained chapters. Although a general introduction to the relevance of the aforementioned issues is given in Chapter 1, it was felt that a more detailed description of each of those issues was needed, resulting in a presentation of earlier results, state-of-the-art, and perspectives for nearly each chapter. For convenience, and in spite of a few duplicates, references are included at the end of each chapter.

It is hoped that this approach contributes to improve the readability of the thesis.

Chapter 1

Introduction

Wavelength division multiplexing (WDM) has been introduced in order to make use of the large bandwidth offered by silica optical fibres, and later on to benefit from new degrees of freedom offered by the possibility to manipulate the different wavelengths for selecting, dropping, adding, and routing channels. Since the first demonstrations to the present reported capacities in excess of 10 Tbit/s in a single fibre [1, 2, 3] and record distances over 10000 km without the need to resort to electrical regeneration [4, 5], numerous challenges have been overcome over a relatively short period of time, such as dispersion compensation [6], introduction of all-optical amplification [7], control of optical fibre non-linearities [8], to name a few. In order to increase the capacity of optical systems even further, the same physical limitations need to be even better controlled or mitigated. Furthermore, one of the next long-awaited steps is the introduction of all-optical networking, requiring not only a complete control of the properties of the transmission link, but also of the components and subsystems enabling to perform the routing and cross-connecting operations. This thesis examines a number of selected topics relevant to the realisation of future high-capacity all-optical networks.

Some issues in optical communication systems pertaining to the work reported in this thesis, namely the management of dispersion and non-linearities in optical fibre links, and the influence of optical filtering devices used in WDM networks, are briefly introduced in Section 1.1. Numerical simulation tools have been widely used throughout this work. Section 1.2 reviews this emerging field and lists a number of issues one should be made aware of when using such tools for the design and optimisation of fibre optics links. Finally, a chapter-by-chapter outline of the thesis can be found in Section 1.3.

1.1 Current trends in high capacity optical communication systems

1.1.1 Evolution of optical communication systems

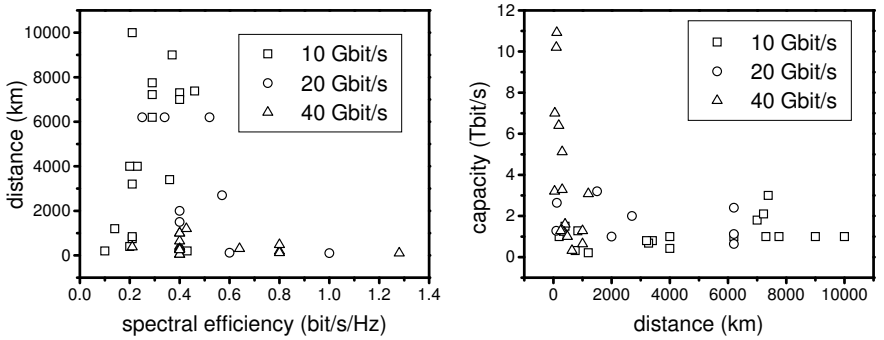

Figure 1.1 Distance versus spectral efficiency (left) and total capacity versus distance (right) as a function of channel bit rate for selected WDM record-breaking experiments reported between 1999 and 2001.

Recent record-breaking WDM transmission experiments reported at major optical communications conferences between 1999 and 2001 are summarised in Figure 1.1. The endeavours to achieve two concurrent goals, namely maximising the transmission distance and the total capacity, are highlighted. For a WDM system carrying N channels spaced Δf GHz apart, each channel carrying a bit rate equal to B Gbit/s, the total capacity is equal to $C = N \cdot B$, while the spectral efficiency is defined as $SE = B/\Delta f$ (in bit/s/Hz). Maximising the spectral efficiency ensures that the highest possible capacity can be transmitted over a bandwidth otherwise limited to the low loss region of optical fibres and to the wavelength ranges where optical amplification can be achieved.

Two trends can be observed in the graphs of Figure 1.1. The longest transmission distances can be reached with 10 Gbit/s channels, while the largest capacities and spectral efficiencies were obtained with 40 Gbit/s channels over rather short distances. Apart from the natural tendency to use the latest available technology (nowadays 40 Gbit/s) to perform these "hero-experiments", some basic transmission limitations inherent to the signal degradation mechanisms through optical fibres, or at the multiplexer and demultiplexer stages, can explain this trend. Since then, record capacities of 10.92 Tbit/s over 117 km [1] and 10.2 Tbit/s over 300 km [3] have been reported.

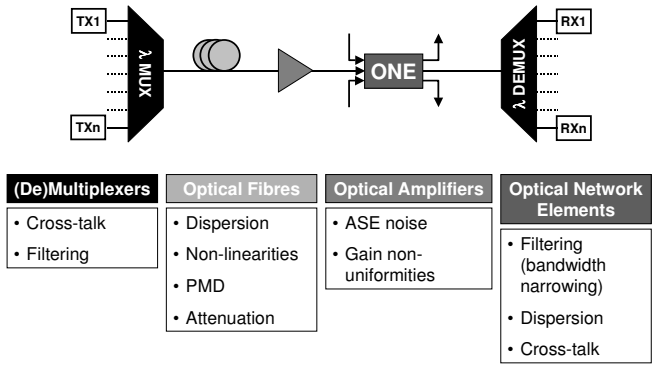

Figure 1.2 Transmission impairments in WDM networks.

Some of the signal impairments to be encountered in a WDM optical network and their origin are summarised in Figure 1.2. Channel selective components are present under the form of terminal (de)multiplexers, but also in optical network elements (ONE) such as wavelength routers, optical add-drop multiplexers (OADM) and optical cross-connects (OXC). The choice of their bandwidth results from a trade-off between cross-talk from adjacent channels and signal distortion resulting from excessive filtering. When cascaded in a link, bandwidth narrowing and accumulation of filter dispersion might become an issue, as will be discussed in depth in this thesis. Optical fibres exhibit group-velocity dispersion as well as polarisation mode dispersion [9]. Furthermore, their non-linear behaviour results in a full range of detrimental effects, either due to the Kerr non-linearity or to stimulated Brillouin and Raman scattering mechanisms [8]. The loss of optical fibres can be compensated by the use of optical amplifiers, typically erbium-doped fibre amplifiers (EDFA) [7]. However, those will add spontaneous emission noise to the signal and might produce unequal amplification for the different WDM channels, which can to some extent be compensated by gain equalisation filters.

Some of the basic signal degradation mechanisms presented above can be avoided, or at least mitigated, by a proper design of components or by the choice of a suitable technology. As we shall see later on in this thesis, this is typically the case of dispersion in optical components. Others are inherent to the transmission medium and cannot be avoided, such as non-linearities in optical fibres. Consequently, design rules should be drawn in order to ensure a particular system is operated within safe parameter areas where those degradations are kept under control. In the following, we focus on two of the limitations investigated further in this thesis: the interaction

of dispersion and non-linearities in optical fibre links, and the influence of non-ideal transfer functions of optical network elements.

1.1.2 Management of dispersion and non-linearities

Group-velocity dispersion (GVD) is due to the frequency dependence of the group index in optical fibres and is known to be responsible for pulse broadening, resulting in inter-symbol interference (ISI) in digital fibre optics communication systems. The impact of GVD scales as the square of the bit-rate, making the effect a severe limitation at high bit-rates. For instance, if an amount of accumulated dispersion of 1000 ps/nm, corresponding to about 60 km standard single mode fibre (SMF), can be tolerated for a 10 Gbit/s system for a 1 dB penalty criterion [6], this amount will be reduced to only about 70 ps/nm (or 4 km SMF) at 40 Gbit/s. Some techniques have hopefully been introduced over the years in order to circumvent this detrimental effect, such as pre-chirping at the transmitter [10], dispersion-supported transmission [11], mid-span spectral inversion [12], the use of negative dispersion devices such as planar lightwave circuits [13], and chirped fibre gratings [14], as well as the use of negative dispersion fibres (the so-called "dispersion compensating fibres", or DCFs) [15]. This last solution has appeared as the most attractive due to the large bandwidth offered. It relies on the fact that engineering the refractive index profile of optical fibres enables to change the contribution of the waveguide dispersion to their total dispersion, and hence to produce negative dispersion fibres.

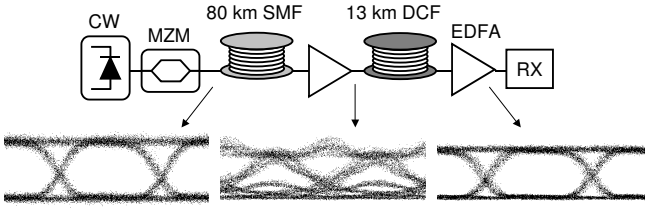

Figure 1.3 Principle of dispersion compensation (here applied to a 10 Gbit/s NRZ signal over 80 km SMF). CW: continuous wave laser; MZM: Mach-Zehnder modulator; EDFA: erbium doped fibre amplifier; SMF: standard single-mode fibre; DCF: dispersion compensating fibre; RX: receiver.

The use of DCF in conjunction with SMF is illustrated in Figure 1.3, where the propagation of a 10 Gbit/s non return-to-zero (NRZ) signal through a 80 km link is examined. It can be seen that, after only 80 km,

the signal is severely distorted by the dispersion of the SMF, of the order of 17 ps/(nm·km). The eye diagram closure resulting from pulse spreading due to dispersion would be responsible for detection errors at the decision circuit at the receiver. Inserting a matching length of DCF - here about 13 km DCF with dispersion parameter equal to -100 ps/(nm·km) - enables the pulse shape to be restored at the end of the link, thus demonstrating the effectiveness of the use of DCFs for dispersion compensation.

In the 80 km link example shown above, even unperfect dispersion compensation might result in an acceptable signal quality at the receiver. The picture will be changed in long-haul multi-span systems where the residual dispersion will accumulate over the entire link, potentially resulting in severe signal degradation. Furthermore, when wavelength division multiplexing is used, it should be ensured that the dispersion compensation scheme is effective for all transmitted channels.

The dispersion compensation task is complicated by the occurrence of optical fibre non-linearities. The intensity dependence of the refractive index of silica can cause the phase of a signal to be modulated by its own intensity (self-phase modulation or SPM), by the intensity of neighbouring channels (cross-phase modulation or XPM), or can be responsible for the generation of mixing products at other wavelengths in WDM systems (four-wave mixing or FWM). Modulation instability (MI) can result in the spontaneous break-up of a long string of "1" in an NRZ signal into pulses. All these effects interact with fibre dispersion by either conversion of phase modulation to intensity fluctuations, frequency chirping, walk-off between WDM channels, or by satisfaction of a phase matching condition. Consequently, the effect of dispersion cannot be considered independently from the non-linearities, hence the concept of "management of optical fibre dispersion and non-linearities" achieved by a proper choice and arrangement of a combination of transmission and dispersion compensating fibres. The general rule for efficient dispersion management in multi-channel systems is to keep the local dispersion sufficiently high to reduce the efficiency of non-linear effects such as XPM and FWM, while ensuring that the total accumulated dispersion is close to zero for each channel over the link. This can be realised with dispersion maps based on SMF, the optimisation of a number of which will be reported in this thesis.

1.1.3 Influence of network elements

Wavelength division multiplexing systems are evolving from point-to-point links where the different wavelengths were merely used as a way to increase the capacity, to more complex network structures where the wavelengths

provide additional degrees of freedom (e.g. routing). Operations on the wavelengths can be performed by a variety of channel manipulation components such as optical add-drop multiplexers and optical cross-connects, which are responsible for new causes of signal degradation. In a straight line WDM system, the channels need to be demultiplexed only at the receiver end. Therefore, signal degradation occurring because of the filtering process at the demultiplexer is not critical as long as the channels can be recovered with acceptable power penalty. In a network context, on the other hand, the signals might be demultiplexed and re-multiplexed at each add-drop or cross-connect node. Consequently, even small degradation induced in each filtering stage will eventually accumulate over the path followed by the signal. New issues concerning non-ideal filtering elements need to be addressed in the study of dense WDM (DWDM) networks, resulting in tight specifications for the (de)multiplexers, especially when a high spectral efficiency is desired. Some of those issues are listed below.

- Amplitude filtering: amplitude filtering occurs by removing spectral contents to the signal. The filter bandwidth with respect to the channel spectral width, as well as the shape of the amplitude transfer function will influence the filtering behaviour and result in more or less pronounced signal distortion. Sharp roll-off associated with small bandwidths might not be always desirable if they remove important spectral content from the signal.

- Component loss: although insertion loss can ideally be compensated by the use of optical amplifiers, this process generates amplified spontaneous emission (ASE) noise. As the requirements on optical signal-to-noise ratio (OSNR) for a given system performance increase with the bit rate, it is highly desirable, especially for systems operating at 40 Gbit/s and above, to reduce as much as possible the loss between optical amplifiers. It is therefore necessary to minimise the loss in network elements.

- Cascading induced filter bandwidth narrowing: unless the (de)multiplexers have a square spectral response, the effective bandwidth of a cascade of filters will decrease with the number of filters. Depending on the filter design, this bandwidth reduction can be more or less pronounced. Typical arrayed waveguide grating (AWG) multiplexers have a Gaussian shaped pass-band [16], which can be shown to be very prone to bandwidth reduction. Designing a WDM system with a high spectral efficiency requires (de)multiplexers having reduced bandwidths. Cascading network elements might then result in

equivalent bandwidths far too small compared to the signal spectral width, which is determined by the modulation format and the bit-rate. Unrecoverable distortion might then be induced on the signal propagating through such a filter cascade.

- Cross-talk accumulation: different cross-talk mechanisms are likely to be introduced in network nodes [17, 18]. This cross-talk could result from insufficient clearing of the dropped signals in add-drop nodes, from multi-path propagation in optical components (both resulting in cross-talk contributions at the same wavelength as the signal), or from insufficient rejection of neighbouring channels in filtering elements such as (de)multiplexers (ranging from power addition to homodyne cross-talk depending on the separation between the channels). The later can be minimised provided the neighbouring channels are sufficiently attenuated. The cross-talk level of a component is usually defined as the ratio of the attenuation experienced by the transmitted channel to the attenuation of its closest neighbour channel. Again, a square spectral response is clearly desirable.

- Filter dispersion: the chromatic dispersion in optical filters is the subject of increased attention [19]. As in optical fibres, dispersion results from wavelength dependent group delay through a filter and will manifest itself by pulse distortion. However, the variation of the group delay with respect to wavelength is usually much more pronounced in optical filters and therefore the full dispersion transfer function needs to be taken into account (whereas in optical fibres, unless very high bit rates in excess of 80 Gbit/s are used, it is usually sufficient to describe the dispersion by a dispersion parameter at the channel centre wavelength). The recent importance of dispersion in optical components is due to several new developments in optical communication systems. First, the increase in bit rate from 2.5 to 10, and now 40 Gbit/s means that this effect can no longer be ignored. Small dispersion values up to a few tens of picoseconds per nanometre which are typically measured in WDM components for 10 Gbit/s systems will need to be taken into account in the system design at 40 Gbit/s and above. Second, optical communications systems are evolving from point-to-point to more complex network structures. Therefore, any path through the network is likely to include an increased number of network elements such as OADMs or OXCs, which are built from dispersive devices. The accumulation of device induced dispersion might then result in significant signal degradation.

Finally, the spectral efficiency of WDM systems is also increasing, and filtering elements having narrower bandwidths are required in order to accommodate such a higher channel density. Depending on the filter technology [19, 20], this bandwidth reduction is sometimes only possible at the expense of increased chromatic dispersion.

- Various other issues include polarisation dependent loss, control of the pass-band centre wavelength and temperature stability.

In this thesis, we will focus on the transmission impairments induced by amplitude and phase filtering (dispersion) of high data rate optical signals. Cross-talk will not be considered.

1.2 Numerical simulation of optical fibre communication systems

A recent trend in the design of optical communication systems is the increased use of sophisticated simulation tools. Although the modelling and simulation of optical fibre links has been reported for many years (see e.g. [21, 22]), the complexity of state-of-the-art systems is such that it is no longer realistic for system designers to invest a significant amount of time in the development of a simulation platform and in the implementation of generic models. Instead, it has become common practice to rely on commercial simulation software packages offered by a number of companies (for instance the following products - with references to some early work on which they are based - are available at the time of writing: VPItransmissionMakerWDM [23], COMSIS [24], FOCUSS [25], OptSim [26], LinkSIM). These general purpose simulation tools usually combine a graphical user interface from which the systems can be easily defined, scheduling functions which determine the order in which the different blocks are executed, and some libraries of models for optical and optoelectronic components.

The main cause behind the need for general purpose simulation tools has been the advent of optical amplifiers, resulting in increased power levels throughout the links, meaning that the weak non-linearity of optical fibres could no longer be ignored. The interaction between group-velocity dispersion and optical fibre non-linearities is a complex process which needs to be evaluated numerically. The wavelength dependence of the gain and noise figure as well as saturation effects in optical amplifiers, detrimental non-linear effects such as four-wave mixing, cross-phase modulation and stimulated Raman scattering, linear and non-linear cross-talk, more complex link or network structures with add-drop nodes or cross-connects, are

some of the additional effects which have to be taken into account in WDM systems, and which are usually not tractable in the most general case without resorting to numerical simulations.

The increasing complexity of optical communication systems has also resulted in an explosion of the dimension of the design parameters space. It has become impractical, as well as costly, to explore such a space experimentally when designing a system. This is especially true since system designers are likely to select fibres or components from different vendors and cannot afford to buy samples from many sources for the single purpose of testing their prototypes. It is therefore necessary to identify the ranges of interest for the different design parameters beforehand. Consequently, computer simulations are customarily used for multi-parameters optimisations, the results of which constitute inputs for the implementation of a test-bed. However, such an optimisation process might prove particularly time consuming.

The calculation of signal propagation in dispersive and non-linear media such as optical fibres is generally performed using the split-step Fourier method [27]. The effect of chromatic dispersion can be expressed as a frequency dependent phase shift in the frequency domain, while the effect of the Kerr non-linearities are accounted for by an instantaneous power dependent phase shift calculated in the time domain. It is assumed that the dispersive and non-linear effects can be treated separately over a small fibre length known as the step size, hence the name of "split-step" given to the method. Conversions between the time and frequency domains are performed numerically using fast Fourier transform (FFT) algorithms whose computational complexity scales as $N \log_2 N$, where $N = 2^k$ is the number of samples [28]. Therefore, increasing the simulation bandwidth, hence the sample rate, to e.g. simulate WDM systems, will result in an increased computation time, especially if all effects (such as four-wave mixing) need to be taken into account. Depending on the split-step algorithm implementation (adaptive versus fixed split-step [27]), enhancing the non-linear effects by increasing the signal power level will require a decrease in the step size for the method to remain accurate [29]. This will in turn increase the number of calls to FFT routines necessary for the calculation of the signal propagation over a given length of fibre, therefore resulting in a substantial increase in computation time.

As the increased use of numerical simulations stems from the necessity to take optical fibre non-linearities into account, as well as the need to perform multi-parameter optimisations, the computation time constraints imposed by the use of split-step algorithms are clearly an issue. Some other

known issues in general purpose simulation tools are:

- Accurate component models usually require computation times that are not in line with the requirements for the simulation of complete systems. A physical model of e.g. an erbium doped fibre amplifier (EDFA) can accurately predict its behaviour, including wavelength dependence and saturation effects [30]. However, optimising a trans-oceanic link, where up to a few hundred EDFAs can be cascaded, by using such a model is clearly impractical. Hence the need for models with different levels of abstraction, from physical to system-oriented, the usual compromise being between the accuracy and the computation time.

- Moreover, physical parameters are very often not accessible to system designers, either because they already deal with subsystems (e.g. an assembled EDFA as opposed to a piece of erbium doped fibre), or because they are proprietary information. Hence the need for so-called "black-box" models which should ideally predict the behaviour of subsystems in most regimes from a few measurements under carefully selected operating conditions.

- The performance of optical systems is usually assessed from measurements of the bit-error-rate (BER) after transmission of repeated random sequences consisting of up to $2^{31} - 1$ bits. Such an approach can clearly not be followed in numerical simulations. General and accurate receiver models enabling a reliable estimation of the BER still have to be found. This is discussed more in details in Appendix D in connection with the description of the models used in this work.

- Some effective ways to deal with statistical effects, such as for instance polarisation mode dispersion, without resorting to a prohibitive number of simulation runs also need to be found.

Based on the issues above, one might argue whether general purpose simulation tools are well suited for all kinds of problems. For instance in [31], wavelength domain simulation was proposed in order to evaluate the power of signals (including cross-talk terms), as well as amplified spontaneous emission noise spectral densities at all points in a network, followed by full simulations of selected paths in the network. This approach was believed to facilitate the study of complex WDM network structures. A different procedure has been reported for the optimisation of long-haul submarine systems [32], where the effects of signal impairment due to optical signal-to-noise ratio degradation, pulse distortion due to dispersion

and non-linearities, and non-linear interaction of noise and signal were decoupled. Such innovative approaches should be checked against experimental results in order to be validated. However, general purpose tools offer the flexibility to be usable for a broad variety of problems, which was the case in the different studies presented in this thesis.

In this work we have heavily relied on the different generations of tools from Virtual Photonics Incorporated (previously known as BNeD GmBH), with whom we have been collaborating either informally or within the framework of the DEMON project supported by the European Commission. Those tools are, in chronological order, BroadNeD, PTDS [23] and lately VPItransmissionMaker™WDM. In most cases, we have favoured the reliability of the simulations and therefore have limited ourselves to rather conservative modelling approaches with a minimum of simplifying assumptions, at the expense of increased computation time. Simplifying assumptions can be made whenever it is known beforehand that a specific effect can be neglected. Clearly, this is not always the case in research work where new directions are explored. Moreover, simulations are often used to define optimum parameter values, which are the result of a trade-off between several competing effects, making it impossible to rule out *a priori* any of those effects. In a number of cases, the simulations have been cross-checked with results obtained from another tool (STONE, Simulation Tool for Optical Networks) developed by Christian Rasmussen in an earlier project at COM [33]. The models and parameters used for the different investigations presented in this thesis will be described in the different chapters. Some general considerations on modelling approaches that have been followed throughout the thesis are also given in Appendix D.

Quantitative agreement between experiments and numerical simulations can be obtained at the expense of a time consuming fine tuning of all the simulation parameters, the knowledge of which would require a detailed characterisation of some of the subsystems used in the experiments (for instance the exact frequency response and thermal noise density of the photodiode and electrical amplifier chain used at the receiver). As the numerical evaluation of the performance of the system by computing the BER has known limitations anyway, it has been preferred instead to focus on qualitative agreement between simulations and experiments, the former being mostly used to investigate the dependance of the system under investigation on a set of parameters.

1.3 Structure of the thesis

The work reported in the present thesis follows two major directions. The first one deals with transmission impairments induced by filtering effects in passive components used in WDM networks. A strong emphasis is given to the influence of the non-linear phase transfer functions of WDM components, which results in wavelength dependent chromatic dispersion. The phase characterisation of components used in WDM networks is first discussed, followed by reports on investigations carried out on two concurrent technologies, namely those based on fibre Bragg gratings [34] and phased array devices [35]. The second major direction deals with the management of dispersion and non-linearities in optical fibre links. These studies focus on systems based on standard single mode fibres. The optimised design of transparent terrestrial network is first discussed in details, followed by a report on the first experimental assessment of wide-band dispersion compensation fibres. Finally, numerical and experimental investigations on new types of dispersion compensating fibres for cabled long-haul applications are presented. A more detailed outline of the thesis is given below.

Chapter 2 concentrates on the determination of the phase transfer function of optical components used in WDM systems for multiplexing, demultiplexing, add-drop multiplexing, as well as for dispersion compensation and in-line filtering. A number of issues related to amplitude-phase relations in optical filters (analogous to Kramers-Kronig relations) are discussed and illustrated by an example of application. A general formulation of amplitude modulation techniques for the phase characterisation of optical components is presented, followed by the description of the implementation of two particular methods, the phase-shift technique and the dispersion offset method, whose feasibility was investigated following an initial suggestion by Fenghai Liu and discussions with Rune Pedersen. Chapter 2 also presents a broad catalogue of complex transfer functions (amplitude and group delay) measured on a variety of optical filters technologies such as fibre Fabry-Pérot, fibre gratings, thin-film filters and arrayed waveguide gratings.

The cascadability of optical filters based on fibre Bragg gratings has been investigated numerically and experimentally and the results are presented in Chapter 3. Simulations are performed in order to assess the detrimental effect of the chromatic dispersion inherent to such devices. An experimental comparison of signal degradation through fibre Bragg grating filters designed for 100 and 50 GHz channel spacings is performed. Using

a re-circulating loop set-up, it is shown that only up to 5 filters designed for 50 GHz channel spacing can be cascaded with finite penalty. The bandwidth narrowing resulting from cascading such filters can be attributed to features in the dispersion of the device. Numerical simulations are performed in order to demonstrate that, even in the presence of non-uniform dispersion, optical duobinary modulation can overcome some of these limitations. The fibre gratings used in the experiments have been kindly provided by Thomas Rasmussen from ADC Denmark (now Ibsen Photonics), while the work on grating cascadability using optical duobinary modulation results from a fruitful collaboration with Alvaro Buxens.

Phased-array (PHASAR) devices, also known as arrayed waveguide gratings (AWG), constitute a promising technology to perform (de)multiplexing at the transmitter, receiver, or within optical cross-connects and add-drop nodes. Although such devices are commercially available for a number of years, their use in a networking environment at high bit rates needs to be investigated. Chapter 4 presents a study of pass-band flattened PHASARs aimed at maximising the spectral efficiency in dense WDM networks at 40 Gbit/s. Different pass-band flattening techniques are compared and it is shown that a parabolic horn input coupler should be preferred to a multi-mode interference (MMI) input coupler to ensure cascadability of the device with spectral efficiency above 0.4 bit/s/Hz in future multi-gigabit metropolitan networks. This work was carried out in the framework of the European Information Society Technologies (IST) project METEOR (Metropolitan Terabit Optical Ring). The modelling of the different PHASAR designs was performed by Chretien Herben from the Delft University of Technology who provided the transfer functions used in this study.

An innovative way to design transparent optical networks is presented in Chapter 5. It relies on the concept according to which each possible path in a network is made of a cascade of "normalised sections" consisting of standard single mode fibre, dispersion compensating fibre and erbium doped fibre amplifiers. Defining the extension of transparent network domains is then equivalent to assessing the cascadability of the normalised sections under varying operating conditions, depending on the power per channel at the input of each fibre span and the degree of compensation. An extensive numerical optimisation of different dispersion compensation schemes suitable for terrestrial networks is performed for NRZ transmission at 10 Gbit/s. Pre- and post compensation with or without pre-distortion at the transmitter are compared. Based on the simulation results, the

transmission performance of such normalised sections are assessed in re-circulating loop experiments for single channel and WDM transmission at 10 Gbit/s. The concept of normalised sections was first proposed by Norbert Hanik from Deutsche Telekom T-Nova and most of the results have been obtained within our participation to the European ACTS DEMON (Demonstrating the Evolution of a Metropolitan Optical Network) project. The re-circulating loop experiments on single channel and WDM NRZ transmission have been performed together with Fenghai Liu from COM and Lutz Molle from the Technical University of Berlin, while the chirped return-to-zero (CRZ) results were obtained together with Fenghai Liu.

Chapter 6 presents results on the use of wide-band dispersion compensating fibres. Such fibres are designed so that their dispersion slope matches that of standard single mode fibre, resulting in zero accumulated dispersion over a wide bandwidth after an integer number of dispersion compensated spans. This feature is obviously highly desirable in WDM systems. Using a re-circulating loop set-up, it is shown that equivalent performance can be obtained over the full C-band after up to 1000 km transmission, corresponding to 20 cascades of 50 km spans. Transmission in the L-band at 1597 nm is also demonstrated over more than 1000 km with a dispersion map optimised at 1550 nm, showing that the need for separate band dispersion compensation can be removed in typical terrestrial systems by using wide-band DCF. The dispersion compensated spans have been provided by Stig Nissen Knudsen from Lucent Technologies Denmark A/S (now OFS Fitel Denmark I/S), while the L-band re-circulating loop experiments were performed together with Irene Muñoz and Alvaro Buxens, both from COM.

New possibilities for the compensation of the dispersion of standard single mode fibre for cabled long-haul applications are presented in Chapter 7. They rely on new types of dispersion compensating fibres known as inverse dispersion fibres (IDF), which have been designed in order to present a lower non-linear coefficient and lower loss than conventional DCF. The optimum IDF to SMF length ratio is determined numerically for long haul transmission at 10 Gbit/s over typical trans-oceanic spans. Transmission of 1.8 ps and 4.8 ps RZ signals at 10 Gbit/s over respectively 2700 and 3000 km of a dispersion managed link made of SMF and IDF is achieved in a re-circulating loop test-bed. When using such a map, the benefit of short RZ pulses over NRZ is clearly demonstrated. Finally, results on the first 40 Gbit/s optical time division multiplexing (OTDM) re-circulating loop

experiment performed at COM over up to 600 km are reported. Prototype IDFs have been made available to us by Stig Nissen Knudsen from Lucent Technologies Denmark A/S with whom the collaboration on novel DCFs was initiated. The experimental results on 10 and 40 Gbit/s short pulses transmission over a SMF+IDF map were obtained together with Torger Tokle and Jorge Seoane from COM.

1.4 References to Chapter 1

[1] K. Fukuchi, T. Kasamatsu, M. Morie, R. Ohhira, T. Ito, K. Sekiya, D. Ogasahara, and T. Ono, "10.92-Tb/s (273 × 40-Gb/s) triple-band/ultra-dense WDM optical-repeatered transmission experiment", in *Technical Digest Optical Fiber Communication Conference, OFC'01*, Anaheim, California, U.S.A., post-deadline paper PD24, 2001.

[2] S. Bigo, Y. Frignac, G. Charlet, W. Idler, S. Borne, H. Gross, R. Dischler, W. Poehlmann, P. Tran, C. Simonneau, D. Bayart, G. Veith, A. Jourdan, and J.-P. Hamaide, "10.2 Tbit/s (256 × 42.7 Gbit/s PDM/WDM) transmission over 100 km TeraLight™ fiber with 1.28 bit/s/Hz spectral efficiency", in *Technical Digest Optical Fiber Communication Conference, OFC'01*, Anaheim, California, U.S.A., post-deadline paper PD25, 2001.

[3] Y. Frignac, G. Charlet, W. Idler, R. Dischler, P. Tran, S. Lanne, S. Borne, C. Martinelli, G. Veith, A. Jourdan, J.-P. Hamaide, and S. Bigo, "Transmission of 256 wavelength-division and polarization-division-multiplexed channels at 42.7 Gb/s (10.2 Tb/s capacity) over 3×100 km of TeraLight™fiber", in *Technical Digest Optical Fiber Communication Conference, OFC'02*, Anaheim, California, U.S.A., post-deadline paper FC5, 2002.

[4] D. G. Foursa, C. R. Davidson, M. Nissov, M. A. Mills, L. Xu, J. X. Cai, A. N. Pilipetskii, Y. Cai, C. Breverman, R. R. Cordell, T. J. Carvelli, P. C. Corbett, H. D. Kidorf, and N. S. Bergano, "2.56 Tb/s (25 × 10 Gb/s) transmission over 11000 km using hybrid Raman/EDFAs with 80 nm of continuous bandwidth", in *Technical Digest Optical Fiber Communication Conference, OFC'02*, Anaheim, California, U.S.A., post-deadline paper FC3, 2002.

[5] C. Rasmussen, T. Fjelde, J. Bennike, F. Liu, S. Dey, B. Mikkelsen, P. Mamyshev, P. Serbe, P. van der Wagt, Y. Akasaka, D. Harris,

D. Gapontsev, V. Ivshin, and P. Reeves-Hall, "DWDM 40G transmission over trans-Pacific distance (10000 km) using CSRZ-DPSK, enhanced FEC and all-Raman amplified 100 km UltraWave™fiber spans", in *Technical Digest Optical Fiber Communication Conference, OFC'03*, Atlanta, Georgia, U.S.A., post-deadline paper PD18, 2003.

[6] A. H. Gnauck and R. M. Jopson, "Dispersion compensation for optical fiber systems", in *Optical fiber telecommunications IIIA* (I. P. Kaminow and T. L. Koch, eds.), San Diego, pp. 162–195, Academic Press, 1997, 1997.

[7] J. L. Zyskind, J. A. Nagel, and H. D. Kidorf, "Erbium-doped fiber amplifiers for optical communications", in *Optical fiber telecommunications IIIB* (I. P. Kaminow and T. L. Koch, eds.), San Diego, pp. 13–68, Academic Press, 1997, 1997.

[8] F. Forghieri, R. W. Tkach, and A. R. Chraplyvy, "Fiber nonlinearities and their impact on transmission systems", in *Optical fiber telecommunications IIIA* (I. P. Kaminow and T. L. Koch, eds.), San Diego, pp. 196–264, Academic Press, 1997, 1997.

[9] C. D. Poole and J. Nagel, "Polarization effects in lightwave systems", in *Optical fiber telecommunications IIIA* (I. P. Kaminow and T. L. Koch, eds.), San Diego, pp. 114–161, Academic Press, 1997, 1997.

[10] A. H. Gnauck, S. K. Korotky, J. J. Veselka, J. Nagel, C. T. Kemmerer, W. J. Minford, and D. T. Moser, "Dispersion penalty reduction using an optical modulator with adjustable chirp", *IEEE Photonics Technology Letters*, vol. 10, no. 3, pp. 916–918, 1991.

[11] B. Wedding, "New method for optical transmission beyond dispersion limit", *Electronics Letters*, vol. 28, no. 14, pp. 1298–1300, 1992.

[12] S. Watanabe, T. Naito, and T. Chikama, "Compensation of chromatic dispersion in a single-mode fiber by optical phase conjugation", *IEEE Photonics Technology Letters*, vol. 5, no. 1, pp. 92–95, 1993.

[13] K. Takiguchi, K. Okamoto, and K. Moriwaki, "Planar lightwave circuit dispersion equalizer", *Journal of Lightwave Technology*, vol. 14, no. 9, pp. 2003–2011, 1996.

[14] F. Ouellette, "Dispersion cancellation using linearly chirped Bragg grating filters in optical waveguides", *Optics Letters*, vol. 12, no. 10, pp. 847–849, 1987.

[15] J. M. Dugan, A. J. Price, M. Ramadan, D. L. Wolf, E. F. Murphy, A. J. Antos, D. K. Smith, and D. W. Hall, "All-optical, fibre-based 1550 nm dispersion compensation in a 10 Gbit/s, 150 km transmission experiment over 1310 nm optimised fiber", in *Technical Digest Optical Fiber Communication Conference, OFC'92*, San Jose, California, U.S.A., post-deadline paper PD14, 1992.

[16] H. Takahashi, K. Oda, H. Toba, and Y. Inoue, "Transmission characteristics of arrayed waveguide N×N wavelength multiplexer", *Journal of Lightwave Technology*, vol. 13, no. 3, pp. 447–455, 1995.

[17] E. L. Goldstein, L. Eskildsen, and A. F. Elrefaie, "Performance implications of component crosstalk in transparent lightwave networks", *IEEE Photonics Technology Letters*, vol. 6, no. 5, pp. 657–660, 1994.

[18] L. Gillner, C. P. Larsen, and M. Gustavsson, "Scalability of optical multiwavelength switching networks: crosstalk analysis", *Journal of Lightwave Technology*, vol. 17, no. 1, pp. 58–67, 1999.

[19] G. Lenz, B. J. Eggleton, C. R. Giles, C. K. Madsen, and R. E. Slusher, "Dispersive properties of optical filters for WDM systems", *IEEE Journal of Quantum Electronics*, vol. 34, no. 8, pp. 1390–1402, 1998.

[20] G. Lenz, B. J. Eggleton, C. K. Madsen, C. R. Giles, and G. Nykolak, "Optimal dispersion of optical filters for WDM systems", *IEEE Photonics Technology Letters*, vol. 10, no. 4, pp. 567–569, 1998.

[21] P. J. Corvini and T. L. Koch, "Computer simulation of high-bit-rate optical fiber transmission using single-frequency lasers", *Journal of Lightwave Technology*, vol. LT-5, no. 11, pp. 1591–1595, 1987.

[22] K. Hinton and T. Stephens, "Modeling high-speed optical transmission systems", *IEEE Journal on Selected Areas in Communications*, vol. 11, no. 3, pp. 380–392, 1993.

[23] A. Lowery, O. Lenzmann, I. Koltchanov, R. Moosburger, R. Freund, A. Richter, S. Georgi, D. Breuer, and H. Hamster, "Multiple signal representation simulation of photonic devices, systems, and networks", *IEEE Journal of Selected Topics in Quantum Electronics*, vol. 6, no. 2, pp. 282–296, 2000.

[24] E. Gay, E. Guillard, M. Le Ligné, and D. Hui Bon Hoa, "Partie I: logiciel de simulation des systèmes de télécommunication: application aux

systèmes de transmission optique", *Annales des Télécommunications*, vol. 50, no. 3-4, pp. 379–388, 1995.

[25] C. Glingener, J.-P. Elbers, J. Kastner, and E. Voges, "Simulation of wavelength multiplexed fibre-optical systems", *AEÜ International Journal of Electronic Communication*, vol. 50, no. 5, pp. 301–309, 1996.

[26] A. Carena, V. Curri, R. Gaudino, P. Poggiolini, and S. Benedetto, "A time-domain optical transmission system simulation package accounting for nonlinear and polarization-related effects in fiber", *IEEE Journal on Selected Areas in Communications*, vol. 15, no. 4, pp. 751–765, 1997.

[27] G. P. Agrawal, *Nonlinear fiber optics*, chapter 2, pp. 50–54, Academic Press, San Diego, 2nd edition, 1995.

[28] A. V. Oppenheim and R. W. Schafer, *Digital signal processing*, pp. 285–336, Prentice Hall, Englewood Cliffs, 1975.

[29] C. Francia, "Constant step-size analysis in numerical simulation for correct four-wave mixing power evaluation in optical fiber transmission systems", *IEEE Photonics Technology Letters*, vol. 11, no. 1, pp. 69–71, 1999.

[30] C. R. Giles and E. Desurvire, "Modeling erbium-doped fiber amplifiers", *Journal of Lightwave Technology*, vol. 9, no. 2, pp. 271–283, 1991.

[31] I. Roudas, N. Antoniades, D. H. Richards, R. E. Wagner, J. L. Jackel, S. F. Habiby, T. E. Stern, and A. F. Elrefaie, "Wavelength-domain simulation of multiwavelength optical networks", *IEEE Journal of Selected Topics in Quantum Electronics*, vol. 6, no. 2, pp. 348–362, 2000.

[32] E. A. Golovchenko, A. N. Pilipetskii, N. S. Bergano, C. R. Davidson, F. I. Khatri, R. M. Kimball, and V. J. Mazurczyk, "Modeling of transoceanic fiber-optic WDM communication systems", *IEEE Journal of Selected Topics in Quantum Electronics*, vol. 6, no. 2, pp. 337–347, 2000.

[33] C. J. Rasmussen, *Transmission analysis in WDM networks.* PhD thesis, COM, Technical University of Denmark, Lyngby, Denmark, 1999.

[34] K. O. Hill and G. Meltz, "Fiber Bragg grating technology fundamentals and overview", *Journal of Lightwave Technology*, vol. 15, no. 8, pp. 1263–1276, 1997.

[35] M. K. Smit and C. van Dam, "PHASAR-based WDM-devices: principles, design and applications", *IEEE Journal of Selected Topics in Quantum Electronics*, vol. 2, no. 2, pp. 236–250, 1996.

Chapter 2

Phase characterisation of optical components

2.1 Importance of the phase characterisation of optical components

Chromatic dispersion results from the frequency dependence of the group delay through a linear optical device. This phenomenon is well known in single mode optical fibres where the frequency dependence of the group refractive index causes the different frequency components of a pulse spectrum to propagate at different group velocities in the fibre. This, in turns, results in pulse broadening or narrowing, depending on the relation between the chirp of the pulse (i.e. whether its instantaneous frequency is an increasing or decreasing function of time), the sign of the dispersion (i.e. whether the group velocity increases or decreases with increasing frequency), and the fibre length [1]. Pulse broadening is responsible for energy leaking from one pulse to the neighbouring bit slots, therefore causing inter-symbol interference resulting in detection errors in digital optical communication systems.

Wavelength division multiplexing (WDM) requires wavelength selective components in order to reduce cross-talk and allow close channel spacing at the transmitter (multiplexers), separate the channels at the receiver (demultiplexers), or allow channel manipulation such as add-drop multiplexing or cross-connecting in all-optical networks. A number of device technologies have been developed recently in order to perform the required operations on the wavelength. Wavelength selective components have been in use for many year in other branches of optics such as spectroscopy under the form of interferometers of various kinds or diffraction gratings [2]. Cur-

rent WDM filter technologies have successfully managed to transpose those basic physical principles in implementations compatible with fibre optics, either as fibre based or integrated planar devices.

Interferometers relying on division of amplitude can be used to perform filtering operations in WDM systems, either as 2-beam interferometers (e.g. Mach-Zehnder type devices [3]) or multiple beam interferometers, such as Fabry-Pérot [4] or thin-film filters [5]. Bulk diffraction gratings have also been proposed as wavelength demultiplexers [6]. An implementation of a diffraction grating which is compatible with the planar waveguide technology is known as the arrayed waveguide grating (AWG) or phased-array (PHASAR)[7, 8], which can be used as wavelength (de)multiplexer or router. Fibre Bragg gratings are very versatile devices whose transfer function can be tailored by a proper choice of the refractive index perturbation distribution [9], enabling them to be used in a wide range of applications, such as bandpass filters, optical add-drop multiplexers (OADM), devices for dispersion compensation, gain flattening filters, etc. For all the aforementioned technologies, selection of a particular wavelength relies on the realisation of constructive interference between a number of beams experiencing different phase shifts, which are realised in practice by different optical path lengths, and are therefore wavelength dependent. As a consequence, depending on the actual frequency dependence of the phase of their transfer function, optical filters are likely to exhibit some amount of dispersion.

According to the theory of linear systems, the group delay can be calculated from the phase of the transfer function $H(\omega)$ of a linear device according to[1]

$$\tau = \frac{\partial \phi}{\partial \omega} \tag{2.1}$$

where $\phi(\omega) = -\arg H(\omega)$. The dispersion $\mathbb{D}$ (usually expressed in ps/nm) is the derivative with respect to wavelength of the group delay[2]

$$\mathbb{D} = \frac{d\tau}{d\lambda} \tag{2.2}$$

[1]Throughout this thesis, the complex representation of a quantity having a magnitude A and a phase ϕ will be written $Ae^{-j\phi}$. Moreover, we adopt the time convention $e^{j\omega t}$ for complex representations of the fields. These conventions might differ from the ones adopted by other authors. However, physical quantities should in any case be represented by the same number, including its sign, indifferently of the phase convention.

[2]Note that in the more restrictive context of optical fibres, $\mathbb{D}$ would actually represent the total accumulated dispersion over a certain length L of fibre. It can be related to the dispersion parameter D (per unit length, customarily expressed in units of ps/(nm·km)) according to $\mathbb{D} = D \cdot L$, provided the dispersion is uniformly distributed with distance along the fibre.

We shall see in the remaining of this chapter that most common optical filter technologies exhibit rather low values of dispersion in the pass-band. However, one of the major concerns with group velocity dispersion is its accumulative nature. Proposed optical cross-connect (OXC) structures [10] require the ability to select a particular channel from an input fibre before switching it, in some cases depending on the required flexibility, wavelength converting it, and finally multiplexing it with other switched channels to an output fibre. In any case, the demultiplexing and multiplexing operations will have to be carried out at each cross-connect, either by using (de)multiplexers such as AWGs, or a combination of bandpass filters and passive couplers. OADMs can be distinguished from OXCs by the fact that they only have two aggregate ports and a number of tributary ports used to add or drop a limited number of wavelengths. Practical implementations which do not require to demultiplex the entire WDM spectrum are based on fibre grating filters, either used in conjunction with optical circulators [11], or in a Mach-Zehnder interferometer structure [12]. As a consequence, the future deployment of large scale WDM all-optical networks will involve a large number of filtering elements to be found in any given path within the network, resulting in a possibly high value of accumulated dispersion stemming from the network elements alone. The dispersion in the fibre links of such transparent networks can be effectively compensated by the use of dispersion compensating fibre (DCF) as will be shown in Chapter 5, and it is the dispersion of network elements which might ultimately limit the size of the transparent domains. Furthermore, the present evolution of WDM systems towards higher bit rate (40 Gbit/s systems are currently under development), where the dispersion tolerance is lower, or smaller channel spacing requiring narrower bandwidth filters, which, for a given technology, are likely to introduce increased dispersion [13], will exacerbate such component-induced dispersion limitations[3]. Modular OXC structures based on building blocks such as fibre Bragg gratings have also been presented in the literature [17], often assuming ideal frequency responses for the filtering elements. However, the scalability of such structures towards an increase in the number of channels will depend, not only on cross-talk accumulation, but also on in-band and out-of-band dispersion induced signal degradation.

[3]Other components which might be introduced in a network are devices for dispersion compensation (such as chirped fibre gratings - see Section 2.6.2) or gain equalisation filters (for instance based on long period gratings [14]). The main concern with both types of grating-based devices are the group delay ripples, which, depending on their pseudo-period and amplitude, might cause system penalties. Those impairments have been discussed elsewhere (see e.g. [15, 16]) and are outside the scope of this thesis.

As a consequence, it is essential to be able to accurately characterise the dispersive behaviour of optical components to be used in WDM systems. The remaining of this chapter focuses on the phase characterisation of optical filters. First, a number of dispersion measurement techniques are reviewed in Section 2.2, and their applicability to the characterisation of wavelength selective components is discussed. Another approach that had been foreseen to provide the phase response of optical filters is via the calculation of amplitude-phase relations (often referred to as Kramers-Kronig relations). Theoretical issues are briefly discussed and an example of application is provided in Section 2.3. Dispersion measurement in devices using radio-frequency amplitude modulation techniques are presented in Section 2.4, where a general formulation is presented, enabling to discuss the accuracy of the commonly used phase-shift technique described in Section 2.5. Section 2.6 presents a wide range of complex transfer functions of the most commonly used WDM devices, as well as of more innovative filter designs, enabling to highlight the major differences between the available filter technologies. Finally, an alternative direct dispersion measurement technique known as the dispersion offset method is presented in Section 2.7.

2.2 Review of dispersion measurement techniques

A number of techniques have been devised over the years in order to measure the dispersion parameter of optical fibres. In the following, we will briefly present a review of selected techniques such as pulse delay measurement, interferometric methods, phase-shift techniques and frequency domain fibre transfer function measurement. We will then assess the additional requirements which are specific to the characterisation of dispersion in optical components. Based on those requirements, some suitable measurement methods will be selected for further investigation.

2.2.1 Dispersion measurements in optical fibres

Interferometric techniques

The phase shift experienced by a lightwave propagating in an optical fibre can be related to the group delay according to (2.1). As a consequence, the determination of phase shifts by interferometric techniques appeared as a natural way to measure dispersion. Several implementations of such techniques have been reported. Usually based on a Mach-Zehnder interferometer structure, they rely on one of the basic principles which are outlined below.

- Wavelength scanning technique with fixed path-length imbalance: a broadband source is used and the intensity of the interference pattern $I(\lambda)$ is measured as a function of wavelength after filtering with a monochromator prior to detection [18]. Curve fitting of the interference fringes enables a direct determination of the dispersion D and dispersion slope $S = \frac{dD}{d\lambda}$.

- Path-length imbalance (Δx) scanning with a narrow-band source: by assessing the shift in position of the envelope of the interferogram $I(\Delta x)$ for successive values of the wavelength, one can measure the relative group delay $\tau(\lambda)$ [19, 20].

- Fourier transform spectroscopy: a broadband source is used and the path-length imbalance Δx is scanned in order to record the interferogram $I(\Delta x)$, which is then Fourier transformed to obtain the relative phase spectrum [20, 21]. The group delay and dispersion can then be calculated by numerical differentiation techniques.

These techniques are usually implemented with an air reference path (although in some cases a length of fibre of known dispersion characteristics can be used), and therefore allow for the characterisation of short pieces of fibres (typically ~ 1 m). Extrapolation to longer fibre lengths has to be done cautiously, as this assumes the dispersion is uniform with fibre length, which might not always be the case, especially for fibre types having a small core diameter.

Phase-shift techniques

In the conventional phase shift technique, light from a non-pulsed source is sinusoidally intensity modulated (typically at a few tens to a few hundreds of MHz) before being launched into the fibre under test. The electrical phase difference between the modulating signal and the component at the modulation frequency of the photo-current can be shown (under certain assumptions to be discussed in Section 2.5) to be equal to

$$\Delta\varphi = 2\pi f_m \tau(\lambda_0) \tag{2.3}$$

where $\tau(\lambda_0)$ is the group delay at the wavelength λ_0 and f_m is the modulation frequency. By measuring $\Delta\varphi$ at different wavelengths and by differentiating it according to (2.2), it is then possible to determine the dispersion accumulated through a certain length of fibre. The method has been first suggested with a broadband source and a monochromator as a wavelength discriminating element before detection [22], and later on using a laser

source tunable in wavelength [23]. Its applicability to the measurement of dispersion in optical components will be discussed in depth in Section 2.5.

One of the drawbacks of the method is that it requires both ends of the fibre to be accessed from the same location, making it unsuitable for measurement of the dispersion of installed fibres. A modified phase shift technique based on supercontinuum generation of a fixed wavelength reference signal as well as a wavelength selectable signal has been proposed to overcomes this limitation [24].

A variant of the phase-shift method known as "differential phase-shift technique" [25] directly measures the electrical phase shifts difference

$$\delta\varphi = \Delta\varphi\left(\lambda + \Delta\lambda/2\right) - \Delta\varphi\left(\lambda - \Delta\lambda/2\right) \tag{2.4}$$

experienced by amplitude modulated signals with a small wavelength separation $\Delta\lambda$. This can be achieved in practice by shifting the wavelength of the laser over $\Delta\lambda$ at a frequency lower than the amplitude modulation frequency f_m. The dispersion can be calculated from $\delta\varphi$ according to

$$\mathbb{D}\left(\lambda\right) = \frac{\delta\varphi}{2\pi f_m \Delta\lambda} \tag{2.5}$$

Note that deriving (2.5) from (2.3) assumes that the dispersion is a smooth function of wavelength, which is usually the case in optical fibres. Practical implementations of the phase-shift and differential phase-shift methods in a metrology environment are discussed in details in [26].

Other methods

A method for the direct determination of $\mathbb{D}$ has been proposed in [27, 28]. It is based on the measurement - following square law detection - of the response of an optical fibre to small index amplitude modulation whose frequency is swept in the radio-frequency (RF) - microwave region (up to a few tens of GHz). This technique, which we will call RF modulation method, is described in detail in Sections 2.4 and 2.7.

As dispersion manifests itself as a frequency dependence of the group delay through a fibre, some early methods have focussed on the comparison of the propagation time of laser pulses at different wavelengths (the so-called "time-of-flight" measurements [29]). However it requires the generation of short pulses at several wavelengths as well as the precise determination of the propagation delay experienced by them. A comparison of early fibre dispersion measurement techniques, including pulse-delay measurement, phase shift, and some implementations of interferometric techniques can be found in [19].

A technique which does not require a closed-loop configuration for the fibre has been reported in [30]. It is based on phase-to-amplitude (PM-AM) modulation conversion experienced in a dispersive medium. It allows the determination of the dispersion of an entire link, including optical amplifiers and wavelength selective devices, from the evaluation of the amplitude modulation of the received lightwave when a sinusoidally phase modulated signal is input to the link.

Another category of techniques relies on the fact that the manifestation of a certain number of non-linear effects in optical fibres depends on the local value of the dispersion parameter. For instance, the power of four wave mixing products can be shown to be an oscillatory function of distance [31]. The period of the oscillations can be related to the phase mismatch between the launched waves, which is a function of the local dispersion. Measuring the period of spatial oscillations (from the temporal oscillations of the Rayleigh back-scattered wave) at a specific distance in the fibre will thus enable a determination of the local dispersion parameter. This technique, which has been demonstrated in [32], allows for distributed dispersion measurements over an entire link.

Some comments

The list above does not pretend to be exhaustive. It merely presents a variety of techniques based on different principles, some of which were believed to be of interest for the problem of dispersion measurement in optical components. Out of the many schemes which have been suggested in order to provide, in some more or less straightforward way, a value of the dispersion in optical fibres, only very few are actually used in practice.

As an example, a recommendation from the International Telecommunication Union (ITU) [33] mentions the phase-shift technique as the reference test method, while the interferogram envelope displacement method and the pulse-delay technique are both cited as alternative test methods. The phase-shift technique is very often preferred in the industry due to its simplicity and the availability of compact set-ups from several manufacturers[4].

It should also be emphasised that, among the methods described previously, only the differential phase-shift and the RF modulation techniques, provide a direct measurement of the dispersion. From all the other methods, the dispersion can be obtained after numerical differentiation of the

[4]See for example, at the time of writing, Nettest's *S18 & S19 Chromatic Dispersion Measurement Systems*, Agilent's *86037C Chromatic Dispersion Test Solution* or Advantest's *Q7760 Optical Network Analyzer*, among others.

phase or group delay, or, in some cases, by more complex signal processing. However, numerical differentiation of noisy measured data might lead to significant errors, which affect the accuracy of those methods for the determination of the dispersion. The usual procedure is to fit the measured relative group delay versus wavelength curve to a suitable functional expression (typically a quadratic function or a three-term Sellmeier [19] expansion are used, depending on the fibre type; those are now defined in standards [33]), and to calculate the derivative with respect to wavelength of this expression. This point will be of critical importance in the context of the determination of the dispersion of optical components.

2.2.2 Dispersion measurements in components

Although the quantity of interest, and therefore its effects, is the same as for optical fibres, some specific requirements due to the nature of the devices are introduced when attempting to characterise the dispersion of optical components. An important consequence is that fibre dispersion characterisation techniques might not be directly transposable to optical filters used in WDM networks. Those specific requirements are:

Devices are expected to exhibit a "small" amount of dispersion in the pass-band. In the case of optical fibre, even if the dispersion per unit length D is small, one has the degree of freedom to arbitrarily increase the fibre length L so that the total accumulated dispersion $\mathbb{D} = D.L$, which is actually measured, is large enough for the sensitivity of the method (defined as the minimum measurable dispersion). A device characterisation technique should therefore be able to measure small dispersion values.

Even extremely small dispersion values (close to the zero-dispersion wavelength in dispersion-shifted fibres for instance) can be characterised accurately in some types of optical fibres by interpolation. This is due to the fact that the group delay is a "well-behaved" and smooth function of wavelength, which can be fitted with a reasonable accuracy to some of the functional expressions discussed above. Therefore, knowledge of the group delay in wavelength ranges where its variations with wavelength are large enough to be measured might prove sufficient to perform the fitting operation enabling to predict lower dispersion values. Note that the problem of extrapolation using the same functional expressions is more hazardous. The standard quadratic or Sellmeier fits only apply in a limited wavelength range, which can be far away from the zero-dispersion wavelength in some kind of fibres. Attempts to predict low dispersion values from measurement of the group delay in a distant wavelength range will, in most cases, prove unreliable. In devices, on the other hand, the group delay is usually a fast-

varying function of wavelength. This means that such a fitting procedure is usually not an option. First, there might not be any physical legitimacy for a chosen functional expression[5]. Even in the cases when modelling of the device can predict a theoretical group delay versus wavelength curve, no analytic expression is usually available to perform a least-square fit to the measured data. As a consequence, interpolation or extrapolation of measured group delay or dispersion data in order to evaluate dispersion values which are too low compared to the sensitivity of the method should be disregarded in the context of optical devices.

The fact that the group delay of optical components can be a fast-varying function of wavelength also means that some of the assumptions upon which a number of fibre dispersion characterisation techniques rely might not be satisfied for optical components. This point will be treated in detail in Section 2.5.1 dealing with the phase-shift characterisation of WDM components.

The desired functionality of most of the devices expected to play an important role in future WDM networks is to provide some degree of amplitude band-pass filtering (cf. Section 1.1.1). The chromatic dispersion exhibited by some of the components is usually considered as an undesired side effect. Nevertheless, both phase and amplitude filtering are expected to be simultaneously present in the devices to be characterised. In optical fibres, on the other hand, the attenuation can be considered to be independent of wavelength, at least locally. This is typically not the case at the edge of the pass-band of an optical filter. Therefore, it should be ensured that having an uniform attenuation is not a strict requirement for the dispersion characterisation technique. Even though there might be no fundamental limitation to the applicability of a given method in the presence of non-uniform attenuation, practical limitations (such as dynamic range requirements between the side-bands of an amplitude modulated signal, or minimum optical power providing the required signal-to-noise ratio for a given measurement accuracy) might arise.

Finally, a certain number of practical considerations have to be taken into account. For an optical system designer, it is important to be able to characterise devices that will be part of a fibre link (in order to e.g. compare different available technologies). Such devices are very often, either based on optical fibres (gratings), or packaged and pig-tailed. This implies that dispersion measurement techniques relying on free space op-

[5]In the case of optical fibres, the Sellmeier expressions - or rather simplified expansions far from resonances - can be used in wavelength ranges where material dispersion dominates [34].

tics (such as low coherence interferometry where one light path length has to be precisely scanned), might not be considered as practical solutions, even though they are known to be suitable for the measurement of small dispersion values. Such practical requirements might of course be different in a device development or production environment.

Techniques used for the measurement of dispersion in optical components

Based on the specific requirements previously described, a number of techniques have been applied to the characterisation of the dispersion of optical filters. Some of those are briefly outlined below.

- Low coherence interferometry based on wavelength scanning with fixed path length imbalance has been used to characterise the dispersion properties of bulk grating pairs [35].

- The precise determination of the intensity of the fringes $I(\lambda)$ obtained from a narrow-linewidth laser used in a Michelson interferometer configuration has allowed the determination of the dispersion of a bulk grating pair and of a linearly chirped waveguide grating [36].

- An all-fibre Michelson interferometer using a low coherence technique based on the determination of the reference path delay maximising the amplitude of the interferogram at a given wavelength has been proposed in [37]. It has been used for the measurement of the group delay of a chirped fibre Bragg grating.

- The group delay of a variety of fibre gratings has been measured using an all-fibre Michelson interferometer where the reference arm was phase modulated [38]. The group delay could be obtained by numerical differentiation of the relative phase of the response of the interferometer when the wavelength was scanned across the device bandwidth. An active temperature stabilisation scheme was required.

- Fourier transform spectroscopy has been used to determine the distributions of phase and amplitude errors in arrayed-waveguide gratings by Fourier transforming the portion of the interferogram corresponding to a given path through the device [39]. The complex transfer function, therefore including the group delay, can then be reconstructed from the knowledge of the attenuations and phase-shifts experienced by the light propagating through each of the individual

waveguides of the array [40]. Alternatively, Fourier transforming the full interferogram will directly lead to the phase spectrum from which the group delay and dispersion can be evaluated numerically [41].

- Inserting a device into the cavity of a mode locked fibre ring laser (MLFRL) has been suggested as a way to measure small amounts of dispersion [42] . This technique relies on the high sensitivity of the laser repetition frequency to the optical length of the cavity.

- The phase-shift technique has been used for the characterisation of a variety of components, including planar lightwave circuit dispersion equalisers [43], chirped fibre gratings for dispersion compensation [44], as well as arrayed-waveguide grating and multilayer interference multiplexers [45].

- Other reported techniques are not universal in the sense that they apply to a single category of device whose particular properties enable to theoretically link its phase response to directly measurable quantities. This is the case of the recovery of the phase from the amplitude response of a grating via Hilbert transform relations [46], or of a proposed method relying on the processing of the interference pattern between the light reflected from a fibre grating and the end facet of the fibre [47]. It has also recently been suggested that the group delay of Bragg grating based Mach-Zehnder optical add-drop multiplexers could be recovered from their drop and back-reflection responses, provided the gratings written in each arm of the Mach-Zehnder are slightly detuned [48].

We have reviewed a number of experimental techniques to characterise the dispersion of optical components (starting with the well known case of optical fibres) and discussed their applicability to the case of optical filters to be used in dense wavelength division multiplexing (DWDM) systems. Our interest is in the implementation of a technique which is universal (i.e. does not depend on the technology of the filter to be characterised) and compatible with fibre optics components, therefore eliminating methods resorting to free space optics. In the following, we will present three alternative characterisation techniques that have been considered in this Ph.D. project. Measuring the amplitude response of an optical device can easily be achieved in the laboratory. We will first discuss whether the phase response of an optical filter can be determined from its amplitude transfer function, and evaluate the practical applicability of such a numerical

method. Based on the discussion on requirements specific to the determination of the dispersion in optical devices, it appeared that the phase-shift technique was particularly well adapted to our purpose, in spite of some inherent limitations. We will discuss those limitations and present a broad catalogue of complex transfer function of DWDM components measured using this method. Finally we will present an adaptation of an optical fibre characterisation technique which allows a direct determination of the dispersion in the pass-band of optical filters.

2.3 Amplitude-phase relations

It is known from the theory of linear systems that the phase response of a filter can be inferred from its amplitude response provided the so-called "minimum-phase" condition is satisfied [49, 50]. It is therefore natural to consider such a numerical approach to retrieve the dispersion from the amplitude transfer function of optical filters. When they exist, the mathematical relations linking the amplitude and the phase of an optical filter are analogous to the Kramers-Kronig relations between the absorption and refractive index (or real and imaginary parts of the dielectric constant) of a material [51]. Mathematically, quantities satisfying such relations are know as Hilbert transform pairs. As a consequence, "amplitude-phase", "Kramers-Kronig" or "Hilbert transform" relations will be used indifferently in this thesis.

Some early work on the applicability of the Kramers-Kronig relations to the determination of the group delay of optical filters was first presented in [52], where it was clearly demonstrated that such relations do not exist for some types of filters to be used around 800 nm (e.g. Gires-Tournois interferometer, dielectric mirror and birefringent filter). It was later shown that a careful consideration of the zeros of the transfer function as well as of the frequency dependence of all optical parameters could enable recovery of the phase response of etalon filters - therefore including Gires-Tournois interferometers - from their amplitude response [53]. At the same time, the determination of the dispersion of components to be used in DWDM systems around 1550 nm became the object of increased attention. Kramers-Kronig relations were successfully applied to the reflectivity of fibre Bragg gratings [46, 54] and a comparison between recovered and theoretical group delay was performed. The first comparison between measured group delay and delay recovered from measured amplitude responses was presented in [55] for uniform fibre gratings. Although some striking similarities could be observed for some devices, discrepancies in other devices raised some

doubts on the practical applicability of the method. It was later on shown that, for real imperfect gratings, the modelling of the group delay of the corresponding perfect grating will often provide a better estimate than the recovery of the group delay by applying the Kramers-Kronig relations to the measured reflectivity [56].

Although the existence of the minimum-phase condition was known and mentioned by the authors of [46, 55], its validity was not discussed in the general case of optical filters, including fibre gratings, until some more thorough studies of the dispersive properties of WDM filters were presented in [13]. It was also shown in [57] that the group delay in transmission of an arbitrary fibre grating could be determined from its amplitude transfer function, whereas the same is true in reflection only if the grating is symmetric.

Our interest in amplitude-phase relations and their use for the determination of the dispersion of DWDM components was raised in the summer of 1997, just before the publication of [54], soon followed by the other publications listed above. Due to concerns on the practical applicability of the method, it was decided not to pursue those investigations further. Nevertheless, we present below some of our considerations on this approach. First the theoretical issues linked to the use of Kramers-Kronig relations will be presented, followed by a description of the algorithm implemented for their calculation. The determination of the phase response of an uniform fibre Bragg grating based on its theoretical amplitude transfer function, as well as on an imperfect measured amplitude response, will be used to illustrate a number of issues linked to the use of amplitude-phase relations for the practical determination of the group delay of optical components.

2.3.1 Theoretical issues

Let us consider a passive optical filter with impulse response $h(t)$. Such a physical system is causal and stable, therefore its impulse response is real valued and verifies the conditions $h(t) = 0$ for $t < 0$ and $|h(t)| < \infty$. Let $H(\omega)$ be the transfer function of the optical filter (i.e. the Fourier transform of its impulse response) and $H_{\mathcal{L}}(s)$, where s is a complex variable, its Laplace transform. The Fourier transform can be evaluated from the Laplace transform according to $H_{\mathcal{L}}(j\omega) = H(\omega)$. The fact that $h(t)$ is causal translates into $H_{\mathcal{L}}(s)$ being analytic in the right-hand plane. Under those assumptions it can be shown that

$$H(\omega) = \frac{1}{j\pi} P \int_{-\infty}^{+\infty} \frac{H(\Omega)}{\Omega - \omega} d\Omega \tag{2.6}$$

where P denotes the Cauchy principal value. Appendix A presents a derivation of (2.6). One important consequence of equation (2.6) is that the real (respectively imaginary) part of the transfer function $H(\omega)$ can be determined from the knowledge of its imaginary (respectively real) part. The real and imaginary parts of $H(\omega)$ are said to constitute a Hilbert transform pair.

The transfer function of the optical filter can be written

$$H(\omega) = |H(\omega)| e^{-j\phi(\omega)} \tag{2.7}$$

taking the logarithm

$$\ln H(\omega) = \ln |H(\omega)| - j\phi(\omega) \tag{2.8}$$

Therefore, by applying the results of (2.6) to the function $\ln H(\omega)$, one should be able to derive Hilbert transforms relations between the logarithm of the amplitude transfer function and the phase of an optical filter. However, this would require the function $\ln H_{\mathcal{L}}(s)$ to fulfill the initial assumptions and to be analytic in the right-hand plane. One important issue is that $H_{\mathcal{L}}(s)$ might have zeros in the right-hand plane, where the logarithm is not defined. If we moreover assume that $H_{\mathcal{L}}(s)$ has no zero for $\mathrm{Re}(s) \geq 0$, then its phase will be uniquely determined from its amplitude response according to

$$\phi(\omega) = \frac{1}{\pi} P \int_{-\infty}^{+\infty} \frac{\ln |H(\Omega)|}{\Omega - \omega} d\Omega \tag{2.9}$$

Filters for which the logarithm of the Laplace transform of their impulse response is analytic in the right-hand plane are said to be of the minimum-phase type.

It is shown in Appendix A that, starting from equation (2.9) a new expression for the phase can be written, which highlights the relation between the variations of the amplitude response with frequency and the phase response

$$\phi(\omega) = \frac{1}{\pi} \int_{-\infty}^{+\infty} \frac{d}{du} \left[\ln |H(\omega e^{u})|\right] \ln \left(\coth \frac{|u|}{2}\right) du \tag{2.10}$$

An immediate consequence is that any attempt to realise sharp edges in the transfer function of a minimum-phase optical band-pass filter will result in increased dispersion at those edges. Recalling our discussion of Section 1.1.3, it can be concluded that, for a minimum-phase optical filter, the two goals of achieving low crosstalk and low dispersion cannot be

reached simultaneously. Filters which are not minimum-phase will offer more degrees of freedom in order to achieve these two desired features. Note, however, that the fact that a filter is non minimum-phase does not prevent it from exhibiting a high dispersion at the edges of its pass-band, but simply means that its dispersion cannot be calculated from the attenuation spectrum.

The minimum phase condition was discussed for different optical filters technologies in [13]. It was shown that generalised Mach-Zehnder filters (including arrayed waveguide gratings) were in general not minimum-phase, therefore allowing for a squaring of their amplitude transfer function without affecting their phase response. Interference filters such as Fabry-Pérot and thin-film filters are inherently of the minimum-phase type when used in transmission. It was also shown in [57] that grating filters were minimum-phase in transmission but that this was not always the case in reflection. Nevertheless, in case the grating is symmetric, its group delay is identical in reflection and transmission, as shown in Appendix B, therefore enabling the reflection group delay to be recovered from the grating transmittivity.

In the following section, we discuss the practical use of the Kramers-Kronig relations based on a concrete example.

2.3.2 Example of application

The applicability of amplitude-phase relations for the practical determination of the group delay of optical filters raises a number of issues. First of all, it is necessary to determine whether the filter one attempts to characterise is of the minimum-phase type or not. The influence of imperfections in the real filter (as opposed to the ideal modelled filter) needs to be assessed. For instance, if a certain type of filter can theoretically be shown to be of the minimum-phase type, one should ensure that the real imperfect implementation of such a filter is also minimum-phase before applying the Kramers-Kronig relations to its measured attenuation spectrum. Equation (2.6) shows that it is theoretically necessary to integrate the amplitude response over all frequencies in order to recover the phase by the Kramers-Kronig relations. However, in practice, the amplitude response is usually known only in a small wavelength region. Intuitively, it makes sense that the amplitude transfer function far from the wavelength of interest should not contribute significantly to the phase transfer function at that wavelength, which is confirmed mathematically from equation (2.10). Nevertheless, the requirements on the range where the amplitude transfer function has to be defined in order to provide a reliable estimation of the phase need to be quantified. Additional concerns arise with the practical implementa-

tion of a given Kramers-Kronig calculation algorithm, more specifically its behaviour close to the zeros of the amplitude transfer function, as well as in the presence of noisy measurement data.

In order to provide an illustration of some of the points mentioned in the previous paragraph, we have applied the amplitude-phase algorithm described in [54] to the case of a uniform fibre grating used in reflection. Its transfer function can be easily calculated using the coupled mode equations formalism [9], leading to the following expression for the reflectivity

$$r = \frac{-j\kappa \sinh(\gamma L)}{\gamma \cosh(\gamma L) + j\Delta\beta \sinh(\gamma L)} \tag{2.11}$$

where L is the grating length, κ is a coupling coefficient between the forward and backward propagating waves, and

$$\Delta\beta = -j\frac{\alpha}{2} + \frac{n_{eff}}{c}(\omega - \omega_B) \qquad \gamma^2 = \kappa^2 - (\Delta\beta)^2 \tag{2.12}$$

In equation 2.12, α is the loss per unit length, n_{eff} is the effective refractive index, c is the speed of light in vacuum and ω_B is the Bragg angular frequency. Those parameters are explicited in detail in Appendix B. We know from [57] that such a grating is minimum-phase in transmission and that, in the case of symmetric gratings (which include uniform gratings), the group delay is identical in transmission and reflection. Therefore the group delay in reflection can be calculated from the transmittivity of the grating via the Kramers-Kronig relations. However, we would like to calculate the group delay in reflection from the measured reflectivity of the grating. We therefore need to ensure that the reflectivity r is a minimum-phase function. As the transfer function of a physically realisable device, r is clearly analytic in the right-hand plane. We should now check about the existence of zeros for $\mathrm{Re}(s) \geq 0$, where s is the complex variable $s = \sigma + j\omega$ in order to determine whether $\ln r$ is also analytic in the right-hand plane. The zeros in the complex plane of the function $\sinh z$ occur for $z = jp\pi$ where $p \in \mathbb{Z}$. After some arithmetic, we obtain the following expressions for the real and imaginary parts of the zeros of the reflectivity r.

$$\sigma = -\frac{c}{n_{eff}}\frac{\alpha}{2} \tag{2.13}$$

$$\omega = \omega_B + \frac{c}{n_{eff}}\sqrt{\kappa^2 + p^2\frac{\pi^2}{L^2}} \tag{2.14}$$

From equation (2.13), we observe that, *in the presence of loss*, the zeros of the reflectivity of a uniform fibre Bragg grating are moved towards the

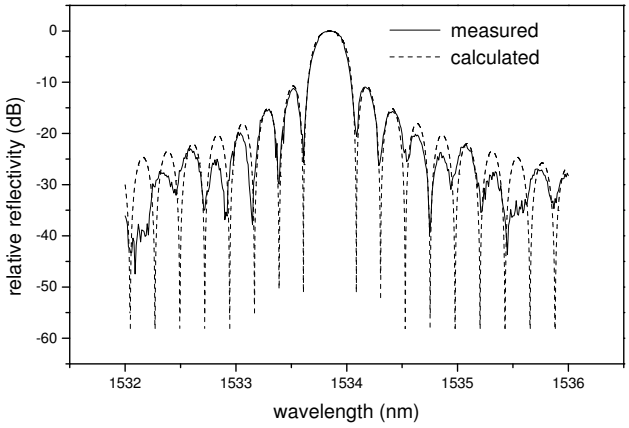

Figure 2.1 Comparison of the measured and calculated power transfer functions in reflection for a 33 GHz bandwidth uniform fibre Bragg grating.

left-hand plane. We can therefore conclude that a uniform grating used in reflection is of the minimum-phase type, for which the Kramers-Kronig relations apply directly.

The reflectivity of an uniform fibre Bragg grating with full-width half-maximum (FWHM) bandwidth equal to 33 GHz has been measured and is plotted in Figure 2.1. The theoretical transfer function of an uniform grating approaching the measured data has been calculated using the coupled mode equations formalism. As can be seen in Figure 2.1, good agreement between measured and calculated transfer functions is obtained for the main lobe and the two neighbouring lobes on both sides, after which imperfections in the real grating are responsible for deviation from the ideal behaviour.

Using the Kramers-Kronig algorithm described in Appendix A, we have calculated the phase of the uniform grating starting from the measured reflectivity, as well as from the calculated reflectivity of the theoretical uniform grating matching the measurements. The results are shown in Figure 2.2, together with the theoretical phase of the grating calculated directly from equation (2.11). For reference, the calculated reflectivity of the grating is also plotted on a linear scale in Figure 2.2. It can be observed that, apart from a linear phase factor [54], and from discontinuities due to limitations from the domain of definition of the functions used for the inversion of the theoretical phase, good agreement is obtained between the calculated phase and the phase recovered from the calculated reflectivity. The aforementioned limitations will obviously vanish when calculating

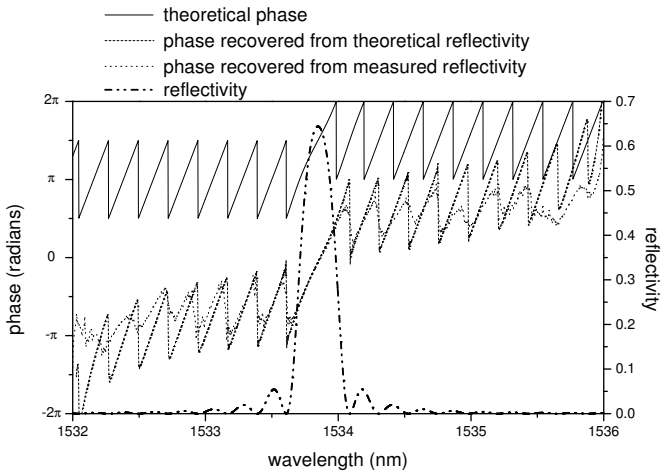

Figure 2.2 Theoretical phase (solid), phase recovered from the theoretical reflectivity (dashes) and phase recovered from the measured reflectivity (dots) for the uniform fibre Bragg grating of Figure 2.1.

the group delay or the dispersion which are the quantities of interest, and therefore no special care has been taken in order to avoid them. Good agreement is also observed between the phases recovered from the calculated and measured transfer functions at the centre of the reflectivity's main lobe. The agreement is also reasonable far from the phase discontinuities at wavelengths corresponding to the neighbouring lobes in the reflectivity spectrum. Further away from the centre wavelength, significant discrepancies are observed, due to the already mentioned deviation between calculated and measured transfer functions. The phase discontinuities occur at the minima of the reflectivity. The effect of loss being quasi-negligible, those minima are located in the vicinity of the zeros of the reflectivity. The calculated reflectivity is very close to zero at those points, whereas, due to imperfections of the real grating and to the limited resolution of the optical spectrum analyser used for amplitude transfer function measurements, the measured reflectivity presents higher values as can be seen in Figure 2.1. Such a difference of several orders of magnitude in the attenuation is the cause for the observed deviations between the phases recovered from the measured and calculated reflectivities close to their discontinuities. Needless to say that such discrepancies for the phase will result in even more severe deviations for the group delay.

In order to allow for a better comparison between the theoretical phase calculated from (2.11) and the phase recovered by applying the Kramers-

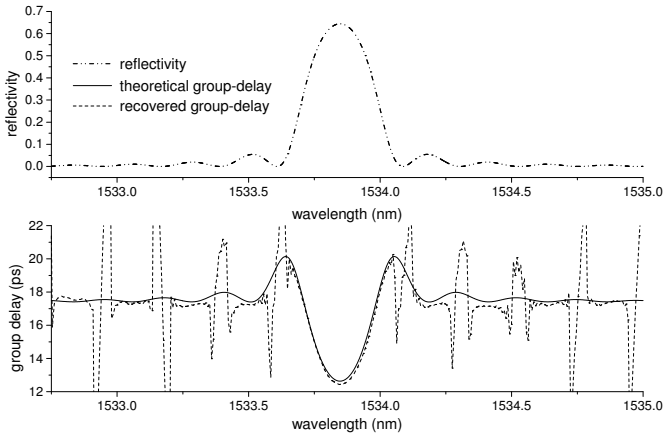

Figure 2.3 Comparison of the theoretical group delay (solid) with the group delay recovered from the theoretical reflectivity (dashes) for the uniform fibre Bragg grating of Figure 2.1.

Kronig relations to the calculated reflectivity, we have calculated the corresponding group delays according to equation (2.1). The results are shown in Figure 2.3, together with the calculated reflectivity plotted on a linear scale. Apart from the spikes in the recovered group delay which occur close to the zeros of the reflectivity, a good agreement is obtained, especially in the main lobe of the transfer function. Note that the theoretical group delay curve has been slightly up-shifted in Figure 2.3 in order to allow for a better comparison.

In conclusion, we have shown that the Kramers-Kronig relations can be successfully applied to the amplitude response of an optical filter of the minimum-phase type (which was demonstrated to be the case for an uniform fibre grating used in reflection). However, difficulties arise for wavelengths close to the zeros of the amplitude transfer function. Even though, by definition of a minimum-phase filter, those zeros do not appear on the imaginary axis in the complex plane, they might be infinitesimally close, resulting in numerical errors when calculating the phase response by the Kramers-Kronig relations. We have also shown that applying amplitude-phase relations to measured data might not prove reliable, due to limitations in the resolution and sensitivity of the measuring instrument close to the minima of the amplitude transfer function. As a consequence, we believe that measurements of the phase response (or equivalently of the group delay or dispersion) should be preferred to a numerical approach via the Kramers-Kronig relations for the characterisation of optical filters.

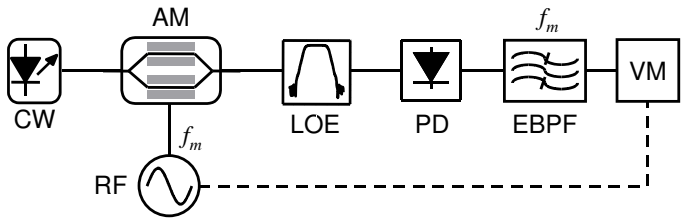

Figure 2.4 Generic set-up for dispersion measurement techniques based on amplitude modulation. CW: continuous wave laser; RF: radio-frequency generator; AM: amplitude modulator; LOE: linear optical element; PD: photodiode; EBPF: electrical band-pass filter; VM: vector voltmeter.

2.4 A general formulation of amplitude modulation techniques

In this section, we present a general formulation of chromatic dispersion measurement techniques based on small-index intensity modulation of a lightwave. This family of methods covers two variants which have been implemented experimentally for the measurement of the group delay or dispersion of optical components: the phase-shift technique which is discussed in Section 2.5, and the small signal transfer function method, which has been adapted to the needs of device characterisation and which is described in Section 2.7. Apart from providing a better understanding of the principles of the aforementioned techniques, this general formulation will also enable to understand their limitations and discuss their validity in the special case of the phase characterisation of devices to be used in WDM networks.

A generic set-up for amplitude modulation based techniques is shown in Figure 2.4. It consists of a continuous wave (CW) laser followed by an external amplitude modulator (AM) which is driven by a radio-frequency (RF) signal at the frequency f_m (corresponding to the angular frequency $\omega_m = 2\pi f_m$). The electric field of the modulated signal can be written

$$E(t) = E_0 \left[1 + m \cos(\omega_m t - \varphi)\right] e^{j\omega_0 t} \tag{2.15}$$

where ω_0 and E_0 are the angular frequency and electric field amplitude of the CW laser (assumed to be perfectly monochromatic) respectively, m is the amplitude modulation index and φ is the initial phase of the modulating signal. The spectrum of the modulated signal described by (2.15) consists of a carrier at ω_0 and of two sidebands of equal amplitude at $\omega_0 \pm \omega_m$, as

can be seen from the expansion[6]

$$E(t) = E_0\Big[\cos(\omega_0 t) + \frac{m}{2}\cos\left((\omega_0+\omega_m)t - \varphi\right) + \frac{m}{2}\cos\left((\omega_0-\omega_m)t + \varphi\right)\Big] \tag{2.16}$$

The modulated signal is then input to a linear optical element (LOE) having a transfer function

$$H(\omega) = |H(\omega)|\, e^{-j\phi(\omega)} \tag{2.17}$$

At this point, the optical element can indifferently be an optical fibre or an optical filter. It will also be referred to as the device under test. Its amplitude transfer function will be defined from now on with the simplified notation $h(\omega) = |H(\omega)|$.

Each frequency component at ω of the spectrum at the input of the linear optical element will experience an attenuation $h^2(\omega)$, as well as a phase shift $-\phi(\omega)$. It is therefore possible to write the electric field at its output as

$$\begin{aligned} E_{out}(t) = E_0\Big[&h(\omega_0)\cos\big(\omega_0 t - \phi(\omega_0)\big) \\ &+ \frac{m}{2}h(\omega_0+\omega_m)\cos\big((\omega_0+\omega_m)t - \phi(\omega_0+\omega_m) - \varphi\big) \\ &+ \frac{m}{2}h(\omega_0-\omega_m)\cos\big((\omega_0-\omega_m)t - \phi(\omega_0-\omega_m) + \varphi\big)\Big] \end{aligned} \tag{2.18}$$

The derivation of the amplitude modulation methods relies on the fact that both the amplitude and phase transfer functions of the optical linear element can be expanded as Taylor series to any integer order n around the carrier frequency ω_0 according to

$$h(\omega) = \sum_{k=0}^{n} \frac{1}{k!}\frac{d^k h}{d\omega^k}(\omega_0)\left(\omega - \omega_0\right)^k \tag{2.19}$$

$$\phi(\omega) = \sum_{k=0}^{n} \frac{1}{k!}\frac{d^k \phi}{d\omega^k}(\omega_0)\left(\omega - \omega_0\right)^k \tag{2.20}$$

[6]For simplicity and in accordance with a widespread usage, we have kept identical notations for the expression of the field - which is a real quantity - as in (2.16) and its complex representation as in (2.15), where it is implicitly assumed that the real part should be considered.

It is then possible to separate the odd and even powers of ω_m in the expansions of the amplitude and phase transfer functions given by (2.19) and (2.20), respectively and write

$$h(\omega_0 + \omega_m) = h(\omega_0) + h_1(\omega_m) + h_2(\omega_m) \tag{2.21}$$

$$\phi(\omega_0 + \omega_m) = \phi(\omega_0) + \phi_1(\omega_m) + \phi_2(\omega_m) \tag{2.22}$$

where h_1 and ϕ_1 are odd functions of ω_m and h_2 and ϕ_2 are even functions of ω_m. Inserting (2.21) and (2.22) into (2.18) and rearranging, leads to a new expression for the electric field at the output of the device under test

$$\begin{aligned} E_{out}(t) =& E_0 h(\omega_0) \cos\big(\omega_0 t - \phi(\omega_0)\big) \\ &+ mE_0 h(\omega_0) \cos\big(\omega_0 t - \Phi_2\big) \cos\big(\omega_m t - \Phi_1\big) \\ &- mE_0 h_1(\omega_m) \sin\big(\omega_0 t - \Phi_2\big) \sin\big(\omega_m t - \Phi_1\big) \\ &+ mE_0 h_2(\omega_m) \cos\big(\omega_0 t - \Phi_2\big) \cos\big(\omega_m t - \Phi_1\big) \end{aligned} \tag{2.23}$$

where

$$\Phi_1 = \phi_1(\omega_m) + \varphi \tag{2.24}$$

$$\Phi_2 = \phi(\omega_0) + \phi_2(\omega_m) \tag{2.25}$$

The lightwave is then finally detected in a photodiode (PD) whose photocurrent $i(t)$ is proportional to the time average over many optical cycles of the squared electric field

$$i(t) = K \left\langle E_{out}^2(t) \right\rangle \tag{2.26}$$

If we only retain the component of the photocurrent at the modulation frequency ω_m, we obtain

$$\begin{aligned} i_{\omega_m}(t) = i_0 m h(\omega_0) \Big[&\big(h(\omega_0) + h_2(\omega_m)\big) \cos\phi_2(\omega_m) \cos\big(\omega_m t - \Phi_1\big) \\ &+ h_1(\omega_m) \sin\phi_2(\omega_m) \sin\big(\omega_m t - \Phi_1\big) \Big] \end{aligned} \tag{2.27}$$

where $i_0 = KE_0^2$.

Using a standard trigonometric identity expressing the weighted sum of a sine and a cosine having the same argument[7] leads to the final expression

[7] $A\cos\theta + B\sin\theta = \sqrt{A^2 + B^2}\cos(\theta - \Gamma)$

for the component of the photocurrent at ω_m

$$i_{\omega_m}(t) = i_0 m h_0 \sqrt{\left(h_0 + h_2\right)^2 \cos^2\phi_2 + h_1^2 \sin^2\phi_2}\cos\left(\omega_m t - \phi_1 - \varphi - \Gamma\right) \tag{2.28}$$

where Γ is defined according to

$$\tan\Gamma = \frac{h_1}{h_0 + h_2}\tan\phi_2 \tag{2.29}$$

It has been attempted to improve the readability of (2.28) and (2.29) by introducing the shorthand notations

$$h_0 = h(\omega_0) \qquad h_1 = h_1(\omega_m) \qquad h_2 = h_2(\omega_m) \tag{2.30}$$

were the explicit dependance of h_1 and h_2 on the modulation frequency has been removed.

Equation (2.28) can be related to two dispersion measurement techniques once restrictive assumptions are made. First, we assume that the amplitude transfer function of the linear optical element can be considered uniform locally. In practice this means that the carrier and the two sidebands of the amplitude modulated signal will experience the same attenuation when propagating through the device under test:

$$h(\omega_0) = h(\omega_0 - \omega_m) = h(\omega_0 + \omega_m) \tag{2.31}$$

which from (2.21) results in

$$h_1(\omega_m) = h_2(\omega_m) = 0 \tag{2.32}$$

We can furthermore make one of the following assumptions:

1. The phase of the transfer function can be accurately described by a first order Taylor expansion around the carrier frequency ω_0, i.e.

$$\phi(\omega) = \phi(\omega_0) + \frac{\partial\phi}{\partial\omega}(\omega_0)\left(\omega - \omega_0\right) \tag{2.33}$$

   By comparing the electrical phase of the component at ω_m of the photocurrent and the phase of the RF signal driving the optical amplitude modulator, we obtain

$$\Delta\varphi = \phi_1(\omega_m) + \Gamma \tag{2.34}$$

which, under our restrictive assumptions, translates to

$$\Delta\varphi = \omega_m \frac{\partial\phi}{\partial\omega}(\omega_0) \tag{2.35}$$

where we can recognise the group delay $\tau(\omega_0)$ of the linear optical element at the optical frequency ω_0. By performing a swept-wavelength measurement of the electrical phase difference $\Delta\varphi$, it is then possible to obtain the wavelength dependence of the group delay from which the dispersion can be evaluated numerically according to (2.2). This is the principle behind the "phase-shift" technique [22, 23], which will be described more in details in Section 2.5. In particular, we will examine the validity of the above assumptions in the case of the measurement of the group delay of optical filtering elements designed for WDM applications.

2. Alternatively, a second order expansion might be necessary to describe the phase of the transfer function around the carrier frequency ω_0

$$\phi(\omega) = \phi(\omega_0) + \frac{\partial\phi}{\partial\omega}(\omega_0)\left(\omega-\omega_0\right) + \frac{1}{2}\frac{\partial^2\phi}{\partial\omega^2}(\omega_0)\left(\omega-\omega_0\right)^2 \tag{2.36}$$

The magnitude of the photocurrent can be measured as a function of the modulation frequency ω_m while keeping the carrier frequency ω_0 constant.

$$|i_{\omega_m}| = i_0 m h_0^2 \left|\cos\phi_2(\omega_m)\right| \tag{2.37}$$

where, under the assumption (2.36)

$$\phi_2(\omega_m) = \frac{1}{2}\left[\frac{\partial^2\phi}{\partial\omega^2}(\omega_0)\right]\omega_m^2 = -\frac{1}{2}\left[\frac{\lambda^2}{2\pi c}\mathbb{D}(\lambda_0)\right]\omega_m^2 \tag{2.38}$$

The cosine in (2.37) cancels for $\phi_2(\omega_m) = (2k-1)\frac{\pi}{2}$ where k is a strictly positive integer. It is therefore possible to relate the frequencies at which the magnitude of the photocurrent at ω_m cancels to the value of the chromatic dispersion at the carrier frequency ω_0. Such a RF modulation technique, also known as "fibre transfer function" has been proposed for the measurement of dispersion in optical fibres [28, 27]. We will see in Section 2.7 how it can be extended to the measurement of small dispersion values in optical components.

Remark

The only assumption we have made on the device under test so far is that it has to be linear, so that its effect on the lightwave can be described in the frequency domain by a transfer function according to (2.17). An optical fibre can be considered as a linear optical element as long as its input power is sufficiently low. In this case the transfer function of a length L of fibre having an attenuation per unit length α can be written

$$H(\omega) = e^{-\frac{\alpha}{2}L} e^{-j\beta(\omega)L} \tag{2.39}$$

where $\beta(\omega)$ is the mode propagation constant which can be expressed around ω_0 using the customary expansion (here limited to second order)

$$\beta(\omega) = \beta_0 + \beta_1(\omega - \omega_0) + \frac{1}{2}\beta_2(\omega - \omega_0)^2 \tag{2.40}$$

with

$$\beta_n = \frac{\partial^n \beta}{\partial \omega^n}(\omega_0) \tag{2.41}$$

We therefore have, for a linear optical fibre where no dispersion effects higher than β_2 are considered

$$\phi_1(\omega_m) = \beta_1 L \omega_m \qquad \phi_2(\omega_m) = \frac{1}{2}\beta_2 L \omega_m^2 \tag{2.42}$$

from which original results on phase-shift and RF modulation measurements in optical fibres can easily be derived. Equation (2.28) can therefore be considered as a generalisation of the results described in [23, 28] to any linear optical device.

2.5 Measurements by the phase-shift technique

2.5.1 Description of the method

Our implementation of a phase shift measurement set-up is shown in Figure 2.5. Light from a tunable laser (TLS) is sinusoidally amplitude modulated (typically in the 100 MHz to 20 GHz range) with a small modulation index in a Mach-Zehnder modulator (MZ). After propagating through the device under test (DUT), the lightwave is detected by a photodiode (PD). A network analyser (NA) is used to provide a modulating signal of frequency f_m and to measure electrical phases differences between modulating and detected signals. Synchronisation of the instruments and data acquisition are performed using a computer running an home-made software. We have

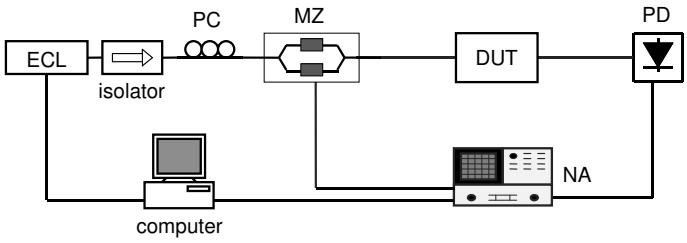

Figure 2.5 Implementation of a phase shift measurement set-up. ECL: external cavity tunable laser source; PC: polarisation controller; MZ: Mach-Zehnder modulator; NA: network analyser; DUT: device under test; PD: photodiode.

seen in Section 2.4 that, assuming a constant amplitude transfer function for the device under test and making a first order approximation for its optical phase, the difference between the phase of the component at f_m of the photocurrent and the phase of the signal driving the modulator can be shown to be equal to

$$\Delta\varphi = 2\pi f_m \tau(\omega_0) \tag{2.43}$$

where $\tau(\omega_0)$ is the group delay of the device under test at the optical angular frequency ω_0. A phase shift measurement is performed by sweeping the optical frequency ω_0 while keeping the modulation frequency f_m constant, therefore enabling a characterisation of the group delay as a function of wavelength, from which the dispersion can be assessed according to equation (2.2). Equation (2.43) shows that, for a given electrical phase measurement accuracy, smaller dispersions can be resolved by increasing the modulation frequency. For instance, if an accuracy of 0.1 degree is achievable by the network analyser, this will result in a group delay resolution of about 3 ps if a modulation frequency of 100 MHz is used, against about 0.03 ps at 10 GHz. However, using a higher modulation frequency results in a larger separation between the sidebands of the amplitude modulated signal, which will probe the device under test at different frequencies and will no longer experience the same level of attenuation. Moreover, a first order approximation might also no longer be sufficient for the optical phase. For instance, if a modulation frequency of 100 MHz is used, the separation between the sidebands is 1.6 pm at 1550 nm, against 0.16 nm for a modulation frequency of 10 GHz. Those values should be compared to the bandwidths of DWDM components that need to be made compatible with current channel spacings of 100 GHz or even 50 GHz and lower, depending on the bit-rate. Therefore, equation (2.43) does not necessary hold when the modulation frequency is high and when the phase and amplitude

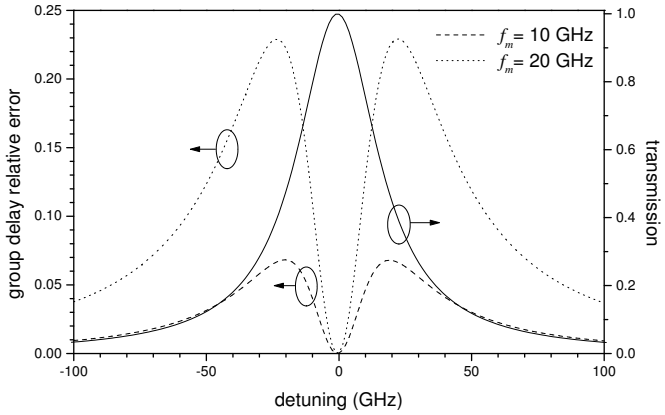

Figure 2.6 Relative error in the determination of the group delay of a 40 GHz Fabry-Pérot filter when using the standard phase-shift approximation with 10 and 20 GHz modulation frequencies.

of the transfer function of the device under test are fast-varying functions of the wavelength. This is especially the case at the band edges of optical filters where dispersion is expected to be non-negligible [58], as shown theoretically in Section 2.3.1 in the case of minimum-phase filters. As a consequence, the general assumptions of the phase-shift technique need to be refined based on the theory of Section 2.4

2.5.2 Limitations of the phase shift technique

Equation (2.34) is a generalisation of (2.43). However, it is unpractical for calculation of the group delay as it contains higher order terms in the expansion of the phase transfer function. Nevertheless, the error induced by using equation (2.43) to calculate the group delay can be evaluated for some kinds of filters for which analytical expressions of the phase transfer function can be derived. If we assume that a second order approximation is necessary for the phase transfer function, then the group delay evaluated using (2.43), τ_{meas}, can be related to the actual group delay τ through

$$\tau_{meas}\left(\omega_0\right) = \tau\left(\omega_0\right) - \frac{1}{\omega_m}\text{atan}\left[\frac{1-\alpha}{1+\alpha}\tan\left(\frac{\pi c}{\omega_0^2}\mathbb{D}\omega_m^2\right)\right] \tag{2.44}$$

where $\mathbb{D}$ is the device dispersion at the optical angular frequency ω_0, c is the light velocity in vacuum, and α is the ratio of the amplitudes of the transfer function at the sidebands frequencies $\alpha = h\left(\omega_0 - \omega_m\right)/h\left(\omega_0 + \omega_m\right)$.

The effect of a modulation frequency which is too high for the basic assumptions on the complex transfer function to be satisfied is therefore

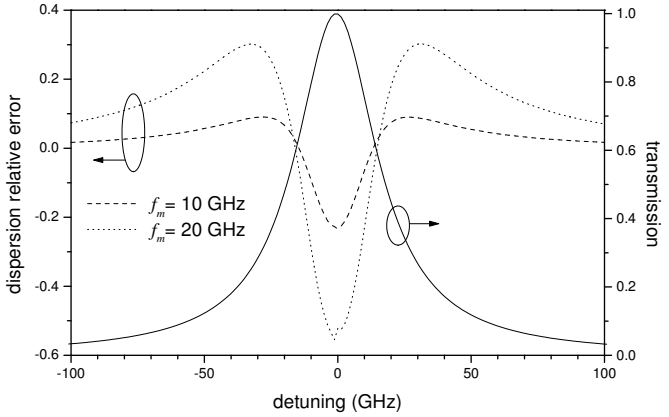

Figure 2.7 Relative error in the determination of the dispersion of a 40 GHz Fabry-Pérot filter when using the standard phase-shift approximation with 10 and 20 GHz modulation frequencies.

to induce some distortion in the group delay curve. This is illustrated in Figure 2.6 where equation (2.44) has been used to evaluate the relative error made in the determination of the group delay for a Fabry-Pérot filter having a 3 dB bandwidth equal to 40 GHz when modulation frequencies of 10 and 20 GHz are used. Here, the relative error is defined as $(\tau_{meas} - \tau)/\tau$. At a modulation frequency of 10 GHz, the maximum relative error in the determination of the group delay is of the order of 7%, whereas it can exceed 20% for a modulation frequency of 20 GHz. The relative error is the largest at the band edges of the filter, where both the amplitude and the phase have a strong wavelength dependence. The dispersion of a device is evaluated by differentiating its group delay curve with respect to wavelength. As the relative error in the determination of the group delay is not constant, the dispersion curve will also suffer from distortion. In Figure 2.7 the group delay curves obtained using (2.43) have been numerically differentiated and compared to the actual dispersion of a Fabry-Pérot filter identical to the one used to generate the results in Figure 2.6. As can be seen, the error in the determination of the dispersion can be significant.

This effect was confirmed experimentally by performing phase shift measurements of a 40 GHz fibre Fabry-Pérot filter with the experimental set-up described in Figure 2.5. Additional details on the device are provided in Section 2.6.1. Results of phase-shift measurements performed at modulation frequencies equal to 10 and 20 GHz are presented in Figure 2.8 together with the calculated group delay response of the filter. If reasonably good agreement is obtained at 10 GHz, this is no longer the case for a modulation

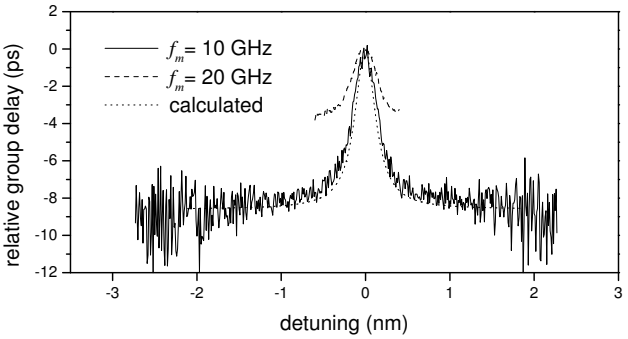

Figure 2.8 Group delay of a 40 GHz fibre Fabry-Pérot filter measured by the phase-shift technique using modulation frequencies of $f_m = 10$ and 20 GHz. The calculated group delay curve is shown for comparison.

frequency of 20 GHz where the measured group delay departs significantly from the theoretical value.

Therefore, we have shown that the choice of a too high modulation frequency can induce significant errors in the experimental determination of the group delay of optical components by the phase shift technique. Moreover, it is at the band edges of filters, where dispersion effects are expected to be the most significant, that the error in the determination of the group delay is the largest. Therefore, the choice of a modulation frequency for phase-shift measurements is a trade-off between resolving small dispersions and obtaining undistorted group delay curves. As WDM systems will evolve towards smaller channel spacing, the phase shift technique might no longer be appropriate to characterise the required narrow band devices. This limitation can be partly overcome by using single side-band modulation [59], which can be generated by creating a 90 degree phase shift between the modulating signals applied to the two arms of a dual drive Mach-Zehnder modulator [60]. Using an integer ratio between the modulation frequency and the frequency step size of the tunable laser in the phase shift technique has also been recently suggested to overcome this limitation [61]. However, it is doubtful this can be implemented in practice due to the high requirements on the control of the tunable laser frequency. Alternatively, a numerical deconvolution method has been recently presented to enable the reconstruction of the group delay based on distorted data obtained by phase shift measurements performed using a too high modulation frequency [62, 63].

An additional difficulty of the phase-shift technique is due to the fact

that it does not allow for a direct determination of the dispersion, which is the quantity of interest, but instead of the group delay as a function of wavelength. The derivative of the group delay with respect to wavelength needs to be calculated numerically, which might be a problem in the case of noisy measurement data, unless some appropriate fitting is performed.

2.6 Devices characterisation using the phase shift technique

In this section, we propose a broad catalogue of complex transfer functions of wavelength selective components used in DWDM systems. In spite of its previously described limitations, the phase shift technique has been used for the characterisation of their group delay. However, it has been ensured that the averaging effect due to a too high modulation frequency was kept to a minimum. This was done by systematically performing group delay measurements with different modulation frequencies (typically from 10 GHz down to a few hundreds MHz) in order to determine the lowest possible modulation frequency offering the best trade-off between phase measurement resolution and averaging distortion. In agreement with a now widespread usage, group delay curves are presented instead of dispersion spectra. In this way, the raw measured data can be seen on the graphs, and no additional error due to the numerical calculation of the derivative of noisy data or from illegitimate curve fitting are introduced. Unless otherwise specified, the amplitude transfer functions presented in this chapter have been measured using an external cavity tunable laser and an optical spectrum analyser with 0.1 nm resolution bandwidth.

The characterised devices were either available commercially or under research or development stages, in which cases they have been kindly provided by colleagues at COM[8] or industrial partners[9]. It should be kept in mind that, if the group delay characterisation of WDM components is now widespread, this was not the case when this work was initiated. Therefore, it is believed that some of the characterisation results presented below were among the first realised for certain device technologies. Moreover, we have been fortunate enough to have access to different types of devices throughout the duration of this work, resulting in what we believe is a fairly broad catalogue of complex transfer functions, which enables a comparison

[8]The devices were designed and realised within the "Glass Competence Area" at COM. Special thanks go to Hans-Jürgen Deyerl for a fruitful collaboration.

[9]Especially thanks to Thomas Rasmussen at Ibsen Photonics (then ADC Denmark), as well as Bo Foged Jørgensen and Rune Pedersen from Tellabs Denmark.

between some of the different WDM filter technologies available today.

2.6.1 Fabry-Pérot filter

A Fabry-Pérot interferometer consists of a slab of dielectric material of refractive index n_2 and thickness h surrounded by a medium of refractive index n_1. Constructive interference between the waves resulting from multiple reflections in the dielectric slab occurs when the phase difference between two consecutive transmitted beams

$$\varphi = \frac{4\pi}{\lambda} n_2 h \cos\theta' \tag{2.45}$$

where θ' is the refraction angle into the slab, is equal to an integer multiple of 2π. The finesse $\mathcal{F}$ of a Fabry-Pérot interferometer, defined as the ratio of its free spectral range to the FWHM bandwidth of one of its transmission peaks, can be simply related to the reflectivity R of the interface between the slab and the surrounding medium according to $\mathcal{F} = \pi \frac{\sqrt{R}}{1-R}$. If a high reflectivity, resulting in a high finesse, can be achieved, a Fabry-Pérot interferometer can be used as an optical bandpass filter. In practice, Fabry-Pérot filters can be realised either by inserting a slab of dielectric material between the tips of lensed optical fibres [4] or by creating an air gap between two high-reflection coated optical fibre facets [64]. Wavelength tunability can be obtained, in the first case, by varying the angle of refraction θ' by rotating the dielectric slab or, in the second case, by controlling the thickness of the cavity h.

The complex transfer function of a Fabry-Pérot filter can be easily calculated by summation of the contributions to the output field of each transmitted beam, leading to

$$\mathbb{T} = \frac{t_{12} t_{21}}{1 - r_{21}^2 e^{-j\varphi}} \tag{2.46}$$

where t_{ij} and r_{ij} are the transmission and reflection coefficients from the medium of refractive index n_i to the medium of refractive index n_j respectively. From the Fresnel relations we have $R = r_{21}^2$ and $t_{12} t_{21} = 1 - R$. Hence the following expressions for the power and phase transfer functions

$$|\mathbb{T}|^2 = \frac{1}{1 + \left(\frac{2\mathcal{F}}{\pi}\right)^2 \sin^2 \frac{\varphi}{2}} \tag{2.47}$$

$$\phi = -\mathrm{atan}\left[\frac{R \sin\varphi}{1 - R\cos\varphi}\right] \tag{2.48}$$

Note that in deriving equation (2.46) we have ignored the phase shift corresponding to propagation through the medium of refractive index n_2, which

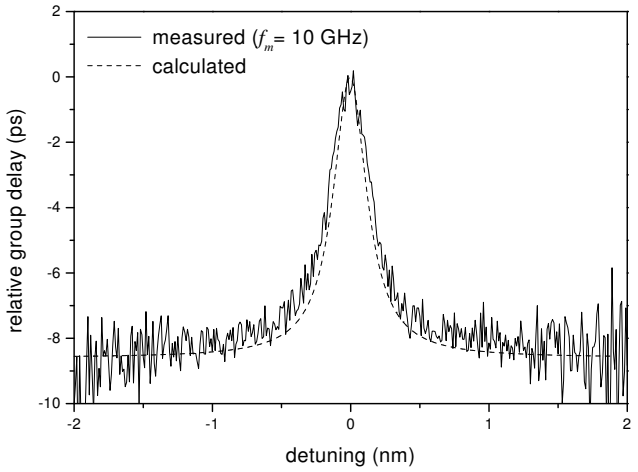

Figure 2.9 Measured (modulation frequency $f_m = 10$ GHz) and calculated group delay as a function of detuning with respect to the centre wavelength for a 40 GHz fibre Fabry-Pérot filter

was moreover assumed to be lossless. As far as the phase transfer function is concerned, the first assumption is physically equivalent to ignoring the contribution of the material dispersion to the total dispersion of the filter.

The fact that Fabry-Pérot filters can be simply modelled offers an opportunity to validate our phase-shift measurement set-up. The amplitude transfer function of a commercial tunable fibre Fabry-Pérot filter (Micron Optics Inc, model FFP-TF) having a 40 GHz FWHM bandwidth and a finesse equal to $\mathcal{F} = 138$ was measured in order to determine the reflectivity R, as well as the cavity length h based on the constructive interference condition, $\varphi = m2\pi$, where m is an integer. As the measured filter was of the air gap type, we considered $n_2 = 1$ and $\theta' = 0$ in equation (2.45). Once the physical parameters of the filter are known, it is possible to calculate its dispersion from equation (2.48). In Figure 2.9, we compare the calculated group delay of the fibre Fabry-Pérot filter with a measurement performed by the phase-shift technique with a modulation frequency of $f_m = 10$ GHz. Good agreement is obtained between the theoretical and measured group delays, in spite of the relatively high modulation frequency used to resolve the small electrical phase differences. The noise floor observed outside the pass-band on the measured group delay curve is due to the attenuation in excess of 10 dB of the filter at those wavelengths. Based on the theoretical complex transfer function, the dispersion of the Fabry-Pérot filter can be calculated, leading to maximum values of ± 37 ps/nm in the 3 dB

bandwidth of the device.

It is therefore confirmed that the phase-shift technique can be used to characterise the group delay of DWDM components and that our implementation is suitable for providing accurate estimates of the dispersive properties of narrow-band components such as a 40 GHz Fabry-Pérot filter.

2.6.2 Bragg grating for dispersion compensation

Waveguide gratings where the period of the effective refractive index changes linearly with the position along the waveguide (known as linearly chirped gratings) have been suggested as a way to compensate for the dispersion accumulated in optical fibre links [65] and can be implemented using the photosensitivity mechanism in Ge doped optical fibres [66]. Their principle of operation can be intuitively understood by observing that the Bragg reflection wavelength ($\lambda_B = 2n_{eff}\Lambda$ where n_{eff} is the effective refractive index and Λ is the corrugation period) varies linearly with position along the waveguide, resulting in different propagation delays for different wavelengths, which are reflected at different locations of the grating. If the grating is linearly chirped, then the variation of the group delay with wavelength should in principle be linear, which is equivalent to a constant dispersion in the pass-band of the device. Some practical concerns about this technology are dealing with their limited bandwidth as compared to the broadband fibre solutions discussed in Chapter 6, as well as the presence of group delay ripples in their pass-band due to grating imperfections [67]. On the other hand, when non-linearly chirped, such devices can offer adaptive dispersion compensation [68], which is a highly desirable functionality in future high speed networks with line rates at 40 Gbit/s and above.

Such devices are by nature designed to exhibit dispersion values large enough to compensate for the dispersion accumulated in several kilometres of standard single mode fibre (SMF). Therefore their characterisation by the phase shift technique should be relatively straightforward with low modulation frequencies, leading to a high accuracy.

We have experimentally characterised a commercial chirped fibre grating for dispersion compensation. This device had been used for unrepeatered transmission at 10 Gbit/s over a record distance of 250 km SMF [69]. It should be mentioned that this particular sample belonged to the first generation of commercially available dispersion compensating gratings, and that equivalent devices manufactured nowadays should present much better properties. The reflectivity was measured using a broadband amplified-spontaneous emission (ASE) erbium doped fibre source and an optical spectrum analyser. The phase-shift technique was used to charac-

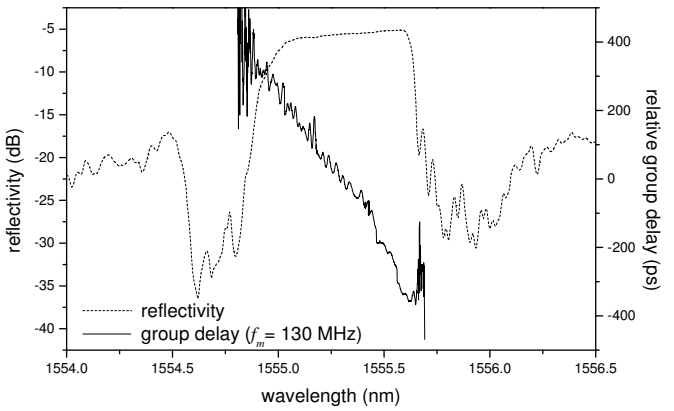

Figure 2.10 Measured reflectivity and relative group delay (modulation frequency $f_m = 130$ MHz) of a chirped fibre Bragg grating for dispersion compensation.

terise the group delay of the device, as shown in Figure 2.10. Owing to the large dispersion of the grating, a modulation frequency of $f_m = 130$ MHz was found to be sufficiently large for the phase resolution of the network analyser, while ensuring that the group delay characterisation would not suffer from the averaging distortions described in Section 2.5.2. It was experimentally confirmed that dispersion of the opposite sign was obtained from the other input of the device. The average dispersion exhibited by the device in the 1555 to 1555.4 nm range is of the order of -800 ps/nm, which would compensate for about 50 km SMF. Group delay ripples can be observed in the pass-band of the grating. Their pseudo-period is around 30 pm, as can be seen in Figure 2.11, which shows details of the group delay curve around 1555.2 nm. Those ripples are due to multiple reflections arising because of imperfections in the grating, resulting in Fabry-Pérot resonances [67]. Because of the group delay ripples, the dispersion can vary significantly within the pass-band. This was confirmed by applying the RF modulation method described in Section 2.7 to this particular chirped fibre grating. This latter method has the benefit of providing a direct measurement of the dispersion. It was found that the device had a dispersion of -858 ps/nm at 1555.2 nm, against about -1300 ps/nm at 1555.5 nm. Nevertheless, this does not mean that this grating could compensate for 1300 ps/nm accumulated dispersion at this particular wavelength, as the period of the ripples (in this case about 4 GHz) needs to be related to the spectral width of a modulated signal (for instance 20 GHz for the main

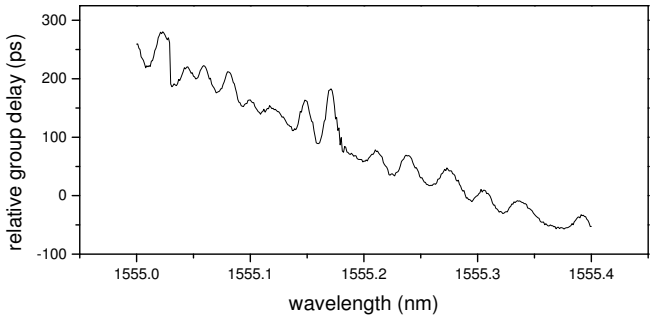

Figure 2.11 Details of the transfer function of Figure 2.10 showing the group delay ripples (measured with a modulation frequency $f_m = 130$ MHz) of a chirped fibre Bragg grating for dispersion compensation.

lobe of a NRZ modulated signal at 10 Gbit/s). Significant research effort has been spent in order to minimise the group delay ripples [67] as well as to understand their effect on system performance [15, 70]. In addition, resolving those group delay ripples requires a precise control of the tunable laser wavelength and necessitates the use of a wavelength meter, which was not employed in the present characterisation (the wavelength step was 0.001 nm). As a consequence, measurement noise due to mode hopping in the external cavity laser might also be present in the group delay curve shown in Figure 2.10. The amplitude noise observed at the edges of the pass-band is simply due to the high attenuation of the grating reflectivity at those wavelengths.

2.6.3 Uniform and apodised fiber Bragg gratings

One of the main advantages of the fibre grating technology is that the transfer function of the filter can be tailored by the proper choice of the distribution of the coupling coefficient along the fibre length, which is itself determined by the longitudinal effective refractive index profile. In this way it becomes possible to "square" the pass-band and to reduce the cross-talk level of fibre grating filters used in reflection, a process known as apodisation. Whether a side effect of this process is to necessarily result in increased group delay at the edges of the transfer function depends on whether the filter is minimum-phase, which is not systematically the case when a fibre grating is used in reflection, as seen in Section 2.3.1. The influence of the apodisation profile (defined as the envelope function of the effective refractive index with position along the grating) on system performance will be studied in details in Chapter 3.

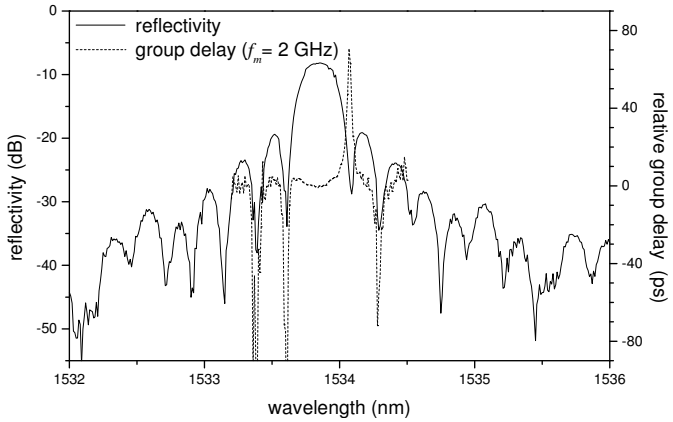

Figure 2.12 Measured reflectivity and relative group delay (modulation frequency $f_m = 2$ GHz) for a uniform fibre Bragg grating.

In this section, we present amplitude and group delay responses measured on a variety of fibre Bragg gratings having increased apodisation profile complexity. The grating structures are described according to their effective refractive index perturbation

$$\delta n_{eff}(z) = \alpha(z)\,\delta n\left[m + \cos\left(\frac{2\pi}{\Lambda(z)} + \phi(z)\right)\right] \tag{2.49}$$

where δn is the amplitude of the refractive index change due to photosensitivity, $\alpha(z)$ is the apodisation function, m controls the average (or "dc") index change, $\Lambda(z)$ is the grating period (including its spatial dependence in case of a chirped grating) , and $\phi(z)$ describes eventual phase shifts. The nomenclature of the gratings follows their apodisation function $\alpha(z)$. We will start by looking at the dispersive properties of a uniform grating for which $\alpha(z) = 1$. Measurements on gratings with conventional apodisation profiles where $\alpha(z)$ is a Gaussian function will be presented for different filter bandwidths, followed by a characterisation of a sinc apodised filter. Finally, the potential of advanced index profiles for the design of low dispersion filters will be illustrated by the first measurement results on a grating with an asymmetric apodisation function with multiple phase-shifts.

Uniform grating

The reflectivity and measured group delay of a uniform fibre grating with 33 GHz FWHM bandwidth is shown in Figure 2.12. From the attenuation in the centre of the pass-band, it is possible to deduce the strength of the

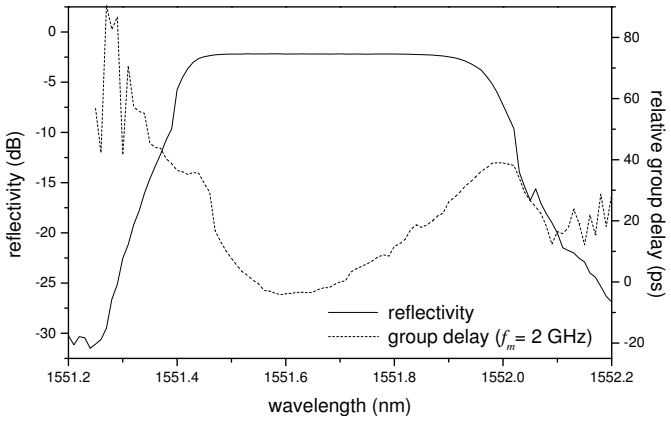

Figure 2.13 Measured reflectivity and relative group delay (modulation frequency $f_m = 2$ GHz) for a Gaussian apodised fibre Bragg grating designed for 100 GHz channel spacing.

grating according to $|r|^2 = \tanh^2 \kappa L$ where κ is the coupling coefficient and L is the grating length. This leads to the value $\kappa L = 0.4$. The dispersion is zero at the centre of the pass-band and increases towards the edges of the main lobe. Resolving the group delay at the filter's pass-band edges is difficult due to the narrow bandwidth of the device. Nevertheless, the shape of the group delay curve in the pass-band matches the theoretical prediction for an equivalent ideal uniform grating, as can be seen by comparing the measured data with the calculated group delay shown in Figure 2.3. Such a uniform grating is not suitable for filtering or demultiplexing applications in DWDM systems due to its high cross-talk level (defined as the difference between the attenuation at the centre frequency and the minimum attenuation of the first side-lobe), estimated to be of the order of 10 dB. This cross-talk can be suppressed by imprinting an envelope function to the effective index along the grating.

Gaussian apodised gratings

A Gaussian apodisation profile can be used to simultaneously square the pass-band while maintaining an acceptable cross-talk level [9]. Two commercial grade devices designed for DWDM systems with 100 and 50 GHz channel spacing have been characterised by the phase shift technique. The results obtained with a modulation frequency equal to 2 GHz are shown in Figure 2.13 and 2.14 respectively. It can be seen that the shape of the group delay curve is similar for both bandwidths. However, the extent of

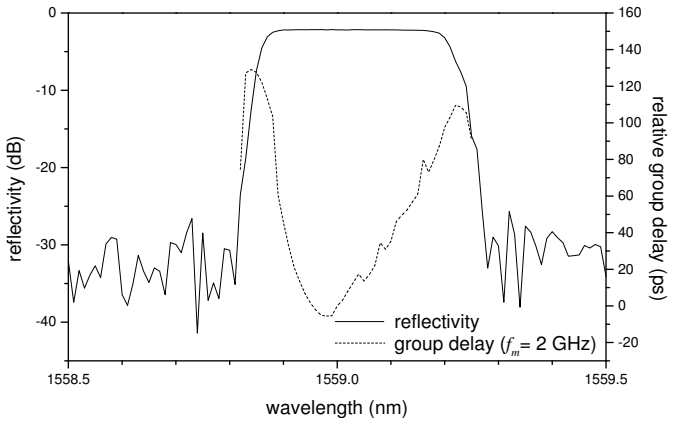

Figure 2.14 Measured reflectivity and relative group delay (modulation frequency $f_m = 2$ GHz) for a Gaussian apodised fibre Bragg grating designed for 50 GHz channel spacing.

the variations of the group delay with wavelength is much higher in the 50 GHz grating case, indicating that this device exhibits higher values of dispersion in the pass-band than its 100 GHz counterpart. In both cases, the zero-dispersion wavelength is not at the centre of the pass-band, as predicted by the theory for an ideal Gaussian apodised grating (see for instance Figure 3.12 in Chapter 3), but is deported towards its short wavelength edge. In agreement with the theory, zero dispersion (corresponding to local extrema in the group delay curve) is also observed at the edges of the pass-band of the reflectivity spectrum. This is clearly visible for the 50 GHz grating. On the long wavelength side, the maximum value of dispersion is estimated to be around 790 ps/nm for the 50 GHz grating against about 175 ps/nm for the 100 GHz device. The discrepancies between the theoretical and measured group delay are believed to be due to imperfections in the writing process of the grating. If no special care is taken, writing a Gaussian apodisation function will result in a Gaussian average effective index (i.e. the parameter m in equation (2.49) is not equal to 0). This is due to the fact that the refractive index can only be raised by the photosensitivity mechanism under UV illumination. This "dc" contribution to the effective index is responsible for some Fabry-Pérot resonances which manifest themselves as side-lobes on the short-wavelength side of the reflectivity spectrum [71]. Suppressing the average index change has been shown to be effective for removing those spectral features [72]. The Gaussian apodised filters whose transfer characteristics are reported in this section had been written using a double exposure technique aimed

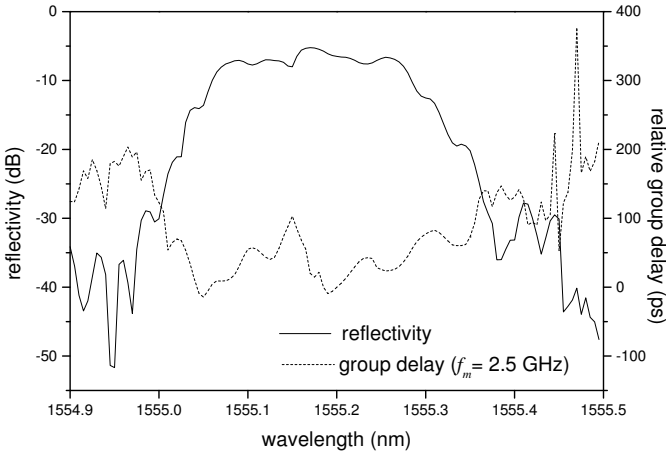

Figure 2.15 Measured reflectivity and relative group delay (modulation frequency $f_m = 2.5$ GHz) for a sinc apodised fibre Bragg grating used in reflection.

at cancelling out the "dc" index change [73]. Imperfect cancellation of the average refractive index change results in a less sharp short wavelength edge in the amplitude transfer function, and is also believed to be responsible for the zero dispersion wavelength not being centred in the middle of the pass-band. This last feature will have serious implications on the system performance of such a device as we shall see in Section 3.2.

Sinc apodised grating

It can be shown that, in the weak coupling regime, the coupling potential due to the refractive index corrugation $q(z)$ and the grating reflectivity $r(\omega)$ are related by a Fourier transform like expression [74]. Although this relation no longer holds for strong gratings, it can nevertheless provide some rough design guidelines for the optimisation of the shape of the reflectivity of grating filters. The coupling potential $q(z)$, introduced in Appendix B, depends directly on the amplitude and phase of the refractive index perturbation [75]. Therefore, in order to achieve a flat-top and low cross-talk "square" transfer function, the apodisation function should follow a $\sin z/z$ dependence. However, this requires the ability to realise π phase shifts in the apodisation profile. Such a technique has been developed within the "Glass Competence Area" at COM [76], and the first produced devices have been characterised using the phase-shift technique. The measured complex transfer functions obtained in reflection and in transmission are shown in Figure 2.15 and 2.16 respectively. The reflectivity presents significant am-

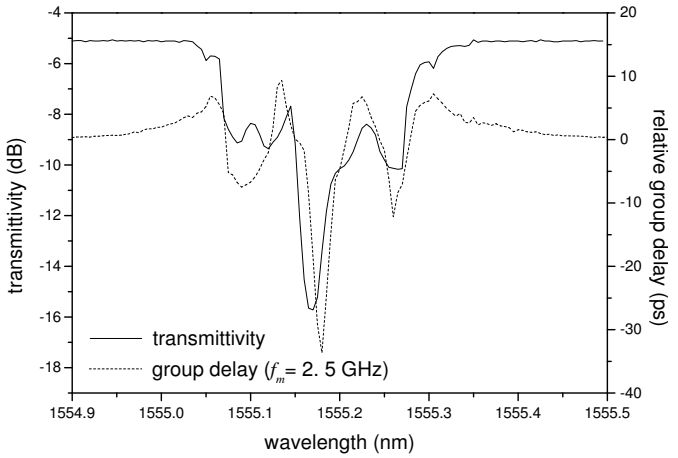

Figure 2.16 Measured transmittivity and relative group delay (modulation frequency $f_m = 2.5$ GHz) for a sinc apodised fibre Bragg grating used in transmission.

plitude ripples in the pass-band due to imperfections at this early stage of the writing method development. Matching group delay ripples can also be observed, resulting in high local dispersion values. It can be seen from the transmittivity that the maximum attenuation of the rejected channel is of the order of 11 dB, making this particular sample unsuitable for use as the filtering element of an add-drop multiplexer. It can also be observed that the variations of the group delay in transmission follow closely those of the attenuation, as was already the case for the reflectivity. Globally, poor control of the writing process is responsible for the weak performance of the characterised device. Progress in the development of the method achieved since then have been shown to result in "square" reflectivities and suppression of the filtered channel of the order of 40 to 50 dB in transmission, as was demonstrated in [76].

Asymmetric grating with phase-shifts

It has been mentioned in Section 2.3 that grating filters were generally not of the minimum-phase type when used in reflection. This opens the possibility to achieve the double goal of synthesising devices with an ideal "square" transfer function and low dispersion at the edges of the pass-band. However, it has also been demonstrated in Appendix B that, if the grating is symmetric, then its group delay is identical in transmission and in reflection. A grating being minimum-phase in transmission [57], the group delay in reflection of a symmetric device will then be uniquely de-

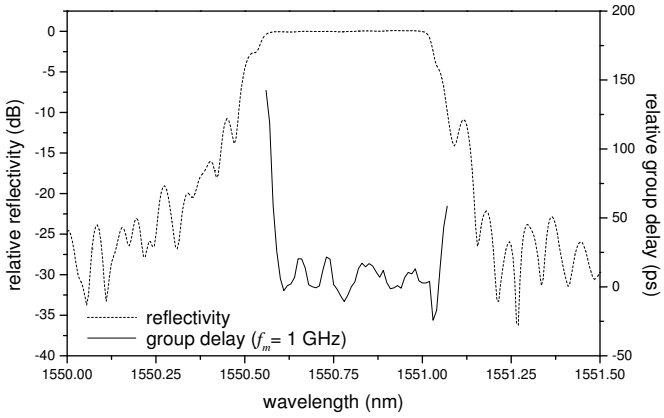

Figure 2.17 Measured reflectivity and relative group delay (modulation frequency $f_m = 1$ GHz) for a low dispersion grating with asymmetric apodisation profile. Amplitude transfer function courtesy of Hans-Jürgen Deyerl.

termined from its reflectivity. Therefore, using an asymmetric apodisation profile offers some more freedom in the design of low dispersion filters with nearly square amplitude responses. Such an approach has been successfully demonstrated for grating filters designed for 50 [77] and later on 25 GHz channel spacing [78]. The polarisation control method developed within the "Glass competence area" at COM allows for the realisation of asymmetric apodisation profiles with multiple phase-shifts [76]. The group delay of an asymmetric grating written using the polarisation control method has been characterised by the phase-shift technique. The transmission of the device was of the order of 20 dB and its FWHM bandwidth was 65 GHz. As can be seen in Figure 2.17, the grating reflectivity exhibits a square pass-band shape with cross-talk suppression of more than 20 dB. The group delay is fairly uniform in the pass-band, with group delay ripples of the order of 20 ps. Steep group delay increases are observed at the edges of the pass-band, similarly to the designs described in [77]. The resulting high dispersion value should not be detrimental in a system context as this behaviour is observed outside the usable bandwidth of the filter. The group delay curve of Figure 2.17 should be compared to the one obtained with a Gaussian apodised grating designed for the same channel spacing of 50 GHz and shown in Figure 2.14. It can clearly be seen that the amplitude of the variations of the group delay within the pass-band is much higher for the Gaussian apodised device. On the other hand, the low-dispersion asymmetric grating exhibits group delay ripples that can be predicted by the coupled-modes modelling of the refractive index structure [79]. Those

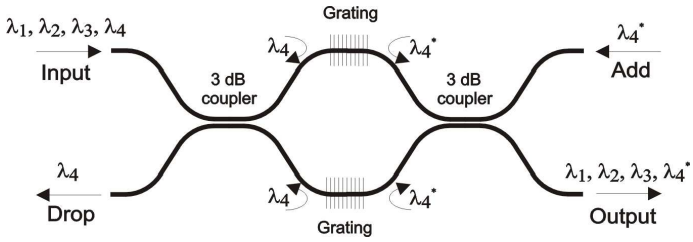

Figure 2.18 Principle of a fibre grating Mach-Zehnder interferometer optical add-drop multiplexer. Figure courtesy of Rune J. S. Pedersen.

short period ripples might result in high dispersion values locally, but the average dispersion of the filter should be close to zero in the pass-band, in contrast to the Gaussian filter of Figure 2.14. As in the case of chirped fibre gratings, and although the pseudo-period of the ripples is larger for the asymmetric structure described here (of the order of 0.1 nm against a few tens of pm), the amplitude and period of the ripples would need to be related to the spectral width of a modulated signal in order to assess their potential detrimental effect. It is also expected that due to the sharp dispersion increase at the edge of the pass-band, the asymmetric grating might exhibit higher penalties than the Gaussian apodised one for large detuning values.

It has also been confirmed experimentally that the group delay measured from the other input of the grating was different, resulting in higher dispersion values within the pass-band, as expected from the use of such an asymmetric apodisation function [79]. As a consequence, this type of grating cannot be used in the conventional add-drop multiplexer structures described in the following section, due to the fact that their dispersion properties are optimised only from one input. Therefore, even though they offer less degrees of freedom, symmetric sinc-type apodisation profile are still investigated by some authors as a trade-off between bi-directional operation and reduced dispersion [80, 81].

2.6.4 Fibre grating Mach-Zehnder optical add-drop multiplexer

A fibre grating Mach-Zehnder optical add-drop multiplexer is represented in Figure 2.18. It consists of two fibre gratings written in the arms of a Mach-Zehnder interferometer made with two 3 dB couplers [12]. For optimum operation, the two gratings should be fabricated in such a way that

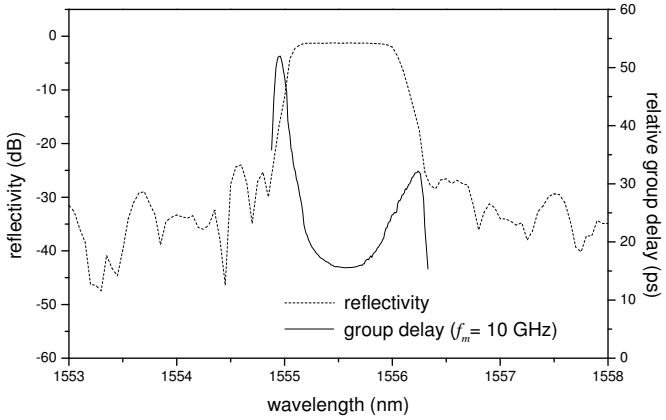

Figure 2.19 Measured transmittivity and relative group delay (modulation frequency $f_m = 10$ GHz) between the input and drop ports of a fibre grating Mach-Zehnder interferometer optical add-drop multiplexer.

both of them have identical reflectivity as well as transmittivity. The principle of operation of the device is as follow. The gratings are designed to be reflective for a specific wavelength, say λ_4, and their pass-band can be tailored using conventional apodisation techniques in order to reduce the cross-talk from adjacent channels. When a comb of WDM channels is input to the device at the port labelled "input" in Figure 2.18, only λ_4 is reflected by the two gratings while the other wavelengths propagate through them, ideally unaffected. Due to the existence of $\pi/2$ phase shifts in the cross paths of the 3 dB couplers, it can easily be checked that the two reflected waves at λ_4 interfere constructively at the "drop" port, while the transmitted signals at λ_1, λ_2, λ_3, etc, interfere constructively at the "output" port. The device has therefore realised the "drop" functionality. It can be shown in a similar way that, if another signal at wavelength λ_4^* (where the star $*$ denotes the fact the signal is different from the one input at λ_4 at the "input" port, although the wavelength is the same) is input to the device at the port labelled "add" in Figure 2.18, constructive interference is observed at the "output" port after reflection by the two gratings, thus realising the "add" functionality. Compared to another known implementation of an optical add-drop multiplexer making use of a grating between two circulators [11], the Mach-Zehnder type device can be integrated using conventional planar lightwave circuit technologies in silica-on-silicon and is potentially cheaper. On the other hand, proper operation requires the two arms of the Mach-Zehnder interferometer to be perfectly balanced, as well

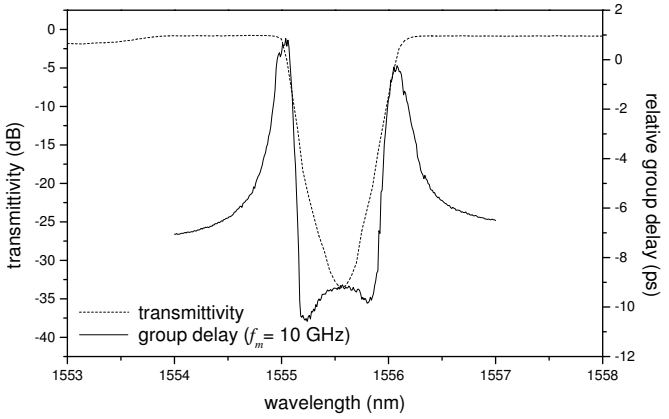

Figure 2.20 Measured transmittivity and relative group delay (modulation frequency $f_m = 10$ GHz) between the input and output ports of a fibre grating Mach-Zehnder interferometer optical add-drop multiplexer.

as the gratings written in each arm to be identical.

We have performed a detailed characterisation of a commercial fibre grating based Mach-Zehnder OADM (Innovative Fibers, S/N MZ1103, centre wavelength $\lambda = 1555.65$ nm). The complex transfer function measured from the "input" to the "drop" port of the device is shown in Figure 2.19. It is essentially similar to the reflectivity of a single apodised fibre grating. The FWHM bandwidth of the device is 130 GHz and its maximum cross-talk is of the order of -23 dB at a frequency spacing of 120 GHz. The group delay response is slightly asymetric and exhibits local maxima at the edges of the pass-band (corresponding to an attenuation of 15 dB) and close to the centre wavelength. By numerically calculating the derivative of the group delay curve in Figure 2.19, it can be shown that the maximum dispersion observed within the 3 dB bandwidth of the device is within ± 140 ps/nm.

When a fibre grating is no longer simply used as an optical band-pass filter, but as part of an add-drop device, its transmission properties also need to be assessed. The channels that are not dropped will propagate through the two gratings in the Mach-Zehnder structure of Figure 2.18, and therefore any imperfection in their transmittivity will affect them. In particular, if the gratings exhibit some out-of-band dispersion, the signals which are closer in wavelength to the one which has been dropped might experience some dispersion induced degradation. Depending on the bandwidth over which the out-of-band dispersion is significant and on the channel spacing, degradation might accumulate in structures designed to drop more than

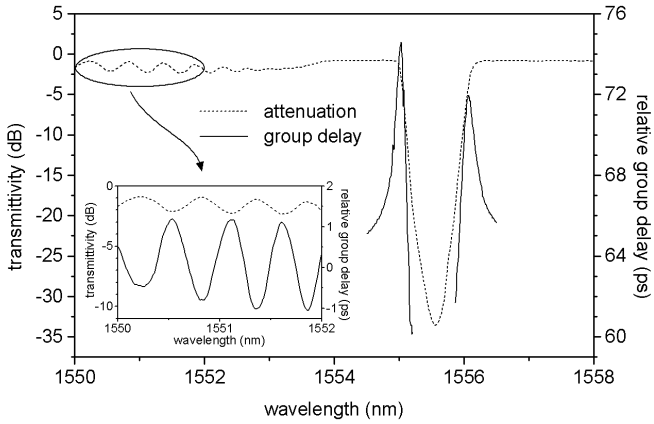

Figure 2.21 Measured transmittivity and relative group delay of a Mach-Zehnder interferometer optical add-drop multiplexer. The group delay around the stop-band was measured at a modulation frequency of $f_m = 5$ GHz, while $f_m = 2.5$ GHz was used to characterise the group delay associated to the amplitude ripples on the short wavelength side (inset).

one channel (i.e. making use of cascaded add-drop multiplexer modules or including several gratings, each designed to reflect a distinct wavelength). The transfer function measured between the "input" and "drop" ports is shown in Figure 2.20 in the vicinity of the design wavelength of the grating. A suppression of more than 30 dB is observed for the dropped channel. The functional shape of the group delay is the same as the one measured in reflection. High dispersion values are measured at the edges of the stop-band and the dispersion decreases towards zero away from the dropped wavelength of the OADM. No dispersion impairments are expected when this device is used in a WDM system with 200 GHz (1.6 nm) channel spacing. On the other hand, operation with 100 GHz channel spacing would result in a dispersion of the order of ± 5 to ± 15 ps/nm for the closest channels on both sides of the stop-band.

Coupling to cladding modes is responsible for amplitude ripples on the short wavelength side of the transmittivity transfer function of fibre gratings [9, 71]. Those ripples can be observed in Figure 2.21 for the device previously characterised. Such amplitude ripples can be detrimental in WDM systems as some of the channels that are not dropped by the device might be present in the wavelength range where they occur. In the best case, the effect of amplitude ripples will result in power unbalance between the channels, and in the worst case in signal distortion due to filtering, depending on the amplitude and period of the ripples with respect to the

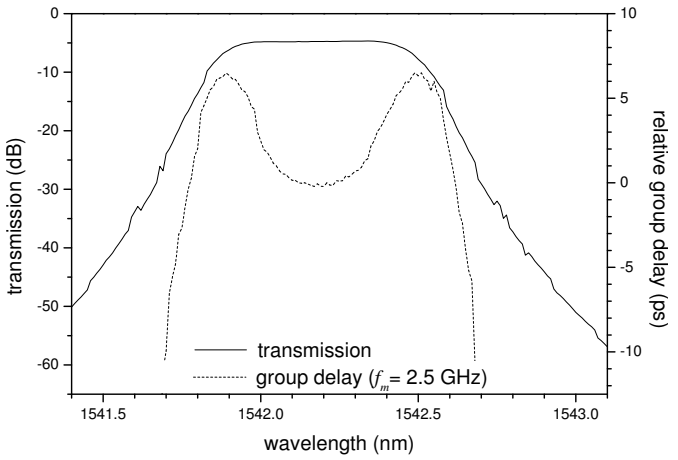

Figure 2.22 Measured transmittivity and relative group delay (modulation frequency $f_m = 2.5$ GHz) for a thin-film filter based demultiplexer.

channel bandwidth. Furthermore, by performing a phase shift characterisation in the wavelength range where those amplitude ripples are observed, we have shown that they are associated with group delay ripples having the same periodicity, as can be seen in the inset of Figure 2.21. For this particular device, the period of the ripples is estimated to be about 0.5 nm around 1551 nm (corresponding to only 3 channels away from the dropped channel if a spacing of 200 GHz is used) and the corresponding maximum dispersion values are ± 15 ps/nm. The evaluation of the system impairments connected to those dispersion and amplitude ripples would require statistical considerations on their amplitude, periodicity and phase, as well as on the topology and wavelength assignment of the WDM network where the OADMs would be used.

2.6.5 Thin-film (de)multiplexer

Multi-layer interference filters, also known as thin-film filters, consist of Fabry-Pérot like half-wave cavities separated by reflectors made of a stack of alternating low and high refractive index quarter-wave layers [5]. The bandwidth and steepness of the resulting filter transfer function can be tailored by engineering the number of cavities and $\lambda/4$ dielectric layers. For instance, increasing the number of cavities enables to realise steeper slopes, although this might also have the side effect to increase the attenuation ripples in the pass-band. Thin-film filters are usually designed to be band-pass in transmission, while the out-of-band channels are reflected by the

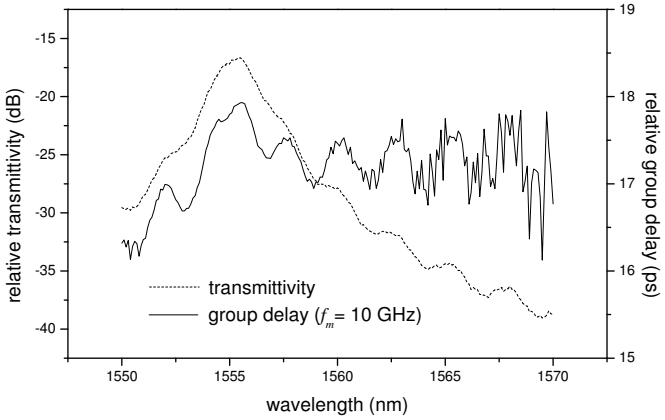

Figure 2.23 Measured transmittivity and relative group delay (modulation frequency $f_m = 10$ GHz) for a commercial thin-film tunable bandpass filter.

device [5]. Contrary to components like arrayed-waveguide gratings, interference filters only select one channel (or alternatively a group of adjacent channels, depending on their bandwidth) and several of them need to be combined in a proper structure to perform demultiplexing operations [82].

A typical amplitude response for a thin-film (de)multiplexer is shown in Figure 2.22, showing a characteristic flat-top and steep-slope response. Its insertion loss is 4.8 dB while its 3 dB bandwidth is 80 GHz and its 20 dB bandwidth is equal to 120 GHz. The associated group delay was measured using the phase shift technique with a modulation frequency of $f_m = 2.5$ GHz. The group delay variation is limited to 7 ps in the passband and the dispersion is equal to 0 ps/nm at the centre wavelength. The maximum dispersion in the 3 dB bandwidth is found to be within the range of -60 to 40 ps/nm. As pointed out in [13], the mechanism of resonant coupling in grating devices means they could be considered to the limit as being equivalent to thin-film filters with a large number of cavities. Our group delay characterisation confirms the similar behaviour of the two types of filters, although the characterised thin-film filter appears to be less dispersive than a grating of equivalent bandwidth such as the one shown in Figure 2.13.

2.6.6 Tunable thin-film filter

The angle of incidence of the light upon a thin-film filter such as the one described in Section 2.6.5 will determine its resonant wavelength. It is

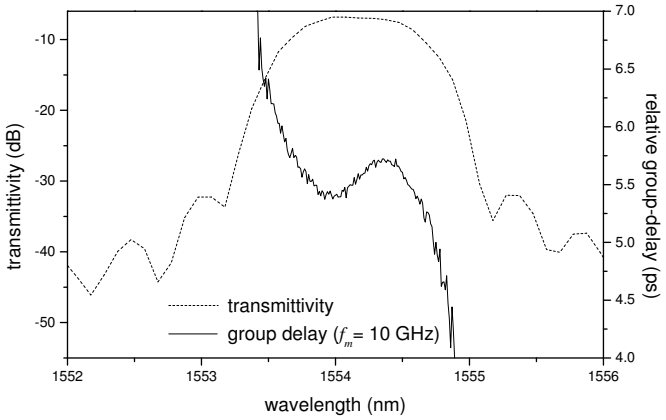

Figure 2.24 Measured transmittivity and relative group delay (modulation frequency $f_m = 10$ GHz) for a commercial arrayed waveguide grating multiplexer.

therefore possible to realise tunable band-pass filters using this principle. The amplitude and group delay of a commercial 1.3 nm bandwidth tunable band-pass filter (JDS model TB4500) are shown in Figure 2.23. Contrary to the transfer function of the thin-film (de)multiplexer shown previously, this band-pass filter is not of the flat-top type. Attenuation ripples are observed outside the pass-band. The device exhibits low dispersion, as can be inferred from the necessity to use a high modulation frequency of 10 GHz to resolve its group delay. Small group delay ripples of less than 1 ps are associated to the aforementioned amplitude ripples. It is not expected that dispersion should be an issue when this device is used at moderate bit rates up to 10 Gbit/s.

2.6.7 Arrayed waveguide grating (de)multiplexer

Arrayed waveguide gratings, also known as phased-arrays, consist of two free-propagation regions linked by an array of waveguides designed in such a way that the optical length difference between two consecutive waveguides is constant. They can be used as (de)multiplexers, add-drop multiplexers or, depending on their cyclic properties, wavelength routers. Reviews of the PHASAR technology can be found for instance in [7, 8]. The system implications of optimised PHASAR designs for high spectral efficiency systems is the topic of Chapter 4. It can easily be shown that, if the excitation of the arrayed waveguides is symmetric, then a PHASAR is a linear-phase device, consequently dispersion-free [13].

In order to verify this theoretical prediction, the group delay of a conventional, non pass-band flattened PHASAR designed for 200 GHz channel spacing has been characterised by the phase-shift method. This commercially available device (AT&T S/N 00428J) presented insertion loss of about 7 dB and a worst case cross-talk of 22 dB. The transmission properties are shown for the channel centred at 1554.245 nm in Figure 2.24. The 3 dB bandwidth of the device is equal to 125 GHz. A modulation frequency as high as 10 GHz was necessary in order to measure the group delay in the pass-band, indicating that the (de)multiplexer presents low dispersion values. The maximum dispersion value in the pass-band is estimated to ± 2 ps/nm. It has therefore been confirmed experimentally that conventional non-flattened AWG (de)multiplexers are linear-phase devices.

A number of channel manipulation components for WDM networks have been successfully characterised by the phase-shift technique. Those devices were selected as representative of different possible available technologies for (de)multiplexing or add-drop multiplexing. Unless their apodisation profile is carefully designed, fibre Bragg grating based components have been shown to be the most dispersive, followed by thin-film interference filter based multiplexers. The conventional arrayed waveguide grating technology is promising as far as its dispersion properties are concerned. However it suffers from a non-ideal pass-band shape which is not suitable for close channel packing in DWDM systems. Whether "squaring" their pass-band results in increased dispersion will be discussed in Chapter 4. Although great care was taken to optimise the modulation frequency in all the phase-shift characterisations presented above, it is clear that the method will show its limits for narrow band devices with small dispersion. An alternative characterisation technique (the so-called "RF modulation" or "dispersion-offset" method), which allows for direct measurement of the dispersion, is presented in the following section.

2.7 The dispersion-offset technique

2.7.1 Description of the method

The experimental set-up for the RF modulation method is depicted in Figure 2.25 [27, 28]. Light from a tunable external cavity laser is intensity modulated with a small modulation index by a $LiNbO_3$ Mach-Zehnder modulator before being coupled into a fibre offset followed by the device under test. A photodiode is used to detect the light at its output. As the

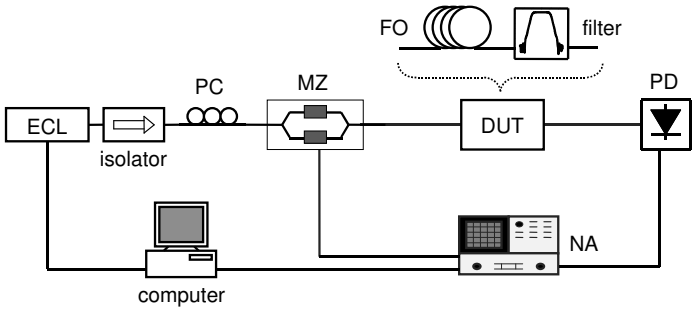

Figure 2.25 Experimental set-up for the RF modulation technique. ECL: external cavity laser; PC: polarisation controller; MZ: Mach-Zehnder modulator; DUT: device under test; FO: fibre offset; NA: network analyser; PD: photodiode.

modulation frequency is continuously swept from 130 MHz to 20 GHz, the small signal frequency response is measured by a network analyser.

The method relies on the fact that, due to the dispersive nature of optical components, the propagation constants of the two sidebands of the amplitude modulated signal are different. For a given dispersion value, modulation frequencies can be found where the components of the beat signal between the carrier and the sidebands are in counterphase, resulting in cancellations of the photocurrent seen as dips in the small signal frequency response. From (2.39) it is found that the total dispersion $\mathbb{D}$ can be calculated from these frequencies according to

$$\mathbb{D} = \frac{\left(k - \frac{1}{2}\right) c}{\lambda^2 f_n^2} \tag{2.50}$$

where f_n is the centre frequency of the n^{th} dip in the small signal frequency response, c and λ are the speed of light and the wavelength respectively. As an illustration, the frequency response measured in the range of 130 MHz to 20 GHz for 50 km of standard single mode fibre is shown in Figure 2.26. From the frequencies of the dips, it is possible to estimate the total dispersion accumulated in the fibre, which is equal to 861 ps/nm at 1557.65 nm. For practical purpose, it can be shown that the width of the dips for a given attenuation is a decreasing function of their order k, resulting in better accuracies in the measured dispersion values when higher order sideband cancellations are used.

From (2.50) we can see that the minimum dispersion that can be measured by this method depends on the maximum frequency at which the Mach-Zehnder modulator can be driven. This limitation arises from the

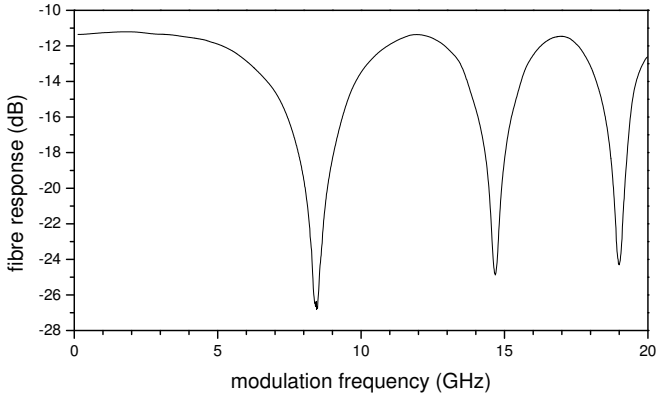

Figure 2.26 Example of frequency response obtained in the modulation frequency range 130 MHz to 20 GHz after propagation through 50 km of standard single mode fibre.

fact that, for a given amount of dispersion, the phase mismatch between the sidebands required for cancellation of the photocurrent is only achieved when the sideband separation is large enough. By inserting a constant dispersion offset (in our case 50 km of standard single mode fibre) in the set-up, we have been able to measure small values of both positive and negative dispersions. Such an offset will increase the total amount of dispersion to a value large enough to be measured by our set-up. The dispersion of the device under test is equal to the change in total dispersion after it has been inserted.

When characterising components such as filters, the two sidebands of the amplitude modulated signal can experience different levels of attenuation. If a and b are the relative amplitude attenuations experienced by the upper and lower sidebands respectively, then it can be shown from equation (2.28) that the detected RF current component at the modulation frequency ω_m can be written

$$i_{\omega_m}(r) = i_0 \frac{m}{2} \sqrt{a^2 + b^2 + 2ab\cos\phi_2}\cos\big(\omega_m t - \phi_1 - \varphi - \Gamma\big) \qquad (2.51)$$

where the notations of Section 2.4 have been kept. The argument $\phi_2(\omega_m)$ of the cosine appearing in the expression of the amplitude of the envelope of i_{ω_m} can be directly related to the dispersion β_2 from equation (2.36).

In this case, imperfect cancellation of the sidebands occurs, resulting in shallower dips in the measured small signal frequency response. However our calculation shows that the frequencies of the dips are the same as in the

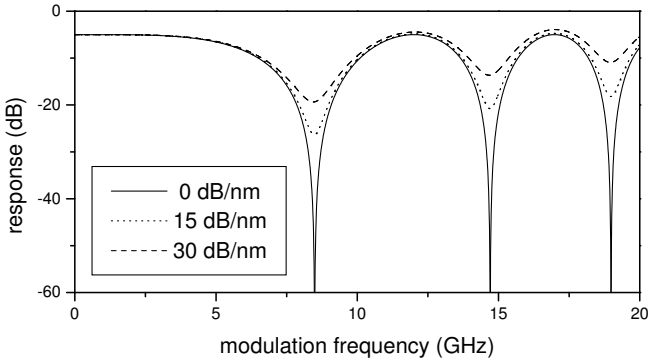

Figure 2.27 Calculated frequency response in the range 0-20 GHz for a total accumulated dispersion of D= 860 ps/nm and power transfer function slopes of 0, 15 and 30 dB/nm.

ideal case when $a = b$ and therefore (2.50) can still be used to evaluate the dispersion. This point is illustrated in Figure 2.27 where the small signal frequency response of a device with a dispersion value of 860 ps/nm has been calculated for power transfer function slopes of 0, 15 and 30 dB/nm. Therefore, this technique does not require the amplitude transfer function of the device to be uniform with respect to wavelength.

Since the method relies on a constant dispersion offset, its stability with time is an important issue. We have investigated the stability of a dispersion offset made of 50 km of standard single mode fibre which had been previously packaged in order to reduce thermal fluctuations. Over a 40 minute period, the frequency of the second dip in the small signal frequency response remained within a 10 MHz frame, which translates into a 1.2 ps/nm uncertainty for a total dispersion of 861 ps/nm at the measurement wavelength of 1557.65 nm. Figure 2.28 shows the measured dispersion of the fibre offset as a function of time. This 40 minute duration is far longer than the time required for performing the two modulation frequency sweeps necessary for evaluating the dispersion of a device at a single wavelength and enables wavelength dependent characterisations. Therefore, such a 50 km length of standard single mode fibre has been shown to constitute a dispersion offset stable enough to measure dispersion values with a resolution which is comparable to that of the phase-shift method.

This technique requires the possibility to perform swept-modulation frequency measurements for each wavelength, therefore necessitating the use of a network analyser, and resulting in a higher cost than the phase-shift technique for which a band-pass electrical filter and a vector voltmeter

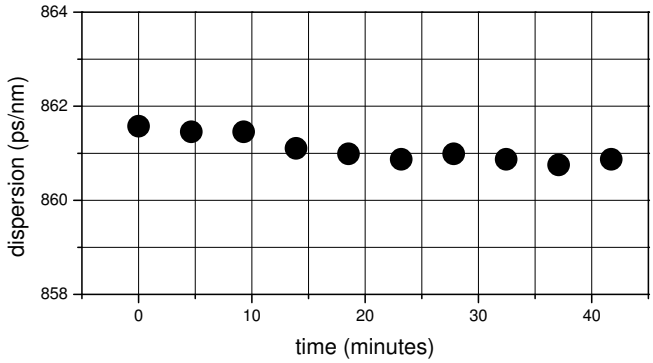

Figure 2.28 Measured dispersion of the fibre offset as a function of time.

are in principle sufficient. However, we have seen that added flexibility can be obtained in the phase-shift technique provided the modulation frequency can be tuned, in which case both configurations become equivalent.

The main advantage of this method is that it enables a direct determination of the dispersion of optical components, contrary to the phase-shift technique which leads to the group delay spectrum, from which the dispersion can be obtained by differentiation. However, the numerical differentiation of noisy phase-shift measurement data is only applicable with difficulty. The resolution of the dispersion-offset method is limited by the accuracy in the determination of the dip frequency influenced by noise and by the short term stability of the dispersion offset.

2.7.2 Example of application

A computer program has been written in order to synchronise the instruments and to record the small signal frequency response traces from the network analyser. All measurements have been performed on the second dip of the transfer function as it allows the determination of a wide range of both positive and negative dispersion values. The technique has been used for the determination of the dispersion of the fibre grating Mach-Zehnder optical add-drop multiplexer already characterised by the phase-shift technique in Section 2.6.4. The dispersion curve measured from the"in" to the "drop" port is shown in Figure 2.29, together with the power transfer function of the device. Values in excess of ± 40 ps/nm have been measured in the considered wavelength range. When reaching the edges of the passband of the filter, the dips in the small signal frequency response become shallower and the determination of their centre frequencies becomes more

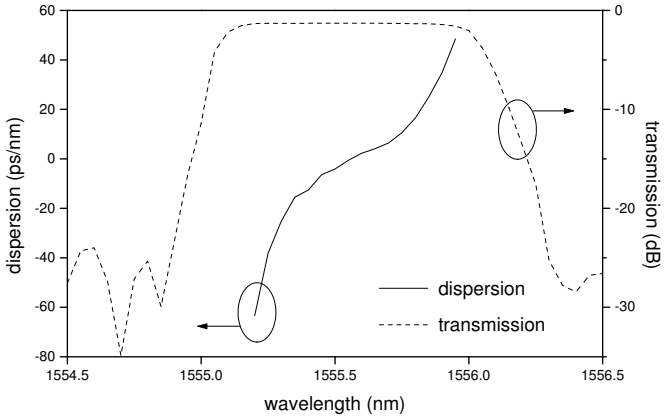

Figure 2.29 Dispersion of a fibre grating Mach-Zehnder optical add-drop multiplexer measured with the dispersion offset technique.

difficult, until they totally vanish in the noise. The values of the dispersion in the pass-band are within ±5 ps/nm of the ones obtained by numerical differentiation of the group delay curve obtained by the phase-shift technique in Figure 2.19. The good reproducibility of the results obtained with the dispersion-offset technique has also been verified.

2.8 Summary of Chapter 2

In this chapter, the needs for characterisation of the dispersion of components to be used in DWDM systems have been assessed. The evolution of optical fibre point-to-point links towards more sophisticated network structures, as well as the increase in spectral efficiency to meet ever increasing demands on capacity, are creating new requirements on the dispersive properties of optical filters. Dispersion characterisation techniques have been reviewed, with particular focus on their suitability for fibre optics devices. The calculation of the group delay of optical filters from their attenuation using Kramers-Kronig like relations has been shown to be of limited practical interest due to both theoretical issues on the minimum-phase criterion and difficulties in applying a suitable algorithm to measured data.

A general formulation of amplitude modulation technique has been presented, enabling a discussion on the accuracy of the commonly used phase-shift technique. It has been shown that a significant distortion of the measured group delay is obtained when a too high modulation frequency is used, which is otherwise required in order to obtain a sufficiently high time

resolution. Therefore, great care has to be taken in the choice of the modulation frequency, especially when characterising DWDM devices with low dispersion and narrow bandwidth.

A broad selection of WDM components has been characterised experimentally using the phase-shift technique. It has been confirmed experimentally that arrayed waveguide gratings, thin-film multiplexers and fibre gratings based devices, in this order, exhibited an increasing amount of dispersion at the edge of their pass-band.

Finally, a new method enabling the direct determination of the dispersion in the pass-band of optical filters has been presented and successfully applied to the characterisation of a fibre grating based optical add-drop multiplexer.

2.9 References to Chapter 2

[1] G. P. Agrawal, *Nonlinear fiber optics*, Academic Press, San Diego, second edition, 1995.

[2] M. Born and E. Wolf, *Principles of Optics*, Pergamon Press, Oxford, sixth edition, 1993.

[3] B. H. Verbeek, C. H. Henry, N. A. Olsson, K. J. Orlowsky, R. F. Kazarinov, and B. H. Johnson, "Integrated four-channel Mach-Zehnder multi/demultiplexer fabricated with phosphorous doped SiO_2 waveguides on Si", *Journal of Lightwave Technology*, vol. 6, no. 6, pp. 1011–1015, 1988.

[4] A. Frenkel and C. Lin, "Angle-tuned etalon filters for optical channel selection in high density wavelength division multiplexed systems", *Journal of Lightwave Technology*, vol. 7, no. 4, pp. 615–624, 1989.

[5] M. Scobey and R. Hallock, "Thin film filter based components for optical add/drop", in *OSA Trends in Optics and Photonics*, WDM components, D. A. Nolan (ed.), 1999, vol. 29, pp. 25–33, 1999.

[6] P. Martin, E. Taufflieb, B. Laloux, and H. C. Lefèvre, "Optimized bulk-optic grating approach for D-WDM demultiplexers", in *Proceedings European Conference on Optical Communication, ECOC'99*, Nice, France, vol. 1, pp. 110–111, 1999.

[7] M. K. Smit and C. van Dam, "PHASAR-based WDM-devices: principles, design and applications", *IEEE Journal of Selected Topics in Quantum Electronics*, vol. 2, no. 2, pp. 236–250, 1996.

[8] H. Takahashi, K. Oda, H. Toba, and Y. Inoue, "Transmission characteristics of arrayed waveguide N×N wavelength multiplexer", *Journal of Lightwave Technology*, vol. 13, no. 3, pp. 447–455, 1995.

[9] T. Erdogan, "Fiber grating spectra", *Journal of Lightwave Technology*, vol. 15, no. 8, pp. 1277–1294, 1997.

[10] E. Iannone and R. Sabella, "Optical path technologies: a comparison among different cross-connect architectures", *Journal of Lightwave Technology*, vol. 14, no. 10, pp. 2184–2196, 1996.

[11] K. P. Jones, M. S. Chaudhry, D. Simeonidou, N. H. Taylor, and P. R. Morkel, "Optical wavelength add-drop multiplexer in installed submarine WDM network", *Electronics Letters*, vol. 31, no. 24, pp. 2117–2118, 1995.

[12] D. C. Johnson, K. O. Hill, F. Bilodeau, and S. Faucher, "New design concept for a narrowband wavelength-selective optical tap and combiner", *Electronics Letters*, vol. 23, no. 13, pp. 668–669, 1987.

[13] G. Lenz, B. J. Eggleton, C. R. Giles, C. K. Madsen, and R. E. Slusher, "Dispersive properties of optical filters for WDM systems", *IEEE Journal of Quantum Electronics*, vol. 34, no. 8, pp. 1390–1402, 1998.

[14] A. M. Vengsarkar, J. R. Pedrazzani, J. B. Judkins, P. J. Lemaire, N. S. Bergano, and C. R. Davidson, "Long-period fiber-grating-based gain equalizers", *Optics Letters*, vol. 21, no. 5, pp. 336–338, 1996.

[15] K. Ennser, M. Ibsen, M. Durkin, M. N. Zervas, and R. I. Laming, "Influence of nonideal chirped fiber grating characteristics on dispersion cancellation", *IEEE Photonics Technology Letters*, vol. 10, no. 10, pp. 1476–1478, 1998.

[16] D. Penninckx, S. Khalfallah, and P. Brosson, "System impact of phase ripples in optical components", in *Technical Digest Optical Fiber Communication Conference, OFC'01*, Anaheim, California, U.S.A., paper ThB4, 2001.

[17] F. Liu, R. J. S. Pedersen, and P. Jeppesen, "Novel 2 × 2 multiwavelength optical cross connects based on optical add/drop multiplexers", *IEEE Photonics Technology Letters*, vol. 12, no. 9, pp. 1246–1248, 2000.

[18] P. Merritt, R. P. Tatam, and D. A. Jackson, "Interferometric chromatic dispersion measurements on short lengths of monomode optical fiber", *Journal of Lightwave Technology*, vol. 7, no. 4, pp. 703–716, 1989.

[19] L. G. Cohen, "Comparison of single-mode fiber dispersion measurement techniques", *Journal of Lightwave Technology*, vol. LT-3, no. 5, pp. 958–966, 1985.

[20] P.-L. Francois, M. Monerie, C. Vassallo, Y. Durteste, and F. R. Alard, "Three ways to implement interferencial techniques: application to measurements of chromatic dispersion, birefringence, and nonlinear susceptibilities", *Journal of Lightwave Technology*, vol. 7, no. 3, pp. 500–513, 1989.

[21] R. K. Hickernell, K. Takada, M. Yamada, M. Shimizu, and M. Horiguchi, "Pump-induced dispersion of erbium-doped fiber measured by Fourier-transform spectroscopy", *Optics Letters*, vol. 18, no. 1, pp. 19–21, 1993.

[22] B. Costa, D. Mazzoni, M. Puleo, and E. Vezzoni, "Phase shift technique for the measurement of chromatic dispersion in optical fibers using LED's", *IEEE Journal of Quantum Electronics*, vol. QE-18, no. 10, pp. 1509–1514, 1982.

[23] S. Ryu, Y. Horiuchi, and K. Mochizuki, "Novel chromatic dispersion measurement method over continuous Gigahertz tuning range", *Journal of Lightwave Technology*, vol. 7, no. 8, pp. 1177–1180, 1989.

[24] K. Mori, T. Morioka, and M. Saruwatari, "Ultrawide spectral range group-velocity dispersion measurement utilizing supercontinuum in an optical fiber pumped by a 1.5 μm compact laser source", *IEEE Transactions on Instrumentation and Measurement*, vol. 44, no. 3, pp. 712–715, 1995.

[25] A. J. Barlow, R. S. Jones, and K. W. Forsyth, "Technique for direct measurement of single-mode fiber chromatic dispersion", *Journal of Lightwave Technology*, vol. LT-5, no. 9, pp. 1207–1213, 1987.

[26] S. E. Mechels, J. B. Schlager, and D. L. Franzen, "Accurate measurements of the zero-dispersion wavelength in optical fibers", *Journal of Research of the National Institute of Standards and Technology*, vol. 102, no. 3, pp. 333–347, 1997.

[27] F. Devaux, Y. Sorel, and J. F. Kerdiles, "Simple measurement of fiber dispersion and of chirp parameter of intensity modulated light emitter", *Journal of Lightwave Technology*, vol. 11, no. 12, pp. 1937–1940, 1993.

[28] B. Christensen, J. Mark, G. Jacobsen, and E. Bødtker, "Simple dispersion measurement technique with high resolution", *Electronics Letters*, vol. 29, no. 1, pp. 132–134, 1993.

[29] L. G. Cohen and C. Lin, "A universal fiber-optic (UFO) measurement system based on a near-IR fiber Raman laser", *IEEE Journal of Quantum Electronics*, vol. QE-14, no. 11, pp. 855–859, 1978.

[30] Y. Yamabayashi, M. Tomizawa, and Y. Sato, "Single-wavelength dispersion measurement for multiple-fiber section connected with narrowband optical amplifiers", *IEEE Transactions on Instrumentation and Measurement*, vol. 45, no. 1, pp. 218–224, 1996.

[31] P. V. Mamyshev and L. F. Mollenauer, "Pseudo-phase-matched four-wave mixing in soliton wavelength-division multiplexing transmission", *Optics Letters*, vol. 21, no. 6, pp. 396–398, 1996.

[32] L. F. Mollenauer, P. V. Mamyshev, and M. J. Neubelt, "Method for facile and accurate measurement of optical fiber dispersion maps", *Optics Letters*, vol. 21, no. 21, pp. 1724–1726, 1996.

[33] ITU-T Recommendation G.650, *Definition and test methods for the relevant parameters of single-mode fibres*, International Telecommunications Union, Geneva, Switzerland, 2000.

[34] M. Born and E. Wolf, *Principles of Optics*, chapter 2, pp. 91–98, Pergamon Press, Oxford, sixth edition, 1993.

[35] X. S. Yao and J. Feinberg, "Simple in-line method to measure the dispersion of an optical system", *Applied Physics Letters*, vol. 62, no. 8, pp. 811–813, 1993.

[36] C. J. Brooks, G. L. Vossler, and K. A. Winick, "Phase response measurement technique for waveguide grating filters", *Applied Physics Letters*, vol. 66, no. 17, pp. 2168–2170, 1995.

[37] M. Volanthen, H. Geiger, M. J. Cole, R. I. Laming, and J. P. Dakin, "Low coherence technique to characterise reflectivity and time delay as a function of wavelength within a long fibre grating", *Electronics Letters*, vol. 32, no. 8, pp. 757–758, 1996.

[38] S. Barcelos, M. N. Zervas, R. I. Laming, and D. N. Payne, "Phase dispersion characterization of fibre gratings", in *Proceedings SBMO/IEEE MTT-S International Microwave and Optoelectronics Conference'95*, vol. 2, pp. 583–589, 1995.

[39] K. Takada, Y. Inoue, H. Yamada, and M. Horiguchi, "Measurement of phase error distributions in silica-based arrayed-waveguide grating multiplexers by using Fourier transform spectroscopy", *Electronics Letters*, vol. 30, no. 20, pp. 1671–1672, 1994.

[40] H. Yamada, H. Sanjoh, M. Kohtoku, K. Takada, and K. Okamoto, "Measurement of phase and amplitude error distributions in arrayed-waveguide grating multi/demultiplexers based on dispersive waveguide", *Journal of Lightwave Technology*, vol. 18, no. 9, pp. 1309–1320, 2000.

[41] J. Gehler and W. Spahn, "Dispersion measurement of arrayed-waveguide gratings by Fourier transform spectroscopy", *Electronics Letters*, vol. 36, no. 4, pp. 338–339, 2000.

[42] Y. Yabuta, H. Furukawa, T. Saitoh, K. Miyagi, and A. Taniguchi, "Measurement of optical device dispersion using mode-locked ring laser", in *Proceedings European Conference on Optical Communication, ECOC'97*, Edinburgh, Scotland, U.K., vol. 2, pp. 277–280, 1997.

[43] K. Takiguchi, K. Okamoto, S. Suzuki, and Y. Ohmori, "Planar lightwave circuit optical dispersion equaliser", in *Proceedings European Conference on Optical Communication, ECOC'93*, paper ThC 12.9, vol. 3, pp. 33–36, 1993.

[44] D. Pastor, B. Ortega, J. Capmany, J. L. Cruz, J. Marti, M. V. Andrés, E. Peral, M. J. Cole, and R. I. Laming, "Fully automatic simultaneous fiber grating amplitude and group delay characterization", *Microwaves and Optical Technology Letters*, vol. 14, no. 6, pp. 373–375, 1997.

[45] C. Caspar, H.-M. Foisel, C. v. Helmolt, B. Strebel, and Y. Sugaya, "Comparison of cascadability performance of different types of commercially available wavelength (de)multiplexers", *Electronics Letters*, vol. 33, no. 19, pp. 1624–1626, 1997.

[46] M. A. Muriel and A. Carballar, "Phase reconstruction from reflectivity in uniform fiber Bragg gratings", *Optics Letters*, vol. 22, no. 2, pp. 93–95, 1997.

[47] J. Skaar, "Measuring the group delay of fiber Bragg gratings by use of end-reflection interference", *Optics Letters*, vol. 24, no. 15, pp. 1020–1022, 1999.

[48] D. Mechin, P. Yvernault, L. Brilland, and D. Pureur, "New practical dispersion measurement technique for Bragg grating based MZI-OADM", *IEEE Photonics Technology Letters*, vol. 14, no. 1, pp. 89–91, 2002.

[49] A. Papoulis, *The Fourier integral and its applications*, chapter 10, McGraw-Hill, New-York, 1962.

[50] H. W. Bode, *Network analysis and feedback amplifier design*, Van Nostrand, New York, 1945.

[51] L. D. Landau, E. M. Lifschitz, and L. P. Pitaevskii, *Electrodynamics of continuous media*, pp. 279–283, Butterworth-Heinenann, Oxford, second edition, 1984.

[52] M. Beck, I. A. Walmsley, and J. D. Kafka, "Group delay measurements of optical components near 800 nm", *IEEE Journal of Quantum Electronics*, vol. 27, no. 8, pp. 2074–2081, 1991.

[53] R. H. Kop, P. de Vries, R. Sprik, and A. Lagendijk, "Kramers-Kronig relations for an interferometer", *Optics Communications*, vol. 138, pp. 118–126, 1997.

[54] A. Carballar and M. A. Muriel, "Phase reconstruction from reflectivity in fiber Bragg gratings", *Journal of Lightwave Technology*, vol. 15, no. 8, pp. 1314–1322, 1997.

[55] D. Pastor and J. Capmany, "Experimental demonstration of phase reconstruction from reflectivity in uniform fibre Bragg gratings using the Wiener-Lee transform", *Electronics Letters*, vol. 34, no. 13, pp. 1344–1345, 1998.

[56] J. Skaar and H. E. Engan, "Phase reconstruction from reflectivity in fibre Bragg gratings", *Optics Letters*, vol. 24, no. 3, pp. 136–138, 1999.

[57] L. Poladian, "Group-delay reconstruction for fiber Bragg gratings in reflection and transmission", *Optics Letters*, vol. 22, no. 20, pp. 1571–1573, 1997.

[58] L. R. Chen and P. W. E. Smith, "Fibre Bragg grating transmission filters with near-ideal filter response", *Electronics Letters*, vol. 34, no. 21, pp. 2048–2050, 1998.

[59] J. E. Román, M. Y. Frankel, and R. D. Esman, "Spectral characterization of fiber gratings with high resolution", *Optics Letters*, vol. 23, no. 12, pp. 939–941, 1998.

[60] G. H. Smith, D. Novak, and Z. Ahmed, "Technique for optical SSB generation to overcome dispersion penalties in fibre-radio systems", *Electronics Letters*, vol. 33, no. 1, pp. 74–75, 1997.

[61] M. Zaacks, A. Zeitouny, M. Horowitz, and U. Mahlab, "Measurement technique of phase aberration induced by fiber Bragg gratings", *IEEE Photonics Technology Letters*, vol. 14, no. 3, pp. 352–354, 2002.

[62] T. Niemi, G. Genty, and H. Ludvigsen, "Group-delay measurements using the phase-shift method: improvement on the accuracy", in *Proceedings European Conference on Optical Communication, ECOC'01*, Amsterdam, The Netherlands, 2001.

[63] G. Genty, T. Niemi, and H. Ludvigsen, "New method to improve the accuracy of group delay measurements using the phase-shift technique", *Optics Communications*, vol. 204, pp. 119–126, 2002.

[64] J. Stone and L. W. Stulz, "Pigtailed high-finesse tunable fibre Fabry-Perot interferometers with large, medium and small free spectral ranges", *Electronics Letters*, vol. 23, no. 15, pp. 781–783, 1987.

[65] F. Ouellette, "Dispersion cancellation using linearly chirped Bragg grating filters in optical waveguides", *Optics Letters*, vol. 12, no. 10, pp. 847–849, 1987.

[66] K. O. Hill, F. Bilodeau, B. Malo, T. Kitagawa, S. Thériault, D. C. Johnson, and J. Albert, "Chirped in-fiber Bragg gratings for compensation of optical-fiber dispersion", *Optics Letters*, vol. 19, no. 17, pp. 1314–1316, 1994.

[67] K. Ennser, M. N. Zervas, and R. I. Laming, "Optimization of apodized linearly chirped fiber gratings for optical communications", *IEEE Journal of Quantum Electronics*, vol. 34, no. 5, pp. 770–778, 1998.

[68] A. E. Willner, K.-M. Feng, J. Cai, S. Lee, J. Peng, and H. Sun, "Tunable compensation of channel degrading effects using nonlinearly

chirped passive fiber Bragg gratings", *IEEE Journal of Selected Topics in Quantum Electronics*, vol. 5, no. 5, pp. 1298–1311, 1999.

[69] R. J. S. Pedersen, B. F. Jørgensen, M. Nissov, and H. Yongqi, "10 Gbit/s repeaterless transmission over 250 km standard fibre", *Electronics Letters*, vol. 32, no. 23, pp. 2155–2156, 1996.

[70] K. Hinton, "Long haul system issues with Bragg fiber grating-based dispersion compensation", *Optical Fiber Technology*, vol. 5, pp. 145–164, 1999.

[71] V. Mizrahi and J. E. Sipe, "Optical properties of photosensitive fiber phase gratings", *Journal of Lightwave Technology*, vol. 11, no. 10, pp. 1513–1517, 1993.

[72] H. Singh and M. Zippin, "Apodized fiber Bragg gratings for DWDM applications using uniform phase mask", in *Proceedings European Conference on Optical Communication, ECOC'98*, Madrid, Spain, vol. 1, pp. 189–190, 1998.

[73] B. Malo, S. Thériault, D. C. Johnson, F. Bilodeau, J. Albert, and K. O. Hill, "Apodised in-fibre Bragg grating reflectors photoimprinted using a phase mask", *Electronics Letters*, vol. 31, no. 3, pp. 223–225, 1995.

[74] H. Kogelnik, "Filter response of nonuniform almost-periodic structures", *Bell System Technical Journal*, vol. 55, no. 1, pp. 109–126, 1976.

[75] G. Hugh Song, "Theory of symmetry in optical filter responses", *Journal of the Optical Society of America A*, vol. 11, no. 7, pp. 2027–2037, 1994.

[76] J. B. Jensen, N. Plougmann, H.-J. Deyerl, P. Varming, J. Hübner, and M. Kristensen, "Polarization control method for ultraviolet writing of advanced Bragg gratings", *Optics Letters*, vol. 27, no. 12, pp. 1004–1006, 2002.

[77] M. Ibsen, R. Feced, P. Petropoulos, and M. N. Zervas, "99.9% reflectivity dispersion-less square-filter fibre Bragg gratings for high speed DWDM networks", in *Technical Digest Optical Fiber Communication Conference, OFC'00*, Baltimore, Maryland, U.S.A., post-deadline paper PD21, 2000.

[78] M. Ibsen, R. Feced, P. Petropoulos, and M. N. Zervas, "High reflectivity linear-phase fibre Bragg gratings", in *Proceedings European Conference on Optical Communication, ECOC'00*, Munich, Germany, vol. 1, pp. 53–54, 2000.

[79] H.-J. Deyerl, N. Plougmann, J. B. D. Jensen, J. El-Bez, H. R. Sørensen, C. Peucheret, and M. Kristensen, "Low-dispersion fibre Bragg gratings written using the polarization control method", in *Proceedings European Conference on Optical Communication, ECOC'02*, Copenhagen, Denmark, paper 7.2.7, vol. 3, 2002.

[80] T. Shibata, M. Shiozaki, M. Ohmura, K. Murashima, A. Inoue, and H. Suganuma, "The dispersion-free filters for DWDM systems using 30 mm long symmetric fiber Bragg gratings", in *Technical Digest Optical Fiber Communication Conference, OFC'01*, Anaheim, California, U.S.A., paper WDD84, 2001.

[81] T. Shibata, K. Murashima, K. Hashimoto, M. Shiozaki, T. Iwashima, T. Okuno, A. Inoue, and H. Suganuma, "The novel dispersion reduced fiber Bragg grating suitable for 10 gb/s DWDM systems", *IEICE Transactions on Electronics*, vol. E85-C, no. 4, pp. 927–933, 2002.

[82] B. Nyman, M. Farries, and C. Si, "Technology trends in dense WDM demultiplexers", *Optical Fiber Technology*, vol. 7, pp. 255–274, 2001.

Chapter 3

Cascadability of fibre gratings for narrow channel spacing systems

Fibre gratings are versatile components that have found a wide range of applications in optical fibre communication systems, including filters, dispersion compensators, optical add-drop multiplexers and gain equalisation devices. Good reviews of their principles and applications can be found for instance in [1, 2].

The principle of fibre gratings relies on the photosensitivity mechanism according to which the refractive index of germanium doped silica can be changed permanently following exposure to ultra-violet radiation, making it possible to write periodic refractive index patterns in the core of optical fibres. These refractive index corrugations act as diffraction gratings, coupling light propagating in the forward and backward directions. In the case of a uniform grating of period Λ, constructive interference between light waves diffracted in the direction opposite to the direction of propagation occurs if the Bragg condition $\lambda_B = 2n_{eff}\Lambda$ is satisfied, where Λ is the corrugation period, n_{eff} is the effective mode index, and λ_B is the wavelength of maximum interaction. More generally, the coupling coefficients depend on the spatial distribution of the refractive index change $\delta n_{eff}(z)$, making it possible to tailor the response of a fibre grating by the proper choice of a refractive index profile.

This property offers some degrees of freedom for the design of filters exhibiting some of the desired features in optical communication systems, namely a nearly square amplitude response resulting in low cross-talk and reduced bandwidth narrowing when several devices are cascaded in a link

or network. However, as discussed in Section 2.3.1, the process of designing such an ideal amplitude response might result in unwanted dispersion at the edges of the pass-band of the device, which becomes critical at high bit rates as we shall see in this chapter. As a consequence, some trade-offs or innovative designs need to be found in order to alleviate those system limitations.

This chapter presents a study of the effects of fibre grating dispersion on transmission performance at 10 Gbit/s. A comparative study of the system penalties induced by different grating apodisation profiles is reported in Section 3.1, establishing a link between device design parameters and impairments encountered when those devices are used in a typical optical communication system. Reducing the channel spacing in wavelength division multiplexing (WDM) systems requires the design of narrow bandwidth filters. This is illustrated by an experimental comparison of the transmission performance through Gaussian apodised gratings when the channel spacing is reduced from 100 to 50 GHz. The results are presented in Section 3.2, together with an investigation of the cascadability of fibre gratings designed for narrow (50 GHz) channel spacing. With such a reduced bandwidth, the grating dispersion is clearly identified as the main cause for transmission impairments. Finally, bandwidth efficient modulation formats such as optical duobinary have been suggested as a way to increase the spectral efficiency in dense WDM systems. A study on the effect of fibre grating dispersion on duobinary modulation is presented in Section 3.3, where it is shown that even in the presence of non-uniform dispersion, the reduced bandwidth associated with the duobinary format results in improved tolerance to filter dispersion.

3.1 Fibre grating dispersion and its implication on high-bit-rate transmission

Since it has been suggested that the dispersive properties of optical filters might affect the performance of WDM systems [3, 4], a number of theoretical and numerical studies have focused on the special case of fibre gratings.

The limitation of the usable bandwidth of fibre Bragg gratings has been evaluated based on dispersion tolerance in [5]. The dispersion of different grating designs had been calculated and compared to the value of 1000 ps/nm, corresponding to 1 dB penalty at 10 Gbit/s, in order to define their usable bandwidth. However, such an approach can be discussed as it does not take into account the fact that the dispersion of fibre gratings is not uniform over the 10 Gbit/s signal spectral width. Moreover,

interactions between amplitude and group delay filtering are ignored. The effect of the dispersion of bandpass transmission filters based on chirped fibre moiré gratings was considered in [6] by examining the broadening of a Gaussian pulse. The wavelength dependance of dispersion has been investigated more in depth in [7] using numerical simulation. It was shown in this work that the dispersion of a grating or thin-film filter could be considered as a linear function of frequency within its pass-band. As a consequence, the dispersive effects of a cascade of gratings could be modelled by considering the dispersion slope and zero dispersion wavelength of the cascade transfer function. Although such a linear dispersion model might be sufficient for small values of the detuning between the laser and the filter centre frequency, it does not account for the dispersive behaviour at the edges of the pass-band.

A few experiments have been reported, whose goal was to highlight the effect of the dispersion of fibre gratings. In [8, 9], penalty measurements have been performed in reflection and transmission for a single apodised grating with 31 GHz bandwidth. The influence of the chirp of a 10 Gbit/s non return-to-zero (NRZ) modulated signal was investigated. Asymmetries in the penalty against wavelength detuning curves for chirped signals were attributed to the grating dispersion which exhibits opposite signs on the short and long wavelength sides. A first experimental comparison with a linear-phase device such as an arrayed waveguide grating was reported in [10], clearly outlining the inherent dispersive limitations of fibre gratings. A measurement of power penalty at 10 Gbit/s due to a single grating designed for 100 GHz channel spacing was performed in [11], and the results were extrapolated using numerical simulation to a cascade of filters in transmission and reflection, assuming some small frequency offsets between the components. Penalty measurements in transmission and reflection for a single tunable grating were also reported in [12]. The last two cited works were aiming at assessing the signal degradation induced by a dynamic tunable add-drop device. Finally, a cascade of 9 gratings having a 64 GHz bandwidth and designed for 100 GHz channel spacing was investigated for 10 Gbit/s transmission in [13]. It was confirmed in this study that the dispersion of the gratings was responsible for the measured penalty.

When a fibre grating is also used in transmission, as is typically the case in the optical add-drop multiplexers structures presented in Section 2.6.4, its out-of-band dispersion might induce degradation to the channels that are immediately adjacent to the dropped one. This might ultimately limit the channel spacing in dense wavelength division multiplexing (DWDM) networks making use of such devices. This potential limitation was recog-

nised early in [14] where a single Gaussian pulse analysis was performed based on an analytical expression for the out-of-band dispersion of a grating used in transmission. An evaluation of grating dispersion in transmission and its consequence on pulse degradation was also performed in [15, 16] where the case of the use of the grating in an optical add-drop multiplexer (OADM) was considered. The cascadability of Gaussian apodised gratings designed for 100 GHz channel spacing was investigated in [17]. This study was also based on an analytical expression for the out-of-band dispersion of the gratings and the tolerance criterion was again the dispersion limit of optical fibres (1000 ps/nm for 10 Gbit/s NRZ), the use of which can be questioned in case of non-uniform dispersion. More recently, the fact that fibre gratings are minimum-phase filters in transmission, meaning that their group delay can be directly evaluated from their transmittivity by the Kramers-Kronig relations, has been exploited to provide some bounds on their dispersion when used in transmission, and to examine the consequences for grating design [18].

Squaring the pass-band of a uniform fibre Bragg grating filter can be realised by increasing the strength of the grating κL, where κ is the coupling coefficient, directly proportional to the effective index change δn_{eff}, and L is the grating length [19]. However, this is known to result in a high level of out-of-band cross-talk, making such a device unsuitable for DWDM applications. A technique known as "apodisation" has been devised in order to reduce this undesired cross-talk. It consists of imprinting an envelope function to the effective refractive index change, resulting in a suppression of the side lobes in the reflectivity spectrum of the grating. Practical examples of apodisation have been presented together with measured complex transfer functions in Section 2.6.3. A number of apodisation functions can be realised with the conventional grating writing techniques [20] in order to approach the desired "flat-top" transfer function and to effectively reduce cross-talk from neighbouring channels. However, the different apodisation functions will also result in different dispersive properties at the pass-band edges, which has not been discussed in a system context so far. This dispersive behaviour will result in a reduction of the usable bandwidth of a grating filter, and therefore to tighter tolerance to laser misalignment with respect to the filter centre frequency, which can be a problem in a real system. In this section, we entirely focus on filtering degradation in the pass-band of fibre Bragg gratings due to the combined effect of amplitude and phase filtering. As a consequence, the respective cross-talk properties of the different grating designs are ignored in the present study. In

what follows, we present a numerical comparison of the detuning tolerance of gratings synthesised using a number of classical apodisation functions. The work is performed for 10 Gbit/s non return-to-zero modulation and for grating transfer functions corresponding to ITU standardised channel spacings of 50 and 100 GHz.

3.1.1 Gratings transfer functions

A number of apodisation functions have been selected and the corresponding grating complex transfer functions have been calculated using the transfer matrix approach described in Appendix B. The following apodisation profiles have been considered:

Uniform:

$$\alpha(z) = 1 \tag{3.1}$$

Gaussian:

$$\alpha(z) = \exp\left[-\frac{4\ln 2}{L_{FWHM}^2} z^2\right] \tag{3.2}$$

Hamming:

$$\alpha(z) = \frac{1 + \eta\cos\left[\frac{2\pi z}{L}\right]}{1+\eta} \tag{3.3}$$

Blackman:

$$\alpha(z) = \frac{1 + (1+\eta)\cos\left[\frac{2\pi z}{L}\right] + \eta\cos\left[\frac{4\pi z}{L}\right]}{2+2\eta} \tag{3.4}$$

In the equations above, L is the grating length and L_{FWHM} is the full-width half-maximum length of the refractive index envelope function $\alpha(z)$. The case of the uniform grating is considered for reference purpose. As the focus of this study is on amplitude and phase filtering in the pass-band of fibre Bragg gratings, cross-talk considerations are ignored. The design target for the gratings is to have a rejection of the filtered channel of at least 25 dB (typically 30 dB) in transmission, so that they can be used as part of add-drop multiplexers without inducing much interferometric cross-talk between the added channel and leakage from the dropped channel [21]. For strong gratings, the bandwidth becomes independent of the grating length [19]. Therefore one can obtain the desired rejection at the centre of the stop-band by increasing the strength of the grating κL via its length, while the refractive index modulation δn is adjusted to provide the desired bandwidth. Values of the apodisaton parameters for the different designs were $L_{FWHM} = 0.43L$ (where L is the grating length) for the Gaussian grating,

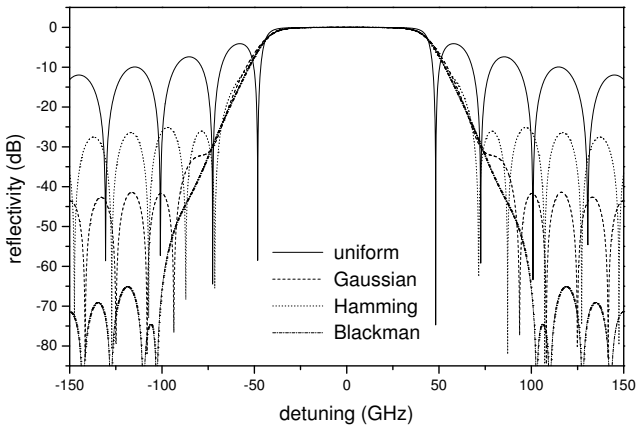

Figure 3.1 Reflectivity as a function of detuning from the centre frequency for uniform as well as Gaussian, Hamming and Blackman apodised fibre gratings designed for 100 GHz channel spacing.

as well as $\eta = 0.25$ and 0.75 for the Hamming and Blackman apodised gratings respectively[1]. The full-width half-maximum (FWHM) bandwidths of the gratings designed for 100, 50 and 25 GHz channel spacing are 88, 44 and 23 Ghz, respectively. The resulting complex transfer functions in the case of gratings designed for 100 GHz channel spacing are shown in Figure 3.1 and 3.2 for the amplitude and the dispersion, respectively.

As anticipated, the uniform grating exhibits strong side-lobes expected to result in poor cross-talk performance. An increased suppression of the side-lobes is observed with Hamming, Gaussian and Blackman apodisation profiles, in this order. Down to about 30 dB attenuation, the shape of the pass-band is fairly similar for all three apodisation functions. As far as dispersion is concerned, maxima are obtained at the edges of the pass-band. The uniform grating exhibits the maximum dispersion value of the four considered apodisations. Then comes the Gaussian grating while the Blackman and Hamming functions result in equivalent dispersion spectra. Nevertheless, the dispersion of the uniform grating is the lowest in the pass-band, and its peak occurs for a slightly higher detuning than for the three apodised gratings, although with a larger amplitude. These observations, performed here on the gratings designed for 100 GHz channel spacing, can also be made for the devices corresponding to 50 and 25 GHz channel

[1]The complex transfer functions considered in this section have been calculated based on parameters provided by Hans-Jürgen Deyerl from the "Glass Competence Area" at COM.

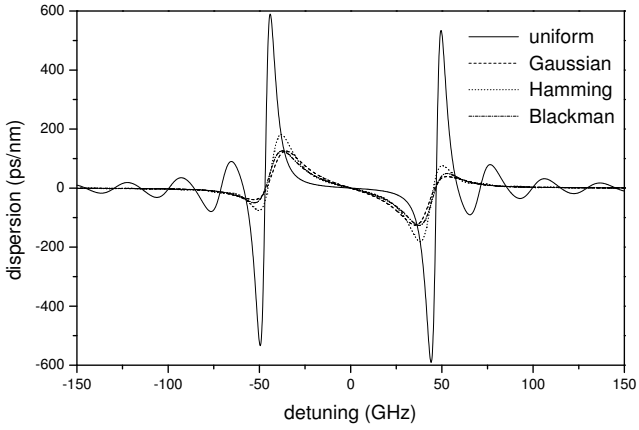

Figure 3.2 Dispersion as a function of detuning from the centre frequency for uniform as well as Gaussian, Hamming and Blackman apodised fibre gratings designed for 100 GHz channel spacing.

spacing. The dispersive properties in the pass-band for the four different types of gratings are summarised in Table 3.1 where their usable bandwidth for an absolute value of the dispersion smaller than 100 ps/nm has been calculated. In order to enable better comparisons, the usable bandwidth has been normalised to the channel spacing. The value of 100 ps/nm would limit the cascadability of network elements based on such gratings to about 10 devices for a NRZ modulated signal at 10 Gbit/s if the dispersion tolerance criterion used in previously reported works [5] was adopted. However, as already emphasised, this 1000 ps/nm limit would correspond to 1 dB dispersion induced penalty assuming the dispersion is uniform with respect to wavelength over the signal bandwidth, a condition which is not fulfilled at the edges of the pass-band of fibre Bragg gratings.

It is confirmed in Table 3.1 that, even though uniform gratings exhibit the highest dispersion value at their pass-band edges, they offer the largest detuning tolerance for less than ± 100 ps/nm dispersion, followed by Blackman, Hamming and Gaussian apodised gratings in this order, apart for the 50 GHz devices where Hamming apodisation results in slightly better detuning tolerance than Blackman apodisation. This last observation can be explained by the fact that the gratings transfer functions have been calculated based on real physical parameters in order to match requirements in terms of 3 dB bandwidth and attenuation in transmission of at least 25 dB at the centre frequency. However, due to the iterative nature of the resolution of this inverse problem, the obtained solution for the grating length

Δf (GHz)	uniform	Gaussian	Hamming	Blackman
100	70.6	58.4	59.2	63.4
50	52.8	23.2	30.4	25.2
25	32.0	7.2	9.2	10.8

Table 3.1 Detuning tolerance (normalised to the channel spacing Δf; in percentage) for less than $\pm$100 ps/nm dispersion for uniform, Gaussian, Hamming and Blackman apodised gratings designed for channel spacings of 100, 50 and 25 GHz.

and refractive index change might result in slightly different values of the target parameters for the different apodisation profiles (e.g. the attenuation at the centre frequency in transmission is not strictly the same for all the grating designs). Nevertheless, the implication on grating properties is expected to be small and should not result in significant performance difference from a system point of view.

From Table 3.1 it is also found that the increase rate of the normalised detuning tolerance is almost the same from 25 to 50 GHz and from 50 to 100 GHz channel spacing for each filter type, suggesting a fairly linear dependence of the dispersion limited bandwidth utilisation on the channel spacing over the limited range investigated here.

3.1.2 Influence of the apodisation profile

The transmission impairments through the four grating designs described in the previous section have been investigated numerically for 10 Gbit/s NRZ modulation. A $2^{11} - 1$ pseudo-random binary sequence (PRBS) was used to externally modulate a continuous wave laser (CW) at 10 Gbit/s in a chirp-free Mach-Zehnder modulator with 15 dB extinction ratio. The signal was then input to a cascade of identical and perfectly aligned gratings and the eye opening penalty (EOP) was calculated as a function of the detuning between the laser frequency and the filter centre frequency. The EOP is defined as the ratio of the normalised eye opening after filtering to the normalised eye opening at the transmitter output, where the normalisation is performed with respect to the signal average power. As the focus is on signal distortion induced by filtering, no optical or electrical noise process was included in the simulation. At the receiver side, an electrical fourth order Bessel low-pass filter with 7.5 GHz 3 dB cut-off frequency was applied to the signal. The EOP calculations were performed for uniform, Gaussian, Hamming and Blackman apodised gratings designed for channel spacings of 100, 50 and 25 GHz. In order to evaluate the influence of the phase

response of the filters, the simulations were repeated with hypothetical transfer functions where the amplitude response is assumed to be identical to the one of the aforementioned gratings, but where the phase response is assumed to be linear, the filter being therefore dispersion-less.

The results are summarised in Figure 3.3 where the frequency detuning corresponding to 1 dB EOP (full-width) is represented as a function of the number of cascaded filters for the four types of gratings designed for 100, 50 and 25 GHz channel spacing and the corresponding hypothetical linear-phase filters. In order to allow for an easier comparison, the allowed detuning has been normalised to the channel spacing. For a single 100 GHz filter, the fraction of the bandwidth that can be used for less than 1 dB EOP is much higher for all apodised devices than for the uniform grating, independently of whether the filter dispersion is taken into account or not. This can be attributed to the sharper edges of the amplitude transfer functions of uniform gratings. When the number of cascaded devices increases, the allowed normalised detuning is proportionally more severely reduced for the apodised gratings than for the uniform filter. This is due to the bandwidth narrowing induced by the filter cascade. Due to the steep edges of the main lobe of the amplitude transfer function of strong uniform gratings, the 10 Gbit/s signal experiences less bandwidth reduction than with the other apodised designs investigated here. Very little difference in bandwidth reduction is observed between the different apodisation profiles. Above three cascaded filters, the influence of filter dispersion starts becoming noticeable, resulting in a divergence of the allowable normalised detuning curves obtained with the complex transfer functions and the corresponding linear phase transfer functions. Nevertheless, for eight cascaded devices, the reduction in allowable normalised detuning induced by the filter dispersion is only of the order of 20% for all the apodised devices when compared to the ideal dispersion-free cases. An even smaller dispersion induced degradation is observed for the uniform grating design. As a consequence, for broad filters to be used in 100 GHz channel spacing WDM systems (corresponding to 0.1 bit/s/Hz spectral efficiency), it can be concluded that the three apodised designs offer equivalent performance in terms of usable bandwidth and should be preferred over uniform gratings up to 6 cascaded filters. The slightly better performance of uniform gratings above 6 cascades is due to their smaller dispersion in the pass-band and to their better resilience to bandwidth narrowing when cascaded. In any case, the influence of grating dispersion remains small for 100 GHz filters at 10 Gbit/s.

The same trends are observed in the case of filters designed for 50 GHz channel spacing. Whichever the grating design, the relative fraction of the

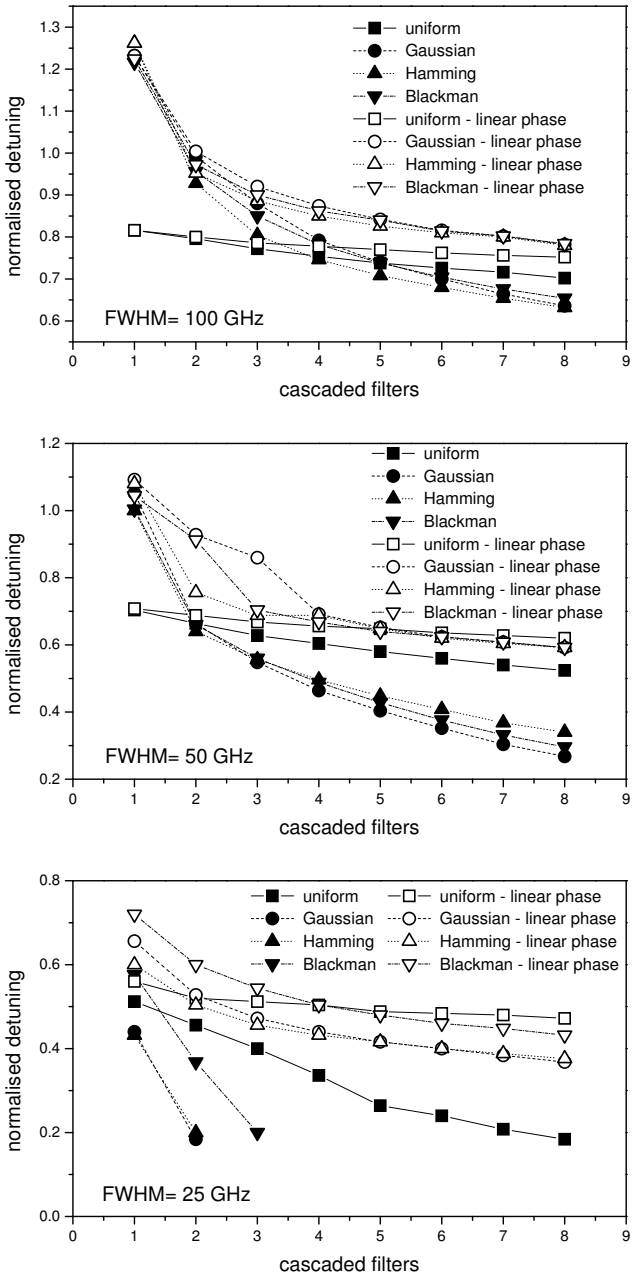

Figure 3.3 Allowed detuning (normalised to the channel spacing) as a function of number of cascaded filters for uniform, Gaussian, Hamming and Blackman apodised fibre gratings designed for 100 (top), 50 (middle) and 25 GHz (bottom) channel spacing. The graphs also present equivalent results for hypothetical linear-phase gratings.

bandwidth which can be used for less than 1 dB EOP is reduced compared to the 100 GHz filters case. The benefit of using uniform gratings can be reached after only 2 cascaded filters. For more than 2 cascaded filters, uniform gratings offer better detuning tolerance than Hamming, Blackman and Gaussian apodised designs in this order. This follows the trends observed in the calculated usable bandwidth of the gratings for less than ±100 ps/nm dispersion reported in Table 3.1. For eight cascaded filters, the reduction in usable bandwidth due to dispersion is now of the order of 50% for the apodised designs.

When a smaller channel spacing of 25 GHz is used (which would correspond to spectral efficiencies of 0.4 bit/s/Hz), only uniform gratings can be cascaded up to eight times, whereas the cascadability of the apodised designs is limited to two or three components for less than 1 dB EOP. The best detuning performance is therefore offered by uniform gratings, followed by the Blackman apodised devices, then the Hamming and Gaussian apodised filters, in agreement with the dispersion detuning tolerances of Table 3.1. However, this observation does not hold for a single device in the case of 25 GHz filters where the 10 Gbit/s NRZ spectrum will be severely affected by both amplitude and phase filtering. Therefore, the estimate of the allowable detuning for less than ±100 ps/nm can be used in order to predict the relative performance of the gratings in a system context, provided it has been ensured first that the filter dispersion is the main source of penalty. Furthermore, it can be observed that the dispersion induced detuning tolerance criterion used in [5] would fail to predict the cascadability behaviour of narrow bandwidth gratings as, for instance, only two 25 GHz Gaussian apodised gratings can be cascaded with less than 1 dB EOP in the pass-band, whereas, based on this criterion, up to 10 devices could be cascaded provided the laser detuning remains within a ±3.6 GHz range from the filter centre frequency. This example emphasises the necessity to take into account both amplitude and phase filtering when edicting cascadabilty guidelines for optical components.

As a conclusion, as far as amplitude and phase filtering performances are concerned, uniform gratings have been shown to offer the best cascadability, in spite of a poorer detuning tolerance when a single device is used. This is due to their steep amplitude response at the edges of the pass-band resulting in reduced bandwidth narrowing when cascaded, and to their lower dispersion in the pass-band. However, this statement must be tempered by the fact that the present analysis focuses strictly on signal degradation induced by amplitude and phase filtering in the pass-band of the devices. Obviously, as can be seen in Figure 3.1, uniform gratings

would suffer from an unacceptably high cross-talk level from neighbouring channels when used in a WDM system. Down to 50 GHz bandwidth, Gaussian, Hamming and Blackman apodisation have been shown to result in equivalent detuning tolerance for up to eight cascaded filters. Therefore, Blackman apodisation should be preferred as it also offers the best cross-talk performance. Furthermore, its detuning tolerance has also been shown to be the largest of the investigated apodised designs for 25 GHz channel spacing. At 10 Gbit/s, the influence of filter dispersion has been shown to start becoming significant below 50 GHz channel spacing, corresponding to WDM systems with over 0.2 bit/s/Hz spectral efficiency.

3.2 Transmission degradation through fibre gratings

A Gaussian apodisation profile is commonly used to approach the desired flat-top and low-crosstalk transfer function for fibre Bragg gratings filters. Such Gaussian apodised gratings can be used for filtering or add-drop multiplexing applications in WDM systems only if the short wavelength sidelobes are sufficiently suppressed (refer to the discussion of Section 2.6.3 in this thesis), which is achieved by cancelling out the average "dc" refractive index change induced by the ultra-violet writing process. This can be performed for instance by using a double exposure technique [20]. However, imperfections in the writing process of a grating might result in signal distortion when the device is used in a system context.

This section presents the results of an experimental investigation of the transmission degradation at 10 Gbit/s through fibre gratings designed for 100 and 50 GHz channel spacing. The increased sensitivity to grating dispersion, as well as the influence of imperfections in the apodisation process will be demonstrated for narrow band devices, resulting in severe limitations to the number of nodes and detuning tolerance when such filters are cascaded in a network.

3.2.1 System impact of 50 and 100 GHz Gaussian apodised gratings

The system impairments induced by imperfect alignment of the transmitter frequency and the centre frequency of a grating filter have been evaluated experimentally. More specifically, the filter detuning tolerance has been compared for Gaussian apodised fibre Bragg gratings designed for 50 and 100 GHz channel spacing. Such an investigation can be used to assess

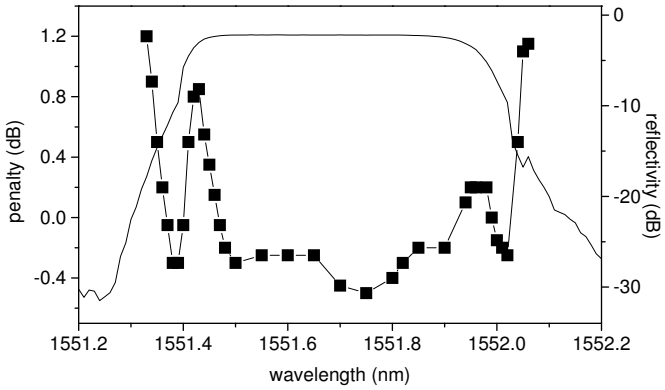

Figure 3.4 Penalty as a function of wavelength for a 10 Gbit/s NRZ signal reflected by a fibre Bragg grating filter designed for 100 GHz channel spacing.

the requirements on laser frequency stability when a DWDM system is upgraded from 100 down to 50 GHz channel spacing at 10 Gbit/s.

The experimental set-up consists of a 10 Gbit/s NRZ transmitter, an optical circulator connected to a fibre grating used in reflection, and a receiver (without optical pre-amplification). The transmitter and receiver configurations correspond to the ones shown in Figure 3.6 and are described in more details in Section 3.2.2. The transmitter is based on an external cavity tunable laser, enabling to scan through the pass-band of the grating under test, and an external chirp-free Mach-Zehnder modulator. The extinction ratio of the NRZ signal was adjusted to 13 dB at the output of the modulator, resulting in a back-to-back sensitivity of -16.7 dBm at a BER of 1.0×10^{-9}. The measured transfer functions have been shown in Figure 2.13 and 2.14 for the fibre gratings designed for 100 and 50 GHz channel spacing respectively.

The measured penalty curve at a BER of 1.0×10^{-9} can be seen in Figure 3.4 for the 100 GHz filter. The penalty is minimum at 1551.75 nm, which approximately corresponds to the centre wavelength of the filter. As expected, the penalty increases towards the edges of the filter's pass-band, although not in a monotonous way. For both positive and negative detunings, the penalty is observed to increase towards local maxima close to the 3 dB limits of the pass-band, before decreasing, then increasing again at its edges. Although perfectly reproducible, the values of the local penalty maxima are only of the order of 0.8 and 0.2 dB on the short and long wavelength sides of the pass-band, respectively.

On the short wavelength side, the increase in penalty could be due to

imperfect cancellation of the average refractive index of the grating by the double exposure method [20], resulting in a residual side lobe which could not be resolved by the amplitude transfer function measurement. Indeed, the group delay curve shown in Figure 2.13 does not exhibit the expected local maximum found at the edge of the transfer function which can be seen in other Gaussian apodised grating reflectivity transfer functions such as in Figure 2.14, or the modelled response of Figure 3.12. Instead, a noise-like behaviour is observed, which could be due to averaging of fast varying spectral features by the phase-shift measurement, as described in Section 2.5.2. Both the observed increase in penalty and the imperfect group delay characterisation hint at the existence of grating imperfections such as a non-resolved side lobe in this wavelength range. The smaller penalty extremum around 1551.95 nm is due to the combined effect of the amplitude transfer function and the dispersion. A secondary zero-dispersion wavelength is measured at 1552 nm, resulting in an improvement of the penalty before it increases again, as expected, towards the pass-band edge. A plateau is observed in the penalty curve around 1551.6 nm, which corresponds to a wavelength region where the attenuation is uniform and where the measured group delay presents a local extremum, corresponding to zero dispersion. The measured negative penalty compared to the back-to-back case observed at some wavelengths is due to filtering of amplified spontaneous emission (ASE) noise by the grating, as well as to some degree of pulse reshaping due to low-pass filtering at the edges of the pass-band.

Therefore, due to grating imperfections, the usable bandwidth of the grating for a 1 dB absolute penalty tolerance is limited to 0.7 nm corresponding to 87 GHz. If the minimum measured penalty is taken as a reference instead, this bandwidth slightly decreases to 0.6 nm (75 GHz). Those two values should be related to the FWHM bandwidth of the device equal to 0.57 nm or 71 GHz.

The power penalty has also been measured as a function of wavelength for the 50 GHz Gaussian apodised grating. The corresponding results are shown in Figure 3.5. Similarly to the case of the 100 GHz device, a local penalty maximum equal to 1.5 dB is observed in the pass-band at long wavelengths, this time well within the 3 dB bandwidth. The bandwidth allowing for 1 dB penalty is limited by this local extremum and is equal to 0.23 nm corresponding to 28 GHz. If a 3 dB penalty can be tolerated, this usable bandwidth can be extended to 0.33 nm or 41 GHz. Again, those two values need to be compared to the filter 3 dB bandwidth, which is 0.35 nm (43 GHz). Contrary to the 100 GHz device, no significant raise in penalty is observed on the short wavelength side. If the local penalty

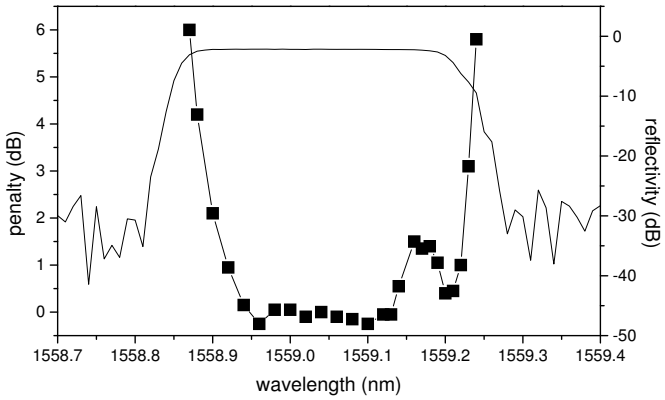

Figure 3.5 Penalty as a function of wavelength for a 10 Gbit/s NRZ signal reflected by a fibre Bragg grating filter designed for 50 GHz channel spacing.

maximum is ignored, and even though the amplitude transfer function is relatively symmetric with respect to its centre frequency, the penalty curve is fairly asymmetric, in contrast with what was observed for the 100 GHz grating. For instance, a penalty of about 6 dB is measured at a detuning corresponding to an attenuation of 0.9 dB on the short wavelength side of the transfer function, against 7.5 dB for long wavelengths. The amplitude transfer function alone cannot therefore account for the measured power penalty, but the combined effects of amplitude and phase filtering need to be considered. The asymmetry in the group delay curve of Figure 2.14, resulting in different dispersion behaviours at short and long wavelengths should therefore be invoked in order to explain the measured penalty. An experimental investigation of the cascadability of the device will be reported in Section 3.2.2 and will enable to establish a link between the penalty curves and the dispersive properties of this particular 50 GHz grating.

It has therefore been shown that grating imperfections are responsible for narrowing the usable bandwidth of fibre gratings designed to be used in DWDM systems with 50 and 100 GHz channel spacing. Some of those imperfections are believed to be due to the writing process of the grating by double exposure and could consequently be suppressed by a better control of the method or by the use of alternative techniques. For a 1 dB penalty criterion, the usable bandwidth of the filter has been shown to be 120% of its FWHM bandwidth for the 100 GHz grating against only 65% for the 50 GHz device. However, it should be noticed that the bandwidth of the filters considered in this study do not scale proportionally to the channel spacing. The bandwidth utilisation factor, defined here as the ratio of

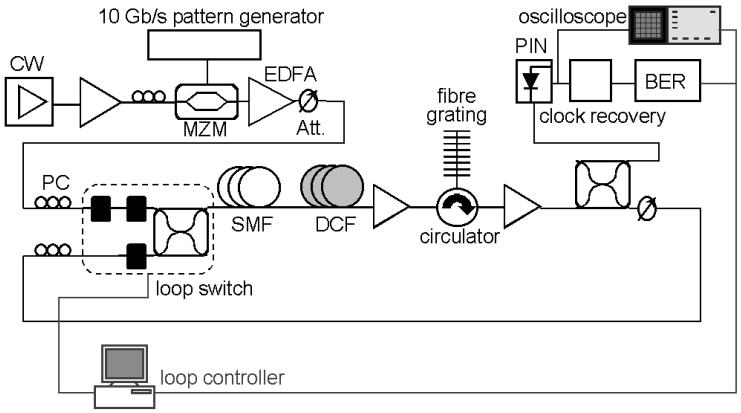

Figure 3.6 Re-circulating loop set-up for the investigation of the cascadability of 50 GHz Gaussian apodised fibre Bragg gratings. CW: continuous wave laser; MZM: Mach-Zehnder modulator; PC: polarisation controller; SMF: standard single mode fibre; DCF: dispersion compensating fibre; PIN: lightwave converter; BER: bit-error-rate analyser.

the filter 3 dB bandwidth to the channel spacing, is equal to 0.71 for the 100 GHz grating against 0.86 for the 50 GHz device. This is simply due to the fact that the filter bandwidth needs to be kept sufficiently large to accommodate a signal at a given bit-rate, here 10 Gbit/s, even though the channel spacing is decreased. Another important consideration is the steepness of the slopes of the transfer function, which can be characterised by a figure of merit defined as the ratio of the 0.5 dB bandwidth of the filter to its 25 dB bandwidth [22], resulting in values of 0.52 for the 100 GHz filter against 0.69 for the 50 GHz grating. Therefore, the low pass filtering due to the amplitude transfer function alone is expected to be more pronounced in the 50 GHz case. This, in conjunction with higher dispersion at the edges of the pass-band (which might itself be related to the slope steepness in case it can be shown the real grating is minimum-phase), explains the reduction of the usable bandwidth when going from the 100 GHz to the 50 GHz filter.

3.2.2 Cascadability of grating filters for 50 GHz channel spacing

It has been shown in Section 3.2.1 that the amplitude transfer function of the 50 GHz grating alone does not account for all the observed system impairments but that its phase needs to be taken into consideration. How-

ever, due to the relatively small dispersion values in the pass-band of the grating, the effect of the phase is difficult to quantify. Its influence can be artificially increased by cascading a number of identical transfer functions in a re-circulating loop, which is the topic of the present section. Furthermore, such an experiment enables to emulate the propagation of a signal in a more complex network where it would be reflected by a number of gratings with strictly identical transfer functions. Although the validity of the last statement is questionable, due to non perfectly reproducible transfer functions or slight detuning of the gratings, such re-circulating loop experiments enable to make a worst-case estimate of the signal degradation induced by multiple reflection by narrow-band fibre grating filters.

The experimental set-up is shown in Figure 3.6. Light generated by an external cavity tunable laser is amplified by an erbium-doped fibre amplifier (EDFA) before being modulated at 10 Gbit/s in a dual drive Mach-Zehnder modulator operated in push-pull mode resulting in chirp-free operation. Only the NRZ modulation format is considered in this experiment where all the measurements have been performed with a $2^{31} - 1$ PRBS word length. The signal is then amplified again before being input to a re-circulating loop switch consisting of a coupler and three acousto-optic modulators. Re-circulating loop operation is possible only if the delay in the loop is long enough to store a sufficiently large amount of data to enable BER measurements. As a consequence, some length of optical fibre is required in the loop, even though only the filtering induced degradation is of interest here. A length of 44 km of standard single mode fibre (SMF) followed by a matching length of 6 km of wideband dispersion compensating fibre (DCF) was inserted in the loop. It was ensured that no penalty was induced by the fibre itself. As we shall see, this was made possible because the cascadability of the grating under test was limited to up to 5 round-trips, resulting in little accumulated dispersion due to the fibre itself in the wavelength range corresponding to the pass-band of the grating. The residual dispersion of the compensated SMF span was only -0.35 ps/nm at 1559 nm. Moreover, the power at the SMF input was kept to a level of 0 dBm, ensuring that spectral broadening due to self-phase modulation would not affect the measurement. After the fibre, the signal was input to the grating under test via a three-port optical circulator. The light reflected from the grating was then amplified by an erbium doped fibre amplifier (EDFA) in order to compensate for the loss accumulated in the fibre span as well as the loop switch. Part of the signal was tapped to the receiver after each round trip by a 10 dB coupler. The receiver consists of a lightwave converter with 11 GHz bandwidth followed by a 18 GHz

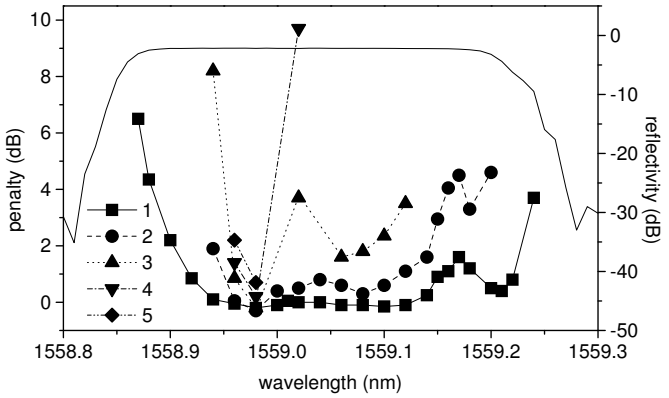

Figure 3.7 Penalty as a function of wavelength for a 10 Gbit/s NRZ signal reflected by a cascade of 1 to 6 fibre Bragg grating filters designed for 50 GHz channel spacing.

broadband electrical amplifier as well as a clock-recovery circuit. Practical details of the loop set-up configuration used in this experiment can be found in [23].

The 25 mm long Gaussian apodised grating with 43 GHz bandwidth whose amplitude and group delay transfer functions are shown in Figure 2.14 has been cascaded in the re-circulating loop set-up described above. For each number of cascade, the sensitivity at a bit-error-rate of 1.0×10^{-9} was measured and compared to the back-to-back sensitivity. The resulting penalty curves obtained with a NRZ signal extinction ratio of 13 dB are shown in Figure 3.7. The back-to-back sensitivity, obtained when the optical attenuator following the booster amplifier at the modulator output was directly connected to the receiver, was measured to be -16.7 dBm. The penalty curve measured in the loop configuration after one single grating filter matches the one obtained in the corresponding straight line experiment, which is shown in Figure 3.5. This confirms the negligible signal degradation induced in the dispersion and dispersion slope compensated fibre span. As expected, it can be seen that the usable bandwidth of the grating is reduced when the number of cascades increases. However, this reduction is not symmetrical with respect to the grating centre wavelength. Cascading the grating while minimising the penalty is possible at the wavelength of 1558.98 nm, which corresponds to an extremum of the group delay and therefore zero dispersion. However, no more than 5 cascades could be achieved with finite penalty for this device. The low-penalty window is deported to the short wavelength side of the pass-band because of the

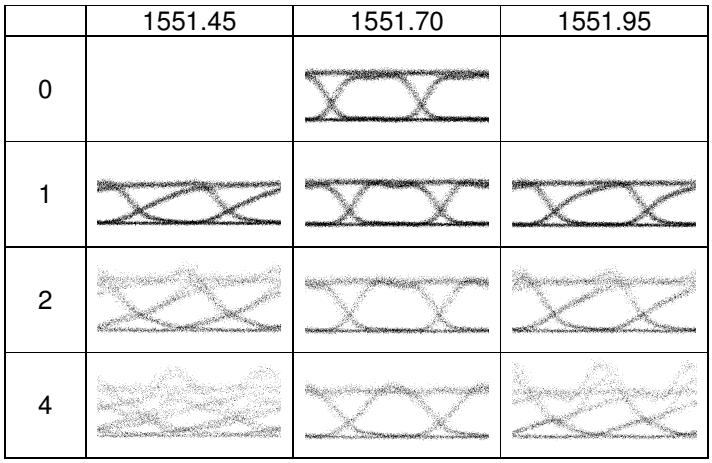

Figure 3.8 Eye diagrams as a function of wavelength detuning after 1, 2 and 4 cascades of the fibre Bragg grating designed for 100 GHz channel spacing illustrated in Figure 3.5. The back-to-back eye diagram is also represented for comparison. Horizontal scale: 20 ps/division.

asymmetry of the grating complex transfer function. This asymmetry is attributed to imperfections in the two exposure technique used to create the apodisation profile. The combination of phase and amplitude filtering is also responsible for a higher penalty area centered around 1559.17 nm. It is clearly seen in Figure 3.7 that the effect of imperfections in the grating complex transfer function on the measured penalty is amplified when the number of cascades is increased. This enables to establish that the dispersion of the device is responsible for narrowing the usable bandwidth of the grating when it is cascaded, as well as for shifting its optimum operation wavelength towards the short wavelength side of its pass-band. In a real network configuration, the transfer functions of the individual gratings encountered in a particular path would not be strictly identical and some degree of averaging would be expected.

In order to confirm the different behaviours of the gratings designed for 50 and 100 GHz channel spacings, eye diagrams were recorded on a 30 GHz sampling oscilloscope for different values of the detuning between the transmitter wavelength and the centre wavelength of the grating. The evolution of the eye diagram when the number of cascaded devices is increased from 1 to 4 is shown in Figure 3.8 for the 100 GHz device. At the grating centre wavelength (1551.70 nm) very little eye degradation is ob-

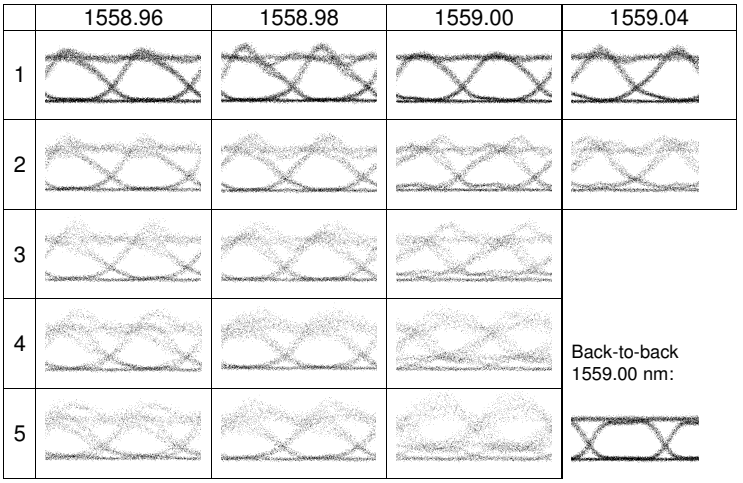

Figure 3.9 Eye diagrams as a function of wavelength detuning after 1 to 5 cascades of the fibre Bragg grating designed for 50 GHz channel spacing illustrated in Figure 3.7. The back-to-back eye diagrams is also represented for comparison. Horizontal scale: 20 ps/division.

served, whereas some low pass filtering effects are observed for both positive and negative detuning. It appears from the eye diagrams that the observed distortion is more severe for negative wavelength detuning, confirming the higher penalty ripple visible in Figure 3.4 for those wavelengths. When the number of cascaded filters is increased, the eye starts getting distorted even at the centre wavelength due to pass-band narrowing, but remains symmetrical with respect to the centre of the time slot, which is an indication that the signal is not significantly affected by the non-uniform dispersion of the filter.

Equivalent eye diagrams obtained with the 50 GHz grating are shown in Figure 3.9. It can be seen that for one single grating the less distorted eye is obtained at 1559.00 nm whereas, when the grating is cascaded the benefit of using the zero dispersion wavelength around 1558.98 nm becomes apparent. Even with a single filter, some reshaping of the 10 Gbit/s NRZ eye is observed, due to the narrow bandwidth of the grating. In case of an ideal grating with a symmetrical amplitude transfer function and antisymmetrical dispersion around the centre frequency, the eye diagrams obtained for the same absolute value of positive and negative detuning are expected to be identical. This is not observed here when moving ± 0.02 nm away from the wavelength of 1558.98 nm corresponding to zero-dispersion, as the mea-

sured group delay curve is not symmetrical around this wavelength, which furthermore does not coincide with the centre of the pass-band of the grating. For wavelengths well into the pass-band (e.g. 1559.00 nm), the eye diagrams are asymmetric with respect to the centre of the time slot, which is a signature of the influence of dispersion as well as excessive low-pass filtering due to the narrow bandwidth of the filter.

We have therefore demonstrated experimentally the limitations of Gaussian apodised fibre Bragg gratings designed for WDM systems with 100 and 50 GHz channel spacing. Imperfections in the grating writing process by the double exposure technique are believed to be responsible for penalty ripples resulting in a reduced usable bandwidth for the 100 GHz grating. Dispersion has been shown to be the main source for system impairments when the narrow bandwidth grating designed for a 50 GHz channel spacing system is used. These limitations can be overcome by novel grating writing methods and designs, as discussed more in depth in Appendix C, as well as by the use of modulation formats more resilient to group-velocity dispersion, as we shall see in the following section.

3.3 Influence of grating dispersion on duobinary modulation

The bandwidth of WDM systems is limited to the low loss region of optical fibres and to the wavelength range where fibre doped optical amplifiers are available. This sets a strong limitation to the number of channels that can be used. The channel density, known as spectral efficiency (in bit/s/Hz), is limited by degradation due to linear cross-talk, as well as optical fibre non-linearities. Higher spectral efficiencies can be achieved by making use of novel modulation formats with reduced bandwidth, so that the frequency spacing of WDM channels can be reduced and the capacity in a given bandwidth increased. The use of optical duobinary modulation [24], which offers a reduction of the spectral bandwidth compared to conventional binary NRZ modulation, has been suggested, first in order to overcome chromatic dispersion limits in optical fibres, but also to increase the spectral efficiency.

However, reducing the frequency spacing between WDM channels means that narrow-band optical filters will be required to perform the (de) multiplexing operation. This is likely to induce more stringent detuning tolerances between the laser wavelength and the filter centre frequency, especially since the dispersion of grating filters is expected to increase when their bandwidth is reduced.

In this section, the effect of filtering by narrow-band (50 GHz) Gaussian

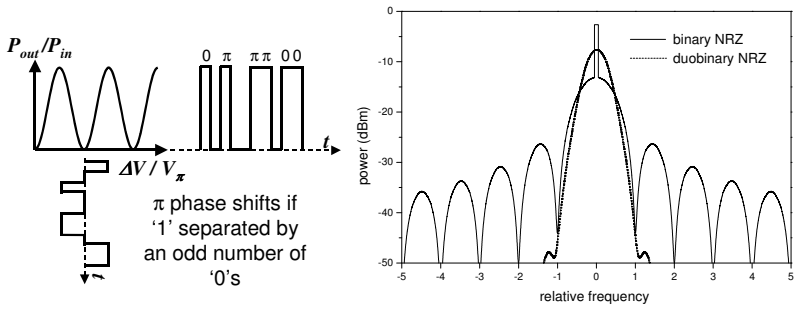

Figure 3.10 Principle of optical duobinary modulation converting a three-level electrical signal to a two-level optical signal with π phase shifts (left) and resulting duobinary NRZ spectrum compared to conventional binary NRZ (right). The spectra are plotted for the same average power as a function of frequency normalised to the bit-rate B (resolution bandwidth 1/10).

apodised fibre grating is compared numerically at 10 Gbit/s for NRZ binary and duobinary modulations. It is shown that duobinary allows a larger filter detuning tolerance in reflection as well as closer channel spacing due to out-of-band dispersion limitations when the grating is used in transmission. This improved performance should alleviate the severe cascadability limitations demonstrated in Section 3.2.

3.3.1 Description of the models

Optical duobinary modulation is obtained by applying a three-level electrical signal to a Mach-Zehnder modulator biased at a null transmission point as illustrated in Figure 3.10. The three-level electrical data is obtained by duobinary encoding the pre-coded NRZ signal to be transmitted. The duobinary encoding operation can be realised by a delay-and-add circuit whose transfer function can be approximated by a low pass-filter with cut-off frequency equal to one quarter of the bit-rate. This latter scheme is traditionally implemented with linear-phase Bessel filters and results in ripples in the "zero" bits which have been shown to be effective at maintaining the "one" bits in their time slot when subjected to group velocity dispersion [25]. The three-level electrical signal is then converted into a two level intensity modulated optical signal with phase shifts of π between consecutive "marks" provided they are separated by an odd number of "spaces". The resulting spectrum is also shown in Figure 3.10 where it is compared to the conventional binary NRZ case. A significant reduction of the width of the main lobe is observed for duobinary modulation. At 10 Gbit/s, the 20 dB

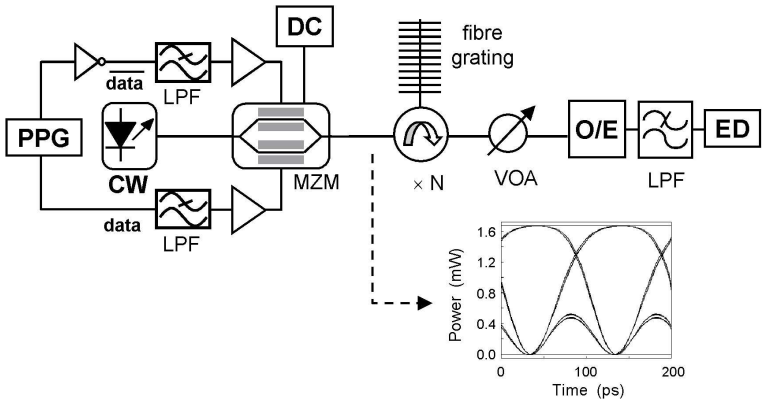

Figure 3.11 Simulation set-up for the investigation of the cascadability of fibre gratings using NRZ and duobinary NRZ modulation. PPG: pulse pattern generator; CW: continuous wave laser; LPF: electrical low-pass filter; DC: modulator bias power supply; MZM: Mach-Zehnder modulator; VOA: variable optical attenuator; O/E: photodetector; ED: error detector.

bandwidth of the spectrum is equal to 18.3 GHz for binary NRZ against only 14.3 GHz for duobinary. Furthermore, the level of the side lobes is considerably reduced in the duobinary spectrum. This narrower spectral bandwidth has enabled to improve the dispersion limit of optical fibre by transmitting over 243 km SMF at 10 Gbit/s [26], as well as to achieve a record spectral efficiency of 1 bit/s/Hz at 20 Gbit/s [27]. Moreover, one of the practical benefits of the optical duobinary modulation scheme is that it is compatible with conventional direct detection receivers. More details on optical duobinary signal generation and transmission can be found for instance in [28, 29].

The simulation set-up used for the filtering tolerance investigation of duobinary signals is shown in Figure 3.11. The duobinary transmitter consists of a CW laser externally modulated by a Mach-Zehnder modulator operated in push-pull mode. The duobinary encoding is performed by filtering the $2^{10}-1$ pseudo random NRZ 10 Gbit/s sequence with a fifth order low-pass Bessel filter with 3 dB cut-off frequency equal to 2.8 GHz. This operation is performed on both the data and inverted data so that chirp-free operation of the modulator is obtained. The eye diagram of the 10 Gbit/s duobinary modulated signal is shown as an inset in Figure 3.11. The presence of ripples in the "spaces", due to the narrow bandwidth low-pass filtering of the NRZ data, is clearly visible. The optical duobinary signal is input to a cascade of N identical fibre grating filters, either in transmission or in reflection. The lightwave is then detected in a photodiode with respon-

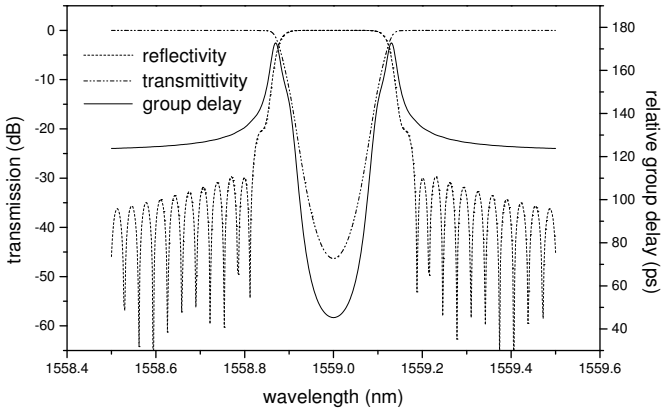

Figure 3.12 Calculated transfer function (reflectivity, transmittivity and group delay) of a Gaussian apodised fibre Bragg grating designed for 50 GHz channel spacing. This transfer function was generated using a commercial grating design software package (IFO gratings; transfer function generated at Ibsen Photonics) and was used for the numerical investigations reported in Section 3.3.2.

sivity of 1.2 A/W (corresponding to 96% quantum efficiency at 1550 nm) and single sided thermal noise density of 15 pA/$\sqrt{\text{Hz}}$, before being filtered by a 4$^{\text{th}}$ order Bessel low-pass filter with 7.5 GHz cut-off frequency. The bit-error-rate is calculated according to the technique taking inter-symbol interference into account described in Appendix D. This calculation is performed by comparing the received data to the inverted transmitted sequence, in accordance with the principles of duobinary transmission. No pre-coder implementation is necessary due to the fact that a shift-register pseudo-random sequence is used in this investigation, meaning that the inverted received data is expected to be a time shifted replica of the transmitted sequence. An identical simulation set-up is used for binary NRZ modulation investigation, apart from the fact that the electrical signals driving the modulator are no longer low-pass filtered at one quarter of the bit-rate, and that the received data is simply compared to the transmitted sequence for BER evaluation. When connecting directly the transmitter and receiver configurations described above, a back-to-back sensitivity of -20.2 dBm is calculated for duobinary NRZ, against -21.7 dBm in the binary case (both at a bit-error-rate of 1.0×10^{-9}). The poorer back-to-back sensitivity obtained for duobinary is in agreement with previous observations [28] and is due to the presence of energy in the "zero" bits caused by low-pass filtering of the electrical signal.

A Gaussian apodised fibre grating designed for 50 GHz channel spac-

ing WDM systems has been modelled using the transfer matrix appoach[2]. The design parameters of the grating were chosen in order to match those of the corresponding fabricated device used in the experimental investigations reported in Section 3.2. The calculated reflectivity, transmittivity and group delay are shown in Figure 3.12 and should be compared to the measured complex transfer function from Figure 2.14. In order to ease the comparison, a number of relevant parameters have been extracted from the measured and calculated complex transfer functions in reflection and in transmission and are summarised in Table 3.2. Two parameters have been introduced to enable a comparison between the calculated group delay and the measured group delay of the imperfect real grating. $\Delta\tau_{max}$ is defined as the difference between the maximum and the minimum group delay in the pass-band, whereas Δf_{max} is the frequency separation between the local maxima of the group delay at both edges of the pass-band. It can be seen from Table 3.2 that a reasonably good agreement is obtained between the fabricated and modelled grating properties, especially since the model does not take imperfections of the writing process into account. The grating structure being symmetric, the group delay is identical in transmission and in reflection, as demonstrated in Appendix B.

Parameter	Real grating	Modelled grating
3 dB bandwidth (GHz)	43	30.6
20 dB bandwidth (GHz)	54	39
Cross-talk (dB)	25	30
Rejection$^{(1)}$ (dB)	60	45
$\Delta\tau_{max}$ $^{(2)}$(ps)	131	130
Δf_{max} $^{(2)}$(GHz)	46.9	30.8

Table 3.2 Comparison of selected properties of the modelled grating used in the numerical investigations of Section 3.3 and the real device used in the experiments reported in Section 3.2. (1) Rejection denotes the attenuation at the centre of the stop-band in transmission. (2) The parameters $\Delta\tau_{max}$ and Δf_{max} have been introduced in order to enable a comparison between the calculated and measured group delay (see text).

[2]The device was modelled by Morten Johansen from Ibsen Photonics using the commercial IFO Gratings software package from Optiwave Corporation, Ottawa, Ontario, Canada.

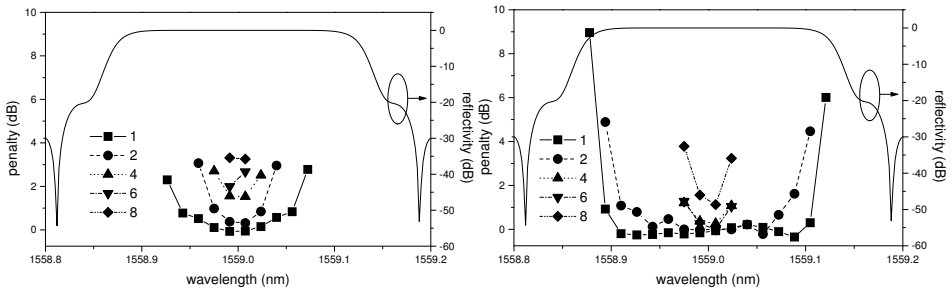

Figure 3.13 Calculated penalty as a function of wavelength for one single grating and a cascade of 2, 4, 6 and 8 identical devices used in reflection. Left: binary NRZ; right: duobinary NRZ.

3.3.2 Filtering of binary and duobinary NRZ signals

The cascadability of the narrow band grating whose transfer function is shown in Figure 3.12 has been assessed numerically for both binary and duobinary NRZ modulation at 10 Gbit/s. The transmitter wavelength has been swept across the pass-band of the device used in reflection or on both sides of the stop-band when the grating was operated in transmission. For each value of the detuning between the laser and the grating centre frequency, the penalty at a BER of 1.0×10^{-9} was calculated for a single device as well as for a cascade of up to 12 filters. In all cases the grating transfer functions are assumed to be strictly identical and perfectly aligned.

The results obtained when the grating is used in reflection are shown in Figure 3.13. Even when a single grating is used, the usable bandwidth of the filter is significantly larger for duobinary compared to binary modulation. For instance, if one allows for 1 dB power penalty, a detuning of ±13 GHz away from the grating centre frequency is allowed for duobinary, against only ±7 GHz for binary NRZ. As expected, a reduction of the usable bandwidth is observed when the number of cascaded filters is increased. After two gratings the detuning tolerance is still ±10 GHz for duobinary while it has been drastically reduced down to ±3 GHz for binary modulation. This larger tolerance towards laser misalignment can be attributed to the better dispersion tolerance of the duobinary modulation. At the same time, the power penalty at the grating centre frequency degrades much faster in the binary case. This is confirmed in Figure 3.14 where the calculated sensitivity is plotted as a function of the number of cascaded filters when the transmitter is tuned to the grating centre wavelength. As stated earlier, the higher back-to-back sensitivity observed for duobinary is

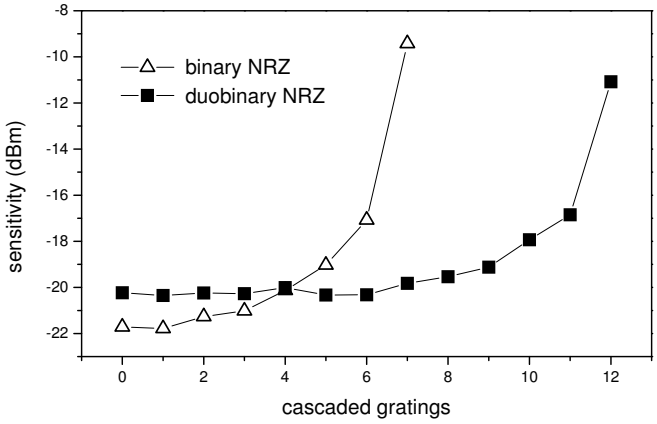

Figure 3.14 Calculated sensitivity as a function of number of cascaded gratings for binary and duobinary NRZ modulation. The transmitter wavelength is assumed to be tuned exactly to the centre of the pass-band of the grating whose transfer function is shown in Figure 3.12.

due to the presence of amplitude ripples caused by low-pass filtering of the NRZ data in order to generate the three-level duobinary encoded signal. However, when the number of cascaded filters is increased, the sensitivity of the duobinary signal becomes lower than the one calculated in the binary case. For a 3 dB power penalty (with respect to back-to-back), up to 5 gratings can be cascaded for binary against 10 for duobinary.

When fibre gratings are used in optical add-drop multiplexer structures such as the ones making use of optical circulators or a Mach-Zehnder interferometer configuration, the channels that are not dropped are expected to propagate unaffected by the grating. However, it has been shown in Section 2.6.4 that some amount of dispersion is present on both sides of the stop-band of a grating used in transmission. The effect of this out-of-band dispersion has also been evaluated numerically for both binary and duobinary NRZ modulation. The results are shown in Figure 3.15 for a single grating as well as for a cascade of 4, 8 and 12 identical and perfectly aligned filters designed to reject (or drop) the channel at the wavelength of $\lambda_0 = 1559.00$ nm. If a 1 dB penalty due to phase and amplitude filtering is acceptable for the channel which is the closest in wavelength to the dropped one, the channel spacing has to be at least 18 GHz for binary NRZ modulation if a single grating designed to drop the channel at λ_0 is encountered in the transmission path. When duobinary NRZ modulation is used, a close value of 17 GHz is found. However, when more than one grating with stop-band centred at λ_0 is present in the link, the channel spacing for the

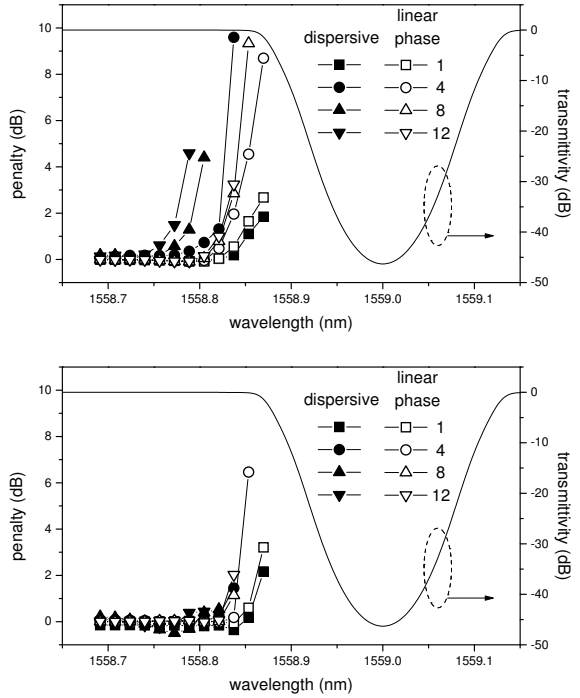

Figure 3.15 Simulated effect of out-of-band dispersion for a Gaussian apodised fibre grating designed for 50 GHz channel spacing. The power penalty is calculated as a function of wavelength for transmission through a single grating and a cascade of 4, 8 and 12 identical and perfectly aligned devices. Penalty curves for an hypothetical linear-phase grating are also shown for comparison. Top: binary NRZ; bottom: duobinary NRZ.

same tolerance criterion of 1 dB penalty needs to be increased for binary modulation up to 23 GHz or even 27 GHz for 4 and 8 devices, respectively. In the duobinary case, a channel spacing of 21 GHz is still allowed, even after 4 filters.

The minimum channel spacing that can be used with this narrow-band grating design is determined by the amplitude and phase filtering in transmission, but also by the cross-talk induced to the selected channel at λ_0 in reflection. A channel spacing of 21 GHz would mean that the closest neighbour to the channel at λ_0 would be suppressed by only 21 dB, which might prove insufficient, especially since the wavelength corresponding to such a detuning still lies in the pass-band of the reflection spectrum. Typical values of adjacent and non-adjacent channel cross-talk often cited are of the order of -25 and -30 dB, respectively, but have not been standardised

yet [30]. It is not clear how a cross-talk value of -21 dB would affect the quality of the signal of interest in a real network as this depends on the network topology, number of cross-talk contributions, sequence of channel added and dropped at the different nodes, power of the cross-talk contributions, etc. Such a study is beyond the scope of the present chapter which focuses solely on filtering induced degradations. Nevertheless, it appears that for the Gaussian apodised fibre grating studied here, the minimum channel spacing will be set by the adjacent channel cross-talk in reflection and not by the out-of-band dispersion in transmission.

It is also of interest to identify whether the limitation to the channel spacing induced by filtering effects alone is due to the low-pass attenuation experienced by a signal at the edges of the grating stop-band, or by its out-of-band dispersion. For this purpose, the penalty as a function of frequency detuning has also ben calculated for an hypothetical linear phase (i.e. dispersion-free) grating whose amplitude transfer function (both in transmission and in reflection) is the same as the one of the narrow-band grating considered throughout this section. The results are shown in Figure 3.15 where they can directly be compared to the behaviour observed for the dispersive grating where both amplitude and phase filtering are considered. No significant benefit is observed in the linear-phase case when one single filter is considered. However, when several identical gratings are cascaded, the hypothetical dispersion-free device would allow a closer channel separation for binary NRZ modulation. On the other hand, very little improvement is observed for duobinary modulation. It is therefore demonstrated that, provided only filtering effects are considered, it is the out-of-band dispersion which limits the channel spacing when conventional binary NRZ modulation is used. Duobinary modulated signals benefit from their narrower spectral width, which simultaneously allows them to be placed closer to the edges of the stop-band without cutting off too much of their high frequency content, as well as not to suffer as much from dispersion as binary NRZ signals. The fact that the use of a linear-phase filter would only result in marginal improvement confirms the resilience of the duobinary format to the non-uniform dispersion present at the edges of the stop-band of optical filters.

We have therefore shown that the duobinary NRZ modulation format presents better filter detuning tolerance at 10 Gbit/s than the commonly used binary NRZ format. This is even more pronounced when several gratings with narrow bandwidth ($\sim$ 30 GHz) are cascaded in a link, as could be a common scenario in future complex meshed networks structures making use of wavelength routing. The better tolerance of the duobinary

format to group-velocity dispersion is believed to be responsible for the observed improvement. If only amplitude and phase filtering is considered, the out-of-band dispersion of fibre gratings has been shown to limit the channel spacing when binary NRZ modulation is used, while its influence was reduced in the case of duobinary modulation. Even though the improved dispersion tolerance of duobinary had already been demonstrated for transmission over optical fibre, those investigations had focussed on transmission media where the dispersion can be considered uniform over the spectral width of the signal. However this is no longer the case in dispersive optical filters such as fibre Bragg gratings, especially at the edges of their pass-band. The duobinary modulation scheme relying on π phase shifts to differentiate the "one" levels, its tolerance towards non-uniform dispersion in grating filters had to be assessed. It can therefore be concluded that, in spite of the non-uniform dispersion of grating filters, the duobinary format is more robust to filtering than NRZ modulation.

Apart from optical duobinary, a number of other modulation formats such as carrier-suppressed return-to-zero (CS-RZ) [31] or optical single sideband (SSB) [32] have been recently proposed in order to alleviate the dispersion or non-linearities induced limitations in optical fibre links, as well as to enable closer channel packing leading to higher spectral efficiencies in dense WDM systems. Moreover, some novel apodisation profile designs have also been recently suggested in order to reduce the dispersion in the pass-band of fibre gratings [33, 34]. A recent experimental study of the resilience of those different modulation formats towards filtering by a low dispersion fibre Bragg grating with high detuning tolerance is presented as a complement to the present chapter and can be found in Appendix C.

3.4 Summary of Chapter 3

The influence of fibre Bragg gratings dispersion on the performance of 10 Gbit/s systems has been investigated numerically and experimentally, with emphasis on the accumulation of filtering degradation along a particular path in an optical network where several devices would be cascaded. We have shown that, for ideal gratings transfer functions, dispersion becomes an issue for filters designed for channel spacings smaller than 50 GHz, and that Blackman apodisation should be preferred over Gaussian and Hamming apodisations, as it simultaneously offers relatively better detuning tolerance for very narrow channel spacing (25 GHz) systems, as well as good cross-talk performance when used in reflection.

The system performance of Gaussian apodised fibre Bragg gratings de-

signed for 100 and 50 GHz channel spacing has been compared experimentally. Grating imperfections believed to be induced by the writing process have been found to induce penalty ripples in the pass-band of the 100 GHz device. Although small (less than 1 dB), those penalty ripples might result in a limitation of the usable bandwidth of the device when cascaded in a network.

The reduction of the usable bandwidth induced by the dispersion of fibre Bragg gratings designed for narrow channel spacings (∼50 GHz) WDM systems has been demonstrated experimentally. Re-circulating loop experiments have been used to prove that, after only five cascaded devices, the usable bandwidth of such a filter is limited to only a small fraction of its 3 dB bandwidth centered around a wavelength corresponding to zero dispersion. Furthermore, the wavelength range over which the device can be operated has been found to be shifted away from its centre frequency when the number of cascaded filters is increased. Therefore, filter dispersion has been clearly identified as the main source of penalty for 50 GHz Gaussian apodised gratings written using the conventional double exposure technique.

As a consequence, new directions should be explored in order to alleviate those dispersion induced limitations in fibre Bragg gratings. Those include a better control of the grating writing process, new grating designs with lower dispersion in the pass-band, and the use of modulation formats with narrower bandwidths known to offer better resilience to group-velocity dispersion. Using numerical simulation, we have shown that, even in the case of non-uniform dispersion of the gratings, the duobinary modulation format is more tolerant towards filtering effects than the usual NRZ format. It therefore results in better tolerances towards laser misalignment, which is a critical issue in the design of high spectral efficiency WDM systems. The system performance of a novel low dispersion fibre Bragg grating practical design has also been presented in Appendix C. Its detuning tolerance has been investigated experimentally for five modulation formats at 10 Gbit/s, showing a bandwidth utilisation above 89% in all cases. Good performance was predicted numerically at 40 Gbit/s.

In case optical communication systems with high spectral efficiencies are designed, it is therefore essential to take into account the properties of the filtering elements present in the link or network path, and not only the non-linear interaction in the fibre. The foreseen evolution of optical systems from point-to-point links towards transparent optical networks with an increasing number of cross-connects or add-drop nodes along the path makes this requirement even more critical. This has been illustrated in this chap-

ter by emphasising the limitations of currently commercially available fibre grating devices designed for narrow channel spacing. However, it has also been shown in this chapter and Appendix C that the inherent dispersive limitations of fibre Bragg grating technology can be overcome by proper filter design, better fabrication methods as well as system considerations such as the choice of the modulation format. Close interaction between components and systems designers will ensure that one can make the most of the degrees of freedom offered by fibre Bragg grating technology.

3.5 References to Chapter 3

[1] K. O. Hill and G. Meltz, "Fiber Bragg grating technology fundamentals and overview", *Journal of Lightwave Technology*, vol. 15, no. 8, pp. 1263–1276, 1997.

[2] C. R. Giles, "Lightwave applications of fiber Bragg gratings", *Journal of Lightwave Technology*, vol. 15, no. 8, pp. 1391–1404, 1997.

[3] N. N. Khrais, F. Shehadeh, J.-C. Chiao, R. S. Vodhanel, and R. E. Wagner, "Multiplexer eye-closure penalties for 10 Gb/s signals in WDM networks", in *Technical Digest Optical Fiber Communication Conference, OFC'96*, San Jose, California, U.S.A., post-deadline paper PD33, 1996.

[4] C. Caspar, H.-M. Foisel, C. v. Helmolt, B. Strebel, and Y. Sugaya, "Comparison of cascadability performance of different types of commercially available wavelength (de)multiplexers", *Electronics Letters*, vol. 33, no. 19, pp. 1624–1626, 1997.

[5] M. Ibsen, H. Geiger, and R. I. Laming, "In-band dispersion limitations of uniform apodised fibre gratings", in *Proceedings European Conference on Optical Communication, ECOC'98*, Madrid, Spain, vol. 1, pp. 405–406, 1998.

[6] L. R. Chen and P. W. E. Smith, "Fibre Bragg grating transmission filters with near-ideal filter response", *Electronics Letters*, vol. 34, no. 21, pp. 2048–2050, 1998.

[7] M. Kuznetsov, N. M. Froberg, S. R. Henion, and K. A. Rauschenbach, "Power penalty for optical signals due to dispersion slope in WDM filter cascades", *IEEE Photonics Technology Letters*, vol. 11, no. 11, pp. 1411–1413, 1999.

[8] G. Nykolak, G. Lenz, B. J. Eggleton, and T. A. Strasser, "Impact of fiber grating dispersion on WDM system performance", in *Technical Digest Optical Fiber Communication Conference, OFC'98*, San Jose, California, U.S.A., paper TuA3, vol. 2, pp. 4–5, 1998.

[9] G. Nykolak, B. J. Eggleton, G. Lenz, and T. A. Strasser, "Dispersion penalty measurements of narrow fiber Bragg gratings at 10 Gb/s", *IEEE Photonics Technology Letters*, vol. 10, no. 9, pp. 1319–1321, 1998.

[10] G. Lenz, G. Nykolak, and B. J. Eggleton, "Dispersion of optical filters in WDM systems: theory and experiment", in *Proceedings European Conference on Optical Communication, ECOC'98*, Madrid, Spain, vol. 1, pp. 271–272, 1998.

[11] H. Bock, P. Leisching, A. Richter, D. Stoll, and G. Fischer, "System impact of cascaded optical add/drop multiplexers based on tunable fiber Bragg gratings", in *Technical Digest Optical Fiber Communication Conference, OFC'00*, Baltimore, Maryland, U.S.A., vol. 2, pp. 296–298, 2000.

[12] P. Leisching, H. Bock, A. Richter, D. Stoll, and G. Fischer, "Optical add/drop multiplexer for dynamic channel routing", *Electronics Letters*, vol. 35, no. 7, pp. 591–592, 1999.

[13] M. Kuznetsov, N. M. Froberg, S. R. Henion, C. Reinke, C. Fennelly, and K. A. Rauschenbach, "Dispersion-induced power penalty in fiber-Bragg-grating WDM filter cascades", in *Technical Digest Optical Fiber Communication Conference, OFC'00*, Baltimore, Maryland, U.S.A., vol. 2, pp. 311–313, 2000.

[14] B. J. Eggleton, G. Lenz, N. Litchinitser, D. B. Patterson, and R. E. Slusher, "Implications of fiber grating dispersion for WDM communication systems", *IEEE Photonics Technology Letters*, vol. 9, no. 10, pp. 1403–1405, 1997.

[15] N. M. Litchinitser, B. J. Eggleton, G. Lenz, and G. P. Agrawal, "Dispersion in cascaded-grating-based add/drop filters", in *Technical Digest Conference on Lasers and Electro-Optics, CLEO'98*, paper CTh015, vol. 6, pp. 395–396, 1998.

[16] N. M. Litchinitser, B. J. Eggleton, and G. P. Agrawal, "Dispersion of cascaded fiber gratings in WDM lightwave systems", *Journal of Lightwave Technology*, vol. 16, no. 8, pp. 1523–1529, 1998.

[17] H. Geiger and M. Ibsen, "Complexity limitations of optical networks from out-of-band dispersion of grating filters", in *Proceedings European Conference on Optical Communication, ECOC'98*, Madrid, Spain, vol. 1, pp. 405–406, 1998.

[18] L. Poladian, "Design constraints for wavelength-division-multiplexed filters with minimal side-channel impairment", *Optics Letters*, vol. 26, no. 1, pp. 7–9, 2001.

[19] T. Erdogan, "Fiber grating spectra", *Journal of Lightwave Technology*, vol. 15, no. 8, pp. 1277–1294, 1997.

[20] B. Malo, S. Thériault, D. C. Johnson, F. Bilodeau, J. Albert, and K. O. Hill, "Apodised in-fibre Bragg grating reflectors photoimprinted using a phase mask", *Electronics Letters*, vol. 31, no. 3, pp. 223–225, 1995.

[21] R. J. S. Pedersen and B. F. Jørgensen, "Impact of coherent crosstalk on usable bandwidth of a grating-MZI based OADM", *IEEE Photonics Technology Letters*, vol. 10, no. 4, pp. 558–560, 1998.

[22] B. Nyman, M. Farries, and C. Si, "Technology trends in dense WDM demultiplexers", *Optical Fiber Technology*, vol. 7, pp. 255–274, 2001.

[23] M. Nissov, *Long-haul optical transmission using distributed Raman amplification*. PhD thesis, Department of Electromagnetic Systems, Technical University of Denmark, Lyngby, Denmark, 1997.

[24] A. J. Price and N. L. Mercier, "Reduced bandwidth optical digital intensity modulation with improved chromatic dispersion tolerance", *Electronics Letters*, vol. 31, no. 1, pp. 58–59, 1995.

[25] D. Penninckx, M. Chbat, L. Pierre, and J.-P. Thiery, "The phase-shaped binary transmission (PBST): a new technique to transmit far beyond the chromatic dispersion limit", *IEEE Photonics Technology Letters*, vol. 9, no. 2, pp. 259–261, 1997.

[26] L. Pierre, J. Thiery, and D. Penninckx, "243 km, 10 Gbit/s transmission experiment through standard fibre and impact of sef-phase modulation using partial response scheme", *Electronics Letters*, vol. 32, no. 7, pp. 673–674, 1996.

[27] T. Ono and Y. Yano, "Key technologies for Terabit/s WDM systems with high spectral efficiency of over 1 bit/s/Hz", *IEEE Journal of Quantum Electronics*, vol. 34, no. 11, pp. 2080–2088, 1998.

[28] K. Yonenaga and S. Kuwano, "Dispersion-tolerant optical transmission system using duobinary transmitter and binary receiver", *Journal of Lightwave Technology*, vol. 15, no. 8, pp. 1530–1537, 1997.

[29] T. Ono, Y. Yano, K. Fukuchi, T. Ito, H. Yamazaki, M. Yamaguchi, and K. Emura, "Characteristics of optical duobinary signals in Terabit/s capacity, high-spectral efficiency WDM systems", *Journal of Lightwave Technology*, vol. 16, no. 5, pp. 788–797, 1998.

[30] ITU-T Recommendation G.671, *Transmission characteristics of optical components and subsystems*, International Telecommunications Union, Geneva, Switzerland, pre-published recommendation, 2002.

[31] Y. Miyamoto, A. Hirano, K. Yonenaga, A. Sano, H. Toba, K. Murata, and O. Mitomi, "320 Gbit/s (8×40 Gbit/s WDM transmission over 367-km zero-dispersion-flattened line with 120-km repeater spacing using carrier-suppressed return-to-zero pulse format", in *Technical Digest Optical Amplifiers and their Applications, OAA'99*, Nara, Japan, post-deadline paper PdP4, pp. PdP4–1/4, 1999.

[32] M. Sieben, J. Conradi, and D. E. Dodds, "Optical single sideband transmission at 10 Gb/s using only electrical dispersion compensation", *Journal of Lightwave Technology*, vol. 17, no. 10, pp. 1742–1749, 1999.

[33] M. Ibsen, R. Feced, P. Petropoulos, and M. N. Zervas, "99.9% reflectivity dispersion-less square-filter fibre Bragg gratings for high speed DWDM networks", in *Technical Digest Optical Fiber Communication Conference, OFC'00*, Baltimore, Maryland, U.S.A., post-deadline paper PD21, 2000.

[34] H.-J. Deyerl, N. Plougmann, J. B. D. Jensen, J. El-Bez, H. R. Sørensen, C. Peucheret, and M. Kristensen, "Low-dispersion fibre Bragg gratings written using the polarization control method", in *Proceedings European Conference on Optical Communication, ECOC'02*, Copenhagen, Denmark, paper 7.2.7, vol. 3, 2002.

Chapter 4

Pass-band flattened PHASARs for 40 Gbit/s systems

Dense wavelength division multiplexing (DWDM) is an effective and flexible technology to simultaneously provide routing, switching, protection and restoration functionalities, as well as capacity increase in optical networks. In order to be able to satisfy the ever increasing demand for bandwidth triggered by the exponential growth of data traffic, some technological breakthroughs are nevertheless required. Increasing the transmission capacity can be realised by exploring new wavelength windows, by increasing the individual channel line rate to 40 Gbit/s and above, by allowing closer channel spacing or by using a combination of those various techniques [1]. Ultimately, the goal will be to increase the spectral efficiency (in bit/s/Hz) to its highest possible limit. Although information theory predicts theoretical limits as high as 6-14 bit/s/Hz in fictitious systems free from degradation other than amplifier noise [2], various issues such as fibre non-linearities, chromatic and polarisation mode dispersion, practical implementation of multiplexing and demultiplexing, etc, have so far limited record spectral efficiencies to values below 1 bit/s/Hz without having to rely on polarisation multiplexing [3]. A lot of effort has been spent worldwide in order to demonstrate record unidirectional link capacities as high as 6.4 Tbit/s [4]. However, the focus has so far mostly been on transmission systems without networking functionalities.

One of the goals of the METEOR (MEtropolitan TErabit Optical Ring) project is to demonstrate a four node optical ring at 40 Gbit/s with potential capacity of more than 1 Tbit/s. Furthermore, the feasibility of DWDM

networking using non-return to zero (NRZ) modulation at 40 Gbit/s with less than 100 GHz channel spacing is being explored within this project. This demonstration relies on the realisation of pass-band flattened phased-array (PHASAR) multiplexers/demultiplexers [5, 6] using silica-on-silicon technology.

In the present chapter, the design of such devices and their system implications at 40 Gbit/s is reported. In Section 4.1, recent progress in high spectral efficiency systems as well as examples of 40 Gbit/s all-optical networking experiments are reported, together with an overview of previous work performed at 10 Gbit/s, dealing with the cascadability of PHASARs. Furthermore, the origin of dispersion in PHASAR devices is briefly discussed. Based on the assumption that linear-phase devices can be fabricated, numerical simulation results on two classes of ideal transfer functions are presented in Section 4.2, which will be used as references against which the real device designs will be compared. Two pass-band flattened PHASAR designs based on multi-mode interference (MMI) coupler and parabolic horn are briefly introduced in Section 4.3, followed by a detailed numerical investigation of their cascadability. The goal of this investigation is to assess the minimum multiplexer bandwidth resulting in acceptable penalty for a four node ring network corresponding to the METEOR demonstrator. The origin of signal degradation is discussed for the different designs, as well as their tolerance towards laser misalignment. Finally, we conclude by identifying the most promising PHASAR design for high spectral efficiency networking at 40 Gbit/s.

4.1 PHASARs for high spectral efficiency systems

In this section, some issues pertaining to high spectral efficiency systems are briefly presented, followed by a description of the few 40 Gbit/s networking experiments reported so far[1]. The origin of dispersion in PHASAR devices is discussed. Finally, experimental results on the cascadability of arrayed waveguide grating (de)multiplexer are reviewed.

4.1.1 High spectral efficiency systems issues and techniques

The bandwidth offered in the third transmission window (centred around 1550 nm) in silica optical fibres has long been thought of being inexhaustible. It has later on been realised that in order to match the ever

[1]This section describes the state-of-the-art as of December 2000, when the work was first reported.

increasing demand for capacity, some new transmission windows such as the L-band (1570-1610 nm, the use of which is now current practice) and the S-band (1480-1510 nm) needed to be explored. Taking into account that, even in extended bands, the available bandwidth is a finite quantity, as well as for system complexity and cost reasons, it is often desirable to obtain as much capacity as possible from a given bandwidth. This can be done by increasing the spectral efficiency of the system by either upgrading individual WDM channels to higher bit rates or by reducing the channel spacing. For a given line rate, the channel density is limited by the spectral width of each channel and therefore one of the current engineering challenges consists in finding the best trade-off that will result in a significant increase of the total capacity in a given bandwidth. This can be achieved by using modulation formats with reduced spectral widths compared to conventional binary NRZ signals [1]. For instance, the highest spectral efficiency reported so far of 1 bit/s/Hz [3] has been obtained using duobinary modulation together with orthogonal polarisation launch of adjacent channels at 20 Gbit/s. The robustness of the duobinary code to narrow band filtering has also been shown to result in increased spectral efficiencies [7]. However, in many cases it is desirable to use well proven modulation techniques to achieve similar goals. Over a period of one year (September 1999 to September 2000), the highest spectral efficiency for 40 Gbit/s NRZ systems has been brought from 0.4 bit/s/Hz [8] to 0.64 [9] and even 0.8 bit/s/Hz [4], while the total capacity simultaneously evolved from 1.6 Tbit/s to 5.12 and 6.4 Tbit/s respectively. A record breaking capacity of 7 Tbit/s was also reported for bi-directional transmission [10]. In [9], unequal alternate channel spacings of 50 and 75 GHz were used in conjunction with vestigial sideband filtering (i.e. the unequal channel spacing relaxes the requirements on narrow band demultiplexing, provided the signal can still be recovered with a small offset between the channel wavelength and demultiplexer centre frequency). In [4], polarisation multiplexing and demultiplexing were used to achieve a channel spacing as small as 50 GHz over 186 km standard single mode fibre (SMF) and reverse dispersion fibre (RDF). State of the art experiments using more conventional techniques have also been reported for 100 GHz channel spacing at 40 Gbit/s NRZ (spectral efficiency of 0.4 bit/s/Hz), resulting in transmission of 1.6 Tbit/s over 400 km non-zero dispersion shifted fibre (NZDSF) [8], 1.28 Tbit/s over 300 km of fibre with 8 ps/nm/km dispersion [11], and 1.28 Tbit/s over 250 km pure silica core SMF [12]. So far the management of dispersion and non-linearities has been the main focus for the high capacity experiments reported above, which exclusively deal with point-to-point

systems. Therefore, a lot of effort has been spent on the design of effective dispersion maps using a variety of optical fibre types, on the reduction of interactions between adjacent channels by launching them with orthogonal states of polarisation, as well as on the reduction of fibre launch power while maintaining a sufficiently high optical signal-to-noise ratio by using Raman amplification [13].

The METEOR project aims at demonstrating the feasibility of 40 Gbit/s networking with increased spectral efficiency. However, only a few 40 Gbit/s networking experiments have been reported so far. In [14] transmission of 1.6 Tbit/s (40×40 Gbit/s) over 4 add-drop nodes was reported with a spectral efficiency of 0.4 bit/s/Hz. Nodes consisting of a fully programmable integrated 40 channel wavelength add/drop device (IWAD) made of a planar silica arrayed waveguide grating router and Mach-Zehnder thermo-optic switches [15] and of flat-top AWGs were compared. It was found that the IWADs were much more tolerant to signal wavelength misalignment, which is a critical factor at those high spectral efficiencies. Transmission through 5 add-drop nodes built from conventional 100 GHz channel spacing arrayed waveguide grating multiplexers designed for 10 Gbit/s WDM systems has also been demonstrated at 40 Gbit/s using return-to-zero (RZ) modulation [16]. The transmission line consisted of 9 AWG filters with flat-top pass-band shape and the 5 nodes were linked by 40 km NZDSF. The dispersion of each AWG pair was estimated at about 20 ps/nm per node while their 3 dB bandwidth was in the range 0.49 to 0.59 nm (61 to 74 GHz), and their pass-band detuning was within ±6.2 GHz from the channel wavelength grid. Optical signal-to-noise ratio degradation was found to be the main cause for system penalty and successful transmission of 25 channels with Q-factors better than 16.7 dB, resulting in bit-error-rates better than 1.0×10^{-9}, was obtained. The spectral efficiency achieved in this experiment was also 0.4 bit/s/Hz, which is of the same order of magnitude as for straight line experiments at 40 Gbit/s. These experimental results show that high capacity networking through a limited number of add-drop nodes is therefore possible at 40 Gbit/s.

4.1.2 PHASAR dispersion

The absence of dispersion, which is equivalent to constant group delay or linear phase, is a desired feature in wavelength (de)multiplexers. An essential optical filter design issue is therefore to know whether it is possible to simultaneously approximate a “square” frequency response while having zero or little dispersion in the pass-band. The concept of minimum-phase filters has been introduced in Section 2.3. The phase and amplitude re-

sponses of a minimum-phase filter cannot be tailored independently. As a consequence, any attempt to obtain an approximation of a square amplitude response will result in a given phase response - equivalent to dispersion behaviour - that cannot be corrected by design. It has actually also been shown in Appendix A that, for a minimum-phase filter, sharp amplitude transfer function edges will result in increased dispersion, and therefore the goal of a nearly square dispersion-less filter cannot be achieved. However, not all transfer functions are minimum-phase [17, 18]. Non minimum-phase filters offer an additional degree of freedom as attempts to tailor their amplitude response might not affect their phase response.

A PHASAR consists of an array of waveguides with a constant length difference between adjacent arms. Accordingly, its frequency response can be written as a sum of fixed delays [17]:

$$H(\omega) = \sum_{n=0}^{N-1} h(n)\, e^{-j\omega n} \tag{4.1}$$

where N is the number of waveguides, ω is the frequency normalised to the constant delay and $h(n)$ is the discrete impulse response for each waveguide in the array. It can be shown that if $h(n) = h(N-1-n)$ (i.e. if the weight distribution in the summation above is symmetric), then the filter is linear phase [17]. Moreover, the filter can be shown to be non-minimum phase and allows for flexible design of the phase and amplitude transfer functions. Loss in real devices has been found to be responsible for small phase distortions at the pass-band edges [19, 20]. The nearly ideal linear phase behaviour of conventional, non pass-band flattened PHASARs, has already been confirmed experimentally in Section 2.6 for a commercial silica-on-silicon multiplexer with $\sim$1 nm bandwidth. Very little dispersion was found in the pass-band.

The origin of dispersion has been investigated in PHASARs multiplexers with a Gaussian spectral response, as well as for pass-band flattened devices [21]. It was found that the dispersion of the pass-band flattened AWG is an even function of the detuning with respect to the centre frequency, whereas the Gaussian device exhibits odd-order dispersion. The main origin of the dispersion was attributed to symmetric phase errors and antisymmetric amplitude errors for the pass-band flattened and Gaussian AWG respectively. Fourier transform spectroscopy measurements performed on InP and silica-on-silicon devices confirmed that slowly-varying phase errors (i.e. non-random contribution to the phase distribution of each path in the waveguides array) were responsible for dispersion imperfections [22]. Furthermore, several dispersion compensating AWG designs

have been reported, showing that it is possible to alter the phase behaviour while conserving the desired amplitude response. For instance, it has been suggested to use a quadratic phase difference between consecutive waveguides in order to obtain a broadened pass-band chirped AWG [23]. Other simulated designs are based on a symmetric parabolic phase profile imposed on the central arrayed waveguide region [24, 25].

Therefore, PHASAR based devices offer some degrees of freedom in order to engineer simultaneously their amplitude and phase responses. One should of course distinguish between the theoretical response of the filter and its actual device implementation where loss or processing induced phase and amplitude errors can create some amount of dispersion. Depending on the applicability of the symmetry condition, flattening the pass-band using diverse techniques might still result in linear phase, but has also been reported to introduce some dispersion [26], as we shall see more in details in Section 4.3.

4.1.3 PHASAR cascadability

The cascadability of arrayed waveguide grating multiplexers has been investigated experimentally by a number of authors [27, 28, 29]. Experiments reported so far have been carried out at 10 Gbit/s. Arrayed waveguide gratings with a Bessel filter pass-band shape, 100 GHz channel spacing and 38 GHz full-width half maximum (FWHM) bandwidth have been cascaded experimentally in [27]. It was found that the penalty versus frequency detuning curve exhibited two minima when the number of cascades was increased. This effect was attributed to single side band generation. Increased penalty due to pass-band narrowing was also demonstrated in this work. The same bandwidth reduction effect has been investigated in [29] by cascading up 60 AWG multiplexers with ∼1 nm FWHM bandwidth and sharp roll-off characteristics. Up to 40 devices could be cascaded penalty free, and the allowable fluctuation of the centre frequency (defined as the range of carrier frequencies for which the 10 Gbit/s signal can achieve a bit-error rate smaller than 1.0×10^{-9}) has been shown to be ∼24 GHz for 40 cascades. Different types of multiplexers based on AWGs or multilayer interference (MI) filters have been compared experimentally in [28] with emphasis on their dispersive properties. It was shown for the first time that the cascadability was also influenced by the dispersive characteristics of the devices. AWGs were found to be nearly dispersion free while the detuning tolerance of a dispersive MI filter was found to be less than one half compared to dispersion free AWG designs. A 1175 km dispersion compensated link with 15 wavelength selective cross-connects based on AWGs has

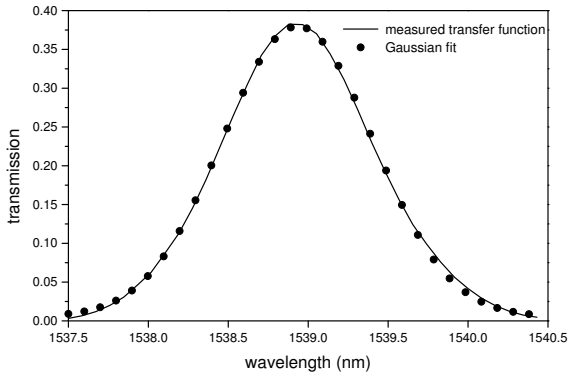

Figure 4.1 Measured conventional silica-on-silicon PHASAR transfer function and Gaussian fit.

also been simulated in a re-circulating loop experiment for 4 channel WDM transmission at 10 Gbit/s [30], showing that as little as 0.2 dB penalty was induced per OXC. The effect of the detuning of the centre frequencies of pass-band flattened AWGs in a cascade of network elements was also investigated based on numerical simulations [31], where it was shown that up to 100 filters designed for 200 GHz channel spacing could be cascaded depending on the laser frequency misalignment. Although the aforementioned experiments demonstrate the feasibility of transparent large area networking, new challenges emerge when the bit rate is increased to 40 Gbit/s and when small multiplexer bandwidths are necessary to accommodate high channel densities.

4.2 Reference simulations

In order to be able to assess improved flat top PHASAR designs for spectrally efficient 40 Gbit/s NRZ systems, we start by investigating a number of reference scenarios. This is performed by defining ideal transfer functions exhibiting some of the desired features of a pass-band flattened PHASAR. Guidelines on "ideal" pass-band flattened PHASAR transfer functions can then be edicted, against which the real modelled designs will be compared.

4.2.1 Classes of ideal transfer functions

Conventional non-flattened PHASARs have a pass-band which can be fairly well approximated by a Gaussian transfer function [6], as illustrated in Figure 4.1, which shows the measured amplitude transfer function of a silica-

on-silicon PHASAR. Higher order Gaussian transfer functions are known to present sharper roll-offs and can be used to approximate the ideal square filter response. Although they do not correspond to any known design of arrayed-waveguide grating, their reduced rate of bandwidth narrowing means that they could be used in order to help defining the filter transfer function shape real designs should try to approximate. Using multi-mode interference couplers is known as one possible way to perform pass-band flattening in PHASARs [32]. The device amplitude transfer function can then be approximated by the sum of two Gaussian functions with small wavelength detuning. Therefore, modelling pass-band flattened PHASARs with double Gaussian transfer functions has some kind of physical legitimacy, even though the dispersive behaviour of the device might be occulted and a more accurate modelling might prove necessary, as described in Section 4.3. The two families of reference transfer functions (Gaussian of order m and double Gaussian with different "flatness" parameters) are presented below.

Gaussian transfer functions

The transfer function of an optical filter can be defined according to:

$$E_{out} = T(\lambda) E_{in} \tag{4.2}$$

where E_{out} and E_{in} are the output and input electric fields respectively. For a Gaussian transfer functions of order m we have:

$$T(\lambda) = \exp - \left[\frac{\lambda - \lambda_0}{a} \right]^{2m} \tag{4.3}$$

where λ_0 is the filter centre wavelength and where the parameter a can be related to the filter full-width half maximum bandwidth according to:

$$(FWHM)_{filter} = 2a \left(\ln \sqrt{2} \right)^{\frac{1}{2m}} \tag{4.4}$$

Gaussian transfer functions of orders m=1, 2, 3 and 4 are represented in Figure 4.2 for the same FWHM bandwidth equal to 100 GHz. The sharper roll-off of higher order Gaussian transfer functions is clearly seen in the figure. It is therefore expected that, when cascaded, their bandwidth narrowing factor should be smaller than for 1$^{\text{st}}$ order Gaussian.

The FWHM bandwidth of a cascade of m^{th} order perfectly aligned Gaussian filters can be expressed as a function of the number of filters n

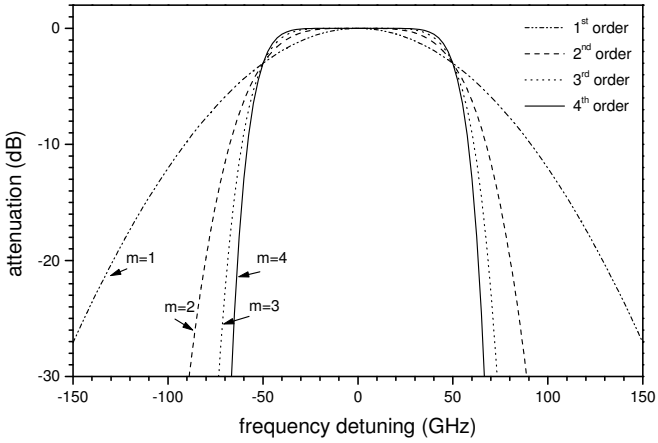

Figure 4.2 Transfer functions of 1st, 2nd, 3rdand 4th order Gaussian band-pass filters with 100 GHz FWHM bandwidth.

according to:

$$(FWHM)_{cascade} = \left(\frac{1}{n}\right)^{1/2m} (FWHM)_{filter} \tag{4.5}$$

A plot of the bandwidth narrowing factor for Gaussian orders 1 to 4 will be shown in Figure 4.7. It is important to mention at this point that we have assumed dispersion-free transfer functions for the diverse orders of Gaussian filters. First order Gaussian transfer functions corresponding to conventional PHASARs have been shown to be linear phase in Section 2.6. However, any design attempting to replicate higher order Gaussian transfer functions (provided this can be accomplished, which is not discussed here) might not result in dispersion-less devices. Therefore, it is emphasised that 2nd, 3rd and 4th order Gaussian filters have to be considered as mathematical transfer functions without any physical legitimacy, and are reported here for reference purpose only.

Double Gaussian flat-top transfer functions

One known technique to broaden the pass-band of PHASAR multiplexers is to use a two-fold imaging MMI coupler at the input of the device [32]. With a Gaussian spatial field distribution at the MMI input, two Gaussian like images are obtained at the output, the separation of which is determined by the width and index contrast of the MMI. Figure 4.3 shows how the sum of two Gaussian functions can approximate a flat-top function depending on

the value of the ratio of the Gaussian width to their centre wavelength offset. One immediate concern is that real implementations of PHASARs with MMI couplers will lead to dispersion [26]. This is ignored in the reference transfer function analysis presented in this section. Real PHASARs based on MMI couplers will be modelled accurately in Section 4.3.

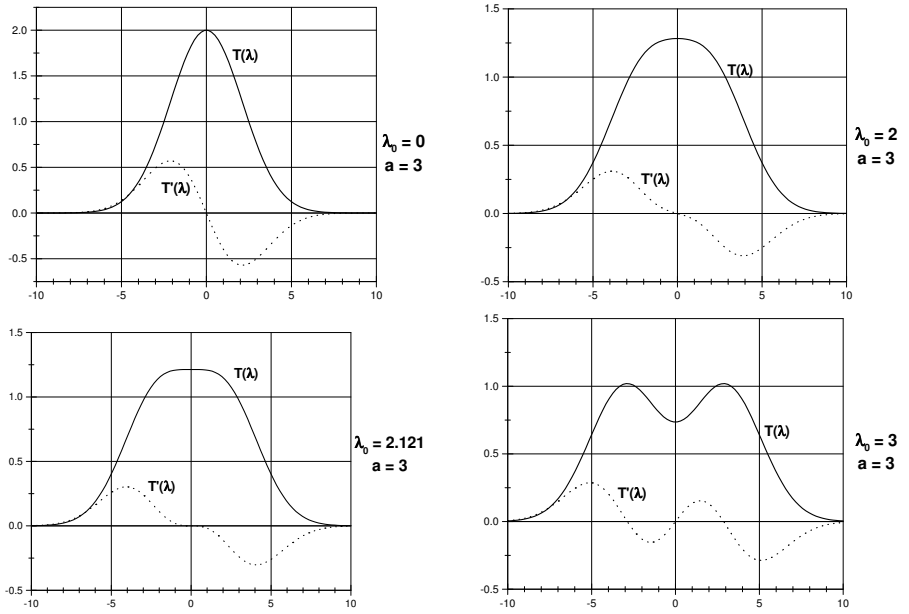

Figure 4.3 Evolution of the sum of two Gaussian functions having the same width (a) as a function of the spacing of their maxima ($2\lambda_0$). The transfer function $T(\lambda)$ as well as its first derivative with respect to wavelength $T'(\lambda)$ are represented.

The sum of two Gaussian transfer functions having the same FWHM bandwidth but centred around λ_0 and $-\lambda_0$ is given by

$$T(\lambda) = \exp - \left[\frac{\lambda - \lambda_0}{a}\right]^2 + \exp - \left[\frac{\lambda + \lambda_0}{a}\right]^2 \tag{4.6}$$

Following [32] we can define a flatness parameter

$$f = \frac{\text{separation of the two Gaussian}}{\text{Gaussian width}} = \frac{2\lambda_0}{a} \tag{4.7}$$

which, for convenience, can also be expressed as

$$f = 2\alpha\sqrt{2} \tag{4.8}$$

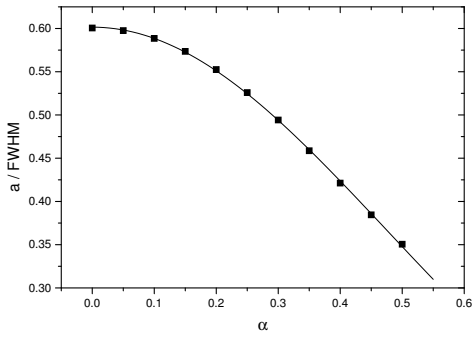

Figure 4.4 Ratio of the individual Gaussian width a to the FWHM bandwidth of the double Gaussian function as a function of the flatness parameter α.

For $\alpha = 0$ the overall transfer function is a Gaussian, while for $0 < \alpha < 0.5$ the transfer function broadens. When $\alpha = 0.5$, we have $f = \sqrt{2}$ and the Gaussian separation is then related to the Gaussian width according to:

$$\frac{\lambda_0}{a} = \frac{\sqrt{2}}{2} \tag{4.9}$$

At this point a transfer function having a flat top is obtained. On the other hand, when $\alpha > 0.5$, the two peaks separate and a dip is produced at the filter centre wavelength. The FWHM bandwidth of the transfer function $T(\lambda)$ can be related to the design parameters a and λ_0. This can be done by extracting the FWHM of filter transfer functions calculated with α in the range $[0 \ldots 0.5]$. The dependence of the Gaussian width on the filter FWHM is linear and depends on the parameter α. By plotting $a/FWHM$ as a function of α, as shown in Figure 4.4, a Gaussian dependence is found according to

$$\frac{a}{FWHM} = 0.6026 \exp - \left(\frac{\alpha}{0.6754}\right)^2 \tag{4.10}$$

Therefore, for a given desired filter FWHM bandwidth and flatness parameter α, it is possible to find the value of the Gaussian width a by using equation (4.10). Figure 4.5 shows the amplitude transfer functions of 100 GHz FWHM bandwidth filters corresponding to flatness parameters α equal to 0 (Gaussian filter), 0.45 and 0.5 ("maximally flat" double Gaussian transfer function).

4.2.2 Simulation models

Numerical simulations have been used in order to investigate the cascadability of various (de)multiplexers transfer functions. Whether performed

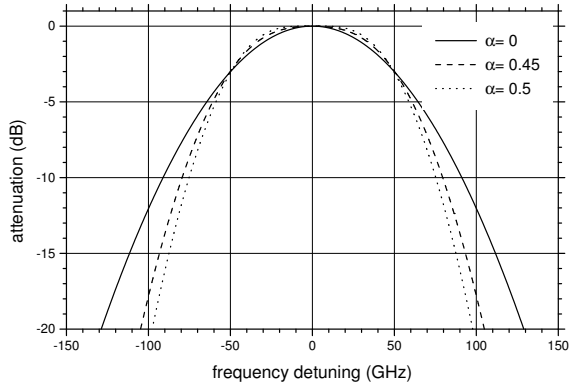

Figure 4.5 Transfer functions of 100 GHz FWHM double Gaussian filters with flatness parameter α equal to 0 (Gaussian), 0.45, and 0.5 ("maximally flat" double Gaussian).

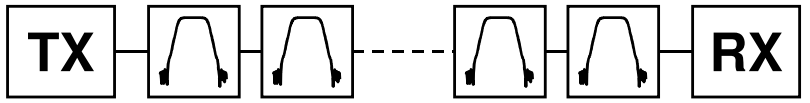

Figure 4.6 Simulation scenario for (de)multiplexer cascadability investigation. TX: 40 Gbit/s transmitter; RX: receiver. n identical and perfectly aligned transfer functions are cascaded between the transmitter and the receiver.

on ideal filter transfer function shapes (reference simulations) or on transfer functions resulting from the accurate device modelling described in Section 4.3, the same system models and parameters have been used. All simulations have been carried out using the Photonic Transmission Design Suite (PTDS 1.0 for Linux) from Virtual Photonics Incorporated [33]. The basic simulation test-bed is shown in Figure 4.6. It consists of a 40 Gbit/s NRZ transmitter, a cascade of filters and a PIN receiver. Note that no optical fibre is connecting the nodes and we are therefore strictly focussing on the signal degradation induced by the multiplexers alone.

The 40 Gbit/s NRZ optical signal is generated by a chirp-free Mach-Zehnder modulator with 30 dB extinction ratio. The signal then propagates through a cascade of (de)multiplexers having identical and perfectly aligned transfer functions. As the focus of the study is on signal degradation induced by the transfer function shapes, the insertion loss of the (de)multiplexers is ignored. The receiver consists of a photodiode with responsivity equal to 1.2 A/W and single sided thermal noise density of

15 pA/$\sqrt{\text{Hz}}$. The low-pass filtering behaviour of the receiver is simulated by a 4$^{\text{th}}$ order low-pass Bessel filter with a cut-off frequency equal to 0.75 times the bit-rate (30 GHz). The BER is then calculated taking inter-symbol interference (ISI) from the two neighbouring bits into account, according to the method proposed in [34] and described in more details in Appendix D. The receiver sensitivity is estimated in an iterative way at a BER of 1.0×10^{-9}.

For each type of filter (i.e. Gaussian of order m, double Gaussian with different values of α, or the real filter designs of Section 4.3), transfer functions corresponding to various 3 dB bandwidths have been calculated, either analytically or by scaling the normalised transfer functions $h(\lambda)$ generated by the accurate device modelling reported in Section 4.3 according to

$$T(\lambda) = h\left(\frac{\lambda - \lambda_0}{S}\right) \tag{4.11}$$

where S is a scaling parameter and the filter 3 dB bandwidth ($\Delta\lambda_{3dB}$) can be related to the normalised transfer function 3 dB bandwidth (Δx_{3dB}) according to

$$\Delta\lambda_{3dB} = S\Delta x_{3dB} \tag{4.12}$$

It is believed that this scaling of normalised transfer functions provides accurate filter amplitude and phase responses for the bandwidth range of interest (typically from 20 to 100 GHz). From the simulations, we could extract values of the filter 3 dB bandwidth giving rise to 1 or 3 dB power penalty after n cascaded filters.

4.2.3 Reference simulations

The bandwidth narrowing of the different types of reference filters can be calculated either analytically or numerically. The bandwidth narrowing factor is defined as the ratio of the 3 dB bandwidth of the equivalent transfer function resulting from the cascading of n identical filters, to the 3 dB bandwidth of the individual filter. A plot of the narrowing factor as a function of number of cascaded filters is shown in Figure 4.7 for Gaussian transfer functions of orders m=1 to 4, and double Gaussian transfer functions with flatness parameters α=0.45 and 0.5. As expected, the 1$^{\text{st}}$ order Gaussian transfer function exhibits very poor bandwidth narrowing behaviour. For a given number of cascaded filters, the narrowing factor of double Gaussian transfer functions is better than that of 1$^{\text{st}}$ order Gaussian but does not match those of transfer functions with sharper roll-off such as 2$^{\text{nd}}$, 3$^{\text{rd}}$ and 4$^{\text{th}}$ order Gaussian. However, double Gaussian transfer functions can

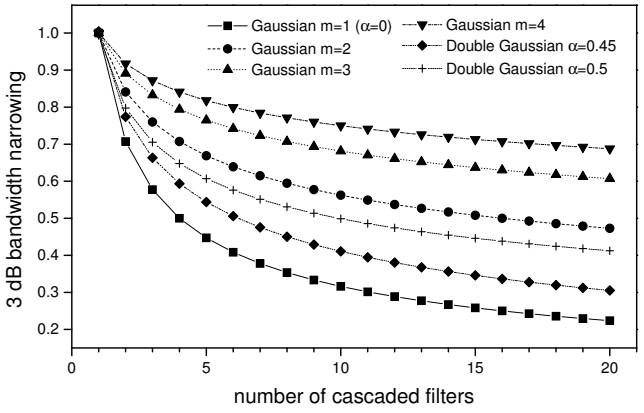

Figure 4.7 Bandwidth narrowing factor as a function of number of cascaded filters for Gaussian and double Gaussian transfer functions.

be synthesised using MMI couplers whereas higher order Gaussian transfer functions might not be realised in practice.

The filters FWHM bandwidths giving rise to 1 or 3 dB penalty are represented as a function of the number of cascades in Figure 4.8 for Gaussian transfer functions, as well as in Figure 4.9 for double Gaussian filters. This representation enables to assess devices requirements (multiplexer FWHM bandwidth) from network dimensioning (number of cascaded filters), depending on the figure of merit (1 or 3 dB power penalty).

For Gaussian filters, it can be seen that the bandwidth giving rise to 1 or 3 dB penalty is much larger for 1st order transfer functions than for 2nd order, which is itself larger than for 3rd order filters, apart when only a couple of devices are cascaded. Up to 2 filters if a 1 dB penalty criterion is adopted, or up to 3 filters for 3 dB penalty, the sharper edges of higher order Gaussian transfer functions induce higher bandwidth requirements for 3rd order than for 2nd and even 1st order Gaussian filters. A similar trend is observed for double Gaussian transfer functions where the higher flatness parameter ($\alpha = 0.5$) enables smaller filter bandwidths than $\alpha = 0.45$, which itself is better than the Gaussian case ($\alpha = 0$). For a reduced number of cascaded filters (i.e. up to 1 for 1 dB penalty or up to 3 for 3 dB penalty), this trend is inverted.

In the METEOR four node ring network configuration, a signal will have to propagate through up to 8 (de)multiplexers. This corresponds to the worst case where one channel is added to the ring traffic at one node, propagates through the remaining 3 nodes and is dropped at the

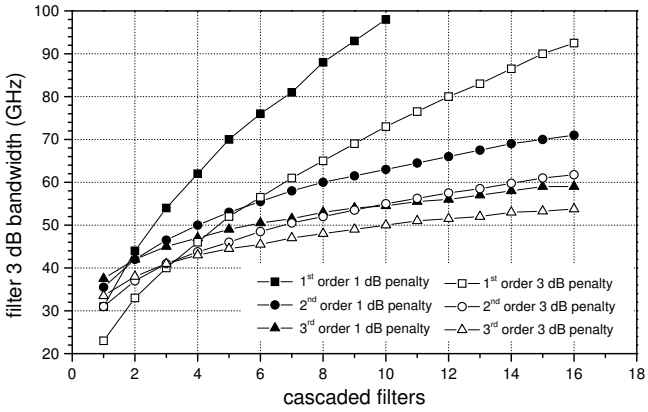

Figure 4.8 Filter 3 dB bandwidth corresponding to 1 and 3 dB power penalty as a function of number of cascaded devices for 1st, 2nd and 3rd order Gaussian transfer functions.

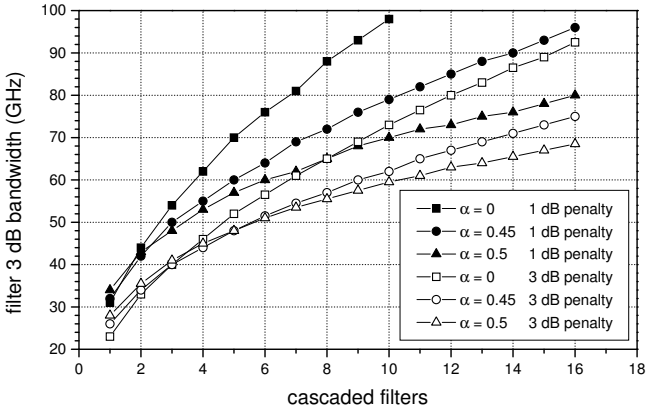

Figure 4.9 Filter 3 dB bandwidth corresponding to 1 and 3 dB power penalty as a function of number of cascaded devices for double Gaussian transfer functions with flatness parameter α= 0, 0.45 and 0.5. Note that α= 0 corresponds to 1st order Gaussian in Figure 4.8.

same node as where it had been added previously. The requirements on (de)multiplexers bandwidths can then be assessed depending on the penalty that can be tolerated. The results for the five types of reference transfer functions are summarised in Table 4.1.

Filter Type	FWHM bandwidth (GHz)	
	1 dB penalty	3 dB penalty
Gaussian 1st order	88	65
Gaussian 2nd order	60	52
Gaussian 3rd order	53	48
Double Gaussian $\alpha = 0.45$	72	57
Double Gaussian $\alpha = 0.5$	65	56

Table 4.1 Filter FWHM bandwidth giving rise to 1 or 3 dB power penalty after 8 cascaded (de)multiplexers with Gaussian or double Gaussian transfer functions.

It can be seen that, by changing the PHASAR design from a conventional 1st order Gaussian transfer function to a maximally flat double Gaussian ($\alpha = 0.5$), a 27% increase in spectral efficiency can be achieved for a 1 dB penalty criterion. This assumes that cross-talk effects, which are not studied here, enable to scale the channel spacing in proportion with the (de)multiplexers bandwidths. If it were moreover possible to synthesise 3rd order Gaussian transfer functions, this spectral efficiency enhancement could be increased to $\sim$39%.

So far, we have determined the filter bandwidth that gives rise to 1 or 3 dB power penalty after n cascaded (de)multiplexers. However, it has already been stated that some amount of bandwidth narrowing will result from the cascading of filters. It is then possible to calculate the effective bandwidth of a cascade of n filters, each having the 3 dB bandwidth determined above. Results are presented in Figure 4.10 for 1st order Gaussian as well as double Gaussian transfer functions with flatness α equal to 0.45 and 0.5. It is clearly seen that the effective bandwidth of the cascade remains nearly constant (within 2 GHz) when the number of cascaded devices is increased. Such a behaviour is expected to be strictly observed for Gaussian filters as the transfer function of a cascade of Gaussian transfer functions remains Gaussian, while its bandwidth is decreased. Figure 4.10 suggests that, for double Gaussian filters, the bandwidth reduction is responsible for the penalty while the overall shape of the equivalent transfer function of the cascade does not experience abrupt changes when n is increased.

Throughout this section, we have presented simulations results on the

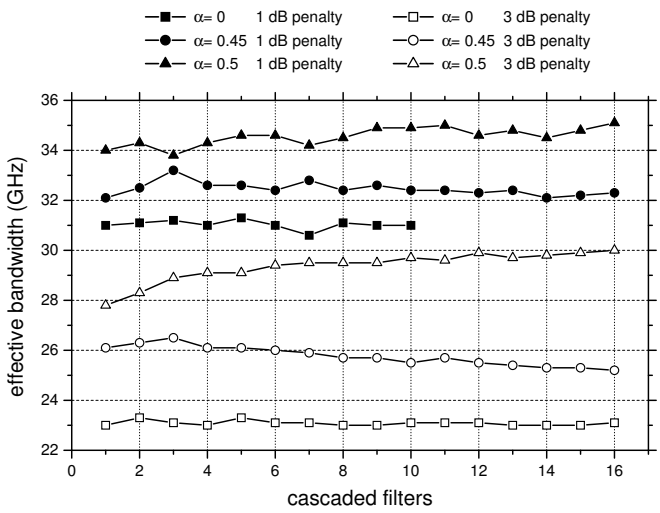

Figure 4.10 Effective bandwidth as a function of number of cascaded (de)multiplexers for double Gaussian transfer functions with flatness parameter α=0, 0.45 and 0.5. The effective bandwidth is defined as the bandwidth of a cascade of n identical filters whose individual FWHM bandwidth value results in 1 or 3 dB power penalty after n cascades.

cascadability of filters with mathematical Gaussian and double Gaussian transfer functions. Using a simple model, it has been shown that flattening the pass-band of a PHASAR using a double Gaussian input field, as could be achieved in a MMI, enables significant increase in spectral efficiency. However, the double Gaussian model provides only an approximate description of the field at the output of a MMI coupler. Moreover, it has also been assumed so far that all PHASARs were strictly linear-phase which might not be satisfied in practice. We have also shown that the sharper roll-off of higher order Gaussian transfer functions does not induce excessive filtering of the 40 Gbit/s NRZ spectrum. As a consequence, 2^{nd} and 3^{rd} order linear-phase Gaussian filters could result in even higher spectral efficiencies provided they can be synthesised. The same simulation procedure will be repeated in Section 4.3 with modelled PHASAR filter responses. These transfer functions will no longer represent hypothetical devices responses, but will result from accurate modelling of multiplexers that can be realised using the silica-on-silicon technology. It will then be possible to compare system simulations results obtained with mathematical and modelled transfer functions in order to assess the effect of the non-ideal behaviour of real devices.

4.3 System implications of pass-band flattened PHASARs

4.3.1 PHASAR pass-band flattening techniques

It has been confirmed experimentally in Chapter 2 that the pass-band of a non-flattened PHASAR exhibits a Gaussian response, as already shown in [6]. Several methods have been proposed in order to approximate the desired "square" or "flat-top" transfer function. Some methods rely on the fact that the electric field distribution at the output of the demultiplexer is the Fourier transform of the field at the junction between the arrayed waveguide and the output slab. If one manages to realise a $\sin x/x$ field amplitude distribution at the output slab input, a rectangular frequency response function can be obtained, as demonstrated in [35, 36], where the amplitude distribution in the arrayed waveguide was modified by introducing loss in some of the arms. Other pass-band flattening approaches consist in creating two frequency shifted responses, for instance by introducing interleaved sub-gratings [37], or by having half of the arrayed waveguides focusing on a slightly different point at the output slab [38]. Realising a double-peaked field at the input of the arrayed waveguide can also enable to achieve pass-band flattening of the PHASAR response. As we have seen in Section 4.2.1, a flat-top response can be realised by the summation of two Gaussian distributions. This principle can be realised in practice by using a multi-mode interference coupler [39] before the input slab, as proposed in [32, 40]. Alternatively, using a parabolic horn (or taper) before the input slab has also been shown to result in pass-band flattening, as proposed in [41]. These last two approaches are the ones considered in the present study. Issues to take into account when introducing a pass-band flattening process in the design of a PHASAR (de)multiplexer are the possible presence of amplitude ripples in the frequency response, the introduction of excess loss, as well as the introduction of dispersion.

Pass-band flattened PHASARs using both MMI input couplers and parabolic horns have been designed and modelled by Chretien Herben from the Delft University of Technology. The designs are those of devices to be realised using silica-on-silicon with waveguide parameters corresponding to the technology available at COM. The two designs were modelled, first by calculating the electric field distribution at the input of the slab by either modal propagation analysis in the case of the MMI input, or by a commercial beam propagation method in the case of the parabolic horn. Based on this input distribution, the PHASAR responses were obtained by calculating the field after diffraction in the input slab, its overlap with the modes

in the array waveguides, followed by simulation of the propagation through the array waveguides, diffraction in the output slab, and finally overlap with the mode in the output waveguide. Such a procedure results in the determination of complex transfer functions where both the amplitude and phase responses are realistic. More details on the physical parameters of the devices and on the modelling approach have been reported in [42].

4.3.2 Transfer functions used for the system simulations

Four different PHASAR designs have been modelled and the corresponding complex transfer functions have been used as inputs to system simulations. The goal of those simulations is to investigate the cascadability of the devices for 40 Gbit/s NRZ transmission. These transfer functions are shown in Figure 4.11. In order to facilitate the reading of Section 4.3, the following nomenclature has been adopted for the four different types of (de)multiplexers transfer functions under investigation.

- *COM03* corresponds to a conventional non-flattened PHASAR design with Gaussian frequency response and nearly linear phase.
- *COM04* corresponds to an arrayed waveguide grating with an artificial perfectly rectangular input field. It therefore represents the maximal amount of flatness which can be achieved but does not correspond to the response of a device which can actually be fabricated.
- *COM05* corresponds to a PHASAR whose pass-band has been flattened using a MMI input coupler.
- *COM06* corresponds to a pass-band flattened PHASAR with a parabolic horn input.

The attenuations of the devices at the centre frequency of their pass-band are equal to 1.8, 7.5, 7.5 and 7.0 dB for COM03 to COM06, respectively. Amplitude ripples are observed in the pass-band for COM05 and COM06. For COM05 these ripples are of the order of 1 dB, whereas they are smaller than 0.1 dB for COM06. One can already predict that cascading 8 times COM05, as in the METEOR network scenario, will result in 8 dB notches in the 40 Gbit/s NRZ signal spectrum, which is expected to result in severe penalty.

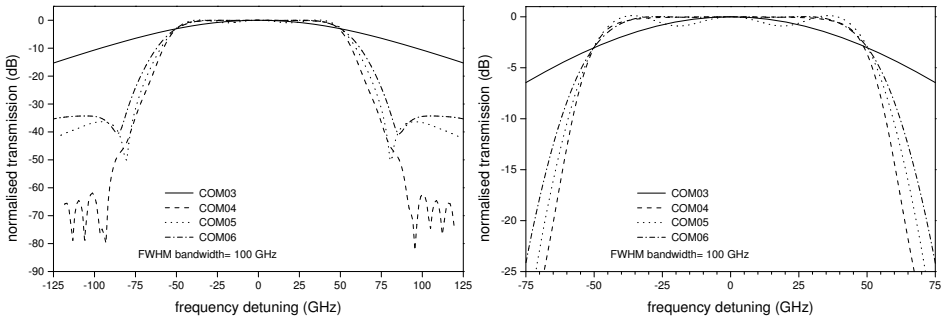

Figure 4.11 Power transfer functions of the four types of pass-band flattened PHASARs represented here for a FWHM bandwidth of 100 GHz. Details in the pass-band are represented to the right.

4.3.3 Dispersion of the various designs

The dispersion of the four different PHASAR designs has been calculated from the phase of their complex transfer functions $H(\omega) = |H(\omega)| e^{-j\phi(\omega)}$. This can be done numerically by differentiating the phase $\phi(\omega)$ twice according to

$$\tau = -\frac{\lambda^2}{2\pi c}\frac{\partial \phi}{\partial \lambda} \tag{4.13}$$

and

$$\mathbb{D} = \frac{d\tau}{d\lambda} = -\frac{1}{2\pi c}\left[2\lambda\frac{\partial \phi}{\partial \lambda} + \lambda^2\frac{\partial^2 \phi}{\partial \lambda^2}\right] \tag{4.14}$$

Dispersion curves for the four types of filters with 100 GHz bandwidth are shown in Figure 4.12. For COM06, details of the dispersion around the pass-band of the device are also provided in Figure 4.13. It can be seen that, for all the designs, the dispersion is reasonably low at the centre wavelength and increases at the filter band-pass edges. In the pass-band, it oscillates around 0 ps/nm with maximum excursion values in the 3 and 25 dB bandwidth given in Table 4.2 for the 100 GHz filter.

COM03 presents no dispersion in the pass-band, as expected from such a PHASAR with Gaussian amplitude transfer function profile. COM04 also exhibits little dispersion in the pass-band. On the other hand, peak dispersion values in the pass-band are fairly high for COM05, even when the multiplexer bandwidth is as large as 100 GHz. The dispersion in the pass-band of COM06 is lower than that for COM05, but starts becoming significant at the filter edges. It can be furthermore noticed that the dispersion profile of COM06 agrees with recent work on the dispersion of PHASAR whose pass-band is flattened using a parabolic taper before the

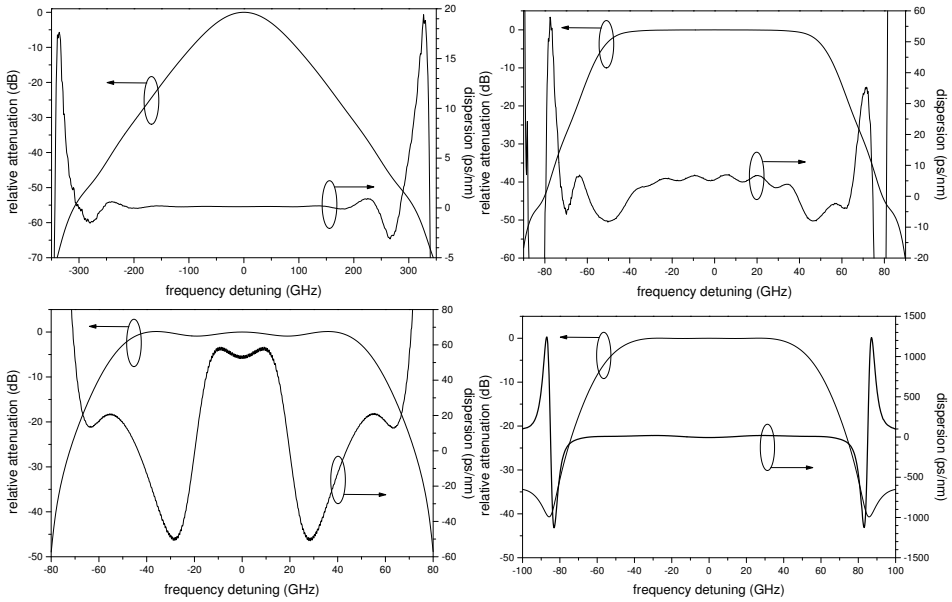

Figure 4.12 Dispersion of the multiplexers COM03 to COM06 for 100 GHz FWHM bandwidth. Top-left: COM03; top-right: COM04; bottom-left: COM05; bottom-right: COM06.

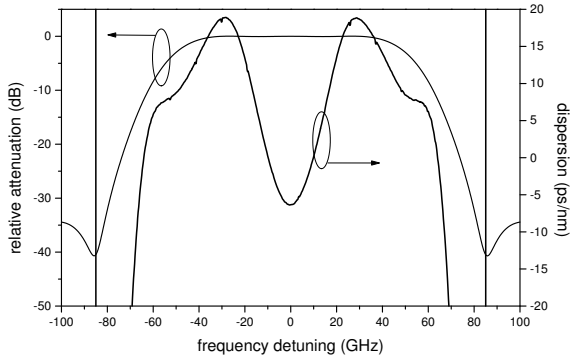

Figure 4.13 Detail of the dispersion of multiplexer COM06 (parabolic horn) for 100 GHz FWHM bandwidth.

Filter	3 dB		25 dB	
	min	MAX	min	MAX
COM03	0.12	0.15	-0.1	0.2
COM04	-8.1	7.0	-8.3	16.9
COM05	-51.0	58.7	-51.0	74.4
COM06	-6.4	18.9	-102.6	18.9

Table 4.2 Minimum and maximum dispersion values (expressed in ps/nm) in the 3 dB and 25 dB bandwidths for the multiplexers COM03 to COM06 with 3 dB bandwidth equal to 100 GHz

input slab region [43]. The important amount of dispersion observed for COM05 corresponds to the presence of three transmission peaks in the pass-band. When the filter bandwidth is decreased to 20 GHz, all dispersion values become prohibitive, apart for the Gaussian shaped multiplexer COM03. It should also be remembered that COM04 corresponds to a maximally flat device which cannot be realised and therefore its phase transfer function is somehow artificial.

4.3.4 Influence of the (de)multiplexer bandwidth

The bandwidth narrowing factors induced by the cascading of the (de)multiplexers COM03 to COM06 have been calculated and are shown in Figure 4.14. COM04 and COM06 exhibit equivalent performance. COM05 presents the best narrowing factor when the number of cascades is increased. However it should be remembered that $\sim$1 dB amplitude ripples are present in the pass-band of the COM05 transfer functions. Therefore, after only 3 cascades, some notches deeper than 3 dB are already present in the cascade equivalent transfer function. In this case, it does not make much sense to define a narrowing factor based on the usual definition of the 3 dB bandwidth. Also represented in Figure 4.14 are the bandwidth narrowing factors for 1^{st} and 2^{nd} Gaussian transfer functions as well as for the double Gaussian function with $\alpha = 0.5$. The narrowing factor for COM03 is in very good agreement with the one obtained for a theoretical 1^{st} order Gaussian transfer function, confirming the Gaussian nature of this multiplexer. If we discard COM03 (Gaussian filter which should be used as reference) and COM05 (because of too high amplitude ripples in the pass-band which will be detrimental to the propagated spectrum), the narrowing factors for both COM04 and COM06 are better than for the double Gaussian filter with $\alpha = 0.5$ and even than for the 2^{nd} order Gaus-

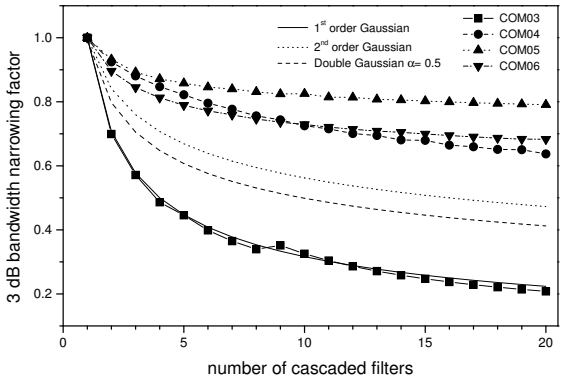

Figure 4.14 Bandwidth narrowing factor as a function of the number of cascaded filters for the designs COM03 to COM06 as well as for 1^{st} and 2^{nd} order Gaussian and double Gaussian transfer function with flatness parameter $\alpha = 0.5$.

sian. Therefore, as far as bandwidth narrowing is concerned, COM04 and COM06 are good candidates for a pass-band flattened multiplexer designed for high spectral efficiency systems.

The simulation procedure described in Section 4.2 has been followed for the multiplexers COM03 to COM06. The filter FWHM bandwidths giving rise to 1 and 3 dB power penalty have been determined as a function of the number of cascaded multiplexers, and the corresponding curves are shown in Figure 4.15.

For the filters whose amplitude transfer functions exhibit some attenuation ripples (namely COM05 and to a lesser extent COM06), some non-monotonous behaviour of the penalty versus filter bandwidth curves are observed. The penalty will first decrease before slightly increasing, and then decrease again with increasing filter bandwidth, as shown in Figure 4.16 for the COM06 transfer function. This behaviour is more visible in the simulations where the phase of the filters is not taken into account. It is believed to be due to the attenuation of spectral contents of the 40 Gbit/s NRZ spectrum by the filter amplitude notches. These non-monotonous features are responsible for some discontinuities in the curves showing the filter bandwidth giving 1 or 3 dB penalty as a function of the number of cascades. For a number n of circulations through the device, the maximum penalty reached at the top of the bump might be below 1 dB while it can get larger than this threshold for $n+1$ cascades as illustrated in Figure 4.16. Such a discontinuity is clearly visible for COM06 in Figure 4.15 even if the phase transfer function was also taken into account to compute this curve. It is therefore essential to ensure that these non-monotonous features have

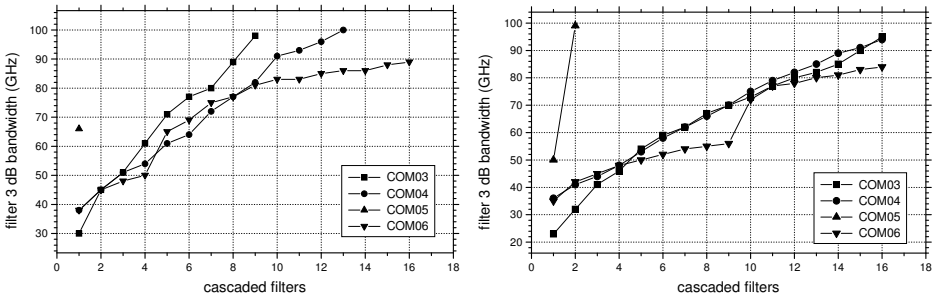

Figure 4.15 Filter 3 dB bandwidth giving rise to 1 dB (left) and 3 dB (right) power penalty as a function of the number of cascaded multiplexers for the designs COM03 to COM06. The full complex transfer function is taken into account in the simulations.

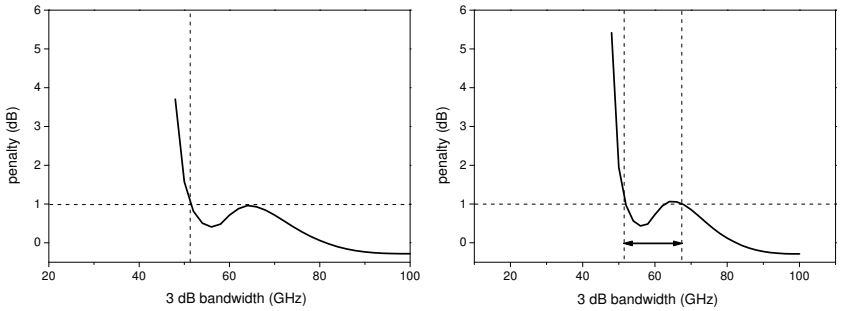

Figure 4.16 Explanation of the presence of discontinuities in the 3 dB bandwidth giving rise to 1 or 3 dB penalty against number of cascades curves. This is illustrated here for the COM06 transfer function where the phase is not taken into account. Left: after 10 cascades the filter bandwidth giving 1 dB penalty is equal to 52 GHz; Right: after 11 cascades this value jumps to 68 GHz.

some real existence and are not just artifacts due to the BER estimation in the simulations. Simulations performed using a home made software [44] have confirmed the existence of these features.

Based on these simulations, we can conclude on the necessary filter bandwidth in order to enable propagation through 4 add-drop nodes (corresponding to 8 cascaded multiplexers and demultiplexers) with a penalty of 1 and 3 dB. The results are summarised in Table 4.3. Therefore, if only 1 dB power penalty is allowed after propagation of the 40 Gbit/s NRZ signal through 4 nodes in the network, a FWHM bandwidth of at least 77 GHz is required when the physically realisable pass-band flattened PHASAR design COM06 is implemented.

Filter Type	FWHM bandwidth (GHz)	
	1 dB penalty	3 dB penalty
COM03	89	67
COM04	77	66
COM05	-	-
COM06	77	55

Table 4.3 PHASAR 3 dB bandwidth giving rise to 1 and 3 dB penalty after 8 cascaded devices corresponding to 4 add-drop nodes.

4.3.5 Identification of the origin of system penalty

The non-ideal transfer functions of the four PHASAR designs have been shown to result in some amount of power penalty. This is due to a combination of amplitude filtering and chromatic dispersion. It is therefore of great interest to try to determine which of the amplitude or the phase transfer function is mainly responsible for the signal degradation. Numerical simulations offer some flexibility in order to answer this question as the effects of the amplitude and phase of the transfer function of an optical filter can be considered separately. Therefore, we have performed cascadability simulations for the following types of transfer functions, either physical or purely hypothetical:

1. *Full complex transfer functions:* both amplitude and phase are included. They do represent the multiplexers models described in Section 4.3.2 and the corresponding system simulation results have been presented in Section 4.3.4.

2. *Amplitude transfer functions:* the amplitude response is the same as for the real multiplexers but the phase is assumed to be linear.

3. *All-pass filters:* the attenuation of the multiplexers is assumed to be uniform and equal to 0 dB while their phase transfer functions are identical to the ones of the real multiplexers.

Obviously type 2 and 3 above have no physical existence. They are merely convenient tools in order to try to identify the origin of system penalty. From a linear system point of view, a real multiplexer (type 1) is equivalent to a cascade of a linear phase filter (type 2) and an all-pass filter (type 3). These three types of transfer functions are represented in Figure 4.17.

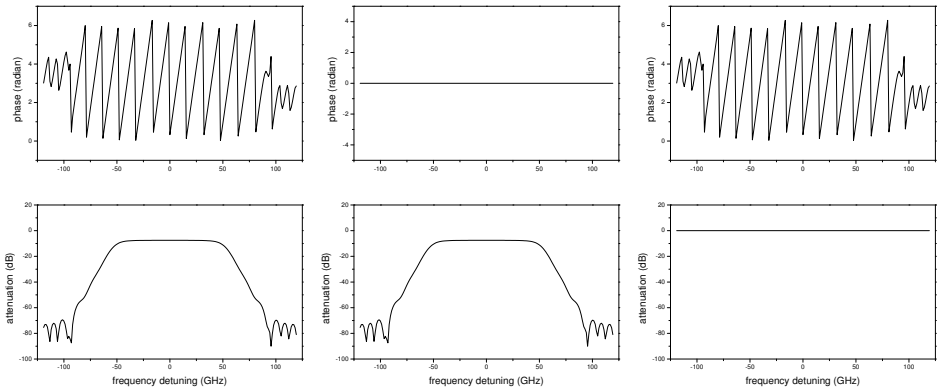

Figure 4.17 The three types of transfer functions used to investigate the origin of system penalty. From left to right: a) complex; b) linear-phase; c) all-pass.

Comparing simulation results obtained with the three types of transfer functions above might prove useful in order to determine which of the phase or the amplitude response is the more responsible for power penalty. One has to be extremely careful when performing such a comparison. For instance, cascading all-pass filters implies maintaining the same power ratio between spectral components of the 40 Gbit/s signal, but shifting them in time through the effect of chromatic dispersion. However, in a real filter, the relative power importance of these spectral components will be determined by the amplitude transfer function. Therefore, in some cases, the amplitude transfer function might be helpful to avoid too large signal distortions seen in the time domain. It is nevertheless possible to learn about the limiting behaviours of the multiplexers when a significant correlation can be established between results obtained from the full complex transfer functions and results obtained with either the linear-phase or all-pass filters.

The penalty versus FWHM bandwidth curves obtained after a given number of cascaded multiplexers for the three types of transfer functions listed above are represented in Figure 4.18 for a single multiplexer corresponding to the transfer function COM04, as well as after a cascade of 5 of those devices. It is clear from this figure that, for one filter, the penalty curve obtained with the complex transfer function is nearly identical to the one obtained with the amplitude transfer function alone. On the other hand, when the number of cascaded devices is increased to 5, the penalty curve for the complex transfer function becomes very similar to the one obtained with the all-pass transfer function. It can also be observed that

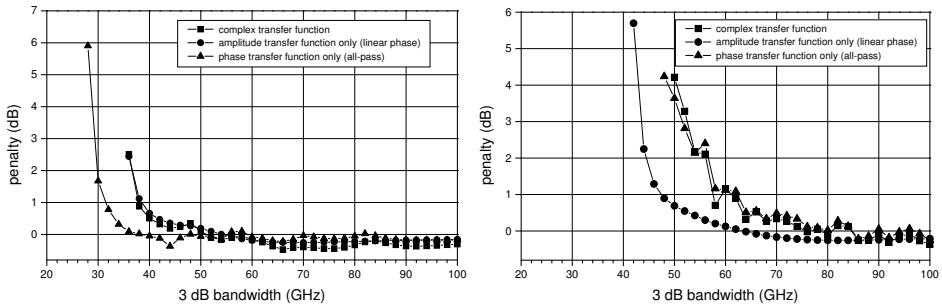

Figure 4.18 Power penalty as a function of filter FWHM bandwidth for complex, linear-phase and all-pass transfer functions representing the COM04 PHASAR design. Left: after one single filter; Right: after 5 filters.

the small variations of the penalty (previously described as "unsmooth" behaviour) match quite well between the complex and all-pass transfer functions. Therefore, the phase characteristics of the transfer functions is believed to be responsible for the unsmooth behaviour observed in the penalty curves. Based on Figure 4.18, it is possible to conclude that for one single COM04 filter, the amplitude transfer function is responsible for the penalty while for 5 filters it is the phase response which mainly causes signal degradation.

Figure 4.19 represents the bandwidth corresponding to 3 dB penalty for the COM04 PHASAR design as a function of the number of cascaded devices. It can clearly be seen that, for one and two filters, the curve representing the effect of the full complex transfer function matches the one representing the amplitude alone transfer function. On the other hand, when the number of cascaded devices is increased to four and more, a good agreement is observed between results obtained with the full complex transfer function and with the phase alone transfer function. As a comparison, a similar set of curves obtained from the COM03 PHASAR design (Gaussian transfer function) is also shown in Figure 4.19. As expected from the linear phase behaviour of the device, the curve representing the full complex transfer function matches the one representing the amplitude alone transfer function over the full bandwidth range of interest. The equivalent bandwidth which would correspond to that of the all-pass transfer function giving 1 or 3 dB power penalty after 1 to 16 cascaded devices is smaller than 20 GHz, which was the lower value in our investigation.

Based on similar investigations for the four PHASAR designs COM03 to COM06, we can conclude on the origin of power penalty when the corresponding devices are cascaded.

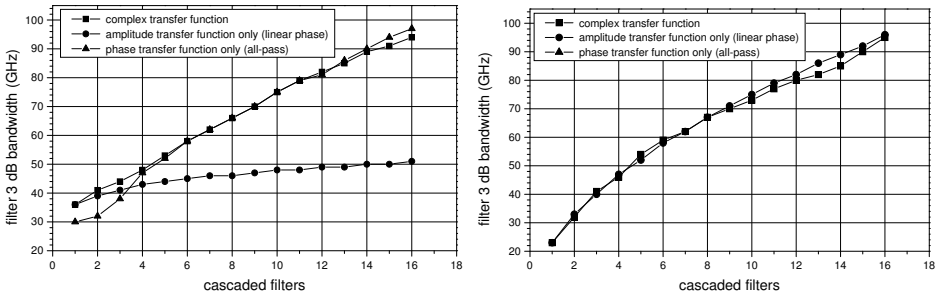

Figure 4.19 Filter FWHM bandwidth resulting in 3 dB power penalty as a function of the number of cascaded devices for complex, linear-phase and all-pass transfer functions corresponding to the COM04 (left) and COM03 (right) PHASAR designs.

- For **COM03** (non-flattened PHASAR with Gaussian amplitude transfer function), there is no dispersion problem as indicated by the nearly linear-phase of the device over its entire bandwidth. The amplitude transfer function is entirely responsible for the penalty.

- For **COM04** (maximal amount of flatness which can be achieved using a rectangular non-physical input field), it has been found that for 1 to 2 devices the amplitude transfer function is mostly responsible for the penalty, while when more than four devices are cascaded, it is the phase transfer function which accounts for the calculated power penalty. Therefore, for such a filter, the amplitude behaviour, including the nice bandwidth narrowing property, cannot account alone for the penalty.

- For **COM05** (pass-band flattened PHASAR using a MMI input coupler), the amplitude transfer function exhibits $\sim$1 dB ripples in the pass-band, which are detrimental to the signal spectrum after only a few cascaded devices. Nevertheless, even for a single filter, it is the phase response which is found mostly responsible for the penalty.

- For **COM06** (pass-band flattened PHASAR using a parabolic horn), it is clear that the phase is the limiting factor when more than a couple of devices are cascaded. This transfer function is more difficult to analyse but it bears similarities with COM04, although correlations between penalty curves are not as good. The influence of the phase response is visible earlier than with COM04. It is also confirmed that it is the amplitude transfer function and not the phase transfer func-

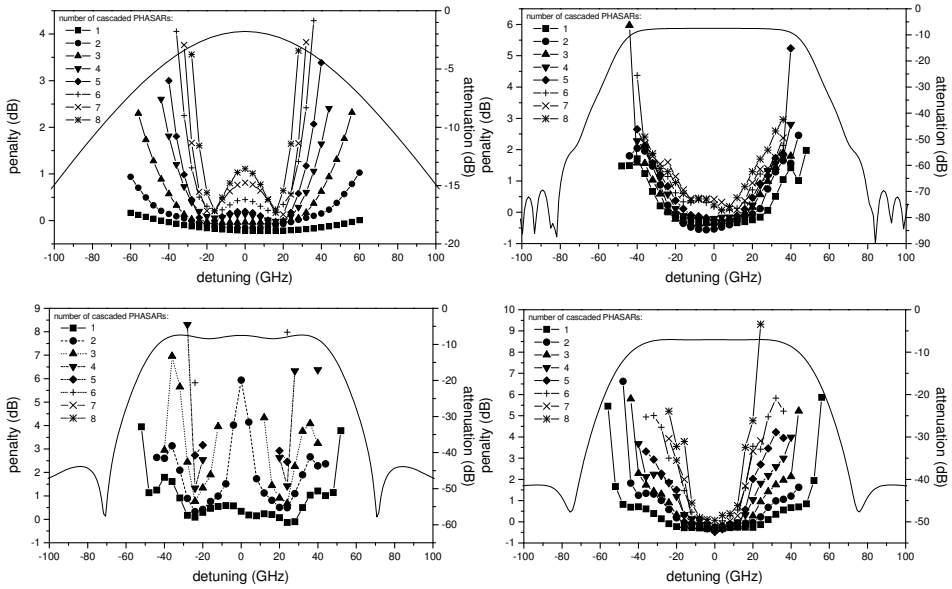

Figure 4.20 Power penalty as a function of laser detuning with respect to filter centre frequency for 1 to 8 cascades of the PHASAR designs COM03 (top-left), COM04 (top-right), COM05 (bottom-left) and COM06 (bottom-right) with 88 GHz FWHM bandwidth.

tion which is responsible for non-uniformities in the penalty versus filter bandwidth curve (not to be confused with unsmoothness which is attributed to the phase response).

Using the flexibility offered by simulation tools, we have been able to demonstrate that the phase transfer functions resulting from pass-band flattened PHASARs modelling need to be taken into account to explain the power penalties calculated when a certain number of multiplexers are cascaded. Even though the dispersion values calculated in the pass-band are fairly low, the reduced tolerance towards chromatic dispersion at 40 Gbit/s makes them critical as soon as more than a couple of pass-band flattened multiplexers are cascaded. Therefore, at such high bit-rates, the departure from ideality of real PHASAR designs can no longer be ignored.

4.3.6 Influence of laser detuning

It has been assumed so far that the transmitter laser was perfectly tuned to the centre frequency of the (de)multiplexer. It has also been assumed that all (de)multiplexers in a cascade were strictly identical and perfectly

aligned. A number of departures from this ideal situation are likely to be encountered in a real network implementation. First, due to device processing issues, the transfer functions of individual multiplexers will be slightly different one from the other, resulting in small differences in the amplitude and phase responses as well as in the devices 3 dB bandwidths. Second, offsets will be present between the centre frequencies of the multiplexers present in a link. This will even be more critical in high spectral efficiency systems, as reduced filter bandwidths will only allow for small detunings of the multiplexers. A comprehensive general study of such real-world links would necessitate a statistical description of the 3 dB bandwidth and centre frequency offset distributions. This task would become even more complex when fibre links between nodes are considered, as in many cases a linear system approach could not be followed any longer. In the present study, we restrict ourselves to the more tractable case where we assume that all (de)multiplexers in a link are strictly identical, and investigate the influence of the laser misalignment with respect to the filter centre wavelength.

Power penalties have been calculated as a function of the number of cascaded devices and frequency detuning for different FWHM bandwidths of the designs COM03 to COM06. Simulations have also been repeated in the hypothetical case where the different designs were strictly linear-phase. Some results are presented in Figure 4.20 for 1 to 8 cascaded COM03 to COM06 multiplexers with 88 GHz FWHM bandwidth. In this case, the full complex modelled transfer function was considered. According to previous calculations, the value of 88 GHz ensures that, with the exception of the COM05 design, less than 1 dB power penalty will be experienced at the filter centre wavelength for 8 cascaded devices. When the COM03 design with Gaussian transfer function is cascaded, two low penalty windows appear due to vestigial sideband filtering, as already reported for Bessel responses in [27]. Similar features are also observed when the MMI input coupler pass-band flattened COM05 design is cascaded. In this case they are due to the $\sim$1 dB amplitude ripples present in the pass-band of the transfer function. For both COM03 and COM05, these transmission windows narrow when the number of cascades is increased and their minimum penalty increases accordingly. The cascading of multiplexers with the COM04 and COM06 designs simply results in a reduction of the usable bandwidth corresponding to a given allowed power penalty. The allowable fluctuations of the laser centre frequency for a 1 dB penalty criterion after 1 and 8 cascaded devices are given in Table 4.4 for both COM04 and COM06.

Even if the usable bandwidth of the COM06 design is larger than that of the maximally flat non-realisable COM04 PHASAR after a single device, it

PHASAR design	Laser misalignment tolerance (GHz)	
	1 filter	8 filters
COM04	±35	±18
COM06	±49	±12

Table 4.4 Laser misalignment tolerance if 1 dB power penalty is allowed after 1 and 8 cascaded PHASARs corresponding to the designs COM04 and COM06 with 88 GHz FWHM bandwidth.

narrows much faster when the number of cascaded multiplexers is increased, resulting in a misalignment tolerance of only 24 GHz after 8 devices. Power penalties as a function of laser detuning have also been calculated assuming all the considered PHASARs were strictly linear-phase. The phase responses of the COM04 and COM06 PHASAR designs have been shown to contribute significantly to the reduction of their usable bandwidth when cascaded. In the case of the parabolic horn pass-band flattened design (COM06) with 88 GHz FWHM bandwidth, the laser misalignment tolerance could be extended from 24 GHz to 40 GHz for 1 dB penalty after 8 cascades, provided the device could be made strictly linear-phase.

4.4 Discussion

Cascadability investigations have been performed on ideal mathematical transfer functions as well as on realistic transfer functions resulting from accurate device modelling. The main goal of the simulations was to determine how small the bandwidth of a PHASAR wavelength (de)multiplexer could be in order to accommodate a 40 Gbit/s NRZ signal with reduced power penalty after 4 cascaded add-drop nodes (each consisting of one multiplexer / demultiplexer pair). The results obtained with reference transfer functions (Section 4.2), as well as modelled conventional and pass-band flattened PHASARs (Section 4.3) are summarised in Table 4.5. The Gaussian and double Gaussian reference transfer functions were considered to be strictly linear phase. For accurately modelled devices, both results obtained with the full complex (amplitude and phase) transfer functions, as well as with hypothetical transfer functions were the phase is assumed to be strictly linear, are presented.

A very good agreement is obtained between the mathematical 1st order Gaussian transfer function and the modelled non-flattened COM03 PHASAR, either with or without phase response. This indicates that the

Filter	FWHM bandwidth (GHz)	
	with phase	without phase
Gaussian 1st order	NA	88
Gaussian 2nd order	NA	60
Gaussian 3rd order	NA	53
Double Gaussian $\alpha = 0.45$	NA	72
Double Gaussian $\alpha = 0.5$	NA	65
COM03	∼89	89
COM04	∼77	51
COM05	-	-
COM06	∼77	50

Table 4.5 Summary of FWHM bandwidths giving rise to 1 dB power penalty after 8 cascaded multiplexers for all reference and modelled transfer functions considered in this work. The mathematical transfer functions assume linear-phase. For the modelled devices, both complex (amplitude and phase) and hypothetical transfer functions where the phase is assumed to be strictly linear are considered.

modelled amplitude response is very close to the expected Gaussian transfer function and that its phase response has a nearly ideal linear behaviour. Although non-idealities such as losses are introduced in the device modelling, a filter response close to the theoretical limits can be obtained. This comparison also enables us to gain confidence in both our devices and systems models. Among the reference transfer functions, the best results are obtained with the transfer functions having the sharper roll-off (3rd order Gaussian). The excessive amplitude ripples (∼1 dB) present in the transfer function of the MMI coupler pass-band flattened PHASAR COM05 prevent it from being cascaded 8 times. It has also been shown that large detrimental dispersion values are associated to these amplitude ripples. It is quite remarkable that the results obtained with the pass-band flattened PHASAR design making use of a parabolic horn (COM06) are extremely close to the ones calculated from the theoretically maximally flat transfer function COM04. The required bandwidth resulting in 1 dB penalty after 4 nodes is identical in both cases. Moreover, if we assume the phase to be linear, a smaller bandwidth is allowed for COM06 than for the mathematical 3rd order Gaussian transfer function. Therefore, from a pure amplitude transfer function point of view, the parabolic horn flattened design exhibits nearly ideal behaviour. Nevertheless, the effects of dispersion prevent this optimum from being reached and require a $\sim 50\%$ increase in filter FWHM

bandwidth in order to match the criterion of 1 dB penalty after 4 nodes. As a consequence, the parabolic horn pass-band flattened PHASAR is the design of choice in order to minimise the filter bandwidth. A FWHM bandwidth of about 78 GHz was shown to fulfil our strict 1 dB power penalty requirement.

Once the study of both amplitude and phase filtering effects has resulted in suggestions for multiplexers design and bandwidth, an appropriate channel spacing needs to be decided. This requires a detailed cross-talk investigation which is outside the scope of the present study. For instance, if we compare the COM04 and COM06 designs, which result in nearly the same bandwidth value in order to obtain less than 1 dB penalty after 8 cascaded PHASARs, it is clear from the transfer functions plot in Figure 4.11 that COM04 would be preferable because of its lower cross-talk level (about 30 dB less than COM06). Unfortunately, COM04 does not represent a physical device and therefore we need to optimise the channel spacing based on the COM06 transfer function. A FWHM bandwidth of 78 GHz and a channel spacing of 88 GHz will result in a -35 dB cross-talk level for COM06. However, due to the relative width of the 40 Gbit/s NRZ spectrum with respect to the filter bandwidth, there is strictly no certitude that this cross-talk level is sufficient, and more detailed investigations are required. As an illustration, Figure 4.21 shows the power spectra of two 40 Gbit/s NRZ signals spaced 88 GHz apart and filtered by the COM06 transfer function with 78 GHz FWHM bandwidth. One of the signals is assumed to be perfectly aligned with the filter centre frequency.

A significant amount of spectral overlap can be observed, and one might be seriously concerned about the cross-talk penalty in this configuration. A channel spacing of 88 GHz results in a spectral efficiency of 0.45 bit/s/Hz at 40 Gbit/s, which is of the same order of magnitude as previously reported networking experiments [14, 16]. Neglecting cross-talk issues, if a 3 dB power penalty is allowed after 4 add-drop nodes, the multiplexer bandwidth could be reduced down to 55 GHz and the spectral efficiency would increase accordingly up to 0.64 bit/s/Hz. It is somehow surprising that in spite of our best efforts to optimise (de)multiplexing elements for 40 Gbit/s NRZ transmission, the maximum achievable spectral efficiency as suggested by our simulations only matches the ones from the few reported networking experiments over a similar number of nodes (0.4 bit/s/Hz) [14, 16]. This is even more surprising when we remember that [16] deals with transmission of return-to-zero signals through flat-top PHASARs designed for 10 Gbit/s systems. However, in those experiments the figure of merit used to assess the quality of the transmission is a Q factor equal to 6 corresponding to a

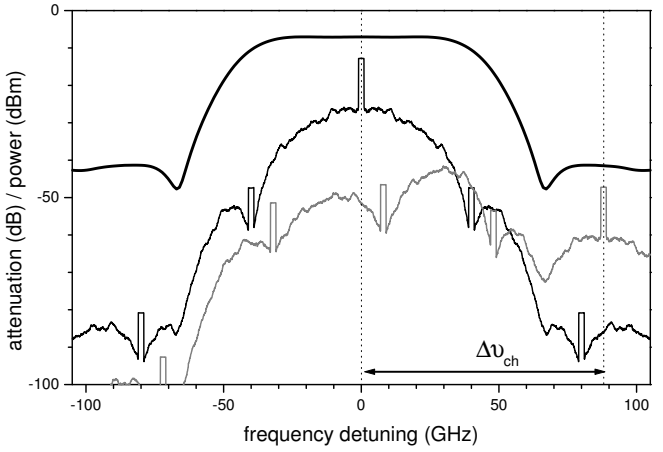

Figure 4.21 Relative power of two 40 Gbit/s NRZ channels spaced $\Delta\nu_{ch}$=88 GHz apart and filtered by a COM06 multiplexer with 78 GHz FWHM bandwidth. The multiplexer amplitude transfer function is also shown in the figure. The significant level of cross-talk (spectral overlap) is clearly visible. The power of the spectra is averaged over a ∼2 GHz square band-pass filter.

BER of 1.0×10^{-9} at the receiver. This might be achieved even in the presence of large penalties and therefore our criterion of 1 dB power penalty after 8 cascaded (de)multiplexers is much stricter and more in line with the requirements of commercial systems. As stated previously, a more relaxed penalty tolerance of 3 dB would also provide a Q value larger than 6 at the receiver, while ensuring an increased spectral efficiency. It should also be kept in mind that, in a real network implementation, the nodes will be linked by optical fibres (the target values for the METEOR field trial are 35–40 km between the nodes corresponding to an optical ring perimeter of 150 km). Non-linearities in these fibres, and more specifically self-phase modulation (SPM) and cross-phase modulation (XPM) might cause some amount of spectral broadening which should be taken into account when deciding for a filter bandwidth. When finally deciding for a filter bandwidth, some provision for spectral broadening should be allowed.

4.5 Summary of Chapter 4

We have performed a thorough investigation of amplitude and phase filtering effects in a cascade of pass-band flattened PHASAR (de)multiplexers. It has been shown that a PHASAR design based on a parabolic horn (or taper) input coupler is the most promising. According to our numerical sim-

ulations, a FWHM bandwidth of 78 GHz results in less than 1 dB power penalty after 8 cascaded multiplexers corresponding to 4 add-drop nodes. A laser misalignment tolerance of about 20 GHz (for less than 1 dB penalty) is allowed after 8 devices. It has also been shown that the dispersion of the device is responsible for increased penalty and accounts for a significant reduction of its usable bandwidth when the multiplexer is cascaded. The PHASAR bandwidth needs to be further adjusted in order to accommodate possible spectral broadening induced by optical fibres non-linearities. The final value of the channel spacing will also need to take into account the effects of cross-talk. Nevertheless, the goal of a channel separation smaller than 100 GHz (resulting in a spectral efficiency above 0.4 bit/s/Hz) seems to be reachable. The extremely demanding criterion of 1 dB power penalty after 4 add-drop nodes also indicates that better spectral efficiencies could be achieved if more relaxed tolerances are allowed.

4.6 References to Chapter 4

[1] M. W. Chbat and D. Penninckx, "High-spectral-efficiency transmission systems", in *Technical Digest Optical Fiber Communication Conference, OFC'00*, Baltimore, Maryland, U.S.A., paper TuJ1, vol. 1, pp. 134–136, 2000.

[2] E. Desurvire, "Fundamental information-density limits in optically amplified transmission: an entropy analysis", *Optics Letters*, vol. 25, no. 10, pp. 701–703, 2000.

[3] T. Ono and Y. Yano, "Key technologies for Terabit/s WDM systems with high spectral efficiency of over 1 bit/s/Hz", *IEEE Journal of Quantum Electronics*, vol. 34, no. 11, pp. 2080–2088, 1998.

[4] T. Ito, K. Fukuchi, K. Sekiya, D. Ogasahara, R. Ohhira, and T. Ono, "6.4 Tb/s (160×40 Gb/s WDM transmission experiment with 0.8 bit/s/Hz spectral efficiency", in *Proceedings European Conference on Optical Communication, ECOC'00*, Munich, Germany, postdeadline paper PD1.1, 2000.

[5] M. K. Smit and C. van Dam, "PHASAR-based WDM-devices: principles, design and applications", *IEEE Journal of Selected Topics in Quantum Electronics*, vol. 2, no. 2, pp. 236–250, 1996.

[6] H. Takahashi, K. Oda, H. Toba, and Y. Inoue, "Transmission characteristics of arrayed waveguide N×N wavelength multiplexer", *Journal of Lightwave Technology*, vol. 13, no. 3, pp. 447–455, 1995.

[7] M. Shtaif and A. H. Gnauck, "The relation between optical duobinary modulation and spectral efficiency in WDM systems", *IEEE Photonics Technology Letters*, vol. 11, no. 6, pp. 712–714, 1999.

[8] T. N. Nielsen, A. J. Stentz, P. B. Hansen, Z. J. Chen, D. S. Vengsarkar, T. A. Strasser, K. Rottwit, J. H. Park, S. Stulz, S. Cabot, K. S. Feder, P. S. Westbrook, and S. G. Kosinski, "1.6 Tb/s (40×40 Gb/s) transmission over 4×100 km nonzero-dispersion fiber using hybrid raman/erbium-doped inline amplifiers", in *Proceedings European Conference on Optical Communication, ECOC'99*, Nice, France, post-deadline paper, pp. 26–27, 1999.

[9] S. Bigo, A. Bertaina, Y. Frignac, S. Borne, L. Lorcy, D. Hamoir, D. Bayart, J.-P. Hamaide, W. Idler, E. Lach, B. Franz, G. Veith, P. Sillard, L. Fleury, P. Guénot, and P. Nouchi, "5.12 Tbit/s (128×40 Gbit/s WDM) transmission over 3×100 km of TeraLight™ fibre", in *Proceedings European Conference on Optical Communication, ECOC'00*, Munich, Germany, post-deadline paper PD1.2, 2000.

[10] A. Färbert, G. Mohs, S. Spälter, J.-P. Elbers, C. Fürst, A. Schöpflin, E. Gottwald, C. Scheerer, and C. Glingener, "7 Tb/s (176×40 Gb/s) bidirectional interleaved transmission with 50 GHz channel spacing", in *Proceedings European Conference on Optical Communication, ECOC'00*, Munich, Germany, post-deadline paper PD1.3, 2000.

[11] S. Bigo, E. Lach, Y. Frignac, D. Hamoir, P. Sillard, W. Idler, S. Gauchard, A. Bertaina, S. Borne, L. Lorcy, N. Torabi, B. Franz, P. Nouchi, P. Guénot, L. Fleury, G. Wien, G. L. Ber, R. Fritschi, B. Junginger, M. Kaiser, D. Bayart, G. Veith, J.-P. Hamaide, and J.-L. Beylat, "1.28 Tbit/s WDM transmission of 32 ETDM channels at 40 Gbit/s over 3×100 km distance", in *Proceedings European Conference on Optical Communication, ECOC'00*, Munich, Germany, vol. 4, pp. 17–19, 2000.

[12] E. Brandon, J.-P. Blondel, F. Boubal, L. Buet, V. Havard, A. Hugbart, L. Labrunie, P. L. Roux, D. Toullier, and R. Uhel, "1.28 Tbit/s (32×40 Gbit/s) unrepeatered transmission over 250 km", in *Proceedings European Conference on Optical Communication, ECOC'00*, Munich, Germany, vol. 4, pp. 21–23, 2000.

[13] P. M. Krummrich, E. Gottwald, A. Schöpflin, C.-J. Weiske, K. Kotten, and G. Fischer, "40 Gb/s ETDM for long haul WDM transmission", in *Proceedings European Conference on Optical Communication, ECOC'00*, Munich, Germany, vol. 4, pp. 13–14, 2000.

[14] H. K. Kim, S. Chandrasekhar, T. Nielsen, C. Doerr, L. Stulz, L. Buhl, R. Monnard, S. Radic, and M. Zirngibl, "1.6 Tbit/s (40×40 Gb/s) total capacity 4-node optical networking with fully programmable A/D devices", in *Technical Digest Optical Fiber Communication Conference, OFC'00*, Baltimore, Maryland, U.S.A., post-deadline paper PD34, 2000.

[15] C. R. Doerr, L. W. Stulz, M. Cappuzzo, E. Laskowski, A. Paunescu, L. Gomez, J. V. Gates, S. Shunk, S. Chandrasekhar, and H. Kim, "40-channel programmable integrated add-drop with flat through-spectrum", in *Proceedings European Conference on Optical Communication, ECOC'99*, Nice, France, post-deadline paper PD3-1, pp. 46–47, 1999.

[16] Y. Horiuchi and S. Yamamoto, "1 Tbit/s (25×40 Gbit/s) transmission over 100 km transparent network with 5 OADM nodes using AWG filters", in *Proceedings European Conference on Optical Communication, ECOC'00*, Munich, Germany, vol. 3, pp. 263–265, 2000.

[17] G. Lenz, B. J. Eggleton, C. R. Giles, C. K. Madsen, and R. E. Slusher, "Dispersive properties of optical filters for WDM systems", *IEEE Journal of Quantum Electronics*, vol. 34, no. 8, pp. 1390–1402, 1998.

[18] G. Lenz, B. J. Eggleton, C. K. Madsen, C. R. Giles, and G. Nykolak, "Optimal dispersion of optical filters for WDM systems", *IEEE Photonics Technology Letters*, vol. 10, no. 4, pp. 567–569, 1998.

[19] G. Lenz, G. Nykolak, and B. J. Eggleton, "Waveguide grating routers for dispersionless filtering in WDM system at channel rate of 10 Gbit/s", *Electronics Letters*, vol. 34, no. 17, pp. 1683–1684, 1998.

[20] C. K. Madsen and J. H. Zhao, *Optical filter design and analysis, a signal processing approach*, chapter 4, pp. 184–198, Wiley, New-York, 1999.

[21] H. Yamada, K. Okamoto, A. Kaneko, and A. Sugita, "Dispersion resulting from phase and amplitude errors in arrayed-waveguide grating

multiplexers-demultiplexers", *Optics Letters*, vol. 25, no. 8, pp. 569–571, 2000.

[22] H. Yamada, H. Sanjoh, M. Kohtoku, and K. Takada, "Measurement of phase and amplitude error distributions in InP-based arrayed-waveguide grating multi/demultiplexers", *Electronics Letters*, vol. 36, no. 2, pp. 136–138, 2000.

[23] A. J. Lowery and P. C. R. Gurney, "270-km 10 Gbit/s WDM dispersion compensation using a chirped AWGM", in *Technical Digest Optical Fiber Communication Conference, OFC'99*, San Diego, California, U.S.A., paper FD5, vol. 4, pp. 74–76, 1999.

[24] M. C. Parker and S. D. Walker, "Virtually ripple-free, multi-channel, adaptive dispersion compensator based on a re-multiplexing AWG cascade", in *Proceedings European Conference on Optical Communication, ECOC'00*, Munich, Germany, vol. 3, pp. 175–176, 2000.

[25] M. C. Parker and S. D. Walker, "Adaptive chromatic dispersion controller based on an electro-optically chirped arrayed-waveguide grating", in *Technical Digest Optical Fiber Communication Conference, OFC'00*, Baltimore, Maryland, U.S.A., paper WM16, vol. 2, pp. 257–259, 2000.

[26] J. E. A. Whiteaway, A. Fielding, T. Bricheno, M. E. Haywood, S. Day, T. V. Clapp, S. M. Ojha, and P. J. Ayliffe, "Novel AWG interleaved filters with a 50 GHz channel spacing exhibiting high 'Figure of Merit' pass-bands, and low loss, cross-talk, dispersion and polarisation sensitivity", in *Proceedings European Conference on Optical Communication, ECOC'00*, Munich, Germany, vol. 3, pp. 25–26, 2000.

[27] C. Caspar, H.-M. Foisel, R. Freund, U. Krüger, and B. Strebel, "Cascadability of arrayed-waveguide grating (de)multiplexers in transparent optical networks", in *Technical Digest Optical Fiber Communication Conference, OFC'97*, Dallas, Texas, U.S.A., paper TuE2, vol. 6, pp. 19–21, 1997.

[28] C. Caspar, H.-M. Foisel, C. v. Helmolt, B. Strebel, and Y. Sugaya, "Comparison of cascadability performance of different types of commercially available wavelength (de)multiplexers", *Electronics Letters*, vol. 33, no. 19, pp. 1624–1626, 1997.

[29] M. Nissov, R. J. S. Pedersen, and B. F. Jørgensen, "Transmission performance through cascaded 1-nm arrayed waveguide multiplexers at

10 Gb/s", *IEEE Photonics Technology Letters*, vol. 9, no. 7, pp. 1038–1040, 1997.

[30] C. Caspar, H.-M. Foisel, R. Freund, and B. Strebel, "Four-channel 10-Gbit/s transmission over 15-wavelength-selective cross-connect paths and 1175-km dispersion-compensated standard single-mode fiber links", in *Technical Digest Optical Fiber Communication Conference, OFC'98*, San Jose, California, U.S.A., paper ThP3, vol. 2, pp. 327–329, 1998.

[31] T. Otani, N. Antoniades, I. Roudas, and T. E. Stern, "Cascadability of passband-flattened arrayed waveguide-grating filters in WDM optical networks", *IEEE Photonics Technology Letters*, vol. 11, no. 11, pp. 1414–1416, 1999.

[32] J. B. D. Soole, M. R. Amersfoort, H. P. LeBlanc, N. C. Andreadakis, A. Rajhel, C. Caneau, R. Bhat, M. A. Koza, C. Youtsey, and I. Adesida, "Use of multimode interference couplers to broaden the passband of wavelength-dispersive integrated WDM filters", *IEEE Photonics Technology Letters*, vol. 8, no. 10, pp. 1340–1342, 1996.

[33] A. Lowery, O. Lenzmann, I. Koltchanov, R. Moosburger, R. Freund, A. Richter, S. Georgi, D. Breuer, and H. Hamster, "Multiple signal representation simulation of photonic devices, systems, and networks", *IEEE Journal of Selected Topics in Quantum Electronics*, vol. 6, no. 2, pp. 282–296, 2000.

[34] C. J. Anderson and J. A. Lyle, "Technique for evaluating system performance using Q in numerical simulations exhibiting intersymbol interference", *Electronics Letters*, vol. 30, no. 1, pp. 71–72, 1994.

[35] K. Okamoto and H. Yamada, "Arrayed-waveguide grating multiplexer with flat spectral response", *Optics Letters*, vol. 20, no. 1, pp. 43–35, 1995.

[36] C. Dragone, T. Strasser, G. A. Bogert, L. W. Stulz, and P. Chou, "Waveguide grating router with maximally flat passband produced by spatial filtering", *Electronics Letters*, vol. 33, no. 15, pp. 1312–1314, 1997.

[37] A. Rigny, A. Bruno, and H. Sik, "Multigrating method for flattened spectral response wavelength multi/demultiplexer", *Electronics Letters*, vol. 33, no. 20, pp. 1701–1702, 1997.

[38] Y. P. Ho, H. Li, and Y. J. Chen, "Flat channel-passband-wavelength multiplexing and demultiplexing devices by multiple-Rowland-circle design", *IEEE Photonics Technology Letters*, vol. 9, no. 3, pp. 342–344, 1997.

[39] L. B. Soldano and E. C. M. Pennings, "Optical multi-mode interference devices based on self-imaging: principles and applications", *Journal of Lightwave Technology*, vol. 13, no. 4, pp. 615–627, 1995.

[40] M. R. Amersfoort, J. B. D. Soole, H. P. LeBlanc, N. C. Andreadakis, A. Rajhel, and C. Caneau, "Passband broadening of integrated arrayed waveguide filters using multimode interference couplers", *Electronics Letters*, vol. 32, no. 5, pp. 449–451, 1996.

[41] K. Okamoto and A. Sugita, "Flat spectral response arrayed-waveguide grating multiplexer with parabolic waveguide horns", *Electronics Letters*, vol. 32, no. 18, pp. 1661–1662, 1996.

[42] C. Peucheret and C. Herben, "First design of band-flattened GHz silica PHASAR", IST-1999-10402 METEOR project, deliverable D11, 2000.

[43] M. E. Marhic and X. Yi, "Calculation of dispersion in arrayed waveguide grating demultiplexers by a shifting-image method", *IEEE Journal of Selected Topics in Quantum Electronics*, vol. 8, no. 6, pp. 1149–1157, 2002.

[44] C. J. Rasmussen, *Transmission analysis in WDM networks.* PhD thesis, COM, Technical University of Denmark, Lyngby, Denmark, 1999.

Chapter 5

Design of all-optical networks using normalised transmission sections

5.1 Introduction

Wavelength division multiplexing (WDM) is an attractive technology to satisfy the needs for capacity and flexibility required by future all-optical networks. The design of such networks is the object of intense research activities dealing with a vast number of issues such as network topology, wavelength allocation, routing, design of effective protection and restoration schemes, etc. [1]. However, in order for this upper-level approach to be implemented practically, a detailed knowledge of the transmission limitations at the physical layer level is required. The necessary degree of transparency for optical networks has been the object of much debate [2]. Different meanings are frequently encountered for the notion of transparency, including transparency to the client signal (e.g. synchronous digital hierarchy (SDH) or asynchronous transfer mode (ATM)), to the line coding (e.g. non-return to zero (NRZ) or return to zero (RZ)), to the modulation format (analogue or digital; amplitude-shift-keying (ASK), frequency-shift-keying (FSK), on-off-keying (OOK), etc.) or to the bit rate (e.g. from 155 Mbit/s to 10 Gbit/s and above). Even if ITU-T recommendations [3] are followed and the so-called "format" transparency is limited to NRZ and RZ line code on an OOK modulation format up to 10 Gbit/s, the transparent extension of optical networks is severely limited by a full range of signal degradation mechanisms. Large scale networks can therefore be naturally divided into transparent domains or sub-networks where end-to-end transparency

could be achieved [4, 5]. It is the object of this chapter to investigate the extension of these transparent domains based upon which network design guidelines are provided. To do so, the concept of "normalised sections" is introduced. Normalised sections facilitate the investigation of the transparency limitations in the network and constitute an efficient tool to ease network planning and management.

In the remaining of Section 5.1, we emphasise the analogue nature of all-optical networks and review signal degradations that are likely to occur and accumulate in the transmission paths. These degradations can be divided into two categories, depending on whether they can be minimised by a proper design of optical components or whether they are inherent to the optical fibre link. Based on this classification, a number of key parameters which will ultimately limit transparent domains extension are identified and their effects studied. As the use of dispersion compensating fibres (DCF) has been suggested as an effective way to upgrade installed links made of standard single mode fibre (SMF) [6], we focus our work on systems based on SMF+DCF transmission spans. The study relies on the division of any transmission path in the network in a cascade of normalised transmission sections consisting of SMF, DCF, and erbium-doped fibre amplifiers (EDFA). The different normalised section candidates are introduced in Section 5.1.2. The goal of the investigation is to maximise the number of cascaded transmission sections with respect to the power levels at the SMF and DCF inputs, as well as the degree of compensation. The optimisation is performed in the first place using extensive numerical simulations. A systematic numerical comparison of normalised sections based on four different dispersion compensation schemes is presented in Section 5.2 for 80 km spans and NRZ modulation at 10 Gbit/s, where it is shown that post-compensation performs better than pre-compensation at the expense of reduced parameters tolerance. Furthermore, pre-distortion at the transmitter is shown to significantly improve the performance of the system. Experimental investigations on 80 km pre-compensated normalised sections are presented in Section 5.3 for single channel, as well as for an eight channel WDM system using NRZ modulation. The influence of the compensation ratio and the effect of pre-distortion at the transmitter are confirmed experimentally. Finally, a systematic experimental comparison of pre- and post-compensation, with and without pre-distortion, is reported for chirped return-to-zero (CRZ) modulation at 10 Gbit/s.

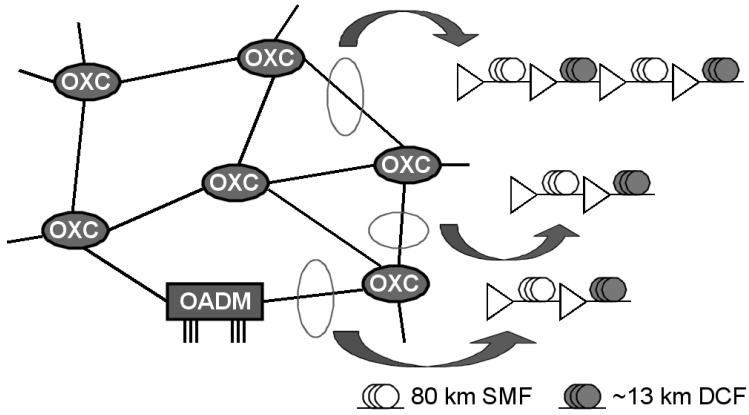

Figure 5.1 Transparent domain within an optical network. Optical network elements such as OXC or OADM are connected with fibre links made of SMF and DCF. No regeneration is present within the transparent domain boundaries.

5.1.1 Physical origin of transparency limitations

A generic configuration for an all-optical network is shown in Figure 5.1. It consists of a number of optical network elements (ONE) such as optical terminal multiplexers and demultiplexers, optical add-drop multiplexers (OADM) and optical cross-connects (OXC), connected together by optical fibre links. The links, which may include optical amplification, can be made of a variety of optical fibre types. We will limit ourselves to the case of SMFs which are already widely used in existing fibre plants. At 10 Gbit/s and above, the use of dispersion compensating fibres will be required in the links. Signal degradations can originate from different sources in such a network. Optical networks elements are responsible for non-ideal transfer functions, including excess loss, amplitude transfer function shape and attenuation ripples, non-linear phase behaviour (dispersion), bandwidth narrowing induced by cascading and cross-talk. These effects are more or less pronounced depending on the used technology [7]. For instance, the pass-band of fibre Bragg gratings can be tailored in order to present the desired flat-top shape, low cross-talk and low insertion loss. However such devices are known to be inherently dispersive, as discussed in Chapter 3. On the other hand, arrayed-waveguide grating devices are inherently dispersion-less, but obtaining ideal flat-top and low crosstalk amplitude transfer functions remains an issue, which has been the topic of Chapter 4. Nevertheless, it can be assumed that such technology challenges

can be solved or that at least tight tolerances on the transfer function of optical network elements can be achieved, so that only minor degradations are induced. Even in the presence of ideal ONE transfer functions, some issues such as tolerance towards laser misalignment would remain. However, these could also be solved in principle by precise laser frequency and multiplexer centre wavelength control. Degradations arising from EDFAs are twofold. Gain tilt in WDM systems can be corrected by adequate gain equalisation techniques. On the other hand, although the noise figure of EDFAs can be minimised by a proper design, the noise generation in amplifiers cannot be avoided. Degradation mechanisms inherent to optical fibres are attenuation, group-velocity dispersion (GVD), polarisation mode dispersion (PMD) [8] and various non-linear effects including self-phase modulation (SPM), cross-phase modulation (XPM), four-wave mixing (FWM) and stimulated Raman scattering (SRS) [9]. Although the effect of these non-linearities can be minimised for a given type of fibre by reducing power levels (at the expense of reduced signal-to-noise ratio), they clearly cannot be totally suppressed. Therefore, it is clear from the above that two kinds of degradation mechanisms are to be encountered in optical networks: those which could ultimately be reduced to a negligible influence by proper component design or sufficiently strict tolerances, and those which are inherent to basic physical mechanisms in amplifiers and optical fibres and which simply cannot be avoided. This statement should not hide the fact that a lot of challenging tasks are ahead of us in order to design optical components and subsystems which would minimise the perturbations belonging to the first category. One of the most detrimental aspect of these degradations is due to their accumulative nature. It is this analogue behaviour of optical networks which limits the extension over which a signal can propagate with sufficient quality. It is also clear that the effects of the basic system degradations will, in most cases, depend on the format and bit rate of the optical signal. Therefore the design of transparent all-optical networks appears as a daunting task.

One possible design approach consists in defining some transparent domains or sub-networks over which the required degree of transparency can be guaranteed [4, 5]. Such sub-divisions in the optical network would be connected via sub-network interfaces (SNI) providing some amount of regeneration (amplification and reshaping (2R) or amplification, reshaping and re-timing (3R), as required). This concept is illustrated in Figure 5.2. Each transparent sub-network would then consist of ONEs, optical amplifiers and fibre links. It would be ensured that no regeneration is necessary within a transparent sub-network, whichever physical path is followed by

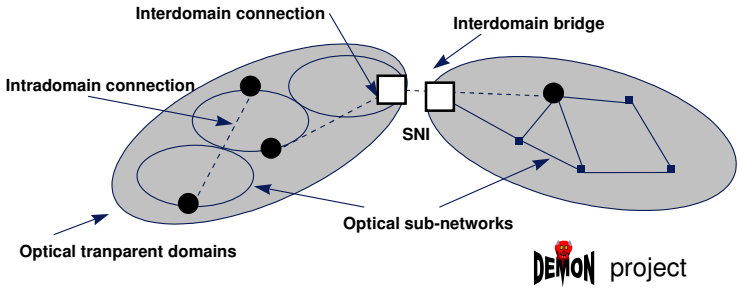

Figure 5.2 Subdivision of an optical network into transparent domains. Regeneration is performed uniquely at the boundary between the transparent domains. SNI: sub-network interface. Source: DEMON project.

the signal within this sub-network. In order to implement such an approach, it is essential to be able to assess the extension of the transparent sub-networks. A pre-requisite is the definition of the level of transparency which is sought. In this work, we limit ourselves to NRZ and RZ line code with OOK modulation at bit rates up to 10 Gbit/s.

5.1.2 The normalised section approach

A simplified approach to the definition of transparent sub-networks consists in dividing each path in the network into a cascade of identical transmission sections, the so-called "normalised sections" [10, 11]. Defining the extension of transparent sub-networks will then be equivalent to finding the maximum number of normalised sections which can be cascaded for an acceptable signal degradation. The signal degradation induced by cascading networks elements has been treated in the context of fibre grating devices and arrayed waveguide gratings in Chapter 3 and 4, respectively. In this chapter, we therefore concentrate on the limitations to the extension of transparent sub-networks set by the interaction of chromatic dispersion, optical fibre non-linearities and amplifier noise. Consequently, we consider these physical mechanisms to be the main cause for system penalty and, as a first approximation, ignore the other sources of signal degradation. Normalised transmission sections consist then of EDFAs, SMF and DCF. Based on ITU-T recommendations for terrestrial networks [12], span lengths of 80 km are considered. Due to the non-linear nature of propagation, the system performance depends on the power levels at the input of the different types of fibres, on the position of the DCF with respect to the SMF and on the amount of residual dispersion. Three different types of spans

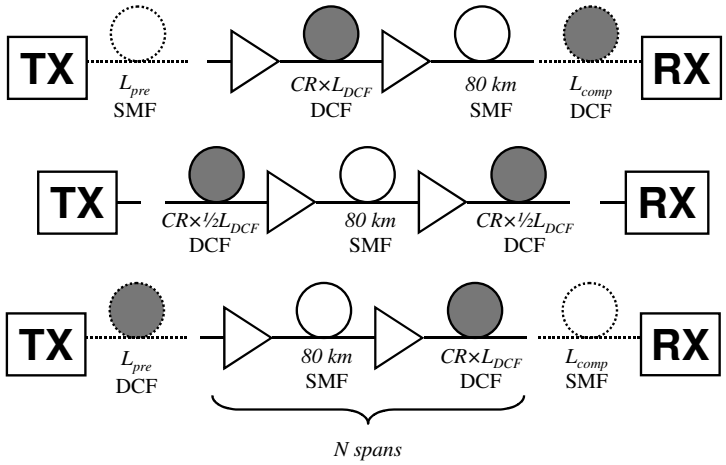

Figure 5.3 Definition of normalised sections. Top: pre-compensation; middle: hybrid compensation; bottom: post-compensation. In the pre- and post-compensation cases, some length L_{pre} of pre-distortion DCF or SMF, respectively, can be added at the transmitter, together with the matching length L_{post} of SMF or DCF at the receiver.

can be considered. Those are represented in Figure 5.3. They correspond to pre-compensation, where the DCF is placed before the SMF for each span, post-compensation, where it is placed after the SMF for each span, and hybrid split-compensation where the dispersion compensation is split into two sections of equal dispersion amount placed before and after the SMF. In a practical system design, dispersion compensating modules will be placed within dual stage optical amplifiers. Additional flexibility can be provided by optional pre-distortion, which consists of an added piece of DCF at the transmitter in the post-compensation scheme, or a piece of SMF in the pre-compensation case, and corresponding compensation at the receiver. Dispersion maps illustrating all these possibilities are represented in Figure 5.4.

The optimisation procedure is carried out as follows. First a set of relevant parameters needs to be identified. In the case of the normalised sections described previously, the power at the input of the SMF, the power at the input of the DCF, the compensation ratio and the amount of pre-distortion appear as natural design parameters. The compensation ratio is defined as the absolute value of the ratio of the total dispersion accumulated in the DCF to the total dispersion accumulated in the SMF for one span. The optimisation is then performed, aiming at maximising the

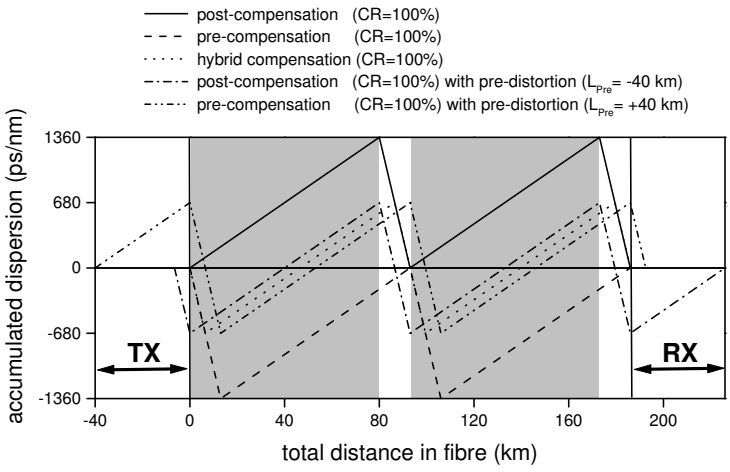

Figure 5.4 Dispersion maps corresponding to post-, pre-, and hybrid dispersion compensation with or without optional pre-distortion. The maps are represented for two periods and correspond to 100% compensation.

number of cascaded normalised sections while achieving sufficiently large parameter tolerance. Due to the occurrence of multi-channel non-linear effects such as cross-phase modulation, four-wave mixing and stimulated Raman scattering, the numerical optimisation procedure should be performed for various WDM configurations (i.e. varying number of channels and channel spacing). However, for sufficiently large channel spacing, both XPM and FWM have been shown to be at the origin of moderate penalties in systems making use of SMF and DCF [13]. The high local dispersion of both types of fibres prevents the phase matching giving rise to FWM and is responsible for small walk-off lengths minimising the interaction between channels at the origin of XPM. Lower wavelength channels depletion due to SRS can be corrected by designing EDFAs having opposite gain tilts. Therefore, the span optimisation can be performed as a first approximation for single channel transmission and the effects of additional degradations introduced with WDM can be assessed at a later stage.

Once the normalised transmission sections have been identified and once their cascadability behaviour has been thoroughly investigated, both network design and network management can be made easier in such a way that the physical complexity of the transmission path can be hidden from the pure networking aspects. From the network planning side, the scalability of the transparent optical sub-networks will be determined by the maximum number of sections which can be cascaded for a given system

penalty. From the management side, the implementation of re-routing, protection switching and restoration schemes will also rely on the availability of information on the maximum cascadability of normalised sections for a given class of signals.

5.2 Numerical comparison of pre- and post-compensation

We have seen that transmission spans made of SMF and DCF are good candidates as normalised sections as their high local dispersion is known to reduce the phase matching giving rise to four wave mixing in wavelength division multiplexing (WDM) systems. Signal degradation in such systems is due to the combined effects of group velocity dispersion, Kerr non-linearity and accumulation of amplified spontaneous emission noise due to periodic amplification. Because of the non-linear nature of propagation, system performance depends on the power levels at the input of the different types of fibres, on the position of the DCF [14] and on the amount of residual dispersion [15, 16].

In this section, the cascadability of 80 km long normalised sections using the post- and pre-compensation schemes is investigated in a systematic fashion using computer simulation for single channel non-return to zero modulation at 10 Gbit/s. We add another degree of freedom compared to earlier work [14, 15] by allowing for independent variation of the SMF and DCF input powers in order to define transmission optima and enable a comparison of the different normalised sections. The influence of the compensation ratio is also systematically investigated. We generalise the results of [15] and show that better performance can be obtained for post-compensation provided correct power levels are used at the SMF and DCF inputs. We also demonstrate that pre-distortion can significantly improve the performance of both pre- and post-compensated systems and shifts the optimum power levels towards higher values, which in turns provides a higher optical signal-to-noise ratio throughout the link.

The systems under investigation are shown in Figure 5.5. Continuous wave (CW) light is externally modulated at 10 Gbit/s with a NRZ pseudo-random binary sequence in a chirpless Mach-Zehnder modulator having a 13 dB extinction ratio and 25 ps rise-time, before being transmitted in a link consisting of a cascade of pre- or post-compensation normalised sections. These sections consist of 80 km of SMF and a variable length of DCF which is adjusted in order to define the compensation ratio. The fibres parameters are given in Table 5.1. Two EDFAs with 5 dB noise figure are used in each

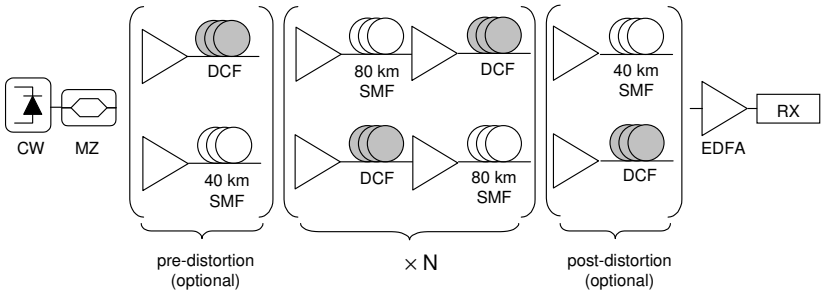

Figure 5.5 Post- (top) and pre-compensation (bottom) systems under investigation, with and without the optional pre-distortion fibres.

section in order to independently set the SMF and DCF input powers. After the desired number of cascades the signal is amplified to a level of 0 dBm, filtered by a 1^{st} order optical band-pass Gaussian filter with a 3 dB bandwidth of 25 GHz and input to the receiver which consists of a PIN photodiode with a responsivity of 1 A/W and a single sided thermal noise density of 15 pA/$\sqrt{\text{Hz}}$, followed by a 5^{th} order low-pass Bessel filter with a 3 dB bandwidth of 10 GHz. Optionally, a piece of DCF (respectively SMF) can be added at the transmitter in the post-compensation (respectively pre-compensation) case, the dispersion of which is compensated for at the receiver by an additional piece of SMF (respectively DCF). EDFAs are used to exactly compensate for the loss in these pre- and post-distortion fibres.

	SMF	DCF
Attenuation (dB/km)	0.25	0.5
Dispersion (ps/nm/km)	16	-102
Dispersion Slope (ps/nm^2/km)	0.06	-0.2
Non-linear index (m^2/W)	2.6×10^{-20}	2.6×10^{-20}
Effective area (μm^2)	80	22

Table 5.1 Fibre parameters used in the simulations of Section 5.2.

The calculation of the propagation in the optical fibres was performed using a standard split-step algorithm with adaptive step-size [17]. The EDFAs were modelled by wavelength independent gain and noise addition. Signal and noise interaction was included during propagation in the fibres. Noise was calculated in a 320 GHz bandwidth centred around the

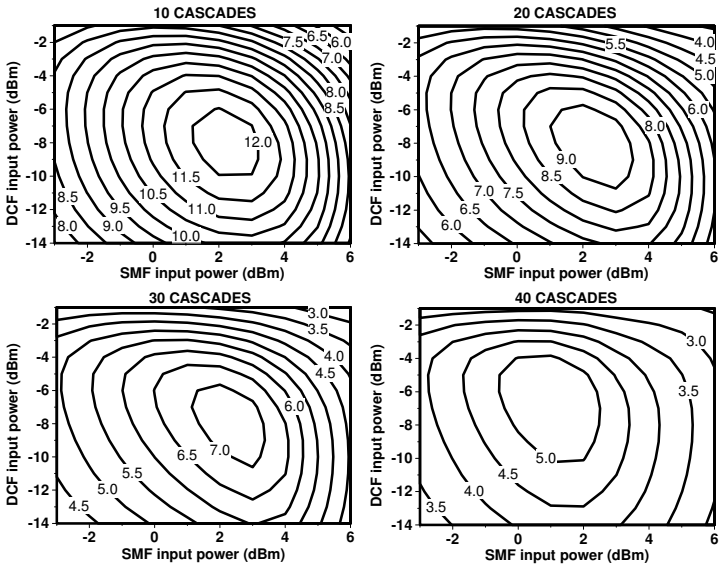

Figure 5.6 Evolution of the Q factor as a function of the SMF and DCF input powers for 10, 20, 30 and 40 cascaded sections in the case of 98% post-compensation without pre-distortion.

transmitter frequency which is equivalent to the use of a 2.5 nm square band-pass in-line filter. Sequence lengths of 1024 bits were used in order to obtain realistic Q factor estimations in the receiver model, as discussed in Appendix D. For each compensation ratio, the powers at the SMF input and DCF input were varied systematically by setting the gains of the EDFAs, and the Q factor was calculated for each set of powers after a defined number of cascaded spans.

Figure 5.6 shows Q factor contour plots obtained after 10, 20, 30 and 40 cascades for 98% post-compensation without any pre-distortion. The powers displayed on the axes are signal average power, meaning that the noise power in a given bandwidth centred on the laser wavelength is not taken into account. The existence of a transmission optimum for certain sets of powers is clearly seen in these contour plots. This optimum corresponds to input powers of about 2 dBm and -7 dBm into the SMF and DCF respectively. It can moreover be observed that, in this case, the position of the optimum does not vary much when the number of cascaded spans is increased. This allows for flexibility in network design as the power levels can be set independently of the path followed by a signal.

The compensation ratio has been varied between 97% and 101% for both

pre- and post- compensation schemes and optimum Q values and fibre input power levels have been extracted from contour plots similar to the ones in Figure 5.6. The results are summarised in Figure 5.7 where the maximum Q factors and the corresponding powers are plotted as a function of the compensation ratio for 30 cascaded sections corresponding to a 2400 km link. Post-compensation shows better performance than pre-compensation and exhibits a clear optimum corresponding to 98%. The Q factor and optimum power levels vary significantly when the compensation ratio is changed, which is not observed for pre-compensation, showing poorer but more stable performance. It should be pointed out that, in our system, a 1% change in the compensation ratio corresponds to only 12.8 ps/nm variation in dispersion, which is a high accuracy requirement when ordering dispersion compensating modules from fibre manufacturers. Moreover, even if we assume that multi-channel non-linear effects have little influence on systems making use of SMF and DCF, and unless DCFs with slope compensation are used, the compensation ratio will vary from one channel to another in WDM systems resulting in unequal channel performance, unless dispersion slope compensating DCFs are used [18]. Therefore running a system at its maximum performance using post-compensation does not allow for much parameter tolerance. It can also be seen on Figure 5.7 that, when the compensation ratio is decreased, optimum powers at both SMF and DCF inputs need to be increased in the post-compensation scheme. For 100% compensation, fibre input power levels are set by signal-to-noise ratio requirements and not by the need to counteract dispersion imbalance by self phase modulation (SPM). On the other hand, when the compensation ratio is decreased, some amount of SPM is required in order to make up for the under-compensation. SPM in the anomalous dispersion regime leads to pulse compression [19] and therefore a higher power into the SMF is desirable. Figure 5.7 shows that some amount of SPM in the DCF can also be beneficial for an under-compensated system, which is in agreement with [16] which studied a single span system. Introducing a pre-distortion fibre reduces the maximum amount of total accumulated dispersion and realises passive pre-chirping at the transmitter.

In Figure 5.8 we show the relative performance of pre- and post-compensation with and without pre-distortion for 100% compensation and 30 cascades. In this case, the absolute value of the dispersion of both pre- and post-distortion fibres corresponds to half of the total dispersion accumulated in one span of SMF. With this value the excursion (from 0 ps/nm) of the total accumulated dispersion is minimised and is moreover the same for pre- and post-compensation. However, it might not correspond to an abso-

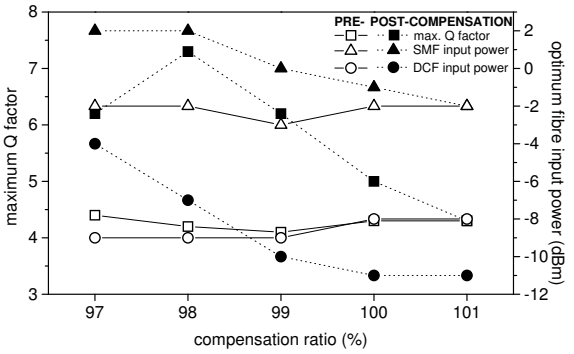

Figure 5.7 Maximum Q factor and corresponding SMF and DCF optimum input powers as a function of the compensation ratio for 30 cascades of the pre- and post-compensation sections.

lute optimum as new design parameters (lengths and input powers of the pre- and post-distortion fibres) are introduced. Again, a higher maximum Q factor is obtained for post-compensation compared to pre-compensation. For a given compensation ratio (here 100% but the same trend has been observed for other ratios), the transmission performance can be significantly improved by using pre-distortion. In the 100% case results are comparable whether pre- or post-compensation is used. This is due to the fact that in this case, if the pre- and post-distortion fibres are excluded, these two dispersion maps are only translated by one DCF length. Pre-distortion has also the effect of shifting the optimum powers towards higher values. This is beneficial as it provides a higher signal-to-noise ratio throughout the system.

We have therefore performed a systematic compensation ratio and fibre input power optimisation of pre- and post dispersion compensation schemes using SMF and DCF. We have shown that, if no pre-distortion is used, post compensation performs better at the expense of more stringent parameter tolerance. A compensation ratio of 98% has been found to constitute an optimum for post-compensation. On the other hand, when pre-compensation is used, little influence of the compensation ratio on the optimum Q factor and power levels has been observed. We have also shown that introducing pre-distortion can significantly improve the performance of both pre- and post-compensation schemes.

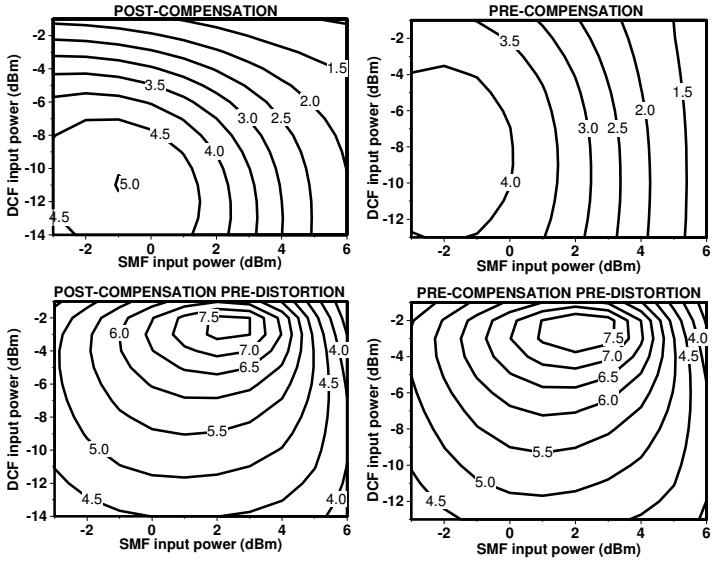

Figure 5.8 Q factor for 30 cascades as a function of SMF and DCF input powers for 100% post- (left) and pre- (right) compensation with (bottom) or without (top) 50% pre-distortion.

5.3 Experimental investigations on normalised sections

Experimental investigations on 80 km normalised sections are presented in this section at a bit rate of 10 Gbit/s. The importance of the choice of the compensation ratio is highlighted by re-circulating loop experiments whose results are reported in Section 5.3.1 for single-channel NRZ modulation. The extension to an 8-channel WDM system presented in Section 5.3.2 confirms the influence of the compensation ratio and demonstrates the benefit of using pre-distortion at the transmitter. Finally, an experimental comparison of pre- and post-compensation, with and without pre-distortion, is reported in Section 5.3.3 for chirped return-to-zero modulation, where it is shown that a 40% increase in transmission distance can be obtained when pre-distortion is used.

5.3.1 Single channel NRZ transmission

Re-circulating loop experiments have been performed on 80 km normalised sections similar to the ones whose numerical optimisation was reported in

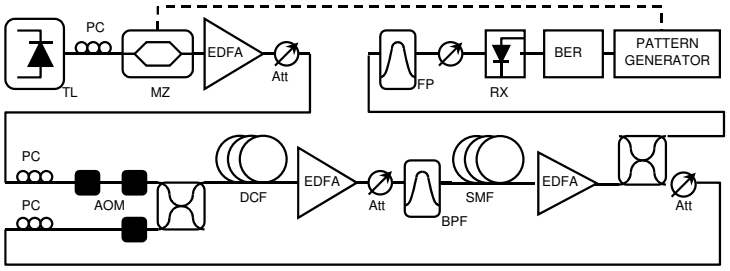

Figure 5.9 Re-circulating loop set-up for single channel transmission over the pre-compensated dispersion map. TL: tunable laser; PC: polarisation controller; MZ: Mach-Zehnder modulator; EDFA: erbium-doped fibre amplifier; Att.: variable optical attenuator; AOM: acousto-optic modulator; DCF: dispersion compensating fibre; SMF: standard single mode fibre; BPF: optical band-pass filter; FP: Fabry-Pérot filter; Rx: optical receiver; BER: error detector.

Section 5.2. The system under investigation is represented in Figure 5.9. CW light from an external cavity tunable laser is modulated at 10 Gbit/s in the NRZ format by a chirp-free Mach-Zehnder modulator, resulting in an extinction ratio of 13 dB. The signal is then boosted in an EDFA before being input into a re-circulating loop consisting of a single normalised section. In order to limit the impact of any additional optical amplifier needed to compensate for the loss of the loop switch and other insertion loss in the loop, a loop configuration making use of only two EDFAs per span was adopted. However, such a configuration did not enable the optimisation of post-compensation sections where SMF is placed first in the loop. The optimum signal power into the SMF in the post-compensation case is expected to be higher than that into the DCF in the pre-compensation scheme, as confirmed numerically in Section 5.2. Such a power budget was not allowed in case post-compensation was used with 80 km spans in our set-up making use of only 2 EDFAs in the loop. Therefore, the post-compensation maps would have been operated in a sub-optimum way (i.e. the power available into the SMF would have been smaller than the value resulting into the best compromise between SPM degradation and limitations by ASE noise accumulation). Consequently, the present investigation with 80 km spans is limited to the case of pre-compensation. Variable attenuators are used to optimise the power levels into the DCF and the SMF. Amplified spontaneous emission noise suppression is achieved using a 1.3 nm optical band-pass filter and a 40 GHz Fabry-Pérot filter in the loop and at the receiver, respectively. The receiver consists of a 12 GHz lightwave converter

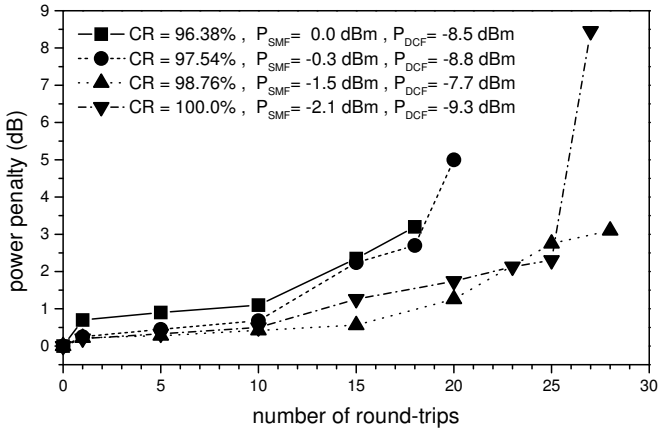

Figure 5.10 Power penalty as a function of number of cascaded sections for single channel transmission over a 80 km pre-compensated dispersion map. The power penalty is plotted for the optimum power levels into the SMF and the DCF and for compensation ratios of 96.4, 97.5, 98.8 and 100%.

followed by a broadband 20 GHz electrical amplifier and a clock-recovery circuit.

The SMF used in this experiment had an attenuation of 0.19 dB/km and a dispersion of 16.6 ps/(nm·km) at the wavelength of 1550 nm. The corresponding quantities for the DCF were 0.49 dB/km and -103 ps/(nm·km). A DCF length of 12.96 km was required in order to compensate for the dispersion accumulated in the 80 km SMF span. The compensation ratio could be varied from 96.4 to 100% by increasing the SMF length by small amounts (up to 3 km in order to obtain 96.4% compensation).

The power penalty at a bit-error-rate (BER) of 1.0×10^{-9} was measured as a function of the number of re-circulations in the loop for compensation ratios equal to 96.4, 97.5, 98.8 and 100.0%. The powers at the SMF and DCF inputs were optimised in order to maximise the transmission distance and were kept to the same level when the number of spans was decreased. The values of the optimum power levels have been shown not to depend significantly on the number of cascaded spans in Section 5.2. The existence of sufficiently large parameter tolerances has also been demonstrated experimentally in similar experiments [20], which justifies this approach. The measured penalties are plotted in Figure 5.10, where the optimum powers to the SMF and the DCF are also indicated. It can be seen that the performance of the system is improved when the compensation ratio is increased from 96.4 to 98.8%. An abrupt increase in penalty is observed above 25

round-trips (corresponding to 2000 km) for 100% compensation. Decreasing the degree of compensation to improve the system performance can be achieved at the expense of a slightly higher power into the SMF, similarly to what had been observed for post-compensation in the numerical analysis of Section 5.2. However, the measured power variations into the SMF and DCF for the different compensation ratios are fairly small, of the order of 2 dB , in agreement with the numerical simulations. Furthermore, the simulations predicted optimum power levels around -8 and -2 dBm into the DCF and SMF, respectively, which is verified in the present experiment.

One difference with the systems modelled in Section 5.2 is the fact that the required degrees of compensation are achieved in the experiments by an increase in SMF length, against a decrease in DCF length in the numerical analysis. Another known limitation of the set-up used for the present investigation is the fact that the wavelength selected in order to obtain the desired degrees of compensation might not coincide with the gain peak of the EDFA chain [21]. Hence the use of a tunable band-pass filter in the loop. A more appropriate gain flattening technique such as the one used in the WDM experiments reported in Section 5.3.2 would be preferable. Furthermore, the bandwidth narrowing induced by cascading the band-pass filter might result in additional penalty for large round-trip counts.

A set of numerical simulation has been performed under the same conditions as the experiments described above in order to validate our simulation procedure. First, the back-to-back simulation was calibrated against the corresponding measurement. The photodiode single-sided thermal noise density was varied in the simulation model until a back-to-back sensitivity equal to the measured one was calculated, resulting in a value of 20 pA/$\sqrt{\text{Hz}}$. In a second phase, the transmission of a 10 Gbit/s NRZ signal was simulated through a cascade of pre-compensated 80 km SMF with compensation ratios of 96.4, 97.5, 98.8 and 100%, and with SMF and DCF input powers equal to the optimum values found from the experiments. As the simulation results are to be compared to the experimental data, the entire loop set-up was modelled, including loop-switch loss. The sensitivity was calculated as a function of the number of round-trips and the results are compared to experimental measurements in Figure 5.11. Good agreement is obtained, in spite of the necessary simplification of the models used to perform those calculations. In particular, the EDFAs were modelled as simple gain blocks delivering a constant output power with Gaussian noise addition. Neither the saturation behaviour, nor the dependence of the noise figure on the gain were taken into account. This good agreement

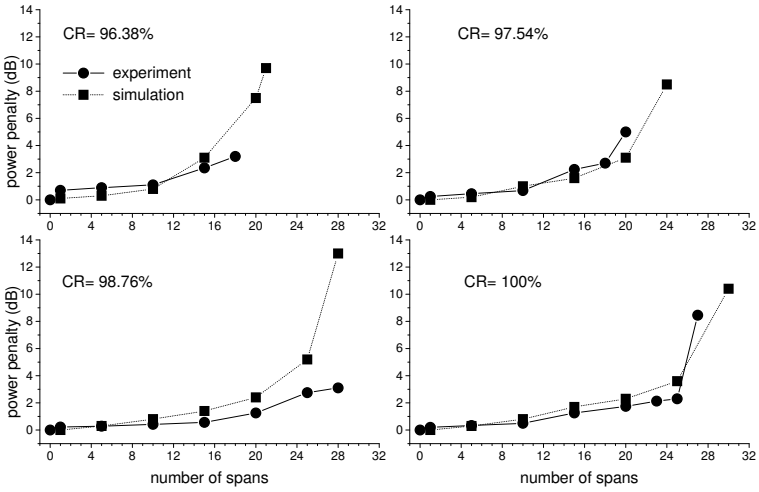

Figure 5.11 Comparison of measured and simulated power penalty as a function of number of 80 km SMF pre-compensated spans for different compensation ratios. Top-left: 96.38%; top-right: 97.54%; bottom left: 98.76%; bottom right: 100%. The power levels at the SMF and DCF inputs correspond to the optima found from the experimental investigation.

with the experimental results confirms that our simple model can provide an appropriate description of the systems under study and legitimates the numerical results of Section 5.2.

5.3.2 8 channel WDM NRZ transmission

In order to verify whether the conclusions obtained from single channel analysis can, as a first approximation, be extended to the case of multi-channel systems, an eight channel WDM experiment has been performed using the pre-compensated normalised section. The re-circulating loop set-up, depicted in Figure 5.12, is essentially similar to the one used in the single channel investigation of Section 5.3.1. Eight CW lasers on a 200 GHz ($\sim$ 1.6 nm) frequency grid are combined in an arrayed waveguide grating (AWG) multiplexer with 1 nm full-width half-maximum (FWHM) bandwidth, before being modulated together in a single $LiNbO_3$ Mach-Zehnder modulator. The WDM signal is then transmitted through a variable length (4 to 30 km) of SMF whose purpose is twofold. First, it enables decorrelation of the eight channels by introducing some walk-off between them in order to emulate real traffic where all eight bit patterns would be different, and reproduce more realistic non-linear cross-talk (due to e.g. cross-

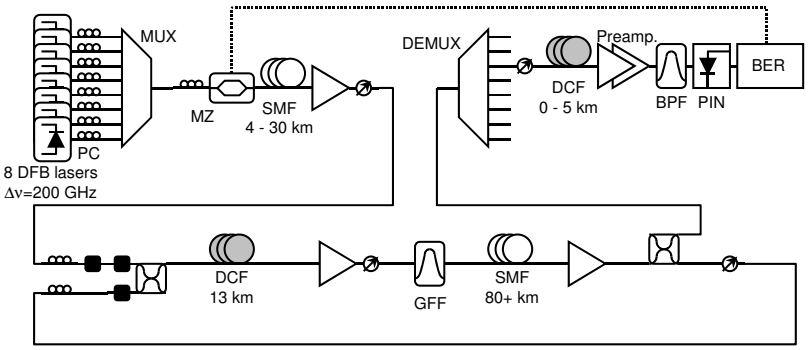

Figure 5.12 Re-circulating loop set-up for 8 channel WDM experiments. PC: polarisation controller; MUX: arrayed-waveguide grating multiplexer; SMF: standard single-mode fibre; DCF: dispersion compensating fibre; GFF: gain-flattening filter; DEMUX: arrayed-waveguide grating demultiplexer; Preamp.: optical preamplifier; BPF: optical band-pass filter; PIN: photodiode; BER: bit-error-rate test-set.

phase modulation) conditions. Second, when its length is larger than 4 km, the SMF enables to realise passive pre-distortion of the channels, as described in Section 5.2. A matching length of dispersion compensating fibre is placed after the wavelength de-multiplexer at the receiver only in case pre-distortion SMF is included (i.e. the SMF length is larger than 4 km). The receiver consists of a dual-stage EDFA preamplifier followed by a 1.3 nm tunable optical filter and a PIN lightwave converter. The transmission spans are similar to the ones used in Section 5.3.1: first 12.96 km DCF followed by 80 km SMF. The SMF length could be increased in order to study the effect of a reduction in the degree of compensation. A novel dispersion compensating fibre providing dispersion slope compensation [18] was used in this experiment, so that the degree of compensation could be reasonably maintained over the eight WDM channels. The residual dispersion of the 80 km span was equal to -0.34 ps/nm at 1550 nm and its dispersion slope was -0.16 ps/nm^2, resulting in only 1.8 ps/nm difference in accumulated dispersion over the 8 WDM channels. Two EDFAs with 5 dB noise figure were used in the loop, together with a tunable Mach-Zehnder gain equalisation filter [22].

New requirements are introduced in the system compared to the single channel case, as an even power of the eight channels has to be ensured throughout the link. This could only be partially realised in our loop set-up where the power development of the WDM channels differed. This point is illustrated in Figure 5.13 where we show the spectra of the WDM sig-

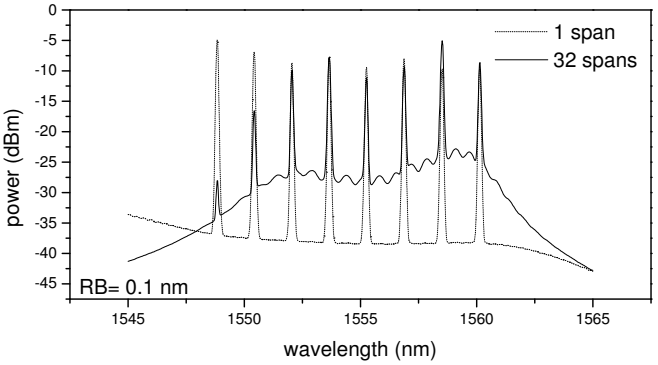

Figure 5.13 Measured spectra (resolution bandwidth: 0.1 nm) after 1 and 32 cascaded spans with 98.8% pre-compensation and 30 km SMF pre-distortion.

nals after 1 and 32 cascaded spans in the case of 98.8% compensation with 30 km SMF pre-distortion. Clearly, different power levels and different optical signal-to-noise ratios are obtained for the different channels. Even when some channel pre-emphasis is applied at the transmitter, and in spite of the gain equalisation filter, the channel with the lowest wavelength cannot be recovered after 32 cascaded spans due to a low optical signal-to-noise ratio (OSNR). This problem could be solved by using two Mach-Zehnder gain equalisation filters with different free-spectral ranges [23], as demonstrated in more recent experiments [24]. Furthermore, due to the wavelength dependence of the Mach-Zehnder modulator, the same extinction ratio could not be guaranteed for all channels. Consequently, it was adjusted to a sub-optimum value of 10 dB for one of the centre channels (channel 4).

BER measurements were performed as a function of distance for all eight channels for a compensation ratio of 100%. The maximum number of normalised sections which could be cascaded was channel dependent due to the different power and OSNR development of each channel. Only 16 spans could be cascaded for the channel with the lowest wavelength (channel 1), against more than 20 for all the other channels. In our re-circulating loop configuration, data is continuously detected at the receiver, corresponding to the different round trips in the loop. Gating of the error counter enables to measure the BER corresponding to the last re-circulation. However, the power meter used to measure the sensitivity is not gated. It therefore measures power averaged over the total number of re-circulations. Due to the fact that the power of each channel is not constant from one round-trip to another in this WDM experiment, it is necessary to correct the measured average sensitivity by taking into account the power distribution of the

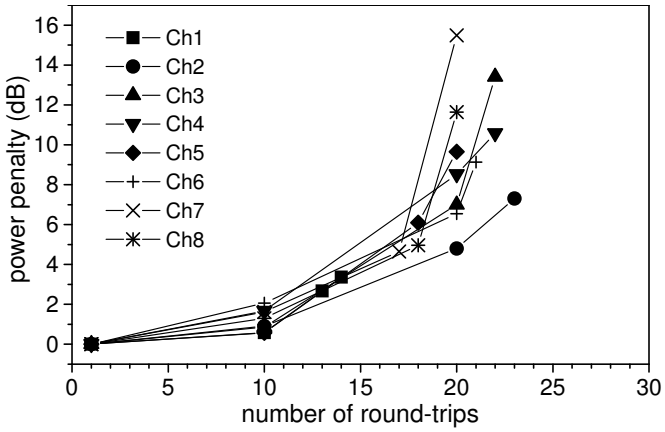

Figure 5.14 Penalty as a function of number of round-trips through 100% pre-compensated spans for an 8 channel WDM system. The measured sensitivities have been corrected to take into account the uneven power development of the different channels. Power corrections by Lutz Molle.

channel over all the round-trips. This has been performed by Lutz Molle from the Technical University of Berlin and Virtual Photonics Incorporated. The resulting penalty plot as a function of cascaded spans is shown in Figure 5.14, where it can be seen that relatively equal performance is obtained for all channels up to 15 round-trips (1200 km).

The performance of the system was assessed by evaluation of channels 2, 4 and 7 when the degree of compensation was reduced to 98.8%. Furthermore, by adding 30 km SMF at the transmitter, and a matching length of 4.8 km DCF at the receiver, the effect of passive pre-distortion could be investigated. The power penalty is shown as a function of number of round-trips in the loop for channel 4 (one of the centre channels at 1554.12 nm that exhibited a uniform power development) in Figure 5.15. It is confirmed that, even in the WDM case, reducing the compensation ratio from 100 to 98.8% results in a performance improvement. When 30 km SMF passive pre-distortion was used at the transmitter, the system performance could be increased even further. Up to 32 normalised sections could be cascaded error-free, corresponding to a 2560 km transmission distance. It has therefore been shown experimentally that the design guidelines edicted from the single channel analysis can be extended to the WDM case when multi-channel degrading effects such as FWM and XPM can be ignored, as it is the case in 80 km normalised sections based on SMF and DCF.

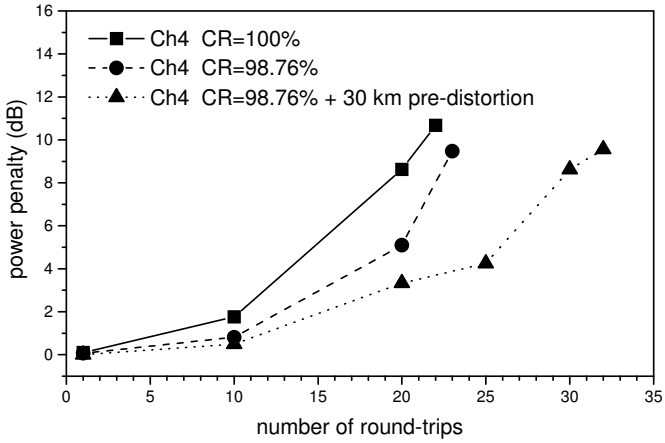

Figure 5.15 Power penalty as a function of number of cascaded sections for 8 channel WDM transmission through a 80 km pre-compensated dispersion map. The power penalty is plotted for channel 4 for 100 and 98.8% compensation ratio without pre-distortion, as well as for 98.8% compensation with 30 km SMF pre-distortion.

5.3.3 Single channel CRZ transmission

Numerical and experimental results on the optimisation of normalised transmission sections have been presented for NRZ modulation at 10 Gbit/s in Sections 5.2 and 5.3 respectively. However, as format transparency is a desirable feature for future optical networks, the different compensation schemes also need to be compared for the return-to-zero format. Numerical simulations based on the propagation of isolated pulses [25] and random sequences [26] have already been reported. In this section, we present a systematic experimental comparison of pre- and post-compensation with and without pre-distortion for chirped return-to-zero transmission (non-soliton) at 10 Gbit/s over cascaded 80 km SMF spans. Using a re-circulating loop set-up, we show that pre-compensation performs better than post-compensation and that a 40% increase in transmission distance (at 5 dB power penalty) can be obtained when using passive pre-distortion at the transmitter.

The re-circulating loop set-up used for these experiments is shown in Figure 5.16. Light from a continuous wave distributed feedback (DFB) laser is amplified in an erbium doped fibre amplifier before being externally modulated with a $2^{31} - 1$ pseudo-random binary sequence (PRBS) in a lithium-niobate Mach-Zehnder modulator (MZM). The electrical 10 Gbit/s RZ signal used to drive the modulator is obtained from a 10 Gbit/s NRZ

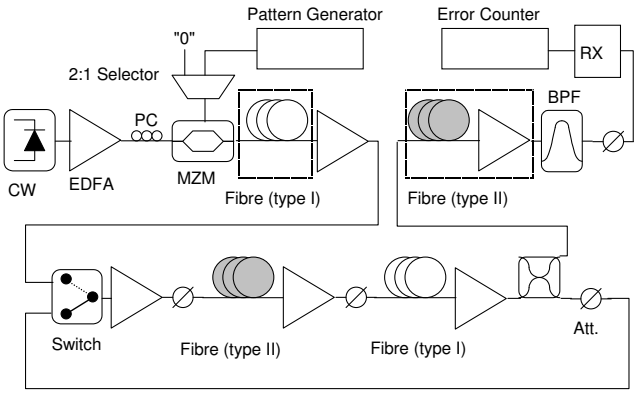

Figure 5.16 Re-circulating loop set-up used for the investigation of the transmission properties of the CRZ format over different 80 km SMF+DCF maps.

PRBS and a constant space in a 2:1 selector [24, 27]. The optical 10 Gbit/s CRZ signal is then amplified before being launched into a loop switch made of three acousto-optic modulators and a 3 dB coupler. The loop consists of a single span made of one 80 km spool of SMF and a 12.96 km spool of DCF providing 100% dispersion compensation. Each spool of fibre is preceded by an EDFA with 13 dBm output power and 5 dB noise, figure followed by a variable attenuator (Att.) used to optimise the launched power in order to obtain the best possible trade-off between high signal-to-noise ratio and enhanced non-linearities in the fibre. A third EDFA is necessary in order to compensate for the loss in the loop switch. The signal is tapped from the loop via a 10 dB coupler, filtered with a 1.3 nm band-pass filter (BPF) and input into a receiver (RX) consisting of a lightwave converter and a clock-recovery circuit. Additionally, one extra fibre spool can be inserted at the transmitter and the corresponding fibre with the opposite amount of dispersion can be inserted at the receiver, together with an extra EDFA used to compensate for the excess loss. These fibres have the effect of reducing the maximum amount of total accumulated dispersion. In all cases, full compensation over the whole link is provided.

The following configurations have been investigated: pre-compensation, post-compensation, pre-compensation with pre-distortion and post-compensation with pre-distortion. In this experiment, pre-distortion means that a 30 km long SMF spool is placed at the transmitter and a 5 km long DCF spool is placed at the receiver in the pre-compensation case whereas these two spools are exchanged in the post-compensation case. The cor-

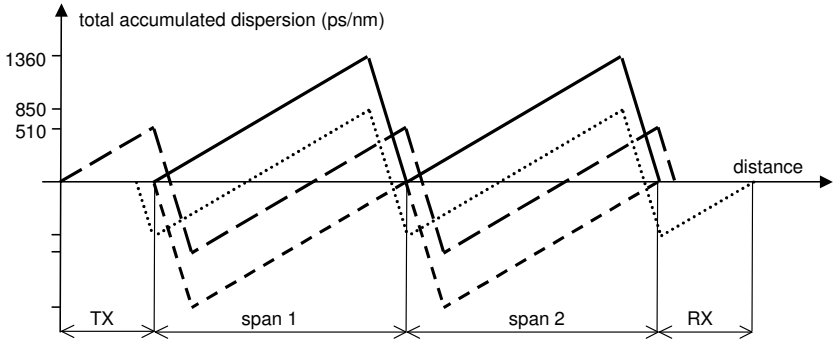

Figure 5.17 Total accumulated dispersion as a function of distance in fibre for the four different SMF + DCF dispersion maps investigated for CRZ transmission: post-compensation (solid line); pre-compensation (short dashes); post-compensation with pre-distortion (dots); pre-compensation with pre-distortion (long dashes).

responding dispersion maps are represented for two 80 km SMF spans in Figure 5.17.

The measured penalties at a BER equal to 1.0×10^{-9} are represented as a function of the number of round trips for each configuration in Figure 5.18. The powers at the input of the SMF and DCF were optimised for the maximum number of round-trips shown for every compensation scheme and were maintained to those values when the number of round-trips was decreased. This was motivated by the fact that, in the normalised section context, it is important that power levels can be set independently of the number of sections a particular signal has to go through, and that these powers need to be chosen so that the transmission over up to a certain number of sections can be guaranteed. As can be seen in Figure 5.18, pre-compensation performed better than post-compensation. This is in good agreement with numerical results presented in [26]. When pre-distortion is introduced, both pre- and post-compensation perform equally well and exhibit significant improvement compared to the case without pre-distortion. Such a behaviour had already been reported in the numerical analysis of Section 5.2 dealing with NRZ modulation. No in-line filtering was used in our set-up and, therefore, its performance was mainly limited by noise accumulation.

Eye diagrams corresponding to one and thirty round-trips for pre-compensation with pre-distortion are shown in Figure 5.19. Optimum fibre av-

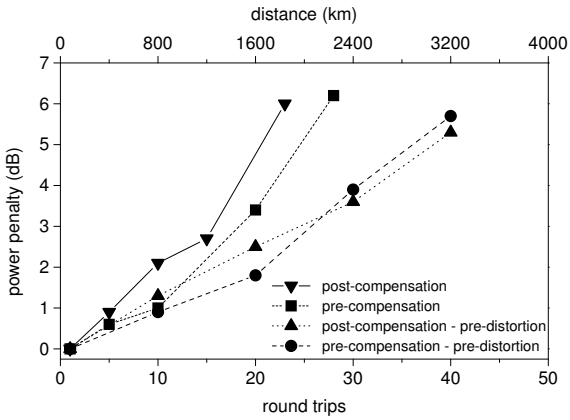

Figure 5.18 Power penalty as a function of number of round trips for the four different maps investigated for CRZ transmission.

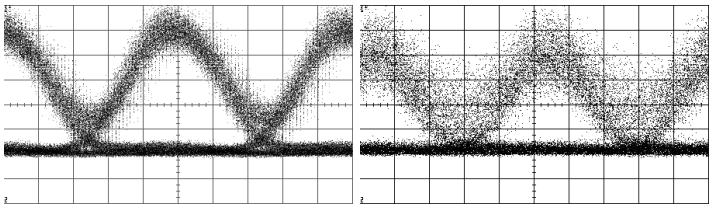

Figure 5.19 Eye diagrams after 1 (left) and 30 (right) pre-compensated SMF + DCF spans. The eyes are recorded using a 30 GHz sampling oscilloscope.

erage input powers were 1 dBm into the SMF and -4 dBm into the DCF in this case. The shape of the pulses is maintained over transmission through 2400 km, showing that they suffer little from the combined effects of dispersion and non-linearities, but that noise accumulation is indeed the main limitation. Comparison with previously reported results for NRZ [4] shows that the pre-compensation scheme can support both the RZ and NRZ formats for transmission up to 2000 km with less than 5 dB penalty and that in both cases this distance can be significantly increased using pre-distortion. Format transparency can therefore be obtained in future networks based on this normalised section.

We have therefore performed an experimental comparison of pre- and post-compensation for 50 ps pulse-width RZ transmission at 10 Gbit/s over 80 km dispersion compensated SMF spans. We have shown that, unless pre-distortion is used, pre-compensation performs better than post-compensation. Together with pre-distortion, both schemes perform equally well. Therefore both pre- and post-compensation normalised sections are good candidates for future optical networks where format transparency is sought.

5.4 Summary of Chapter 5

In this chapter, we have reported a numerical and experimental investigation of signal propagation through 80 km normalised sections based on SMF and DCF. Due to the accumulative nature of signal degradation mechanisms such as group velocity dispersion, optical fibre non-linearities and amplified spontaneous emission noise, the optimum power ranges to the two fibre types, as well as the requirements on the compensation ratio need to be determined in order to maximise the extent of a transparent domain (where no regeneration will take place) with sufficient parameter tolerance.

A numerical comparison of pre- and post-compensation with and without passive pre-distortion at the transmitter has been performed for NRZ modulation at 10 Gbit/s. By independently varying the power at the different types of fibres inputs and the compensation ratio, it has been found that post-compensation performs better than pre-compensation at the expense of stricter parameter tolerances. Moreover, it has also been shown that both pre- and post-compensated systems can be significantly improved by using passive pre-distortion at the transmitter. The optimum power levels to both SMF and DCF have been found not to vary significantly with the number of cascaded sections, which makes the practical design of transparent domains based on normalised sections feasible.

The ability of our simulation tool to accurately model the conjugated effects of GVD, SPM and ASE noise on the transmission through normalised sections has been validated by comparison with measurements performed in our re-circulating loop test-bed, justifying our entire numerical optimisation procedure.

Experimental assessment of the pre-compensation normalised section has been performed for 10 Gbit/s NRZ modulation in the single channel case, as well as for an 8×10 Gbit/s WDM system with 200 GHz channel spacing. The benefit of introducing passive pre-distortion at the transmitter in order to maximise the transmission distance has been confirmed experimentally. Finally, the positioning of the DCF in 80 km SMF spans has been investigated experimentally for 10 Gbit/s CRZ transmission with 50 ps pulse-width. A 40% increase in transmission distance (at 3 dB power penalty) was obtained when adding pre-distortion to pre-compensation.

As a conclusion, we have shown that, with a proper optimisation of the dispersion management, transparent domains with a diameter of the order of 1000 km should be feasible for a performance criterion better than 3 dB power penalty in terrestrial networks with large (80 km) amplifier spacings. Such an extension of a transparent domain would ensure format transparency (NRZ and RZ), as well as a limited impact of the extension towards WDM.

5.5 References to Chapter 5

[1] Special Issue on "High Capacity Optical Transport Networks", *IEEE Journal on Selected Areas in Communications*, vol. 16, no. 7, September 1998.

[2] R. W. Tkach, E. L. Goldstein, J. A. Nagel, and J. L. Strand, "Fundamental limits of optical transparency", in *Technical Digest Optical Fiber Communication Conference, OFC'98*, San Jose, California, U.S.A., paper WJ1, pp. 161–163, 1998.

[3] ITU-T Draft Recommendation G.873, *Optical Transport Network Requirements*, International Telecommunications Union, Geneva, Switzerland, 1999.

[4] C. Caspar, R. Freund, N. Hanik, L. Molle, and C. Peucheret, "Using normalised sections for the design of all optical networks", in *New Trends in Optical Network Design and Modeling, IFIP TC6 Fourth Working Conference on Optical Network Design and Modeling,*

ONDM'00 (A. A. Stavdas, ed.), Athens, Greece, pp. 163–172, Kluwer Academic Publishers, 2001.

[5] A. A. M. Saleh, "Transparent optical networking in backbone networks", in *Technical Digest Optical Fiber Communication Conference, OFC'00*, Baltimore, Maryland, U.S.A., paper ThD7, 2000.

[6] N. Kikuchi, S. Sasaki, and K. Sekine, "10 Gbit/s dispersion-compensated transmission over 2245 km conventional fibres in a recirculating loop", *Electronics Letters*, vol. 31, no. 5, pp. 375–377, 1995.

[7] G. Lenz, B. J. Eggleton, C. K. Madsen, C. R. Giles, and G. Nykolak, "Optimal dispersion of optical filters for WDM systems", *IEEE Photonics Technology Letters*, vol. 10, no. 4, pp. 567–569, 1998.

[8] C. D. Poole and J. Nagel, "Polarization effects in lightwave systems", in *Optical fiber telecommunications IIIA* (I. P. Kaminow and T. L. Koch, eds.), San Diego, pp. 114–161, Academic Press, 1997, 1997.

[9] F. Forghieri, R. W. Tkach, and A. R. Chraplyvy, "Fiber nonlinearities and their impact on transmission systems", in *Optical fiber telecommunications IIIA* (I. P. Kaminow and T. L. Koch, eds.), San Diego, pp. 196–264, Academic Press, 1997, 1997.

[10] E.-J. Bachus, M. Eiselt, K. Habel, K.-D. Langer, E.-U. Scheuing, and F.-C. Tischer, "Photonic network design based on reference circuits", in *Proceedings Optical Network Design and Modelling Conference, ONDM'97*, Vienna, Austria, pp. 56–69, 1997.

[11] N. Hanik, A. Gladisch, and G. Lehr, "An effective method to design transparent optical WDM-networks", in *Proceedings Conference on Networks and Optical Communication, NOC'98, Technology and Infrastructure*, Manchester, England, U.K., pp. 190–197, 1998.

[12] ITU-T Draft Recommendation G.692, *Optical interfaces for multichannel systems with optical amplifiers*, International Telecommunications Union, Geneva, Switzerland, 1998.

[13] S. Bigo, G. Bellotti, and M. W. Chbat, "Investigation of cross-phase modulation limitations on 10 Gbit/s transmission over various types of fiber infrastructures", in *Technical Digest Optical Fiber Communication Conference, OFC'99*, San Diego, California, U.S.A., paper ThC3, vol. 3, pp. 40–42, 1999.

[14] D. M. Rothnie and J. E. Midwinter, "Improved standard fibre performance by positioning the dispersion compensating fibre", *Electronics Letters*, vol. 32, no. 20, pp. 1907–1908, 1997.

[15] G. Bellotti, A. Bertaina, and S. Bigo, "Dependence of self-phase modulation impairments on residual dispersion in 10-Gb/s-based terrestrial transmissions using standard fiber", *IEEE Photonics Technology Letters*, vol. 11, no. 7, pp. 824–826, 1999.

[16] R. J. Nuyts, Y. K. Park, and P. Gallion, "Performance improvement of 10 Gb/s standard fiber transmission systems by using the SPM effect in the dispersion compensating fibre", *IEEE Photonics Technology Letters*, vol. 8, no. 10, pp. 1406–1408, 1996.

[17] G. P. Agrawal, *Nonlinear fiber optics*, chapter 2, pp. 50–54, Academic Press, San Diego, 2nd edition, 1995.

[18] L. Grüner-Nielsen, T. Veng, S. N. Knudsen, C. C. Larsen, and B. Edvold, "New dispersion compensating fibres for simultaneous compensation of dispersion and dispersion slope of non-zero dispersion shifted fibres in the C or L band", in *Technical Digest Optical Fiber Communication Conference, OFC'00*, Baltimore, Maryland, U.S.A., vol. 1, pp. 101–103, 2000.

[19] G. P. Agrawal, *Nonlinear fiber optics*, Academic Press, San Diego, second edition, 1995.

[20] N. Hanik, C. Caspar, F. Schmidt, R. Freund, L. Molle, and C. Peucheret, "Optimised design of transparent optical domains", in *Proceedings European Conference on Optical Communication, ECOC'00*, Munich, Germany, paper P3.5, vol. 3, pp. 195–197, 2000.

[21] N. S. Bergano and C. R. Davidson, "Wavelength division multiplexing in long-haul transmission systems", *Journal of Lightwave Technology*, vol. 14, no. 6, pp. 1299–1308, 1996.

[22] J.-Y. Pan, M. A. Ali, A. F. Elrefaie, and R. E. Wagner, "Multiwavelength fiber-amplifier cascades with equalization employing Mach-Zehnder optical filter", *IEEE Photonics Technology Letters*, vol. 7, no. 12, pp. 1501–1503, 1995.

[23] M. Suyama, H. Iwata, N. Shimojoh, S. Harasawa, and T. Naito, "Transoceanic WDM system with more than 100 Gb/s capacity", *Optical Fiber Technology*, vol. 3, pp. 309–319, 1997.

[24] F. Liu, X. Zheng, C. Peucheret, S. N. Knudsen, R. J. S. Pedersen, and P. Jeppesen, "Chirped return-to-zero source used in 8×10 Gbit/s transmission over 2000 km of standard singlemode fibre", *Electronics Letters*, vol. 36, no. 16, pp. 1399–1400, 2000.

[25] D. Breuer, F. Küppers, A. Mattheus, E. G. Shapiro, I. Gabitov, and S. K. Turitsyn, "Symmetrical dispersion compensation for standard monomode-fiber-based communication systems with large amplifier spacing", *Optics Letters*, vol. 22, no. 13, pp. 982–984, 1997.

[26] D. Breuer, K. Petermann, A. Mattheus, and S. K. Turitsyn, "Combatting fibre nonlinearity in symmetrical compensation schemes using RZ-modulation format at 120 km amplifier spacing over standard fibre", in *Proceedings European Conference on Optical Communication, ECOC'97*, Edinburgh, Scotland, U.K., vol. 2, pp. 261–264, 1997.

[27] F. Liu, C. Peucheret, X. Zheng, R. J. S. Pedersen, and P. Jeppesen, "A novel chirped return-to-zero transmitter and transmission experiments", in *Proceedings European Conference on Optical Communication, ECOC'00*, Munich, Germany, paper 8.3.5, vol. 3, pp. 113–114, 2000.

Chapter 6

Wide-band dispersion compensation

6.1 Introduction

The optimisation of the use of dispersion compensating fibre (DCF) to compensate for the dispersion accumulated in standard single mode fibre (SMF) has been discussed in Chapter 5 in the context of terrestrial networks with large (80 km) amplifier spacing. One of the drawbacks of the previous generation of DCFs was their inability to compensate for the dispersion of SMF over a broad bandwidth, inducing limitations in wavelength division multiplexing (WDM) systems were channel-per-channel dispersion compensation might be required, depending on the link length and individual channel bit-rate [1].

This point is illustrated in Figure 6.1 where the dispersion map of a link made of ten 80 km fully dispersion compensated SMF spans is represented. The dispersion and dispersion slope of the SMF at 1550 nm are equal to $D_{\mathrm{SMF}} = 17$ ps/(nm·km) and $S_{\mathrm{SMF}} = 0.055$ ps/(nm^2·km) respectively. If conventional DCF with dispersion parameter of $D_{\mathrm{DCF}} = -100$ ps/(nm·km) at 1550 nm and dispersion slope of $S_{\mathrm{DCF}} = -0.23$ ps/(nm^2·km) is used[1] with a length adjusted to provide 100% dispersion compensation at 1550 nm, it can be seen that some residual dispersion (± 25.4 ps/nm per span at 1530 or 1570 nm) is experienced by channels away from 1550 nm after each span in the link. It is therefore important to be able to reduce the total dis-

[1]The fibre parameters used for this calculation are based on typical values extracted from data-sheets for the following products by Lucent Technologies: DK:1360 dispersion compensating module (C-band) and WBDK:1360 wide band dispersion compensating module (C-band) - February 2000.

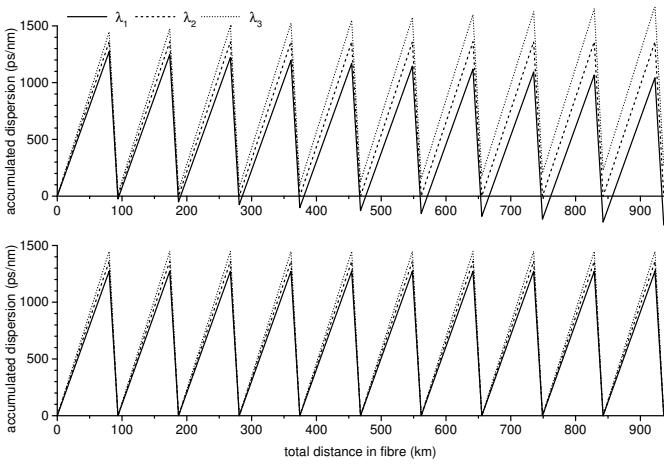

Figure 6.1 Dispersion maps corresponding to 80 km SMF + DCF spans. Top: without dispersion slope compensation. Bottom: with dispersion slope compensation. The map is optimised for $\lambda_2 = 1550$ nm. $\lambda_1 = 1530$ nm, $\lambda_3 = 1570$ nm.

persion accumulated by all channels in WDM systems in order to increase their reach or allow upgrade to higher bit rates.

Considering a two-step dispersion map made of a length L_{SMF} of SMF and a length L_{DCF} of DCF, the total accumulated dispersion per-span $\mathbb{D}_{acc}(\lambda)$ is

$$\mathbb{D}_{acc}(\lambda) = D_{\mathrm{SMF}}(\lambda) L_{\mathrm{SMF}} + D_{\mathrm{DCF}}(\lambda) L_{\mathrm{DCF}} \tag{6.1}$$

Assuming dispersion orders higher than the dispersion slope $S = \frac{dD}{d\lambda}$ can be neglected in a certain wavelength range, the dispersion of either the SMF or the DCF can be expressed as a function of wavelength according to

$$D_i(\lambda) = D_i(\lambda_0) + S_i(\lambda - \lambda_0) \tag{6.2}$$

From (6.1) and (6.2), and assuming that complete dispersion compensation is achieved at λ_0, a condition for having full dispersion compensation for all wavelengths can be easily derived

$$\mathrm{RDS}_{\mathrm{SMF}} = \frac{S_{\mathrm{SMF}}}{D_{\mathrm{SMF}}(\lambda_0)} = \frac{S_{\mathrm{DCF}}}{D_{\mathrm{DCF}}(\lambda_0)} = \mathrm{RDS}_{\mathrm{DCF}} \tag{6.3}$$

Equation (6.3) states that the relative dispersion slope (RDS) should be equal for both SMF and DCF. It should be observed that satisfying this condition does not mean that the accumulated dispersion at all points in the map is the same for all wavelengths, as can be seen in Figure 6.1 where a second map for which equation (6.3) is satisfied has been represented.

The condition (6.3) simply states that the accumulated dispersion returns to zero after each span for all wavelengths for which the approximation (6.2) can be made. In the calculations of Figure 6.1, the dispersion slope of the DCF was changed to $S_{\mathrm{DCF}} = -0.322$ ps/(nm^2·km) so that its RDS matches that of SMF.

A new DCF based on a triple-clad design has been introduced, which enables simultaneous compensation of the dispersion and dispersion slope of SMF [2]. Optimisation of the fibre core and depressed cladding diameters enables to achieve dispersion slope compensation, at the expense of a slightly higher dispersion parameter [3, 4]. The design of such slope-compensating DCFs, also known as wide-band dispersion compensating fibres (WBDCF), has been published for the first time by Lucent Technology Denmark A/S at the Optical Fiber Communication Conference in February 1999. In May 1999, we were given the opportunity to perform system experiments using the newly developed WBDCFs in order to assess their suitability for broad-band compensation. The results of this evaluation are presented in what follows.

In this chapter, two experimental studies of the use of wide-band dispersion compensating fibres are presented. Those experiments were performed in our re-circulating loop test-bed using some of the very first produced WBDCF kindly made available to us by Lucent Technologies Denmark A/S (now OFS Fitel Denmark I/S). The effectiveness of the new WBDCFs to compensate for the dispersion of standard single mode fibre over the entire C-band (1530-1565 nm) is demonstrated in Section 6.2 for 50 km spans. Up to 20 dispersion managed spans (1000 km) are cascaded with identical power penalty at 1540, 1550 and 1560 nm. The extension of the third transmission window towards the L-band (1570-1610 nm) has been made possible in the late nineties by the development of gain shifted erbium-doped fibre amplifiers [5]. New dispersion compensation schemes are therefore required in order to accommodate the entire extended band. In Section 6.3, we demonstrate transmission of a 10 Gbit/s signal over 1000 km at 1597 nm using SMF and WBDCF in a pre-compensation configuration. We show that a dispersion map optimised for 1550 nm can be successfully used in the L-band, removing the need for separate band dispersion compensation.

6.2 Wide-band compensation in the C-band

In order to evaluate the potential of wide-band DCFs, a re-circulating loop experiment similar to the one described in Section 5.3 has been performed. Non return-to-zero (NRZ) modulation generated from a chirp-free Mach-

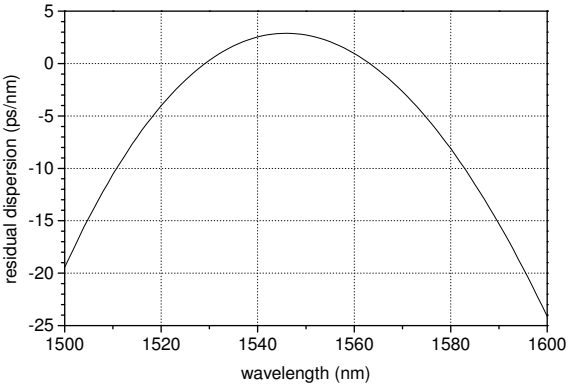

Figure 6.2 Residual dispersion as a function of wavelength for the 50 km SMF+WBDCF span used in the experiment.

Zehnder modulator at 10 Gbit/s was used. The signal extinction ratio was set to 12.5 dB and the back-to-back sensitivity was -18.3 dBm at 1550 nm. The transmission span consisted of a gain-flattened erbium-doped fibre amplifier (EDFA) with 5 dB noise figure and 12 dBm saturated output power, followed by 50.8 km SMF and a matching length of 8.6 km WBDCF. The attenuation of the SMF and WBDCF at 1550 nm was equal to 0.19 and 0.5 dB/km respectively. The residual dispersion of the full span is plotted as a function of wavelength in Figure 6.2, where it is seen to be equal to 2.5, 2.7 and 1.0 ps/nm at the wavelengths of 1540, 1550 and 1560 nm, respectively. The in-line EDFA was followed by a tunable optical band-pass filter (OBF) with full-width half-maximum (FWHM) bandwidth of 1.3 nm and a variable attenuator used to optimise the power level to the SMF. The average signal power to the SMF was adjusted in order to provide the best trade-off between optical signal-to-noise (OSNR) ratio degradation and non-linear distortion, resulting in values of 1 dBm when the transmitter was tuned to 1540 and 1550 nm against only 0.2 dBm at 1560 nm. This last value is lower due to the reduced gain of the EDFAs at this wavelength. An extra gain-flattened EDFA was inserted after the fibre span in order to compensate for the 6 dB loss of the loop switch. At the receiver, a tunable 40 GHz fibre Fabry-Pérot filter was used to suppress amplified spontaneous emission (ASE) noise before the signal was detected in a PIN photodiode.

The signal wavelength was tuned over the entire C-band at wavelengths of 1540, 1550 and 1560 nm, and the penalty at a bit-error-rate (BER) of 1.0×10^{-9} was measured as a function of number of round-trips in the recirculating loop. The measured penalty curves are shown in Figure 6.3 for up to 20 spans. The performances obtained at the different wavelengths

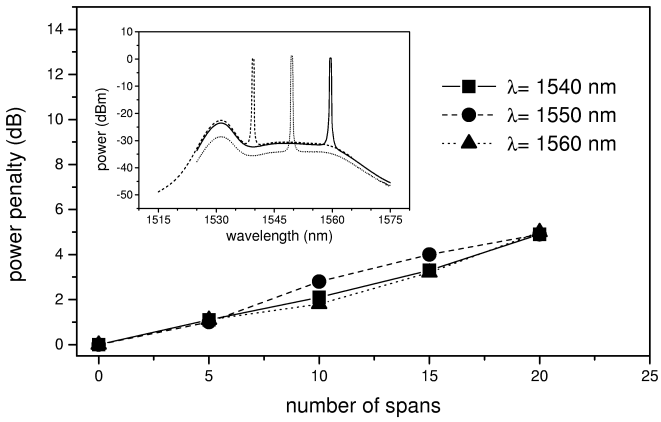

Figure 6.3 Penalty as a function of number of spans for a 50 km post-compensated system at λ = 1540, 1550 and 1560 nm. The inset shows the individual signal spectra after 20 spans (resolution bandwidth: 0.5 nm).

are nearly identical. A power penalty of 5 dB is measured after 20 cascaded spans corresponding to 1000 km. The shape of the penalty curves suggests that the system was limited by OSNR degradation rather than by accumulation of dispersion. Indeed, the largest total accumulated dispersion was obtained at 1550 nm, where it is equal to 54 ps/nm after 20 spans, corresponding to only 3.2 km of standard single mode fibre. The optical spectra measured in a resolution bandwidth of 0.5 nm after 20 round-trips in the loop are also shown as an inset in Figure 6.3. The signal-to-noise ratio at the different wavelengths is difficult to estimate from those spectra because of the presence of the OBF in the loop. This filter was made necessary because of the unfavourable loop configuration where an extra EDFA per span is needed to compensate for the loop switch loss, as well as the insertion loss of other components in the loop such as optical attenuators. Those variable attenuators were used to regulate the power level at the fibre span input, but also to ensure that a round-trip gain of 1 is reached. Having more fibre spans in the loop should definitively result in better performance as the influence of this extra EDFA would be distributed over the number of spans. The bandwidth narrowing induced by cascading the OBF is also believed to contribute to the penalty. Nevertheless, no significant difference could be noticed at the three wavelengths, confirming that the dispersion compensation was effective from 1540 to 1560 nm, i.e. over the whole C-band.

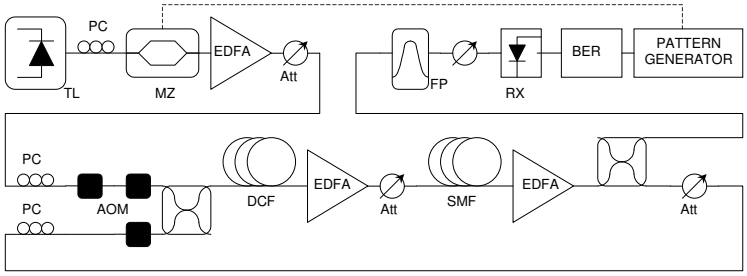

Figure 6.4 Re-circulating loop set-up used for the L-band experiments. TL: tunable laser; PC: polarisation controller; MZ: Mach-Zehnder modulator; EDFA: erbium-doped fibre amplifier; Att.: variable optical attenuator; AOM: acousto-optic modulator; DCF: dispersion compensating fibre; SMF: standard single mode fibre; FP: Fabry-Pérot filter; Rx: receiver; BER: error-counter.

6.3 L-band compensation

One possible way to meet the ever increasing demand for capacity in dense wavelength division multiplexing (DWDM) optical communication systems is to extend the conventional C-band transmission window into the L-band. The successful development of gain-shifted EDFAs has made this approach extremely promising [6]. Terabit WDM transmission using both C and L-bands has been demonstrated [7, 8] and continuing progress in the design of L-band EDFAs with low noise figure and better gain flatness should lead to increased transmission distances [9]. However, over such wide bandwidths, the issue of dispersion management becomes even more critical. Most system experiments reported before the present work have been conducted with dispersion shifted fibres (DSF) whose small residual dispersion in the long wavelength region is used to counteract four-wave mixing [10, 11]. An alternative is to use fibres having a higher local dispersion over the entire bandwidth such as standard single mode fibre in conjunction with dispersion compensating fibre. But wide-band dispersion slope compensation is required if the same piece of DCF is to be used for both the C and L bands.

In this section, we report 10 Gbit/s single channel transmission at 1597 nm over distances in excess of 1000 km using a re-circulating loop set-up. In particular, we demonstrate that dispersion maps designed for 1550 nm and utilising SMF and wide-band DCF [2] can be used successfully without any modification in the L-band, opening the way for wide-band long distance transmission over standard fibres.

The re-circulating loop set-up is shown in Figure 6.4. Light from an ex-

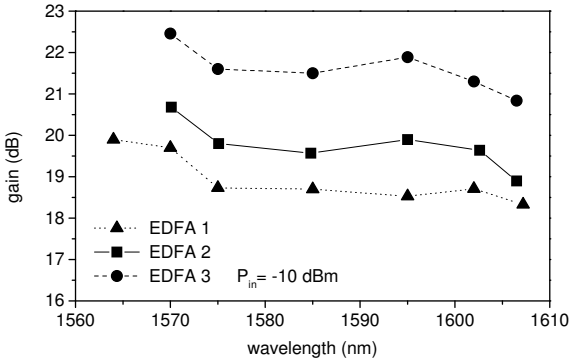

Figure 6.5 Measured gain as a function of wavelength for the three L-band EDFAs used in the re-circulating loop experiment. The numbers correspond to the position of the amplifier according to Figure 6.4. The EDFA input power is $P_{in} = -10$ dBm. Measurement courtesy of Alvaro Buxens.

ternal cavity laser tuned to 1597 nm was externally modulated at 10 Gbit/s with a non return-to-zero pseudo-random binary sequence in a chirpless Mach-Zehnder modulator. It was then amplified before being fed into a loop switch made of three acousto-optic modulators and a 3 dB coupler. The transmission span consisted of two L-band EDFAs, one spool of SMF (50.8 or 80 km) and a matching spool of wide-band DCF. The WBDCF was placed either before (pre-compensation) or after (post-compensation) the SMF. The wide-band DCF used in these experiments exhibited a dispersion of -100 ps/(nm·km) and a dispersion slope of -0.37 ps/(nm^2·km) at 1550 nm. The WBDCF was cut at lengths corresponding to full compensation at 1550 nm. The wavelength dependence of the total residual dispersion for the 50 km SMF span is shown in Figure 6.2. A small residual dispersion of +2.7 ps/nm (corresponding to 99.7% compensation) was measured at 1550 nm for this span. The measured values of the residual dispersion at 1597 nm were -21.3 ps/nm and -13.4 ps/nm for the 50 and 80 km spans respectively. Variable attenuators were placed after each EDFA in order to optimise the power levels in the loop. The signal was tapped from the loop with a 10 dB coupler placed after the last amplifier in the span and was input via a 40 GHz Fabry-Pérot filter to a receiver consisting of a lightwave converter and a clock recovery circuit.

The L-band EDFAs consisted of commercial C-band EDFAs followed by a length of 100 or 130 m erbium doped fibre (EDF). Gain shifting towards the L-band was achieved by forward amplified spontaneous emission pumping into the extra length of EDF, according to the principle described in [12]. The optimum performance for the three L-band EDFAs used in this

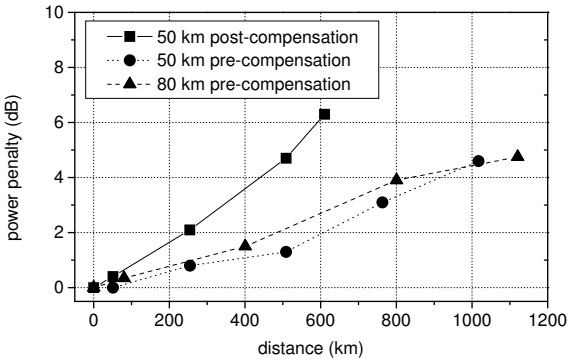

Figure 6.6 Measured penalty as a function of distance for 50 km post-compensation, 50 km pre-compensation and 80 km pre-compensation spans. The transmitter wavelength is $\lambda = 1597$ nm.

experiment were reached around 1597 nm. Gains between 18.5 and 22 dB and noise figures of 5 dB were measured for an input power of -10 dBm at this wavelength. The gain spectra of the three L-band EDFAs are shown in Figure 6.5.

BER curves were measured at 1597 nm for both pre- and post-compensation schemes with 50 km SMF in the loop and for pre-compensation only with the 80 km SMF span. The resulting penalties as a function of distance are shown in Figure 6.6. Only the SMF length is taken into account in the calculation of the transmitted distance in this graph. Using the 50 km SMF span, a power penalty of 4.6 dB was measured in the pre-compensation case for 20 re-circulations corresponding to 1017 km. Penalties were significantly higher for post-compensation. In our experiment the powers at the SMF and DCF inputs were set to values which maximised the transmission distance. In the pre-compensation case, the power at the SMF and DCF inputs was 2.6 dBm and -2.7 dBm respectively for the 50 km span, against -0.5 dBm and -4.2 dBm for the 80 km span. However power budget limitations in the loop set-up due to the 6 dB attenuation of the loop switch and the limited gain of the amplifiers restricted the power at the input of the SMF in the post-compensation case. As self-phase modulation (SPM) in the anomalous dispersion regime is known to lead to pulse compression [13], a higher power into the SMF would be desirable in the post-compensation case. The power levels are consequently not fully optimised in this case, which explains the significant difference in penalty compared to pre-compensation. Using 80 km SMF spans and pre-compensation, a penalty of 4.7 dB was measured for 14 round-trips cor-

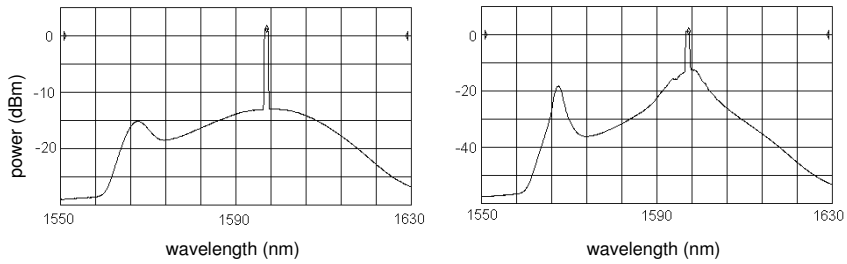

Figure 6.7 Spectra (in a 1 nm resolution bandwidth) after 1 (left) and 20 (right) 50 km pre-compensated spans.

responding to 1120 km. As can be seen in Figure 6.6, similar performances are obtained for the two pre-compensated systems making use of 50 and 80 km spans. From a pure optical signal-to-noise ratio point of view, one would expect the system with the shorter span length to perform better, as the loss between repeaters is the lower in this case. However, the fact that the systems under investigation enable an independent optimisation of the power levels to both the SMF and WBDCF complicates the analysis since the fibre launch conditions of both 50 and 80 km systems were determined from the best compromise between SPM and OSNR degradations.

Figure 6.7 shows the spectra recorded for 1 and 20 re-circulations in the pre-compensation case for 50 km SMF spans. In the experiment, no in-line filtering was used, causing a significant build-up of amplified spontaneous emission noise. With a total residual dispersion of only -426 ps/nm, noise accumulation becomes the limiting factor for such a system.

Proposed repeater schemes for dual C- and L-band WDM systems usually consist of a wavelength division de-multiplexer used to separate the C- and L band channels, followed by an EDFA and a dispersion compensating module (DCM) for each of the wavelength bands. The channels from the C- and L-band are then recombined in the transmission fibre via a coarse wavelength division multiplexer [7, 14]. At least two EDFAs are required (one for the C-band and one for the L-band), as well as two expensive DCMs optimised for both transmission bands. We have demonstrated above that a single DCM made of WBDCF could be used to compensate for the span dispersion in both the C- and L-band. Hence the new proposed repeater structure shown in Figure 6.8.

We have therefore successfully transmitted a 10 Gbit/s signal at 1597 nm over distances in excess of 1000 km using 50 and 80 km spans of SMF and DCF in the pre-compensation configuration. We have demonstrated experi-

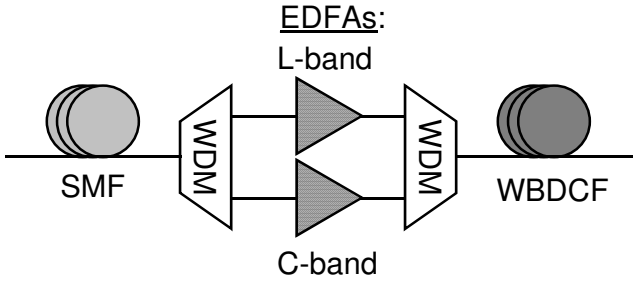

Figure 6.8 Configuration of a dispersion-compensated span for dual C- and L-band WDM transmission making use of wideband DCF. One single spool of DCF is used to simultaneously compensate for the dispersion experienced by the C and L-band channels. WDM: wavelength division (de)multiplexer (C/L band).

mentally that long distance L-band transmission is feasible using wide-band dispersion compensating fibre lengths tailored for dispersion compensation in the C-band. A practical implication is that long distance dual L- and C-band WDM transmission using a parallel amplifier configuration should be feasible without the need for separate band dispersion compensation.

6.4 Summary of Chapter 6

The benefit of using wide-band dispersion compensating fibres in conjunction with standard single mode fibre has been demonstrated using some of the first produced dispersion slope compensating DCFs. It has been shown that the novel WBDCFs could be used successfully to provide dispersion compensation over the entire C-band without the need for compensation of the residual dispersion at 10 Gbit/s.

Three different dispersion maps optimised for transmission at 1550 nm have been used successfully at a wavelength of 1597 nm without the need for fine tuning of the dispersion compensation. The spans consisted of modified C-band EDFAs making use of forward amplified spontaneous emission pumping into an erbium doped fibre, 50 or 80 km SMF, and a matching length of WBDCF optimised for nearly 100% dispersion compensation at 1550 nm. Transmission over more than 1000 km was achieved using pre-compensation with both the 50 and 80 km spans. It has therefore been shown that L-band transmission over more than 1000 km was feasible using a dispersion compensation scheme optimised for the C-band, thus removing the need for separate band dispersion compensation.

6.5 References to Chapter 6

[1] K. Oda, M. Fukutoku, M. Fukui, T. Kitoh, and H. Toba, "16-channel × 10-Gbit/s optical FDM transmission over a 1000 km conventional single-mode fiber employing dispersion-compensating fiber and gain equalization", in *Technical Digest Optical Fiber Communication Conference, OFC'95*, San Diego, California, U.S.A., post-deadline paper PD22, 1995.

[2] L. Grüner-Nielsen, S. N. Knudsen, T. Veng, B. Edvold, and C. C. Larsen, "Design and manufacture of dispersion compensating fibre for simultaneous compensation of dispersion and dispersion slope", in *Technical Digest Optical Fiber Communication Conference, OFC'99*, San Diego, California, U.S.A., paper WM13, vol. 2, pp. 232–234, 1999.

[3] L. Grüner-Nielsen, S. N. Knudsen, B. Edvold, D. Magnussen, T. Veng, and C. C. Larsen, "Design and manufacture of dispersion compensating fibre for simultaneous compensation of dispersion and dispersion slope", in *OSA Trends in Optics and Photonics*, 1999, vol. XXIX, pp. 134–141, 1999.

[4] L. Grüner-Nielsen, S. N. Knudsen, B. Edvold, T. Veng, D. Magnussen, C. C. Larsen, and H. Damsgaard, "Dispersion compensating fibers", *Optical Fiber Technology*, vol. 6, pp. 164–180, 2000.

[5] J. F. Massicott, J. R. Armitage, R. Wyatt, B. J. Ainslie, and S. P. Craig-Ryan, "High gain, broadband 1.6 μm Er^{3+} doped silica fibre amplifier", *Electronics Letters*, vol. 26, no. 20, pp. 1645–1646, 1990.

[6] J. F. Massicott, R. Wyatt, and B. J. Ainslie, "Low noise operation of Er^{3+} doped silica fibre amplifier around 1.6 μm", *Electronics Letters*, vol. 28, no. 20, pp. 1924–1925, 1992.

[7] S. Aisawa, T. Sakamoto, M. Fukui, J. Kani, M. Jinno, and K. Oguchi, "Ultra-wideband long distance WDM demonstration of 1 Tbit/s (50 × 20 Gbit/s) 600 km transmission using 1550 and 1580 nm wavelength bands", *Electronics Letters*, vol. 34, no. 11, pp. 1127–1129, 1998.

[8] A. K. Srivastava, Y. Sun, J. W. Sulhoff, C. Wolf, M. Zirngibl, R. Monnard, A. R. Chraplyvy, A. A. Abramov, R. P. Espindola, T. A. Strasser, J. R. Pedrazzani, A. M. Vengsarkar, J. L. Zyskind, J. Zhou, D. A. Ferrand, P. F. Wysocki, J. B. Judkins, and Y. P. Li, "1 Tb/s

transmission of 100 WDM 10 Gb/s channels over 400 km of TrueWave™fiber", in *Technical Digest Optical Fiber Communication Conference, OFC'98*, San Jose, California, U.S.A., post-deadline paper PD10, 1998.

[9] H. S. Chung, M. S. Lee, D. Lee, N. Park, and D. J. DiGiovanni, "Low noise, high efficiency L-band EDFA with 980 nm pumping", *Electronics Letters*, vol. 35, no. 13, pp. 1099–1100, 1999.

[10] A. K. Srivastava, J. W. Sulhoff, L. Zhang, C. Wolf, Y. Sun, A. A. Abramov, T. A. Strasser, J. R. Pedrazzani, R. P. Espindola, and A. M. Vengsarkar, "L-band 64 × 10 Gb/s DWDM transmission over 500 km DSF with 50 GHz channel spacing", in *Proceedings European Conference on Optical Communication, ECOC'98*, Madrid, Spain, vol. 3, pp. 73–75, 1998.

[11] T. Sakamoto, M. Fukui, M. Jinno, J.-I. Kani, S. Aisawa, H. Ono, M. Yamada, and K. Oguchi, "Recirculating loop experiment for 1580-nm-band large-scale WDM network using dispersion-shifted fiber", *IEEE Photonics Technology Letters*, vol. 10, no. 4, pp. 618–620, 1998.

[12] A. Buxens, H. N. Poulsen, A. T. Clausen, and P. Jeppesen, "Gain flattened L-band EDFA based on upgraded C-band EDFA using forward ASE pumping in an EDF section", *Electronics Letters*, vol. 36, no. 9, pp. 821–823, 2000.

[13] G. P. Agrawal, *Nonlinear fiber optics*, chapter 4, pp. 89–132, Academic Press, San Diego, 2nd edition, 1995.

[14] M. Yamada, H. Ono, T. Kanamori, S. Sudo, and Y. Ohishi, "Broadband and gain-flattened amplifier composed of a 1.55 μm-band and a 1.58 μm-band Er^{3+}-doped fibre amplifier in a parallel configuration", *Electronics Letters*, vol. 33, no. 8, pp. 710–711, 1997.

Chapter 7

System performance of new types of dispersion compensating fibres

Increasing the capacity of optical communication systems relies on the effective management of group-velocity dispersion (GVD) and optical fibre non-linearities. The choice of the type of fibre used for transmission as well as the dispersion management scheme are therefore of prime importance for the design of optical fibre links. The use of dispersion compensating fibres (DCF) [1] is a mature technique to compensate for the dispersion of already deployed standard single mode fibre (SMF), and the effectiveness of the newest generation of DCFs for wide-band compensation has already been demonstrated in Chapter 6 . Moreover, due to its high local dispersion value (around 17 ps/(nm·km) at 1550 nm), SMF suffers little from four-wave mixing [2] and has also been shown to be resilient to cross-phase modulation in wavelength division multiplexing (WDM) systems [3, 4]. It therefore offers a reliable alternative for the design of future links.

Over the past few years, new DCF designs have been introduced - reverse dispersion fibre (RDF) [5] or inverse dispersion fibre (IDF) [6, 7] - which enable the cabled compensation of the dispersion and dispersion slope of SMF with various SMF to DCF length ratios [8]. These new fibres will hereafter be referred to as IDF$\times n$ where n is the SMF to DCF length ratio. Such fibres have been used successfully in a number of high capacity WDM [9, 10, 11, 12, 13] and optical time division multiplexing (OTDM) [14] experiments.

However, when the dispersion compensating fibre design is changed to provide dispersion in the range -100 ps/(nm·km) (conventional DCF) to

-17 ps/(nm·km) (IDF×1), the intrinsic properties of the fibre (attenuation and non-linear coefficient), as well as its position with respect to the transmitter and optical amplifiers in the link are changed. A consequence is that, due to non-linear effects, it is not clear *a priori* which type of dispersion compensating fibre performs the best for a given system.

After summarising the essential properties of the new dispersion compensating fibres in Section 7.1, we report a systematic comparison of the system performance of new types of IDF×n with $n = 1, 2, 3$ and conventional DCF. In Section 7.2, short spans (50 km) typical of long-haul submarine systems are optimised numerically with respect to span input power for 10 Gbit/s non return-to-zero (NRZ) as well as return-to-zero (RZ) modulation. IDF×1 is shown to provide the best performance for single channel NRZ transmission, while IDF×2 or 3 should be preferred in WDM systems. The benefits of using IDF×1 instead of conventional wide-band dispersion compensating fibre (WBDCF) for a 50 km span system making use of chirped return-to-zero modulation (CRZ) is demonstrated experimentally in Section 7.3. Finally, the performance of short (1.8 and 4.8 ps) RZ pulses at 10 Gbit/s is compared to conventional NRZ modulation in a link made of SMF and IDF×1 in Section 7.4. The short RZ pulses are shown to be more resilient to non-linearities, resulting in a two-fold increase in transmission distance over NRZ modulation for a 3 dB power penalty criterion.

7.1 New types of dispersion compensating fibres

Transmission systems requirements impose constraints on the properties of optical fibres, in terms of loss, group-velocity dispersion, polarisation mode dispersion, as well as effective area, which governs the impact of non-linear effects. Two main options for the transmission fibre are being explored today, namely those based on SMF and those based on non-zero dispersion shifted fibres (NZDSF) [15]. The influence of non-linear effects needs to be scaled before choosing a particular fibre infrastructure for a given system. To this respect, SMF might be the preferred choice as the transmission fibre due to its resilience to both four-wave mixing (FWM) and cross-phase modulation (XPM) in WDM systems [3, 4]. In any case, dispersion compensation is required for systems running at bit rates above 10 Gbit/s. From the WDM side, dispersion compensation is expected to be achieved over a broad bandwidth in order to limit expensive and unpractical channel-by-channel compensation schemes to the receiving end of the link. From the OTDM side, transmission at 160 Gbit/s over 160 km SMF [16], 320 Gbit/s over 200 km NZDSF [17] and even 640 Gbit/s over 92 km SMF

and RDF [14] have been achieved in the laboratory. Owing to the short pulse durations, the amount of dispersion experienced during transmission might change significantly over the signal spectrum width, and therefore careful compensation of first and higher dispersion orders are required. As a consequence, one of the important requirements for the dispersion compensating technique to be used in either WDM or high-speed OTDM systems is its ability to compensate for the dispersion of the transmission fibre over a broad bandwidth. So far, only DCFs have been able to satisfy this requirement over the large bandwidths used by high-capacity WDM systems [18].

Some important limitations of conventional dispersion compensating fibres are their high loss (of the order of 0.5 dB/km against only 0.2 dB/km for SMF) and high non-linear coefficient (typically 7-8 $W^{-1} \cdot km^{-1}$ against only about 1.3 $W^{-1} \cdot km^{-1}$ for SMF) induced by the combined effects of a reduced effective area and higher doping of the core necessary to raise its refractive index. Both the high refractive index contrast and the reduced effective area enable high negative dispersions to be obtained [1]. However, reducing the core diameter also increases the sensitivity towards bending loss, which has prevented DCFs from being cabled so far. As a consequence, conventional DCFs are used as lumped elements, usually in-between optical amplifier stages at repeaters. Such an utilisation is not very favourable from an optical signal-to-noise ratio (OSNR) point of view, as the DCF modules induce loss in the link but do not contribute to the transmission distance.

A new type of dispersion compensating fibre has been suggested in order to overcome some of those limitations. First proposed by Furukawa [5], reverse dispersion fibres offer reduced loss and non-linearity compared to conventional DCFs and can be cabled in order to compensate for the dispersion of SMF in a 1:1 length ratio. Consequently, they contribute to the transmission distance, a feature particularly attractive for long-haul submarine links. Fibres exhibiting similar properties, although based on a different refractive index profile design and manufactured using a different technology, were later proposed by Lucent Technologies Denmark A/S (now OFS Fitel Denmark I/S) and named IDF for "inverse dispersion fibre" [6]. Fibres with intermediate properties in terms of loss, dispersion and non-linear coefficient have been later proposed and demonstrated [8, 19]. IDFs form the basis of the novel types of DCFs investigated in this chapter. Some of their key properties are outlined below.

1. They exhibit a smaller attenuation than conventional DCFs. Therefore, for a given transmission length, the span loss can be reduced significantly compared to the "classic" SMF + conventional DCF con-

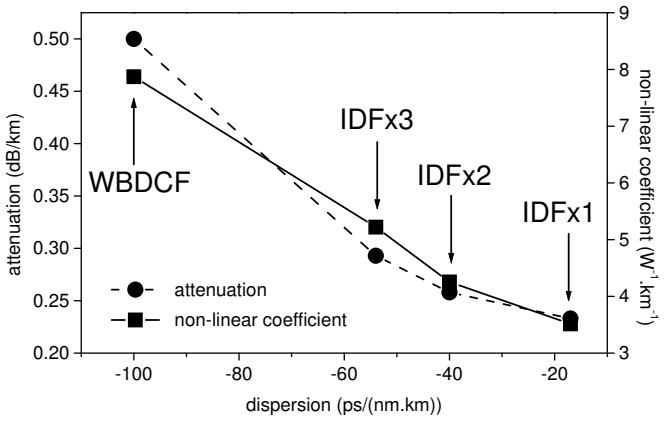

Figure 7.1 Properties of new types of dispersion compensating fibres as a function of their dispersion parameter. Left: attenuation; Right: non-linear coefficient. The evolution of fibre properties is illustrated from conventional DCF to IDF (corresponding to $D = -100$ ps/(nm·km) to -17 ps/(nm·km) respectively).

figuration. This is beneficial in terms of signal-to-noise ratio.

2. Their effective area is increased compared to conventional DCFs. This has the effect of reducing non-linear effects such as self-phase modulation (SPM), cross-phase modulation and four-wave mixing, which are detrimental to the quality of transmission.

3. Unlike older generations of DCFs that were spooled within repeaters where they constituted additional losses, these fibres can be cabled and are therefore part of the transmission distance. This feature makes them especially attractive for long-haul submarine applications.

4. Moreover, they also provide dispersion slope compensation, and can therefore compensate for SMF over a large bandwidth, making them particularly suitable for wavelength division multiplexing and high-speed (above 40 Gbit/s) systems.

5. These new fibres have been designed in order to compensate for the dispersion of SMF with different SMF to DCF length ratios. This offers an additional degree of freedom when dealing with the difficult management of dispersion and non-linearities in optical fibre communication systems.

	SMF	IDF×1	IDF×2	IDF×3	WBDCF
Attenuation (dB/km)	0.18	0.23	0.26	0.29	0.5
Dispersion (ps/nm/km)	17	-17	-40	-54	-100
RDS (nm^{-1})	0.0034	0.0034	0.0034	0.0034	0.0034
Effective area (μm^2)	85	35	30	26	19
n_2 ($\times 10^{-20}$ m^2/W)	2.2	3.0	3.2	3.3	3.7

Table 7.1 Properties of SMF, WBDCF and novel IDF×n with $n = 1, 2, 3$. The parameters are given at 1550 nm.

Throughout this chapter, the dispersion and dispersion slope compensating fibres with dispersion of the order of -100 ps/(nm·km) will be referred to as wide-band dispersion compensating fibres (WBDCF), whereas the novel types of inverse dispersion fibres will be described as IDF×n where n is the SMF to dispersion compensating fibre length ratio. The acronym DCF will be used as a general term to describe all types of dispersion compensating fibres (either WBDCF or IDF). All the DCFs considered in this chapter offer simultaneous dispersion slope compensation. Conventional slope compensating DCFs (WBDCF) correspond to a SMF to DCF length ratio of about 6.

The evolution of dispersion compensating fibres properties when the absolute value of their dispersion is reduced from conventional DCF values (-100 ps/(nm·km)) to IDF×1 values (-17 ps/(nm·km)) is illustrated in Figure 7.1. It can be seen that both the fibre attenuation and non-linear coefficient are significantly reduced. The plotted attenuation and effective area data were obtained from averaged values of measurements performed on a large sample of IDFs manufactured by Lucent Technologies Denmark A/S [8], while the non-linear refractive indices were estimated from dopant concentrations. Typical values for the main optical properties of the novel IDFs are given in Table 7.1 together with the corresponding values for SMF and WBDCF. Those values will be used in all calculations and numerical simulations presented in Sections 7.1 and 7.2. As previously mentioned, all the DCFs were designed in order to also provide compensation of the dispersion slope of SMF. Hence their relative dispersion slope (RDS), defined as the ratio of their dispersion slope to their dispersion at 1550 nm, is the same as that of SMF.

As described previously, the new IDFs are designed to be deployed in the transmission cable. It has also been shown recently that WBDCF could also be cabled successfully [1, 20]. In spans made of SMF followed by

DCF, the new IDFs will however be placed closer to optical amplifiers (for a constant span length) than conventional WDBCFs and, although their non-linear coefficient is smaller, the higher input power means that it is not clear whether such a combination is optimal with respect to non-linear penalty. A trade-off has to be found between increased input power and decreased non-linear coefficient, resulting in an optimal dispersion map. It is the purpose of the remaining of this chapter to investigate the benefits of using IDF$\times n$ when compared to WBDCF in dispersion managed links based on SMF.

Even though the new IDFs have been introduced in a number of record-breaking long-distance and high capacity experiments, this has been done conjointly with other technologies, meaning that it is not always clear whether the introduction of the fibres themselves provided a clear advantage over older configurations. To the best of our knowledge, the only systematic comparison between SMF+WBDCF and SMF+RDF has been reported for a 32×10.7 Gbit/s WDM system using the CRZ modulation format in [21]. It has been shown experimentally that, in such a system with 45 km span length, a dispersion map based on SMF and WBDCF was more robust to fibre non-linearities than a SMF+RDF map. More recently, a numerical optimisation of the dispersion of hybrid links using cabled IDF or lumped dispersion compensating modules with high negative dispersion has been reported in [22] for WDM systems at 40 Gbit/s with 80 km spans. In this case, benefits of using the hybrid solution with transmission fibre dispersion above 12 ps/(nm·km) were highlighted. The rapid development of distributed Raman amplification [23, 24] is likely to complicate even more the choice between IDF$\times n$ or WBDCF, as smaller effective areas, otherwise detrimental in terms of non-linear degradation experienced by the signal, are beneficial in terms of Raman gain efficiency [25]. However, the joint use of IDF and Raman amplification is not considered in the present study.

As a consequence, there is no clear answer to the problem of knowing which of the SMF+WBDCF or SMF+IDF$\times n$ solution performs the best as the conclusion depends on all other parameters in the system (span length, bit rate, modulation format, pulse width, amplification scheme, etc). It is therefore more important to get an understanding of the physical limitations encountered for each type of fibre, which is our ambition in the remaining of this chapter.

The importance of the choice of a proper SMF to DCF length ratio can be highlighted by considering the influence of non-linearities alone and

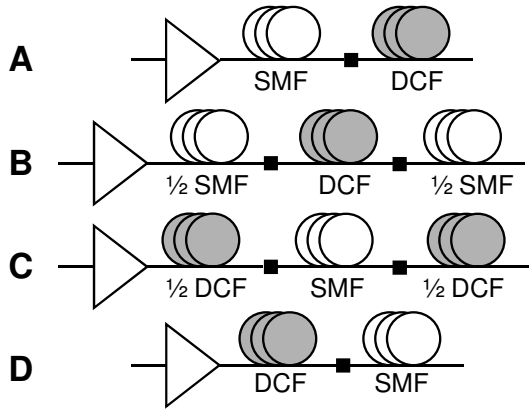

Figure 7.2 Dispersion maps considered in the non-linear phase shift analysis.

calculating the phase shift induced by self-phase modulation throughout a given link. This calculation ignores the influence of other degrading effects such as group-velocity dispersion and amplified spontaneous emission (ASE) noise accumulation. However, it has been shown to be practical in order to evaluate the relative performance of systems known beforehand to be limited by non-linearities. The validity of using the non-linear phase shift as a criterion to assess the performance of terrestrial WDM systems has been recently discussed in [26]. The accumulated non-linear phase shift through a link of length L is defined as

$$\Phi_{NL} = \frac{2\pi}{\lambda} \int_0^L \frac{n_2(z)}{A_{eff}(z)} P(z)\, dz \tag{7.1}$$

where n_2 is the fibre non-linear index, A_{eff} its effective area, λ the signal wavelength and $P(z)$ the signal power distribution over the link. The dependence of the fibre parameters on the propagation distance z enables to take into account links with non-uniform fibre properties, such as those made of dispersion compensated spans.

The non-linear phase shifts induced by a single dispersion compensated span have been calculated for dispersion maps based on WBDCF or IDF$\times n$, where $n = 1, 2, 3$. In these calculations, the span length was set to 50 km, a value typical of long-haul submarine systems. As throughout this chapter, the span length is calculated as the sum of the SMF and DCF lengths, as the new IDFs were designed for cabled dispersion compensation. The four different dispersion maps depicted in Figure 7.2 were considered. Maps A

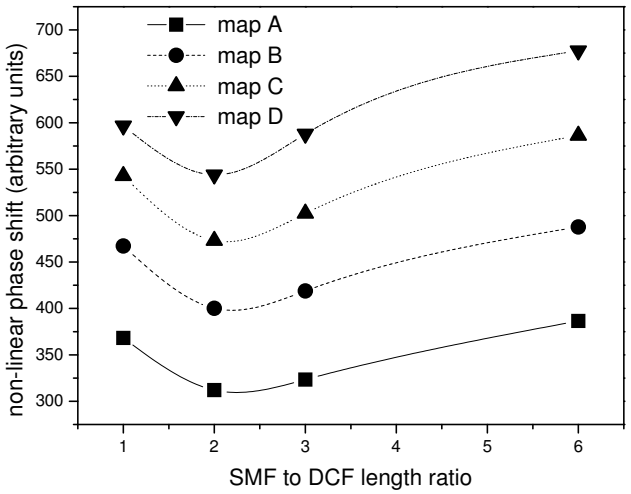

Figure 7.3 Normalised non-linear phase shifts as a function of SMF to DCF length ratio for the four span configurations shown in Figure 7.2. The non-linear phase shifts are calculated for a fixed span output power. The span length is 50 km.

and D correspond to post and pre-compensation, respectively, while the two possible schemes where the length of either the SMF or the DCF is split equally at the beginning and the end of the span are represented by maps B and C, respectively. The span loss being different for each type of DCF, the non-linear phase shifts are calculated for a fixed span output power P_{out}. In this way, a constant electrical signal-to-noise (SNR) ratio at the receiver that would follow the span is ensured for all fibre types. As a consequence, the difference in performance induced by the use of DCFs with different SMF to DCF length ratios are due to the distinct fibres properties, but also to the different span input power P_{in} required to maintain the SNR at the receiver. Accordingly, we calculate the quantity

$$y = \left(\frac{\Phi_{NL}}{P_{in}a}\right) = \left(\frac{\Phi_{NL}}{P_{out}}\right) \tag{7.2}$$

where a represents the span loss, including 0.25 dB splicing loss between SMF and DCF, for a fixed P_{out}.

The calculated non-linear phase shifts normalised to a span output power of 1 W are represented in Figure 7.3 for the four dispersion maps A, B, C and D as a function of the value of the SMF to DCF length ratio. The globally higher values of the non-linear phase shifts for maps D and

C in this order confirm the fact that SPM in the dispersion compensating fibre is the limiting factor. This can also explain the fact that map B exhibits a higher non-linear phase shift than map A, as the DCF is placed closer to the span input in the former map. The curves present an optimum corresponding to IDF×2, reflecting the trade-off between the value of the non-linear coefficient of the DCF and its proximity to the beginning of the span where the signal power is the highest. For all four fibre arrangements, the calculated non-linear phase shift is higher when WBDCF are used than for any of the novel IDF×n. Although such a calculation suggests that it could be beneficial to use the new IDFs when the system is limited by SPM, it does not provide a complete description of the transmission impairments, as interactions betwen dispersion, non-linearities, as well as ASE noise are ignored. In order to take into account all these effects and their interactions, full numerical simulations based on the resolution of the non-linear Schrödinger equation by the split-step method are required.

7.2 Numerical comparison of novel IDF-based dispersion maps

In this section, we report for the first time to our knowledge a numerical comparison of new types of DCFs with different SMF to DCF length ratios. We investigate the origin of signal degradation for single channel transmission at 10 Gbit/s in either the return to zero or non-return to zero format using amplified multi-span systems with a fixed span length (SMF+DCF) of 50 km. Our calculations are based on typical parameters measured on manufactured novel DCFs. In order to illustrate the degradations induced by inter-channel non-linear effects and their influence on the optimum choice for the DCF, an 8-channel WDM system is also considered in the simulations.

7.2.1 Systems under investigation

The dispersion maps under investigation are shown in Figure 7.4 for one period. The link is made of identical spans consisting of an erbium doped fibre amplifier (EDFA) with 5 dB noise figure followed by SMF and DCF with a total span length of 50 km. Splice losses of 0.25 dB are assumed at the DCF ends. The gain of the EDFA compensates exactly for the span loss, meaning that the signal power remains constant at the input of each span. The dispersion of the various types of DCF is -17, -40, -54, and -100 ps/(nm·km), corresponding to SMF to DCF length ratios of about 1,

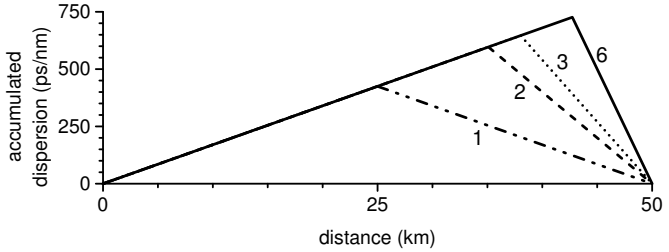

Figure 7.4 Representation of one period of the dispersion maps under investigation for a total span length of 50 km and SMF to DCF length ratios equal to 1, 2, 3 and 6.

2, 3 and 6 (conventional DCF), respectively. The DCFs are designed for compensation of the dispersion slope of SMF and therefore their relative dispersion slope is equal to that of SMF. The fibre parameters used in the simulations correspond to the ones given in Table 7.1. Full dispersion compensation is achieved after each span. Keeping the span length constant for the different dispersion maps makes sense as the new types of fibres are designed for cable deployment [6] and it has also been shown that conventional DCFs can be cabled successfully [1].

The transmission of a 1024 bit pseudo random sequence modulated at 10 Gbit/s in either the NRZ or the RZ format is considered in our simulations. For NRZ modulation, the optical signal is generated from a chirp-free Mach-Zehnder modulator and its extinction ratio is set to 15 dB. Raised cosine pulses with 50 ps full-width half-maximum (FWHM) are considered in the RZ simulations. The receiver consists of a PIN photodiode with a responsivity of 1.2 A/W and single sided thermal noise density of 15 ps/$\sqrt{\text{Hz}}$ followed by a fourth order low-pass Bessel filter with 3 dB cut-off frequency equal to 7.5 GHz. The sensitivity at a bit-error-rate (BER) of 1.0×10^{-9} is then calculated according to the method described in [27]. The calculation of the propagation through the fibre is performed using an adaptive split-step algorithm. Noise is added at each optical amplifier and therefore the non-linear interaction between signal and noise is taken into account in the calculations.

7.2.2 Influence of the modulation format

Figure 7.5 represents the maximum number of cascaded spans resulting in a power penalty smaller than 1 or 3 dB as a function of the span signal average input power in the NRZ case. An optimum signal input power of -3 dBm is found for all four dispersion maps. It is also found that

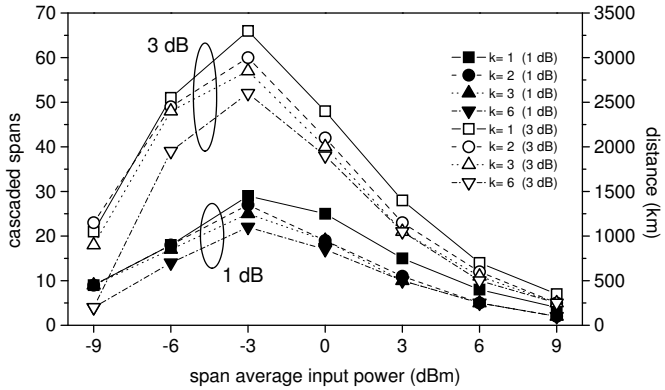

Figure 7.5 Number of cascaded 50 km spans corresponding to 1 and 3 dB power penalty as a function of span average input power. Single channel NRZ transmission with SMF to DCF length ratios equal to k= 1, 2, 3 and 6 (simulation results).

the use of IDF×1 results in the longest transmission distance whatever the power level, while WBDCF exhibits the poorest results. Intermediate performances are obtained with IDF×2 and 3. The significantly shorter reach of systems based on WBDCF at low power levels can be simply explained by the larger loss of the SMF+WBDCF span compared to the three IDF solutions. The loss of the span based on WBDCF is 11.8 dB against 10.8, 10.7 and 10.9 dB for IDF×1, 2 and 3 respectively.

An equivalent plot for the RZ format is given in Figure 7.6, which shows that the transmission distance for a given penalty is maximum for -6 dBm input power with the maps using SMF to DCF length ratios equal to 2 and 3. At low power levels, the conventional configuration (WBDCF) gives the poorest result, while the other three maps exhibit equivalent results. This is due to the fact that the system is then limited by noise accumulation and that WBDCF presents the highest span loss. On the other hand, at high power levels, the SMF+IDF×1 configuration results in the poorest performance, in contrast with what was observed for NRZ modulation. This can be attributed to self-phase modulation in the DCF, as the product of the non-linear coefficient, input power and effective length of the DCF is about 2.5 times higher for IDF×1 than for WBDCF.

At the lower end of the investigated power range (noise limited system), RZ performs better than NRZ independently of the dispersion map, owing to the larger eye opening for a given average power. On the other hand, for higher power values, longer transmission distances are predicted when using

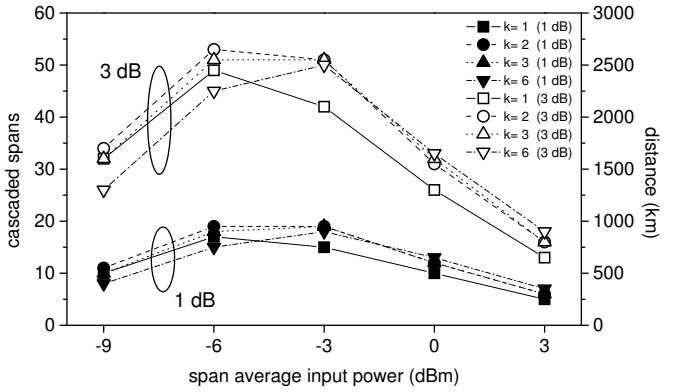

Figure 7.6 Number of cascaded 50 km spans corresponding to 1 and 3 dB power penalty as a function of span average input power. Single channel RZ transmission with SMF to DCF length ratios equal to k= 1, 2, 3 and 6 (simulation results).

NRZ modulation. SPM in the DCF can account for this behaviour. The higher peak power of the RZ pulses for a given average input power when compared to NRZ, as well as their relatively broad pulse width ($\sim$ 50 ps), which ensures that they do not disperse significantly in the relatively short SMF length, contribute both to enhanced SPM in the DCF. This is in contrast with the behaviour observed with the transmission of shorter RZ pulses, as we shall see in the experimental results of Section 7.4. For the investigated dispersion maps and RZ pulse width, NRZ is more robust to non-linearities than RZ at the optimum power level.

7.2.3 WDM transmission

In order to investigate the effects of multi-channel non-linear effects such as FWM and XPM, simulations were also performed on the same set of dispersion maps by considering an 8-channel WDM system with 35 GHz channel spacing. The channels are modulated at 10 Gbit/s in the NRZ format. The wavelength (de)multiplexers were modelled as second order Gaussian filters with 25 GHz FWHM bandwidth.

The channel spacing of 35 GHz corresponds to a spectral efficiency of 0.29 bit/s/Hz. Although not a value standardised by the International Telecommunication Union (ITU), this channel spacing has been selected in order to enhance the influence of cross-phase modulation which is the main focus of this study. Indeed, it has been shown in [28] that, when the

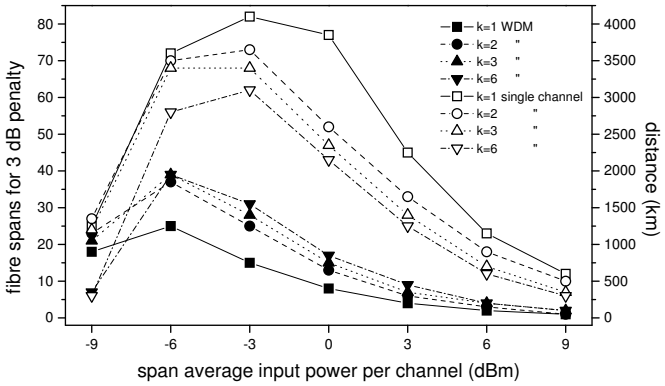

Figure 7.7 Number of cascaded 50 km spans corresponding to 3 dB power penalty as a function of span average input power per channel for single and 8 channel WDM transmission (worst case channel).

walk-off length in the fibre

$$L_{wo} = \frac{\Delta t}{|D|\,\Delta\lambda} \tag{7.3}$$

is much shorter than the effective length

$$L_{eff} = \frac{1 - e^{-\alpha L}}{\alpha}, \tag{7.4}$$

the effect of XPM scales as the inverse of the channel spacing $\Delta\lambda$. The walk-off length is defined here as the length over which XPM interaction from one channel to another channel spaced $\Delta\lambda$ apart occurs, corresponding to the distance over which a transition edge of the interfering channel overlaps spatially with a particular instant t in the perturbed channel. In the definitions of the walk-off length and effective length above, Δt corresponds to the duration of a transition edge of the NRZ modulated signal (either rise time or fall time), D is the fibre dispersion and α is the fibre loss. In our case, for a channel spacing of 35 GHz, dispersion $D = 17$ ps/(nm·km) and rise time equal to one fifth of the bit-slot, we obtain $L_{wo} = 4.2$ km against $L_{eff} = 15.6$ km for 25 km SMF. Similar conclusions on the relative values of L_{wo} and L_{eff} can be obtained with the different types of DCFs considered in this study for a 50 km span. Therefore, the effect of XPM in fibres with high absolute value of dispersion such as the ones considered here, can be increased by reduction of the channel spacing.

The maximum number of spans resulting in a power penalty smaller than 3 dB are plotted as a function of the span average signal input power

per channel in Figure 7.7. For each dispersion map and each span input power value, the performance of the worst-case channel, usually one of the innermost channels in the WDM spectrum, is represented. In order to ease the comparison between the behaviours observed for single channel and in the WDM case, the single channel results of Figure 7.5 are shown in the graph. In contrast with what was observed in the single channel case, IDF×1 performs the worst for all power levels in this WDM system, apart when the input power is reduced down to -9 dBm per channel. In this case, the dispersion map making use of WBDCF displays the worst performance due to the higher span loss. The optimum span input power value is equal to -6 dBm per channel and is the same for all four types of DCFs. This optimum value is decreased by 3 dB compared to the single channel case, while the maximum transmission distance for less than 3 dB power penalty is reduced from 4100 to 1250 km when IDF×1 is used and from 3100 to 1950 km with WBDCF. The fact that the optimum signal power needs to be reduced compared to the single channel system suggests that a new non-linear mechanism is the limiting factor when WDM is introduced. The large dispersion of all the fibres involved prevents the phase-matching leading to effective four wave mixing generation. When two channels with equal power are present at the fibre input, the ratio of the four-wave mixing product power to the signal power at the fibre output can be calculated in the undepleted pump approximation according to [29]

$$\eta = \frac{P_{FWM}}{P_{in}e^{-\alpha L}} = \gamma^2 P_{in}^2 \frac{1 + e^{-2\alpha L} - 2e^{-\alpha L}\cos(\Delta\beta L)}{\Delta\beta^2 + \alpha^2} \tag{7.5}$$

where γ is the fibre non-linear coefficient, P_{in} is the span input power of a single channel, L is the fibre length and $\Delta\beta$ is the difference between the propagation constants of the interacting waves, which depends on the dispersion slope S according to

$$\Delta\beta = -2\pi c S \lambda_0^4 \left(\frac{\lambda_0 - \lambda_1}{\lambda_0\lambda_1}\right)\left(\frac{\lambda_2 - \lambda_1}{\lambda_2\lambda_1}\right)^2 \tag{7.6}$$

where c is the velocity of light in vacuum, λ_1 and λ_2 are the signal wavelengths and λ_0 is the fibre zero-dispersion wavelength. For a channel spacing of 35 GHz and an input power of -6 dBm per channel, we find $10\log\eta$ =-67 dB after 25 km SMF. If we neglect the power of the four-wave mixing tones generated in the SMF and calculate the relative power of the four-wave mixing tones generated in the IDF×1, a value of $10\log\eta$ =-65 dB is found. An equivalent calculation performed with the SMF+WBDCF map leads to $10\log\eta$ =-67 dB in the 42.7 km SMF against -80 dB in the matching 7.3 km WBDCF. As a consequence, it is confirmed that FWM alone

cannot account for the degraded performance observed with the IDF×1 map compared to the WBDCF map.

For span input power levels above -3 dBm, WBDCF results in the best performance in the WDM case. It is therefore suggested that cross-phase modulation in the dispersion compensating fibre is responsible for the poorer performance observed in the IDF×1 case according to the following mechanism. In short spans such as those studied here, the 10 Gbit/s pulses are not totally dispersed when they reach the DCF. This is especially true in the case of IDF×1 where the negative dispersion fibre is placed only 25 km away from the repeaters. This, acting together with the relatively high residual power still available (as only 4.5 dB are lost in the SMF part of the span when IDF×1 are used), means that non-linear effects are still likely to occur in the negative dispersion fibre, as already discussed in the single channel case. IDF×1 presents the lowest dispersion of the various types of DCFs, and therefore the largest walk-off length, which increases the effectiveness of the non-linear interaction induced by XPM between WDM channels. However, the dispersion of IDF×1 is still sufficiently large to efficiently convert the XPM induced phase modulation to intensity distortion. When WBDCF is used instead, both the reduction in power level at the negative dispersion fibre input and the reduction of the walk-off length contribute to lower the influence of XPM. Furthermore, the 100% span-per-span compensation scheme adopted in the systems investigated in this study is not favourable from a XPM point of view as bit patterns are realigned at each span input where the power is the highest, resulting in an accumulation of the non-linear impairments from one span to another.

We have shown that cross-phase modulation is the limiting non-linear effect in WDM systems making use of short 50 km spans made of SMF and IDF×1. Unlike in the single channel case where IDF×1 have been shown to offer the best performance for NRZ modulation, IDF×2 or 3 should be preferred in WDM systems, as they simultaneously present lower span loss than WBDCF, which is beneficial at low power levels, and are more resilient to XPM than IDF×1. They therefore constitute a good trade-off for the design of WDM links making use of novel cabled dispersion compensating fibres.

7.3 Experimental comparison of SMF+WBDCF and SMF+IDF maps

In this section we report the first experimental comparison of the system performance of wide-band DCF and IDF×1 for 50 km spans using the

chirped return-to-zero modulation format. We show that the reach of such a short span system making use of discrete amplification can be significantly increased when IDF×1 are used. Transmission over 40 spans (corresponding to 2000 km) could be achieved with less than 3 dB penalty for IDF×1, corresponding to a 2 dB improvement for the same number of spans when conventional wide-band DCFs are used.

7.3.1 Experimental set-up

The benefit of using new types of dispersion compensating fibres has been demonstrated for the first time in our re-circulating loop test-bed. The experimental set-up is essentially similar to the one shown in Figure 5.16. As the experiment was performed with some of the first IDF spools kindly made available to us by Lucent Technologies Denmark A/S, only one single dispersion compensated span could be included into the loop. A post-compensation scheme was adopted in the experiment and the span length was fixed to approximatively 50 km, depending on the fibre type. In agreement with the numerical study reported in Section 7.2, the dispersion compensating fibre length is included in the span length as the new DCFs have been designed for cabled applications. The re-circulating loop consisted of a gain-flattened EDFA followed by an optical attenuator used to optimise the power level at the span input, a length of SMF followed by a matching length of WBDCF or IDF×1, and an extra gain-flattened EDFA used to compensate for the loss in the loop switch. This loop configuration is obviously not optimum as it includes one extra EDFA per span as compared to a real straight-line system, therefore producing excessive ASE noise accumulation. Having more spans in the loop would mean that the influence of the EDFA compensating for the loop switch loss would be distributed over the spans, hence improving the effectiveness of the loop at emulating a long-haul straight line system. The spans consisted of either 40 km SMF followed by 6.3 km WBDCF or 25.1 km SMF followed by 24.9 km IDF×1. Chirped return-to-zero modulation at 10 Gbit/s was used in this experiment. An electrical RZ signal was generated by applying a 10 Gbit/s NRZ signal to one input of a 10 to 20 Gbit/s electrical multiplexer, the second input being grounded, according to the method described in [30]. The RZ signal was then amplified in a broadband (20 GHz) amplifier before driving one of the arms of a dual-drive Mach-Zehnder modulator. At the receiver side, a 1.3 nm optical band-pass filter was applied to the signal which was subsequently detected using a PIN lightwave converter.

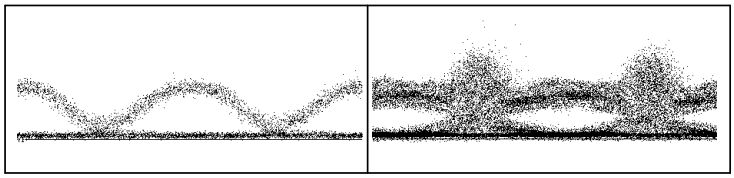

Figure 7.8 Eye diagrams (recorded with a 30 GHz sampling oscilloscope) after propagation through 30 SMF + WBDCF 50 km spans with average input power equal to -2 dBm (left) and 0 dBm (right).

7.3.2 First experimental results

First, the optimum signal power at the span input was determined for the SMF+WBDCF dispersion map. A power level of -2 dBm (as measured using an optical spectrum analyser with a 0.5 nm resolution bandwidth) was found to be optimum in order to maximise the number of spans for which error-free (defined at a bit-error-rate of 1.0×10^{-9}) performance could be obtained. The influence of the span input power is illustrated in Figure 7.8 where eye diagrams recorded after 30 spans (corresponding to 1390 km) are shown. Overshoots due to self-phase modulation and its subsequent conversion to amplitude distortion by fibre dispersion can clearly be seen on the eye diagram measured when the span input power was set to 0 dBm. On the other hand, the eye diagram recorded with -2 dBm span input power still preserves its RZ shape and remains open. Consequently, it was decided to use a power level of -2 dBm for the SMF+WBDCF map, as well as for the SMF+IDF×1 map in order to allow for performance comparison.

Bit-error-rate curves were measured as a function of number of round-trips in the loop for both dispersion maps. The results are shown in Figure 7.9. A sensitivity of -17.1 dBm at a BER of 1.0×10^{-9} was obtained after one single SMF+WBDCF span. This value is indistinguishable from the back-to-back sensitivity. A power penalty of 4.4 dB is measured after 40 SMF+WBDCF spans, corresponding to a distance of about 1850 km. For the same number of spans, the penalty is decreased to 2.5 dB when IDF×1 are used instead of WBDCF. It is still possible to transmit over 45 spans using IDF×1 with a power penalty smaller than the one obtained after 40 SMF+WBDCF spans. Error free transmission can still be achieved with a power penalty of 5.4 dB after 50 spans corresponding to 2500 km when using IDF×1.

Eyes diagrams recorded for both dispersion maps after 40 spans are shown in Figure 7.10. It can be seen that the signal obtained when WB-

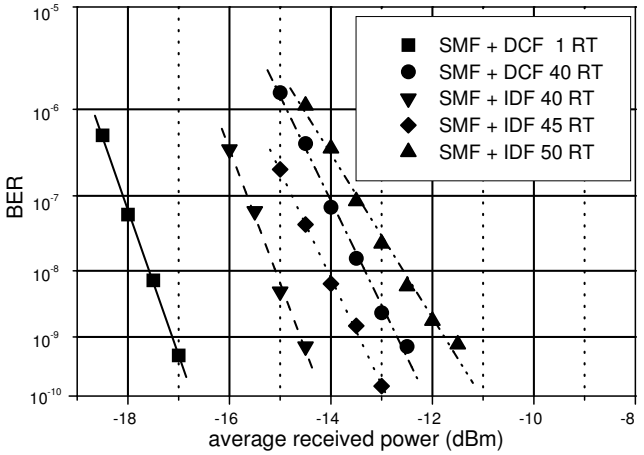

Figure 7.9 BER curves measured after 1 and 40 SMF+WBDCF spans as well as after 40, 45 and 50 SMF+IDF×1 spans.

DCFs are used is more strongly affected by ASE noise than in the case of IDF×1. This is due to the higher loss of the SMF+WBDCF span (estimated to 11.4 dB against only 10.5 dB for the IDF×1 span). The eye is slightly distorted in the SMF+IDF×1 case, which might be attributed to the effect of self-phase modulation in the IDF. As discussed earlier, for fixed span input power (which is the case in this experiment), the power at the input of the fibre which is the most non-linear in the span is higher for IDF than for WBDCF. The residual dispersion of the SMF+IDF×1 span was measured to be 1.6 ps/nm at the wavelength of 1557 nm used in this experiment. This value results in a total accumulated dispersion of 64 ps/nm after 40 spans, corresponding to a length of only 3.8 km SMF. It is therefore expected that the residual dispersion of the link should not significantly affect the quality of the transmitted signal. In any case, the eye diagram obtained after propagation through 40 SMF+IDF×1 spans confirms the measured error-free performance.

It has been pointed out earlier that the lengths of the two spans used in this experiment slightly differ, resulting in an extra 160 km distance after 40 spans for SMF+IDF×1. From a noise accumulation point of view, the same number of EDFAs being present in each type of span, the length difference should benefit the WBDCF-based span, as its loss is reduced compared to a 50 km span. From a fibre non-linearity point of view, it has been suggested that the reach of repeatered systems is limited by the number of spans rather than the span length [31]. The argument behind such a

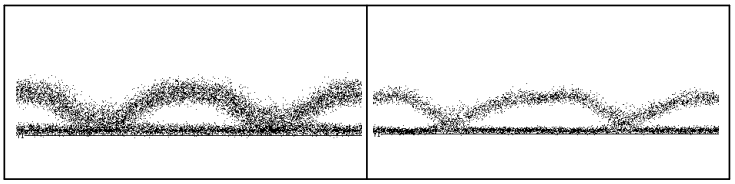

Figure 7.10 Comparison of eye diagrams (recorded with a 30 GHz sampling oscilloscope) after propagation through 40 SMF+WBDCF (left) and SMF+IDF×1 (right) spans with -2 dBm span average input power.

statement is that the influence of self-phase modulation is the largest at the beginning of the span where the signal power is the highest. However, this implies that the span length is much larger than the SMF effective length and that the dispersion compensating fibre can be considered linear. For the short spans used in this experiment, these assumptions might not be satisfied. The effective length of the SMF is 18 km when WBDCF is used, against 15 km in the case of IDF. Furthermore, in short span systems, the dispersion compensating fibre is placed close to the EDFAs, resulting in a higher possible accumulation of non-linearities than if longer spans were used. Having a full 50 km span might slightly improve the resilience towards non-linearities of the SMF+WBDCF system. Nevertheless, as the main limitation of this latter systems is believed to be due to noise accumulation as suggested from the inspection of the eye diagrams of Figure 7.10, a comparison of the two dispersion maps with exact span lengths of 50 km would still benefit the IDF-based solution.

In Section 7.2 it had been shown numerically that, for RZ modulation and 50 km spans, the performance of IDF×1 was significantly better than that of WBDCF only when the system was noise-limited. In the experiments, we still benefit from using IDF×1 at significantly higher span input power than those predicted by the simulations. This discrepancy can be partly explained by the difference in the mode of operation of the EDFAs in the simulations and in the experiments. In the calculations, the gain of the EDFAs was kept constant, resulting in fixed signal span input power. In contrast, the EDFAs used in the experiment were self-running, resulting in a decrease of the signal power induced by amplifier saturation due to the build-up of ASE noise [32]. The extra EDFA added to each span in order to compensate for the loop switch loss (6 dB in loop mode) also caused excess noise accumulation. A more favourable configuration using more spans in the loop would have definitively reduced the influence of this parasitic element. As a consequence, the system was noise limited at

a power level significantly higher than predicted by numerical simulation. Moreover, chirped RZ modulation was used in the experiments and it is believed that the influence of the chirp can also account for the better performance observed with IDF×1. However, the sign and value of the chirp had not been characterised, preventing us from confirming the experimental conclusions by numerical simulations.

Using some of the first available IDF×1 fibres, we have been able to perform an experimental comparison of the relative performance of a 10 Gbit/s CRZ system using 50 km dispersion compensated spans made of either SMF+WBDCF or SMF+IDF×1. We have shown that more than 45 SMF+IDF×1 spans (corresponding to 2250 km) could be cascaded for a penalty lower than that obtained after only 40 spans (corresponding to 1852 km if it is assumed the dispersion compensating fibre can be cabled) made of SMF and WBDCF, clearly demonstrating the benefits of using IDF×1 in such short span systems.

7.4 Short pulse transmission at 10 and 40 Gbit/s over a dispersion managed link made of SMF and IDF

Novel inverse dispersion fibres have been used widely in many high capacity and long haul experiments since their introduction. In parallel, the concept of highly dispersed pulse transmission has been introduced for high bit-rate systems [33, 34]. Short pulses disperse faster in the transmission fibre, leading to a reduced peak power after a short fibre length, and therefore reduced impact of non-linearities such as self-phase modulation. This, in turn, enables the launch power to be increased in order to overcome the more stringent optical signal-to-noise limitations of high bit rate systems.

One of the already mentioned possible limitations of the use of novel IDFs is that, for a fixed span length, they are placed closer to the optical amplifiers than conventional DCFs. Consequently, the numerical investigations reported in Section 7.2 have shown that 10 Gbit/s systems making use of IDF over short 50 km dispersion compensated spans did not benefit from using broad ($\sim 50\%$ duty cycle) RZ pulses instead of NRZ modulation, unless operated with a low span input power. It therefore remains to be seen, whether the transmission of shorter RZ pulses over dispersion maps based on SMF and IDF can present significant advantages over conventional NRZ transmission.

In this section, we present an experimental comparison of the trans-

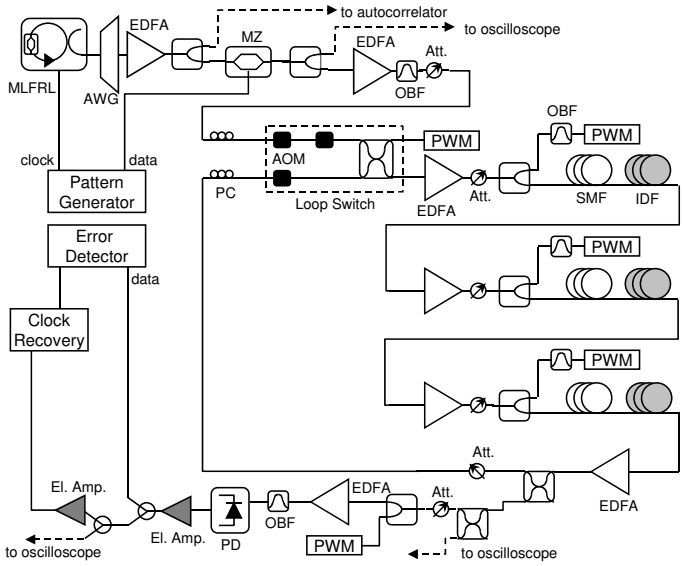

Figure 7.11 Experimental re-circulating loop set-up for 10 Gbit/s short pulse propagation through a SMF+IDF×1 map.

mission properties of the NRZ and short RZ (1.8 and 4.8 ps) modulation formats over a dispersion map made of 50 km SMF+IDF. We highlight the benefits of using short RZ pulses by demonstrating transmission over more than 2700 km. Furthermore, we report the first 40 Gbit/s OTDM experiment performed in our re-circulating loop test-bed, showing the feasibility of transmission over 600 km.

7.4.1 Experimental set-up

The experimental set-up is shown in Figure 7.11. A 1.8 ps full-width half-maximum 10 GHz pulse train was generated by an actively mode-locked erbium-doped fibre ring laser (MLFRL). Broader (4.8 ps) pulses were obtained after filtering in an arrayed waveguide grating (AWG) multiplexer having a 3 dB bandwidth of 0.8 nm. The pulse train was modulated at 10 Gbit/s with a 2^{31}-1 pseudo-random binary sequence (PRBS) in a $LiNbO_3$ chirp-free Mach-Zehnder modulator (MZ), before being amplified, filtered, and sent to a re-circulating loop consisting of 3 identical spans made of an EDFA, 25 km of SMF and 25 km of IDF. For each span, a variable optical attenuator enabled to optimise the input power, which could be monitored using a power meter (PWM) after the signal was tapped in an asymmetric coupler and the ASE noise filtered by an optical band-pass filter. An extra

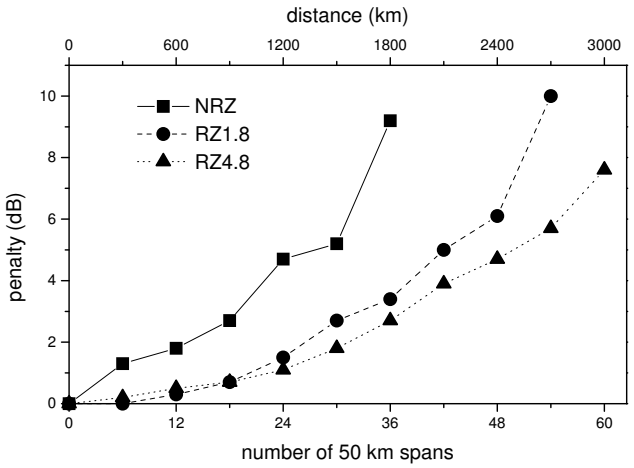

Figure 7.12 Penalty as a function of distance for 1.8 and 4.8 ps RZ as well as NRZ transmission through a SMF+IDF×1 link at 10 Gbit/s.

EDFA was inserted after the third span in order to compensate for the loss in the loop switch. After the desired number of round-trips, the signal was tapped from the loop by a 10 dB coupler and input into a receiver consisting of a double stage pre-amplifier, a 1.3 nm optical band-pass filter (OBF), a lightwave converter and a clock recovery circuit. The receiver exhibited a back to back sensitivity of -35.5 dBm for the 4.8 ps RZ pulses against -34.8 dBm for NRZ modulation. In case NRZ modulation was investigated, the MLFRL was simply replaced by a CW external cavity laser.

7.4.2 Short pulse RZ transmission at 10 Gbit/s

The power penalty at a BER of 1.0×10^{-9} was measured as a function of the transmitted distance (SMF+IDF length) for the two RZ pulse widths and for NRZ and is represented in Figure 7.12. The power at the input of each fibre span was optimised for the longest transmission distance and was kept to this value when the number of round-trips was decreased, corresponding to an average power of 2.5 dBm for the 4.8 ps pulses. The performance of the NRZ modulated signal is consistently worse than those of the RZ signals with both pulse widths. Error free transmission could be obtained up to only 1800 km with NRZ (although with 9 dB power penalty) against 3000 km for 4.8 ps RZ. For a 3 dB power penalty criterion, the transmission distance can be doubled by using 4.8 ps RZ (1880 km) as compared to NRZ modulation (940 km). Figure 7.12 also suggests the existence of an optimum duty cycle for RZ transmission as performances obtained with

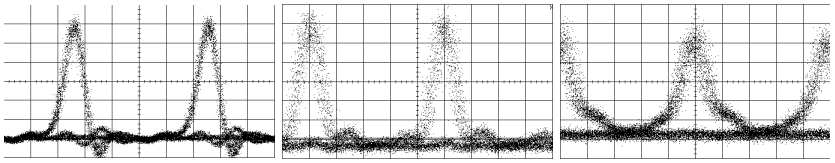

Figure 7.13 Eye diagrams of the 10 Gbit/s signal with 4.8 ps pulses at the transmitter output (left), the 10 Gbit/s signal with 4.8 ps pulses after 12 spans (centre) and the 10 Gbit/s signal with 1.8 ps pulses after 12 spans (right). Horizontal scale: 20 ps per division.

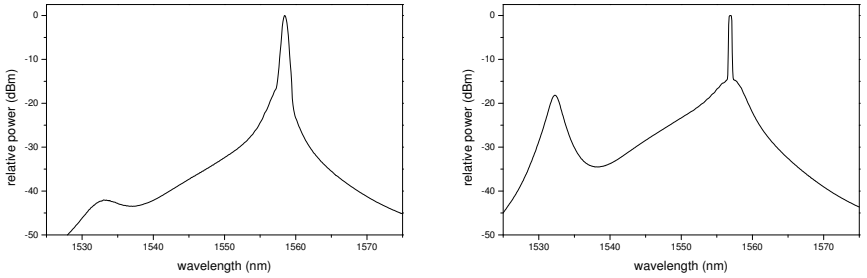

Figure 7.14 Normalised spectra (0.5 nm resolution bandwidth) corresponding to 3000 km and 1800 km transmission for 4.8 ps RZ (left) and NRZ (right), respectively.

1.8 ps FWHM are deteriorated compared to 4.8 ps.

Eye diagrams measured with a 30 GHz sampling oscilloscope are shown in Figure 7.13. After 12 spans (corresponding to 600 km transmission distance), the shape of the eye diagram obtained with 4.8 ps pulses is well preserved compared to the back-to-back case, whereas the pulses start becoming distorted when their width is reduced down to 1.8 ps. The residual dispersion of the link (estimated to 1.1 ps/nm at the transmitter wavelength of 1558.5 nm) is believed to be the cause for this behaviour, the pulses of the shorter duration being naturally more severely affected. In this particular case of 12 spans, the 1.8 ps eye is still open though, resulting in no penalty degradation over the 4.8 ps pulses.

The spectra recorded at the output of the link after transmission over 2700 km for 4.8 ps RZ and 1800 km for NRZ (corresponding to the maximum distance allowing a BER better than 1.0×10^{-9}) are shown in Figure 7.14. Although both spectra correspond to optimum power levels at the spans inputs (and therefore best trade-off between reduced signal-to-noise ratio and enhanced self-phase modulation), it is clearly seen that the

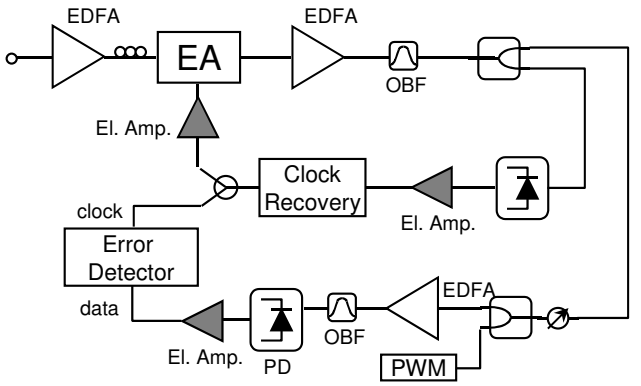

Figure 7.15 Receiver for 40 Gbit/s short-pulse transmission over SMF+IDF dispersion map.

saturation behaviour of the EDFAs is different in both cases because of the smaller optimum average input power required for NRZ. Due to their broader spectra, the RZ pulses will disperse faster, resulting in reduced influence of self-phase modulation and allowing for a higher span input power than for the NRZ signal. The lower optimum span input power for NRZ will in turn reduce the input power to the following EDFA in the link. This effect will accumulate over all the EDFAs in the chain, which will operate in an unsaturated regime as indicated by the spectrum shown in Figure 7.14.

7.4.3 40 Gbit/s transmission over a SMF + IDF map

A 40 Gbit/s OTDM transmission experiment was also performed with the same dispersion map using 1.8 ps pulses. A two-stage fibre delay time multiplexer was inserted directly after the MZ modulator in the transmitter while the receiver was modified as shown in Figure 7.15. De-multiplexing from 40 to 10 Gbit/s was performed using an electro-absorption (EA) modulator. The 10 GHz signal used to drive the EA in order to generate the proper switching window was obtained via a feedback loop from a 10 GHz clock recovery circuit following signal detection in a photodiode (PD). The whole process initiated on the spurious 10 GHz tone present in the electrical spectrum of the 40 Gbit/s signal due to imperfect multiplexing. A 1 dB penalty for the multiplexing and de-multiplexing operations was measured back-to-back as compared to the 10 Gbit/s configuration described earlier. The eye diagrams of the 40 Gbit/s time multiplexed signal at the transmitter output and of one of the de-multiplexed channels at 10 Gbit/s are

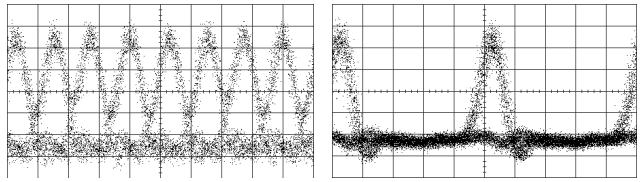

Figure 7.16 Eye diagrams of the 40 Gbit/s signal at the transmitter output and of one de-multiplexed 10 Gbit/s channel. Horizontal scale: 20 ps per division.

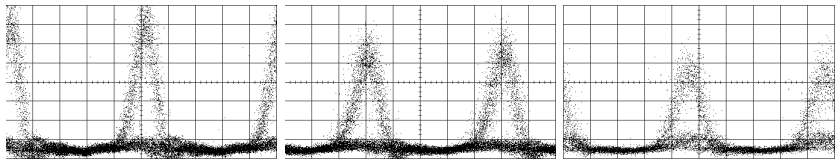

Figure 7.17 Eye diagrams of a 10 Gbit/s channel de-multiplexed from the 40 Gbit/s signal after 3, 6 and 12 SMF+IDF×1 dispersion compensated spans. Horizontal scale: 20 ps per division.

shown in Figure 7.16. The optical bandpass filter following the additional EDFA made necessary in the receiver in order to compensate for the insertion loss of the EA is believed to induce some broadening of the pulses prior to detection.

Polarisation effects in the re-circulating loop acting together with the polarisation sensitive de-multiplexing scheme were found to be the main limiting factor in this experiment, resulting in unstable BER measurements. Nevertheless, eye diagrams could be recorded after up to 12 dispersion compensated spans, corresponding to 600 km transmission distance, as shown in Figure 7.17. The eyes, measured with a 30 GHz photodetector, are clearly open prior to optical and electrical filtering at the receiver. Due to non-ideal multiplexing, the quality of the four multiplexed 10 Gbit/s channels might differ. The measured eye diagrams actually correspond to an average of the four 10 Gbit/s channels and their quality is limited by that of the channel exhibiting the poorest performance. This experiment was the first attempt to use our re-circulating loop test-bed at 40 Gbit/s. An improved clock-recovery scheme compatible with the 40 Gbit/s OTDM signal, or alternatively simultaneous transmission of a 10 GHz clock signal through the same link, but at a different wavelength, as demonstrated in more recent experiments [35], would have made a better evaluation of the performance of the system possible. Nevertheless, the feasibility of 40 Gbit/s OTDM transmission over up to 600 km of a dispersion map made of SMF+IDF×1

could be demonstrated.

In conclusion, using a dispersion map made of SMF and novel IDF×1, we have demonstrated 10 Gbit/s transmission of 4.8 and 1.8 ps pulses over 3000 and 2700 km respectively, as compared to only 1800 km for conventional NRZ modulation. Transmission of a 40 Gbit/s OTDM signal based on 1.8 ps pulses over up to 600 km of the same dispersion map has also been shown to be feasible.

7.5 Summary of Chapter 7

The properties of novel dispersion compensating fibres designed to compensate for the dispersion and dispersion slope of standard single mode fibre have been investigated numerically and experimentally in a system context.

A numerical optimisation of four different dispersion maps making use of novel IDF or WBDCF has been conducted, showing that for short spans (50 km) a combination of IDF and SMF in a 1 to 1 length ratio (IDF×1) performs the best for single channel NRZ transmission at 10 Gbit/s. In contrast, such a map has been shown to be limited by cross-phase modulation in WDM systems with narrow (35 GHz) channel spacing, where the use of IDF×2 or 3 should be preferred. Systems making use of broad (50 ps) RZ pulses are limited by the proximity between the repeaters and the DCF, resulting in a more severe impact of self-phase modulation in the DCF than when NRZ modulation is used. This is especially true for spans based on IDF×1. As a consequence IDF×2 or 3 should also be preferred for broad RZ pulses transmission at 10 Gbit/s.

The benefits of using IDF×1 over WBDCF has been demonstrated experimentally for a 50 km dispersion map using the chirped RZ modulation format at 10 Gbit/s. Using one of the first prototype IDF×1, we have shown that more than 45 spans could be cascaded for a power penalty less than that obtained with 40 spans based on SMF+WBDCF. Error free transmission over 50 spans made of SMF+IDF×1, corresponding to a distance of 2500 km, has been achieved with less than 5.5 dB power penalty.

Finally, a comparison of the transmission performance of NRZ and short pulse RZ modulation at 10 Gbit/s has been performed over a map made of 50 km spans of SMF and IDF×1. The short (1.8 and 4.8 ps) RZ pulses have been shown to be more resilient to self-phase modulation than the NRZ signal, due to the fact that they disperse extremely fast in the transmission fibre, enabling to increase the span input power, which in turn results in a better saturation behaviour of the EDFAs and higher signal-to-noise ratio. For a 3 dB power penalty limit, the transmission distance could be doubled

when using 4.8 ps RZ pulses as compared to conventional NRZ modulation. Transmission over up to 3000 km was demonstrated using the short 4.8 ps RZ pulses.

7.6 References to Chapter 7

[1] L. Grüner-Nielsen, S. N. Knudsen, B. Edvold, T. Veng, D. Magnussen, C. C. Larsen, and H. Damsgaard, "Dispersion compensating fibers", *Optical Fiber Technology*, vol. 6, pp. 164–180, 2000.

[2] R. W. Tkach, A. R. Chraplyvy, F. Forghieri, A. H. Gnauck, and R. M. Derosier, "Four-photon mixing and high-speed WDM systems", *Journal of Lightwave Technology*, vol. 13, no. 5, pp. 841–849, 1995.

[3] S. Bigo, G. Bellotti, and M. W. Chbat, "Investigation of cross-phase modulation limitation over various types of fiber infrastructures", *IEEE Photonics Technology Letters*, vol. 11, no. 5, pp. 605–607, 1999.

[4] M. Eiselt, L. D. Garrett, and R. W. Tkach, "Experimental comparison of WDM system capacity in conventional and nonzero dispersion shifted fiber", *IEEE Photonics Technology Letters*, vol. 11, no. 2, pp. 281–283, 1999.

[5] K. Mukasa, Y. Akasaka, Y. Suzuki, and T. Kamiya, "Novel network fiber to manage dispersion at 1.55 μm with combination of 1.3 μm zero dispersion single mode fiber", in *Proceedings European Conference on Optical Communication, ECOC'97*, Edinburgh, Scotland, U.K., vol. 1, pp. 127–130, 1999.

[6] S. N. Knudsen and T. Veng, "Large effective area dispersion compensating fiber for cabled compensation of standard single mode fiber", in *Technical Digest Optical Fiber Communication Conference, OFC'00*, Baltimore, Maryland, U.S.A., paper TuG5, vol. 1, pp. 98–100, 2000.

[7] S. N. Knudsen, *Optimization of fibers used for dispersion compensation in WDM systems*. PhD thesis, COM, Technical University of Denmark, Kgs. Lyngby, Denmark, 2002.

[8] S. N. Knudsen, M. Ø. Pedersen, and L. Grüner-Nielsen, "Optimisation of dispersion compensating fibres for cabled long-haul applications", *Electronics Letters*, vol. 36, no. 25, pp. 2067–2068, 2000.

[9] K. Yonenaga, A. Matsuura, S. Kuwahara, M. Yoneyama, Y. Miyamoto, K. Hagimoto, and K. Noguchi, "Dispersion-compensation-free 40-Gbit/s × 4-channel WDM transmission experiment using zero-dispersion-flattened transmission line", in *Technical Digest Optical Fiber Communication Conference, OFC'98*, San Jose, California, U.S.A., post-deadline paper PD20, 1998.

[10] Y. Miyamoto, Y. Yonenaga, S. Kuwahara, M. Tomizawa, A. Hirano, H. Toba, K. Murata, Y. Tada, Y. Umeda, and H. Miyazawa, "1.2 Tbit/s (30 × 42.7 Gbit/s ETDM channel) WDM transmission over 3 × 125 km with forward error correction", *Electronics Letters*, vol. 36, no. 9, pp. 812–813, 2000.

[11] C. R. Davidson, C. J. Chen, M. Nissov, A. Pilipetskii, N. Ramanujam, H. D. Kidorf, B. Pedersen, M. A. Mills, C. Lin, M. I. Hayee, J. X. Cai, A. B. Puc, P. C. Corbett, R. Menges, H. Li, A. Elyamani, C. Rivers, and N. S. Bergano, "1800 Gb/s transmission of one hundred and eighty 10 Gb/s WDM channels over 7000 km using the full EDFA C-band", in *Technical Digest Optical Fiber Communication Conference, OFC'00*, Baltimore, Maryland, U.S.A., post-deadline paper PD25, 2000.

[12] J.-X. Cai, M. Nissov, A. N. Pilipetskii, A. J. Lucero, C. R. Davidson, D. Foursa, H. Kidorf, M. A. Mills, R. Menges, P. C. Corbett, D. Sutton, and N. S. Bergano, "2.4 Tb/s (120 × 20 Gb/s) transmission over transoceanic distance using optimum FEC overhead and 48% spectral efficiency", in *Technical Digest Optical Fiber Communication Conference, OFC'01*, Anaheim, California, U.S.A., post-deadline paper PD20, 2001.

[13] D. G. Foursa, C. R. Davidson, M. Nissov, M. A. Mills, L. Xu, J. X. Cai, A. N. Pilipetskii, Y. Cai, C. Breverman, R. R. Cordell, T. J. Carvelli, P. C. Corbett, H. D. Kidorf, and N. S. Bergano, "2.56 Tb/s (25 × 10 Gb/s) transmission over 11000 km using hybrid Raman/EDFAs with 80 nm of continuous bandwidth", in *Technical Digest Optical Fiber Communication Conference, OFC'02*, Anaheim, California, U.S.A., post-deadline paper FC3, 2002.

[14] T. Yamamoto, E. Yoshida, K. R. Tamura, K. Yonenaga, and M. Nakazawa, "640-Gbit/s optical TDM transmission over 92 km through a dispersion-managed fiber consisting of single-mode fiber and "reverse dispersion fiber"", *IEEE Photonics Technology Letters*, vol. 12, no. 3, pp. 353–355, 2000.

[15] ITU-T Recommendation G.655, *Characteristics of a non-zero dispersion-shifted single-mode optical fibre cable*, International Telecommunications Union, Geneva, Switzerland, 2000.

[16] R. Ludwig, U. Feiste, S. Diez, C. Schubert, C. Schmidt, H. J. Ehrke, and H. G. Weber, "Unrepeatered 160 Gbit/s RZ single-channel transmission over 160 km of standard fibre at 1.55 μm with hybrid MZI optical demultiplexer", *Electronics Letters*, vol. 36, no. 16, pp. 1405–1406, 2000.

[17] G. Raybon, B. Mikkelsen, R.-J. Essiambre, A. J. Stentz, T. N. Nielsen, D. W. Peckham, L. Hsu, L. Gruner-Nielsen, K. Dreyer, and J. E. Johnson, "320 Gbit/s single-channel pseudo-linear transmission over 200 km of nonzero-dispersion fiber", in *Technical Digest Optical Fiber Communication Conference, OFC'00*, Baltimore, Maryland, U.S.A., post-deadline paper PD29, 2000.

[18] L. Grüner-Nielsen, S. N. Knudsen, T. Veng, B. Edvold, and C. C. Larsen, "Design and manufacture of dispersion compensating fibre for simultaneous compensation of dispersion and dispersion slope", in *Technical Digest Optical Fiber Communication Conference, OFC'99*, San Diego, California, U.S.A., paper WM13, vol. 2, pp. 232–234, 1999.

[19] S. N. Knudsen, D. W. Peckham, M. Ø. Pedersen, D. Philen, T. Veng, L. R. Pritchett, and L. Grüner-Nielsen, "New dispersion-slope managed fiber pairs for undersea fiber optic transmission systems", in *Proceedings Suboptic'01*, 2001.

[20] L. Grüner-Nielsen and S. N. Knudsen, "Cabling of dispersion compensating fibres", in *Proceedings International Wire & Cable Symposium 1999*, pp. 483–487, 1999.

[21] T. Tsuritani, K. Tanaka, N. Edagawa, and M. Suzuki, "Performance comparison between SCDCF-based system and RDF-based system in slope-compensating transoceanic WDM transmission", *Electronics Letters*, vol. 36, no. 5, pp. 447–448, 2000.

[22] K. Nakajima and M. Ohashi, "A study on the relationship between DWDM transmission performance and chromatic dispersion", *IEEE Photonics Technology Letters*, vol. 14, no. 9, pp. 1276–1278, 2002.

[23] M. N. Islam, "Raman amplifiers for telecommunications", *IEEE Journal of Selected Topics in Quantum Electronics*, vol. 8, no. 3, pp. 548–559, 2002.

[24] S. Namiki and Y. Emori, "Ultrabroad-Raman amplifiers pumped and gain-equalized by wavelength-division-multiplexed high-power laser diodes", *IEEE Journal of Selected Topics in Quantum Electronics*, vol. 7, no. 1, pp. 3–16, 2001.

[25] R. Hainberger, J. Kumasako, K. Nakamura, T. Terahara, H. Onaka, and T. Hoshida, "Optimum span configuration of Raman-amplified dispersion-managed fibers", in *Technical Digest Optical Fiber Communication Conference, OFC'01*, Anaheim, California, U.S.A., paper MI5, 2001.

[26] J.-C. Antona, S. Bigo, and J.-P. Faure, "Nonlinear cumulated phase as a criterion to assess performance of terrestrial WDM systems", in *Technical Digest Optical Fiber Communication Conference, OFC'02*, Anaheim, California, U.S.A., paper WX5, pp. 365–367, 2002.

[27] C. J. Anderson and J. A. Lyle, "Technique for evaluating system performance using Q in numerical simulations exhibiting intersymbol interference", *Electronics Letters*, vol. 30, no. 1, pp. 71–72, 1994.

[28] M. Shtaif and M. Eiselt, "Analysis of intensity interference caused by cross-phase modulation in dispersive optical fibers", *IEEE Photonics Technology Letters*, vol. 10, no. 7, pp. 979–981, 1998.

[29] D. Marcuse, A. R. Chraplyvy, and R. W. Tkach, "Effect of fiber nonlinearity on long-distance transmission", *Journal of Lightwave Technology*, vol. 9, no. 1, pp. 121–128, 1991.

[30] F. Liu, X. Zheng, C. Peucheret, S. N. Knudsen, R. J. S. Pedersen, and P. Jeppesen, "Chirped return-to-zero source used in 8×10 Gbit/s transmission over 2000 km of standard singlemode fibre", *Electronics Letters*, vol. 36, no. 16, pp. 1399–1400, 2000.

[31] J.-P. Elbers, A. Färbert, C. Scheerer, C. Glingener, and G. Fischer, "Reduced model to describe SPM-limited fiber transmission in dispersion-managed lightwave systems", *IEEE Journal of Selected Topics in Quantum Electronics*, vol. 6, no. 2, pp. 276–281, 2000.

[32] C. R. Giles and E. Desurvire, "Propagation of signal and noise in concatenated Erbium-doped fiber optical amplifiers", *Journal of Lightwave Technology*, vol. 9, no. 2, pp. 147–154, 1991.

[33] S.-G. Park, A. H. Gnauck, J. M. Wiesenfeld, and L. D. Garrett, "40-Gb/s transmission over multiple 120-km spans of conventional single-mode fiber using highly dispersed pulses", *IEEE Photonics Technology Letters*, vol. 12, no. 8, pp. 1085–1087, 2000.

[34] B. Mikkelsen, G. Raybon, R.-J. Essiambre, A. J. Stentz, T. N. Nielsen, D. W. Peckham, L. Hsu, L. Gruner-Nielsen, K. Dreyer, and J. E. Johnson, "320-Gb/s single-channel pseudolinear transmission over 200 km of nonzero-dispersion fiber", *IEEE Photonics Technology Letters*, vol. 12, no. 10, pp. 1400–1402, 2000.

[35] M. Girimondo, "Study of 40 Gbit/s transmission in optical fiber communication systems", Master thesis, COM, Technical University of Denmark, Kgs. Lyngby, Denmark, 2002.

Chapter 8

Conclusion

All-optical networks are becoming a reality, driven by recurrent needs for capacity mostly triggered by the increase in data traffic, and by the necessity to remove electronic bottlenecks. Large scale transparent networks are foreseen. However, the analogue nature of transmission through an all-optical network means that signal degradations will accumulate along any given path, unless some form of regeneration is applied. Consequently, the extension of so called "transparent domains" where no regeneration will take place needs to be defined.

Network planning and dimensioning, elaboration of routing algorithms, network management and path restoration, depend all on the knowledge of the accumulated signal degradation that can be tolerated for a given signal quality at the end node. Two main forms of signal degradation are encountered: those induced by the non-ideal transfer functions of the filtering devices to be found in optical network elements such as optical cross-connects (OXC) and optical add-drop multiplexers (OADM), and those induced by group-velocity dispersion, optical fibre non-linearities, amplifier noise and their interaction in the optical fibre link.

Design rules are therefore required, which would hide the physical layer complexity from the network operator. A modular approach has been suggested [1, 2, 3]. It relies on the knowledge of the maximum number of "normalised transmission sections" and optical network elements that can be cascaded for an acceptable signal quality, and on the definition of appropriate tolerance margins.

The present work contributes to this approach by examining the influence of dispersion in optical network elements, and by optimising the dispersion management of optical fibre links based on standard single mode fibre (SMF).

8.1 Summary

The influence of the phase transfer function (dispersion) of fibre optics components will become increasingly important due to the systems upgrades towards higher bit rates, the larger number of optical network elements expected to be cascaded in a link, and the increased spectral efficiency resulting in the need for narrower bandwidth - and potentially more dispersive - devices. The applicability of various techniques enabling the experimental determination of the phase response of fibre optics filters has been discussed in depth. The use of Kramers-Kronig like relations has been shown to be of limited practical interest due to difficulties in determining whether real filters of a given type satisfy the minimum-phase criterion, and to computation issues. A general formulation of amplitude modulation techniques has been presented, based on which the validity of the now commonly used phase-shift technique could be discussed, highlighting the influence of the choice of the modulation frequency for accurate group-delay measurements. The phase response of a broad range of fibre optics components has been characterised experimentally. Those include fibre Fabry-Pérot filters, fibre chirped gratings for dispersion compensation, fibre Bragg gratings with uniform, Gaussian, sinc or asymmetric apodisation profiles, fibre grating Mach-Zehnder optical add-drop multiplexers, multi-layer interference demultiplexers, tunable thin-film filters and arrayed waveguide grating routers. A novel measurement technique (the so-called "RF modulation" or "dispersion-offset" method), which enables the direct determination of the dispersion in the pass-band of optical filters, has been described and implemented. The choice of a particular filter technology for a given application should therefore depend, not only on the on the amplitude response (pass-band shape and cross-talk), but also on the amount of dispersion that can be tolerated for an allowed detuning. This has been investigated further by examining two technologies, namely fibre gratings and phased-array multiplexers, in a system context.

The effect of dispersion in fibre grating components has been studied at 10 Gbit/s. The influence of the apodisation profile on dispersion-induced penalty has been investigated numerically when the channel spacing in a WDM system is reduced from 100 to 25 GHz. The effect of dispersion on the allowable signal detuning with respect to the grating centre frequency has been shown to become significant for channel spacings smaller than 50 GHz. Among "classic" apodisation functions, Blackman apodisation should be preferred due to its larger detuning tolerance and good cross-talk properties. The relative detuning tolerance of Gaussian apodised gratings designed for 100 and 50 GHz channel spacings has been studied ex-

perimentally. Dispersion has been identified as the main source of penalty for the narrower bandwidth device, limiting its cascadability to a maximum of five filters. Beyond the intrinsic dispersive properties of Gaussian apodised gratings, imperfections in the writing process due to the conventional double exposure technique are also believed to contribute to the observed system impairments. The use of reduced bandwidth modulation formats such as optical duobinary has been shown to be an effective way to improve the detuning tolerance of Gaussian apodised gratings. Alternatively, novel asymmetric apodisation functions with multiple phase-shifts have been used to demonstrate reduced dispersion in the pass-band, resulting in large detuning tolerances for non return-to-zero (NRZ), return-to-zero (RZ), carrier-suppressed return-to-zero (CS-RZ), upper and lower side-band return-to-zero (USB-RZ and LSB-RZ) modulation formats at 10 Gbit/s.

Conventional phased-array (PHASAR) devices can be shown to be inherently dispersion-less, apart from phase and amplitude errors introduced in the fabrication process, but exhibit a Gaussian-shaped pass-band resulting in a poor cascadability behaviour. Squaring the pass-band might, however, result in unwanted dispersion. The system implications of two PHASAR pass-band flattening techniques have been compared numerically in the context of a high spectral efficiency Terabit metropolitan ring network carrying 40 Gbit/s channels. The simulation results indicate that a PHASAR whose pass-band has been flattened with a parabolic taper input should be preferred over a design based on an input multi-mode interference (MMI) coupler. A full-width half-maximum bandwidth of 78 GHz has been shown to result in less than 1 dB power penalty after eight cascaded multiplexers, corresponding to four add-drop nodes, while still allowing for a 20 GHz detuning tolerance after four nodes. The dispersion of the pass-band flattened PHASAR has also been shown to account for a significant reduction of the device usable bandwidth.

"Normalised transmission sections" based on standard single mode fibres and dispersion compensating fibres (DCF) have been introduced and optimised with respect to the position of the DCF, degree of compensation, and power levels at the SMF and DCF inputs. The study has been conducted numerically for NRZ modulation at 10 Gbit/s. For 80 km spans typical of terrestrial networks, post-compensation has been found to perform better than pre-compensation at the expense of more stringent parameters tolerance. The existence of an optimum compensation ratio equal to 98% has been demonstrated for post-compensation, while little influence of the compensation ratio and power levels has been observed for pre-

compensation, which makes this scheme more attractive when large tolerances are required. When passive pre-distortion is added at the transmitter, both schemes can be significantly improved and perform equally well. The feasibility of the normalised section approach has been demonstrated experimentally for single channel and an eight channel WDM system with 200 GHz channel spacing. The benefit of adding passive pre-distortion at the transmitter and the influence of the compensation ratio have been confirmed experimentally. Pre- and post-compensation with or without pre-distortion have been compared experimentally for chirped return-to-zero (CRZ) transmission at 10 Gbit/s. Unless pre-distortion is used, pre-compensation was found to perform better than post-compensation. The addition of pre-distortion has been shown to result in a 40% increase in transmission distance for a 3 dB power penalty when used in conjunction with pre-compensation. Therefore, based on the experimental results, transparent domains with a diameter of the order of 1000 km (for a maximum penalty of 3 dB) should be feasible after optimisation of the dispersion management.

The potential of the newest generation of DCFs to compensate for the dispersion slope of SMF has been demonstrated experimentally. In particular, 10 Gbit/s NRZ transmission in the L-band (at 1597 nm) has been reported over more than 1000 km with a dispersion map optimised in the C-band (around 1550 nm).

Novel dispersion compensating fibres enabling for the cabled compensation of the dispersion and dispersion slope of SMF (the so-called inverse dispersion fibres, or IDF$\times n$ where n is the SMF to DCF length ratio) have been introduced and their performance compared numerically for single channel RZ or NRZ transmission, as well as WDM NRZ transmission over 50 km repeatered spans. IDF$\times$1 has been shown to enable the longest transmission distance in the single channel NRZ case, whereas its proximity to the repeaters results in enhanced self-phase modulation (SPM) for RZ modulation with 50% duty cycle. Cross-phase modulation has been shown to result in the poorer performance of IDF$\times$1 in WDM systems where the use of IDF$\times$2 or 3 should be preferred. The first comparison of transmission over a SMF+DCF and SMF+IDF$\times$1 maps has been reported for CRZ modulation at 10 Gbit/s, demonstrating the potential of the new IDF. Finally, a comparison between NRZ and short pulse (1.8 and 3.8 ps) RZ transmission has been performed at 10 Gbit/s over a 50 km SMF+IDF$\times$1 map. The 3.8 ps RZ pulses have been found to enable a doubled transmission distance compared to NRZ for a 3 dB power penalty criterion. This significant improvement has been attributed to the fact that short pulses

disperse faster in the transmission fibre, offering better resilience to SPM, which in turns enable their power to be increased in order to guarantee a better optical signal-to-noise ratio.

We have therefore examined high bit-rate (10 and 40 Gbit/s) signal degradation mechanisms induced by network elements, with an emphasis on dispersion in wavelength selection devices, as well as group-velocity dispersion, optical fibre non-linearities and their intricate interaction in transmission links based on standard single-mode fibre and dispersion compensating fibre (either conventional DCF or IDF). The knowledge gained from these studies is expected to ease the design of future high-capacity transparent optical networks by providing a better understanding of some of the basic physical layer limitations, and by enabling choices between competing technologies. However, some additional investigations are required before the modular approach advocated in this thesis can be practically implemented in network design and management tools.

8.2 Future work

So far, the effects of filtering and signal distortion in optical fibre links have been considered independently. However, some interaction between those two categories of signal degradation mechanisms are expected. For instance, spectral broadening induced by self-phase modulation in the transmission fibre is foreseen to affect the penalty and the consecutive detuning tolerance when the transmitted signal reaches a network element. This will be particularly sensitive in high spectral efficiency systems.

The cascadability of network elements has been studied by assuming identical and perfectly aligned transfer functions, either in the simulations or in the re-circulating loop experiments. Some differences between real transfer functions of fabricated components, as well as statistical detunings, should also be taken into account. Furthermore, the influence of optical cross-talk, which has been deliberately ignored in the present work, should be considered, as it will also result in limitations of the dimensions of transparent domains. Some worst-case scenarios should be elaborated for hybrid links making use of different fibre types and/or different span lengths, and optical paths where network elements based on different technologies would be encountered (e.g. fibre grating based OADM and arrayed waveguide grating based OXC). Polarisation effects have also been neglected in the present work.

The foreseen upgrade of the bit rate in the near future will also require some of the studies reported here to be conducted at 40 Gbit/s and above.

This will be necessary in order to take into account the reduced tolerance to group-velocity and polarisation mode dispersion, and the higher requirements in terms of optical signal-to-noise ratio (OSNR) due to the larger signal bandwidths. Two technologies have been introduced to enable an increase of the OSNR at the receiver, while allowing for a higher SPM tolerance, namely highly-dispersed pulses (also known as pseudo-linear) transmission, and distributed Raman amplification. In this thesis, the concept of highly dispersed transmission has been demonstrated to be beneficial for 10 Gbit/s systems making use of SMF and IDF×1. However, pseudo-linear systems at 40 Gbit/s and above have been shown to be prone to new manifestations of the Kerr non-linearity such as intra-channel four-wave mixing (IFWM) and intra-channel cross-phase modulation (IXPM)[4, 5]. Distributed Raman amplification has also attracted increasing interest over the past few years [6], introducing new design trade-offs in the dispersion managed link. A small effective area fibre is desirable in order to improve the Raman gain efficiency, which will in turn increase the signal path average power in the fibre, resulting in a potentially higher influence of non-linearities such as self- and cross-phase modulation. Consequently, the dispersion management scheme should be optimised by taking those new effects into account, which might lead to different conclusions regarding the use of DCF and IDF×n at high bit-rates.

A strong interest in modulation formats has also been recently observed. New modulation formats such as optical duobinary [7], carrier-suppressed return-to-zero [8], optical single side-band [9] and differential phase-shift keying [10, 11] have been introduced mostly because of their transmission properties in terms of tolerance to group-velocity dispersion and/or resilience to optical fibre non-linearities, but also because of the fact that some of them might allow for an increased spectral efficiency. The focus of most experimental and theoretical studies reported so far has been on the transmission aspects. However, the filtering tolerances of all those new modulation formats also need to be assessed. Some preliminary steps in this direction have been reported in this thesis with the experimental comparison of the detuning tolerance of five modulation formats through a low dispersion fibre Bragg grating.

In a more distant future, non-linear limitations in the transmission link might be alleviated by the use of a new class of optical fibres, the so-called photonic crystal fibres (PCF), offering additional design degrees of freedom compared to conventional step index fibres. An attractive property is the possibility to increase the fibre effective area while conserving its single-mode properties [12]. Pioneering work has been initiated in this new

exciting field [13, 14].

A number of those research goals have been, or are being pursued within the "Systems Competence Area" at COM, ensuring the continuation of the work presented in this Ph.D. thesis.

8.3 References to Chapter 8

[1] N. Hanik, A. Gladisch, and G. Lehr, "An effective method to design transparent optical WDM-networks", in *Proceedings Conference on Networks and Optical Communication, NOC'98, Technology and Infrastructure*, Manchester, England, U.K., pp. 190–197, 1998.

[2] C. Caspar, R. Freund, N. Hanik, L. Molle, and C. Peucheret, "Using normalised sections for the design of all optical networks", in *New Trends in Optical Network Design and Modeling, IFIP TC6 Fourth Working Conference on Optical Network Design and Modeling, ONDM'00* (A. A. Stavdas, ed.), Athens, Greece, pp. 163–172, Kluwer Academic Publishers, 2001.

[3] N. Hanik, C. Caspar, F. Schmidt, R. Freund, L. Molle, and C. Peucheret, "Optimised design of transparent optical domains", in *Proceedings European Conference on Optical Communication, ECOC'00*, Munich, Germany, paper P3.5, vol. 3, pp. 195–197, 2000.

[4] R.-J. Essiambre, B. Mikkelsen, and G. Raybon, "Intra-channel cross-phase modulation and four-wave mixing in high-speed TDM systems", *Electronics Letters*, vol. 35, no. 18, pp. 1576–1578, 1999.

[5] M. J. Ablowitz and T. Hirooka, "Resonant intrachannel pulse interactions in dispersion-managed transmission systems", *IEEE Journal of Selected Topics in Quantum Electronics*, vol. 8, no. 3, pp. 603–615, 2002.

[6] K. Rottwitt and A. J. Stentz, "Raman amplification in lightwave communication systems", in *Optical fiber telecommunications IVA* (I. P. Kaminow and T. Li, eds.), San Diego, pp. 196–264, Academic Press, 2002, 2002.

[7] T. Ono and Y. Yano, "Key technologies for Terabit/s WDM systems with high spectral efficiency of over 1 bit/s/Hz", *IEEE Journal of Quantum Electronics*, vol. 34, no. 11, pp. 2080–2088, 1998.

[8] Y. Miyamoto, A. Hirano, K. Yonenaga, A. Sano, H. Toba, K. Murata, and O. Mitomi, "320 Gbit/s (8×40 Gbit/s WDM transmission over 367-km zero-dispersion-flattened line with 120-km repeater spacing using carrier-suppressed return-to-zero pulse format", in *Technical Digest Optical Amplifiers and their Applications, OAA'99*, Nara, Japan, post-deadline paper PdP4, pp. PdP4–1/4, 1999.

[9] M. Sieben, J. Conradi, and D. E. Dodds, "Optical single sideband transmission at 10 Gb/s using only electrical dispersion compensation", *Journal of Lightwave Technology*, vol. 17, no. 10, pp. 1742–1749, 1999.

[10] M. Rohde, C. Caspar, N. Heimes, M. Konitzer, E.-J. Bachus, and N. Hanik, "Robustness of DPSK direct detection transmission format in standard fibre WDM systems", *Electronics Letters*, vol. 36, no. 17, pp. 1483–1484, 2000.

[11] C. Rasmussen, S. Dey, F. Liu, J. Bennike, B. Mikkelsen, P. Mamyshev, M. Kimmit, K. Springer, D. Gapontsev, and V. Ivshin, "Transmission of 40×42.7 Gbit/s over 5200 km UltraWave fiber with terrestrial 100 km spans using turn-key ETDM transmitter and receiver", in *Proceedings European Conference on Optical Communication, ECOC'02*, Copenhagen, Denmark, post-deadline paper PD4.4, 2002.

[12] T. A. Birks, J. C. Knight, and P. St. J. Russell, "Endlessly single-mode photonic crystal fiber", *Optics Letters*, vol. 22, no. 13, pp. 961–963, 1997.

[13] B. Zsigri, C. Peucheret, M. D. Nielsen, and P. Jeppesen, "Transmission over 5.6 km large effective area and low loss (1.7 dB/km) photonic crystal fibre", *Electronics Letters*, vol. 39, no. 10, pp. 796–798, 2003.

[14] C. Peucheret, B. Zsigri, P. A. Andersen, K. S. Berg, A. Tersigni, P. Jeppesen, K. P. Hansen, and M. D. Nielsen, "Transmission over photonic crystal fiber at 40 Gbit/s using mid-span spectral inversion in a highly nonlinear photonic crystal fiber", in *Technical Digest Conference on Lasers and Electro-Optics, CLEO'03*, Baltimore, Maryland, U.S.A., post-deadline paper CThPDB4, 2003.

Appendices

Appendix A

Amplitude-phase relations in optical filters

A.1 The Kramers-Kronig relations

In this section, we follow [1] and provide a derivation of the Kramers-Kronig relations directly based on the causality assumption for a linear system. Alternative expressions of the amplitude-phase relations used in Chapter 2 are also derived.

Let $h(t)$ be the impulse response of a linear system. The principle of causality can be expressed as

$$h(t) = h(t)\, u(t) \tag{A.1}$$

where $u(t)$ is the unit step function (or Heaviside function) defined as

$$u(t) = \begin{cases} 1 & t \geq 0 \\ 0 & t < 0 \end{cases} \tag{A.2}$$

The Fourier transform[1] of the unit step function is

$$H(\omega) = \pi\delta(\omega) - \frac{j}{\omega} \tag{A.3}$$

[1] As throughout the thesis, we define the Fourier transform $H(\omega)$ of a function $h(t)$ as $H(\omega) = \int_{-\infty}^{+\infty} h(t)\, e^{-j\omega t} dt$. Therefore the expression of the Fourier transform of the unit step might differ from some tabulated functions which assume an alternative definition of the Fourier transform.

By taking the Fourier transform of Equation (A.1), we obtain[2]

$$H(\omega) = \frac{1}{2\pi} H(\omega) * \left(\pi\delta(\omega) - \frac{j}{\omega} \right) \tag{A.4}$$

from which we get

$$H(\omega) = \frac{1}{j\pi} P \int_{-\infty}^{+\infty} \frac{H(\Omega)}{\Omega - \omega} d\Omega \tag{A.5}$$

where P denotes the Cauchy principal value. From Equation (A.5) it can be seen that the real (respectively imaginary) part of the transfer function can be determined from the knowledge of its imaginary (respectively real) part[3]. The real and imaginary parts of $H(\omega)$ are said to constitute a Hilbert transform pair. If we decompose the transfer function $H(\omega)$ into its real and imaginary parts

$$H(\omega) = H_r(\omega) + jH_i(\omega) \tag{A.6}$$

we find the generalised Kramers-Kronig relations

$$H_r(\omega) = \frac{1}{\pi} P \int_{-\infty}^{+\infty} \frac{H_i(\Omega)}{\Omega - \omega} d\Omega \tag{A.7}$$

$$H_i(\omega) = -\frac{1}{\pi} P \int_{-\infty}^{+\infty} \frac{H_r(\Omega)}{\Omega - \omega} d\Omega \tag{A.8}$$

As the impulse response $h(t)$ is causal, we can write

$$H(\omega) = \int_0^{+\infty} h(t) e^{-j\omega t} dt \tag{A.9}$$

$$= \int_0^{+\infty} h(t) \cos(\omega t)\, dt - j \int_0^{+\infty} h(t) \sin(\omega t)\, dt \tag{A.10}$$

Moreover, the impulse response is real valued. Therefore we can deduce from equation (A.10) that H_r and H_i are even and odd functions of the frequency respectively.

[2]Where the 2π factor arises from our definition of the Fourier transform.

[3]A derivation of (A.5) usually involves the integration of $f(\Omega) = \frac{H(\Omega)}{\Omega - \omega}$ around a contour $\mathcal{C}$ where $H(\Omega)$ is analytical and avoiding the singularity at $\Omega = \omega$, as well as the use of Cauchy's theorem according to which $\oint_{\mathcal{C}} f(\Omega)\, d\Omega = 0$.

Starting from (A.7) and using the fact that H_i is an odd function of frequency, we obtain

$$H_r(\omega) = \frac{1}{\pi} P \int_0^{+\infty} \frac{H_i(\Omega)}{\Omega - \omega} d\Omega + \frac{1}{\pi} P \int_0^{+\infty} \frac{H_i(\Omega)}{\Omega + \omega} d\Omega \tag{A.11}$$

We can proceed in a similar way starting from (A.8) and using the even properties of H_r. This leads to alternative expressions for the Kramers-Kronig relations

$$H_r(\omega) = \frac{2}{\pi} P \int_0^{+\infty} \frac{\Omega H_i(\Omega)}{\Omega^2 - \omega^2} d\Omega \tag{A.12}$$

$$H_i(\omega) = -\frac{2\omega}{\pi} P \int_0^{+\infty} \frac{H_r(\Omega)}{\Omega^2 - \omega^2} d\Omega \tag{A.13}$$

The transfer function of an optical filter can be written

$$H(\omega) = |H(\omega)| e^{-j\phi(\omega)} \tag{A.14}$$

Taking the logarithm

$$\ln H(\omega) = \ln |H(\omega)| - j\phi(\omega) \tag{A.15}$$

If the filter is minimum-phase, the Kramers-Kronig relations can be applied to the real and imaginary parts of $\ln H(\omega)$, resulting in the following alternative expressions for the phase:

$$\boxed{\phi(\omega) = \frac{1}{\pi} P \int_{-\infty}^{+\infty} \frac{\ln |H(\Omega)|}{\Omega - \omega} d\Omega} \tag{A.16}$$

$$\boxed{\phi(\omega) = \frac{2\omega}{\pi} P \int_0^{+\infty} \frac{\ln |H(\Omega)|}{\Omega^2 - \omega^2} d\Omega} \tag{A.17}$$

Performing the change of variable $u = \ln \frac{\Omega}{\omega}$ in equation (A.17) leads to

$$\phi(\omega) = \frac{1}{\pi} \int_{-\infty}^{+\infty} \frac{\ln |H(\omega e^u)|}{\sinh u} du \tag{A.18}$$

Recalling that

$$\int \frac{1}{sinhu} du = -\ln\left(\coth \frac{u}{2}\right) + C \tag{A.19}$$

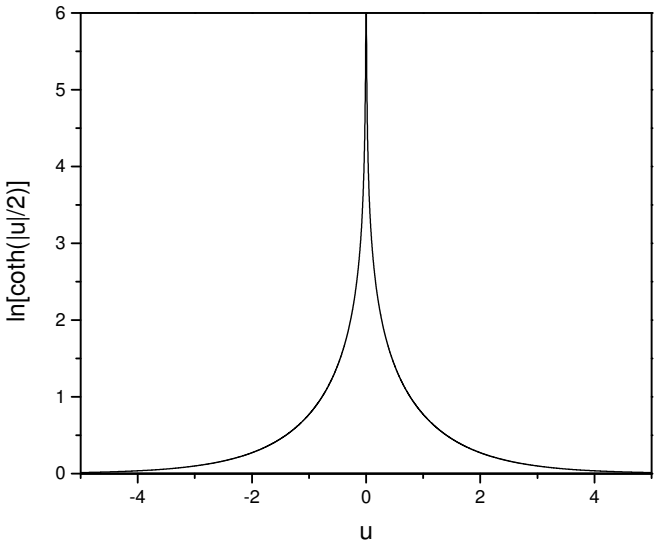

Figure A.1 Representation of the weighting factor $\ln\left(\coth\frac{|u|}{2}\right)$ in the phase integral of equation (A.20).

equation (A.18) can be integrated by parts (in the Cauchy principal value sense) leading to

$$\boxed{\phi(\omega) = \frac{1}{\pi}\int_{-\infty}^{+\infty}\frac{d}{du}\left[\ln|H(\omega e^{u})|\right]\ln\left(\coth\frac{|u|}{2}\right)du} \tag{A.20}$$

The factor $\ln\left(\coth\frac{|u|}{2}\right)$ is plotted in Fig. A.1. It can be seen that this factor peaks around $u = 0$ corresponding to $\Omega = \omega$ and exhibits a fast decrease when $|u|$ increases. As a consequence, the main contribution to the integral (A.20) arises from values in the vicinity of $u = 0$. Therefore, equation (A.20) states that, *for a minimum-phase filter*, the phase of the transfer function at the frequency ω depends mostly on the slope of the amplitude transfer function around ω. The practical implications of this observation are discussed in Section 2.3.

A.2 The minimum-phase condition

We have seen above that the condition for Kramers-Kronig relations to exist between the real and imaginary parts of a complex transfer function

$H(\omega)$ is that its impulse response $h(t)$ is causal, or equivalently that the associated Laplace transform $H_{\mathcal{L}}(s)$ is analytic in the right-hand plane. Therefore, the existence of Kramers-Kronig relations between the logarithm of the amplitude transfer function $\ln|H(\omega)|$ and its phase $\phi(\omega)$ requires the function $\ln H_{\mathcal{L}}(s)$ to be analytic in the right-hand plane. In particular, $H_{\mathcal{L}}(s)$ should not have any zero for $\mathrm{Re}(s) \geq 0$.

From a practical point of view, we are interested in knowing whether amplitude-phase relations can be applied to a certain type of optical filter. Modelling the filter response and checking for its analyticity in the right-hand plane could answer this question provided an analytical expression can be found for the complex transfer function over all complex frequencies. Nevertheless, this does not necessarily mean that a real imperfect transfer function of the same type of filter will also satisfy the analyticity condition or vice versa. Indeed, it has been reported that the effect of loss in arrayed waveguide grating filters can move the zeros of their complex transfer functions from the imaginary axis to the left-hand plane [2], making the real filters satisfy the minimum-phase condition. Note that in the case when its zeros in the right-hand plane are known, a transfer function can be decomposed as the product of a minimum phase function and an all-pass transfer function [3, 4], from which the phase response can be be calculated. Nevertheless, in most cases, the only information available about the filter whose phase needs to be characterised, is a measured amplitude response over a small part of the real frequency axis.

The Paley-Wiener criterion is often invoked in order to determine whether a given function is the Fourier transform of a causal function. Writing $H(\omega) = A(\omega)\, e^{-j\theta(\omega)}$, this theorem states [5] that a necessary and sufficient condition for a positive and square integrable function $A(\omega)$ to be the Fourier spectrum of a causal function is the convergence of the integral

$$\int_{-\infty}^{+\infty} \frac{|\ln A(\omega)|}{1+\omega^2} d\omega < \infty \tag{A.21}$$

The Paley-Wiener condition might prove difficult to apply when a measurement of the magnitude of the transfer function is the only available information about a filter.

A.3 Practical computation of the Kramers-Kronig relations

A number of techniques have been proposed in the literature in order to compute Kramers-Kronig relations. The main difficulty consists in per-

forming the numerical calculation of the principal value integrals (A.16) or (A.17), which are by nature difficult to handle. The use of efficient fast Fourier transform algorithms has been proposed in a method based on Fourier's allied integrals [6], and a method based on a digital signal processing technique has been recently applied to the case of fibre Bragg gratings [7]. An exhaustive list of references pertaining to the numerical calculation of Kramers-Kronig relations can be found in [8].

In this work, we have implemented a Kramers-Kronig relation calculation algorithm based on a non-linear frequency translation known as the Wiener-Lee transform [5, 9]. This algorithm, which is identical to the one described in [10], has been used to generate the results presented in Section 2.3.2. A short description of the algorithm is given below.

We consider the real and imaginary parts of the complex transfer function[4] $H(\omega)$ according to equation (A.6). The real variable ω can be expressed in terms of a new variable δ according to

$$\omega = -\tan\frac{\delta}{2} \tag{A.22}$$

where $\delta \in]-\pi, \pi[$. We can therefore write

$$H\left(-\tan\frac{\delta}{2}\right) = \rho(\delta) - j\chi(\delta) \tag{A.23}$$

where $\rho(\delta)$ and $\chi(\delta)$ are odd and even functions of δ respectively. These two functions can be expanded in Fourier series in the $]-\pi, \pi[$ interval, resulting in

$$\rho(\delta) = \sum_{n=0}^{+\infty} a_n \cos(n\delta) \tag{A.24}$$

$$\chi(\delta) = \sum_{n=1}^{+\infty} b_n \sin(n\delta) \tag{A.25}$$

It can be shown (see for instance [5] or [9]) that, if the impulse response $h(t)$ associated to the transfer function $H(\omega)$ is causal, then

$$b_n = -a_n \tag{A.26}$$

Thus, if we know either the real or imaginary part of a transfer function, we can perform the transformation (A.22), evaluate its Fourier coefficients,

[4] This algorithm will of course be applied to the function $\ln H(\omega)$ after having ensured that it is of the minimum-phase type.

deduce those of the other component according to (A.26) and inverse transform its Fourier series before reverting to the original angular frequency scale.

The method is therefore simple to implement when fast-Fourier transform routines are used. However, its major drawback lies in the non-linear nature of the frequency transformation (A.22), which requires a large number of samples in order to reach an adequate resolution when one attempts to transform a function known only over a small range of the real frequencies axis, as it is often the case for measured amplitude responses of optical filters.

A.4 References

[1] D. C. Hutchings, M. Sheik-Bahae, D. J. Hagan, and E. W. van Stryland, "Kramers-Krönig relations in nonlinear optics", *Optical and Quantum Electronics*, vol. 24, pp. 1–30, 1992.

[2] G. Lenz, B. J. Eggleton, C. R. Giles, C. K. Madsen, and R. E. Slusher, "Dispersive properties of optical filters for WDM systems", *IEEE Journal of Quantum Electronics*, vol. 34, no. 8, pp. 1390–1402, 1998.

[3] R. H. Kop, P. de Vries, R. Sprik, and A. Lagendijk, "Kramers-Kronig relations for an interferometer", *Optics Communications*, vol. 138, pp. 118–126, 1997.

[4] J. Skaar and H. E. Engan, "Phase reconstruction from reflectivity in fibre Bragg gratings", *Optics Letters*, vol. 24, no. 3, pp. 136–138, 1999.

[5] A. Papoulis, *The Fourier integral and its applications*, chapter 10, McGraw-Hill, New-York, 1962.

[6] B. Harbecke, "Application of Fourier's allied integrals to the Kramers-Kronig transformation of reflectance data", *Applied Physics A*, vol. 40, pp. 151–158, 1986.

[7] K. B. Rochford and S. D. Dyer, "Reconstruction of minimum-phase group delay from fibre Bragg grating transmittance/reflectance measurements", *Electronics Letters*, vol. 35, no. 10, 1999.

[8] F. W. King, "Efficient numerical approach to the evaluation of Kramers-Kronig transforms", *Journal of the Optical Society of America B*, vol. 19, no. 10, pp. 2427–2435, 2002.

[9] F. W. King, "Analysis of optical data by the conjugate Fourier-series approach", *Journal of the Optical Society of America*, vol. 68, no. 7, pp. 994–997, 1978.

[10] A. Carballar and M. A. Muriel, "Phase reconstruction from reflectivity in fiber Bragg gratings", *Journal of Lightwave Technology*, vol. 15, no. 8, pp. 1314–1322, 1997.

Appendix B

Properties and modelling of grating filters

B.1 Some properties of grating filters

A grating waveguide filter relies on perturbations of the core refractive index to couple energy between some forward propagating and backward propagating modes. In case only one forward and one backward propagating mode are considered, as it is the case in a single mode waveguide (ignoring coupling to cladding modes), the grating can be described by a scattering matrix between the forward and backward propagating modes. Following the notation of Figure B.1, the scattering relations between the forward and backward modes at the input ($z = 0$) and output ($z = L$) of

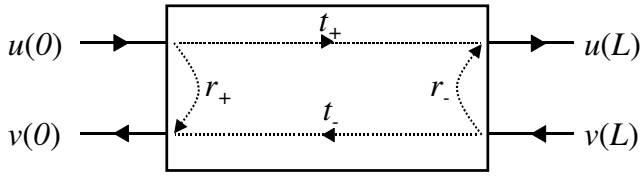

Figure B.1 Notations for the coupled-modes analysis and scattering matrix formalism used in Appendix B. $u(z)$ and $v(z)$ are the forward and backward propagating waves respectively.

the grating can be written

$$\begin{pmatrix} v(0) \\ u(L) \end{pmatrix} = \begin{pmatrix} S_{11} & S_{12} \\ S_{21} & S_{22} \end{pmatrix} \begin{pmatrix} u(0) \\ v(L) \end{pmatrix} \tag{B.1}$$

By considering the special cases where $v(L) = 0$ and $u(0) = 0$, the scattering matrix can be expressed simply in terms of the forward and backward transmission and reflection coefficients of the grating

$$S = \begin{pmatrix} r_+ & t_- \\ t_+ & r_- \end{pmatrix} \tag{B.2}$$

where r_+ and t_+ are the reflection and transmission coefficients, respectively, when a signal is input from the left-hand side of the grating, while r_- and t_- are the corresponding quantities when the right-hand side is used as the input. In the following, some useful relations between the transmission and reflection coefficients of a grating described by the scattering matrix formalism and coupled modes equations are derived. Some of those results are provided without derivation in [1]. They can also be derived using the more sophisticated resonance mode expansion formalism described in [2].

If the grating is assumed to be lossless, its scattering matrix is unitary and therefore

$$r_+ = -\frac{t_-}{t_+^*} r_-^* \tag{B.3}$$

The grating can also be described by the well-known coupled modes equations, which can take the following reduced form (see e.g. [2])

$$\frac{du}{dz} + j\delta u = q(z)\, v \tag{B.4}$$

$$\frac{dv}{dz} - j\delta v = q^*(z)\, u \tag{B.5}$$

where $\delta = (\omega - \omega_B)\, n_{eff}/c$ and where $q(z)$ is a coupling potential depending on the grating structure, i.e. on the spatial variations of the refractive index $n(z)$. It is straightforward to show that, if (u_1, v_1) and (u_2, v_2) are two sets of solutions of the coupled modes equations (B.4) and (B.5), then

$$\frac{d}{dz}(u_1 v_2 - u_2 v_1) = 0 \tag{B.6}$$

We apply this result to the following two particular solutions

$$\begin{aligned} v_1(L) &= 0 & u_2(0) &= 0 \\ v_1(0) &= r_+ u_1(0) & u_2(L) &= r_- v_2(L) \\ u_1(0) &= t_+ u_1(0) & v_2(0) &= t_- v_2(L) \end{aligned}$$

corresponding to input from the left and right-hand side of the grating, respectively. We obtain immediately

$$\boxed{t_+ = t_-} \tag{B.7}$$

We observe that, in order to derive equation (B.7), we have not made any assumption on the symmetry properties of the coupling potential $q(z)$. Therefore, we have shown based on coupled modes equations that the transmittivity of a grating is identical whichever side of the structure is used as an input. As a consequence, we can re-write equation (B.3) under the form

$$\boxed{r_+ = -\frac{t}{t^*} r_-^*} \tag{B.8}$$

where $t = t_+ = t_-$.

If we moreover express the complex reflection and transmission coefficients in terms of their amplitude and phase

$$r_\pm = \sqrt{R_\pm} e^{-j\phi_{r\pm}} \tag{B.9}$$

$$t = \sqrt{T} e^{-j\phi_t} \tag{B.10}$$

then we can derive relations between measurable quantities such as the reflectivities $R_\pm$ and the transmittivity T, as well as the dispersion in reflection $\mathbb{D}_{r_\pm}$ and in transmission $\mathbb{D}_t$.

$$R_+ = R_- \tag{B.11}$$

and

$$\mathbb{D}_t = \frac{1}{2}\left[\mathbb{D}_{r_+} + \mathbb{D}_{r_-}\right] \tag{B.12}$$

If moreover the grating is symmetric, then $r_+ = r_- = r$ and

$$\mathbb{D}_t = \mathbb{D}_r \tag{B.13}$$

From the unitary nature of the scattering matrix, we also obtain the power conservation equation

$$R_\pm + T = 1 \tag{B.14}$$

We have therefore derived the following properties used in this thesis:

1. The transmission coefficient of a grating does not depend on the input
2. For an ideal symmetric grating, the group delay is identical in transmission and in reflection
3. When using an asymmetric apodisation profile, the same power reflectivity can be obtained from both ends of the gratings, while the dispersion might be different.

B.2 Modelling of fibre gratings

Fibre gratings have been modelled using a conventional transfer matrix approach based on coupled-modes equations [3]. The grating is divided into M sections of length Δz where the period of the refractive index perturbation $\Lambda(z)$ is assumed to be constant. Based on coupled mode equations, the coupling coefficients between forward and backward travelling waves can be derived analytically, resulting in the following transfer matrix relation for each section

$$\begin{bmatrix} E^+(z+\Delta z) \\ E^-(z+\Delta z) \end{bmatrix} = \mathbb{T}(z) \begin{bmatrix} E^+(z) \\ E^-(z) \end{bmatrix} \tag{B.15}$$

where E^+ and E^- are the electric fields of the forward and backward propagating waves respectively. The transfer matrix of each uniform section of length Δz is

$$\mathbb{T}(z) = \begin{bmatrix} \left(\cosh(\gamma\Delta z) - j\frac{\Delta\beta}{\gamma}\sinh(\gamma\Delta z)\right) e^{-j\beta_B\Delta z} & -j\frac{\kappa}{\gamma}\sinh(\gamma\Delta z)\, e^{-j(\beta_B\Delta z+\varphi)} \\ +j\frac{\kappa}{\gamma}\sinh(\gamma\Delta z)\, e^{j(\beta_B\Delta z+\varphi)} & \left(\cosh(\gamma\Delta z) + j\frac{\Delta\beta}{\gamma}\sinh(\gamma\Delta z)\right) e^{j\beta_B\Delta z} \end{bmatrix}$$

where the following parameters have been introduced.

$$\beta_B = \frac{\pi}{\Lambda} \qquad \Delta\beta = j\frac{g}{2} + n_{eff}\frac{2\pi}{\lambda} - \frac{\pi}{\Lambda} \tag{B.16}$$

$$\kappa = \frac{\pi}{\lambda_B}\alpha(z)\,\delta n \qquad \gamma^2 = \kappa^2 - (\Delta\beta)^2 \tag{B.17}$$

The refractive index profile can be written

$$n(z) = n_{eff}(z) + \alpha(z)\,\delta n\cos\left[\frac{2\pi}{\Lambda}z + \phi(z)\right] \tag{B.18}$$

where δn is the amplitude of the refractive index change due to photosensitivity. The effective refractive index n_{eff} can furthermore be written

$$n_{eff}(z) = n_0 + m\alpha(z)\,\delta n \tag{B.19}$$

where n_0 is the refractive index of the fibre core, $\alpha(z) \in [0,1]$ is the apodisation function and the parameter $m \in [0,1]$ controls the average refractive index. ϕ is the phase of the grating and should follow the phase continuity relation

$$\phi(z + \Delta z) = \phi(z) + 2\beta_B \Delta z + \Delta\phi \tag{B.20}$$

where $\Delta\phi$ is an eventual phase shift. The transfer matrix of the grating $\mathbb{T} = (T_{ij})$ is obtained by multiplication of the transfer matrices of each uniform section

$$\mathbb{T} = \prod_{i=1}^{M} \mathbb{T}(z_i) \tag{B.21}$$

with $z_i = -\frac{L}{2} + i\Delta z$. Note that in order to simplify the expressions of commonly used symmetric apodisation functions $\alpha(z)$, the origin of the z-axis has been changed to the middle of the grating compared to the notations of Figure B.1. The transfer matrix of the entire grating is therefore

$$\begin{bmatrix} E^+(L/2) \\ E^-(L/2) \end{bmatrix} = \begin{bmatrix} T_{11} & T_{12} \\ T_{21} & T_{22} \end{bmatrix} \begin{bmatrix} E^+(-L/2) \\ E^-(-L/2) \end{bmatrix} \tag{B.22}$$

from which we can express the complex reflectivity r and transmittivity t of the grating according to:

$$r = -\frac{T_{21}}{T_{22}} \tag{B.23}$$

$$t = T_{11} - \frac{T_{21}T_{12}}{T_{22}} \tag{B.24}$$

This transfer matrices approach has been applied to the calculation of the complex reflectivities of the gratings with different apodisation profiles considered in Chapter 3.

B.3 References

[1] L. Poladian, "Group-delay reconstruction for fiber Bragg gratings in reflection and transmission", *Optics Letters*, vol. 22, no. 20, pp. 1571–1573, 1997.

[2] L. Poladian, "Resonance mode expansions and exact solutions for nonuniform gratings", *Physical Review E*, vol. 54, no. 3, pp. 2963–2975, 1996.

[3] M. Yamada and K. Sakuda, "Analysis of almost-periodic distributed feedback slab waveguides via a fundamental matrix approach", *Applied Optics*, vol. 26, no. 16, pp. 3474–3478, 1987.

Appendix C

Low dispersion fibre Bragg grating with high detuning tolerance[1]

C.1 Introduction

Fibre Bragg gratings (FBG) are attractive components for wavelength division multiplexing (WDM) applications due to the possibility to tailor their apodisation profile in order to realise nearly ideal amplitude responses with low-crosstalk and reduced bandwidth narrowing when cascaded. However, this might result in unwanted dispersion at the edges of the filter's pass-band [1], which is critical for high bit rate applications and will ultimately limit their usable bandwidth. Some designs have been recently proposed to alleviate such limitations [2, 3, 4]. In parallel, the optical system technology is witnessing the introduction of advanced modulation formats for higher resilience to fibre nonlinearities and increased spectral efficiency [5]. These formats present different spectral widths resulting in different tolerance to amplitude and phase (dispersion) filtering. Consequently, novel FBG designs should be tested against a large variety of modulation formats. In this section, we present a new design for a low dispersion FBG filter. It is based

[1] This section presents results obtained in December 2002, therefore outside the official Ph.D. project duration. Nevertheless, this study is a continuation of the work reported in Chapter 3 and it has therefore been decided to include it as an appendix to the thesis. The grating apodisation profile was designed by Simon J. Hewlett from AOFR Pty Limited, Canberra, Australia and the grating was fabricated and characterised by Hans-Jürgen Deyerl from COM. The experimental determination of the frequency detuning tolerance was performed together with Beáta Zsigri.

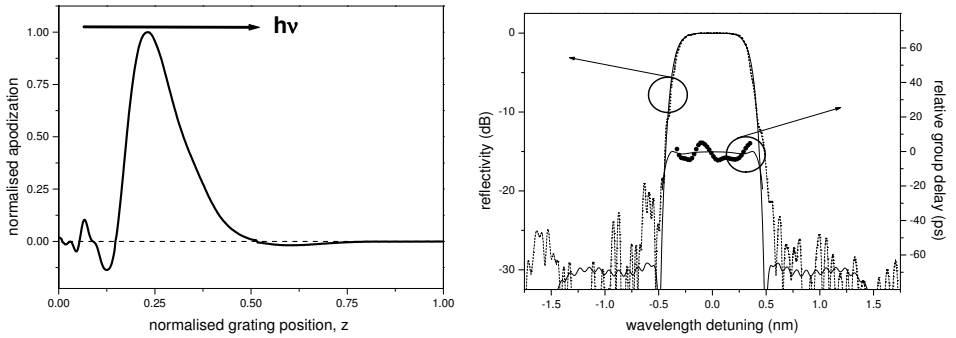

Figure C.1 Left: normalised apodisation profile $\kappa(z)$ for the low dispersion FBG. Right: measured and simulated reflection spectrum along with the measured (modulation frequency: 500 MHz) and simulated group-delay. Figures courtesy of Hans-Jürgen Deyerl.

on an asymmetric apodisation profile with multiple phase shifts that can be easily fabricated using the novel polarisation control method [6]. A group-delay fluctuation of less than 10 ps is obtained over the 1 dB bandwidth for a FBG designed for 100 GHz channel spacing. Furthermore, the grating is only 20 mm long, making it easily packageable by conventional techniques. The good dispersion properties of the grating are confirmed by penalty measurements at 10 Gbit/s where, for the first time to our knowledge, we systematically compare the filtering tolerance of five different modulation formats and show that over 89% bandwidth utilisation can be reached in all cases. In addition, numerical simulations are used to predict the behaviour of the device at 40 Gbit/s.

C.2 Grating properties

The apodisation profile of the grating was designed using an iterative, constraint-based solver. Figure C.1 shows the normalised apodisation profile $\kappa(z)$ of the designed grating. The apodisation profile exhibits four regions with a formally negative index-change, which can be induced by seven phase shifts in the manufacturing process. The designed grating with a length of $L = 20$ mm was fabricated using the recently introduced polarisation control method for UV-writing of FBGs [6]. The resulting grating transfer function is also shown in Figure C.1 and shows a 20 dB bandwidth of 120 GHz for the fabricated device. The measured relative group-delay shows a maximum fluctuation of 10 ps and a RMS group-delay

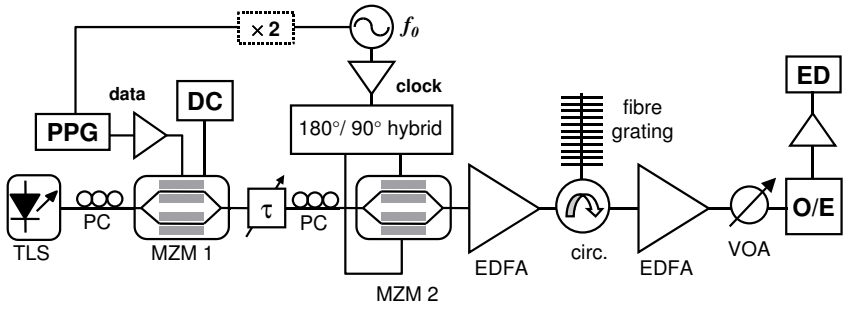

Figure C.2 Experimental set-up.

ripple of ~ 2.5 ps within the 1 dB reflection bandwidth, in good agreement with simulations based on coupled mode theory.

C.3 Experimental results

The filter detuning tolerance was determined experimentally at 10 Gbit/s for the following modulation formats: non return-to-zero (NRZ), return-to-zero (RZ), carrier-suppressed return-to-zero (CS-RZ), upper and lower side-band return-to-zero (USB-RZ and LSB-RZ). The experimental set-up is shown in Figure C.2. Light from a continuous wave tunable laser was first modulated with a $2^{31} - 1$ pseudo-random sequence in the NRZ format in a chirp-free Mach-Zehnder modulator (MZM 1). A second dual-drive Mach-Zehnder modulator (MZM 2), driven by a sinusoidal clock signal was used to shape the data to the different RZ formats. Depending on the clock signal frequency, bias, voltage swing and phase relation between the electrical signals applied to the two arms of the second modulator, either RZ, CS-RZ, USB-RZ or LSB-RZ modulation could be obtained [5]. In the case of RZ modulation, MZM 2 was biased at quadrature and driven with a 10 GHz clock signal and 180° phase shifted clock signal with peak-to-peak amplitudes equal to half of the modulator half-wave voltage V_π. For single side-band RZ modulation, the biasing condition and peak-to-peak voltage remained the same as for RZ, but the phase shift between the 10 GHz clock signals driving each of the arms of MZM 2 was equal to 90°. Either USB-RZ or LSB-RZ could be obtained by selecting which of the two clock signals was retarded compared to the other. In the case of CS-RZ modulation, the frequency of the clock generator was set to half of the bit rate (here $f_0 = 5$ GHz), MZM 2 was biased at a null transmission point, the peak-to-peak amplitude of each clock signal was V_π and they

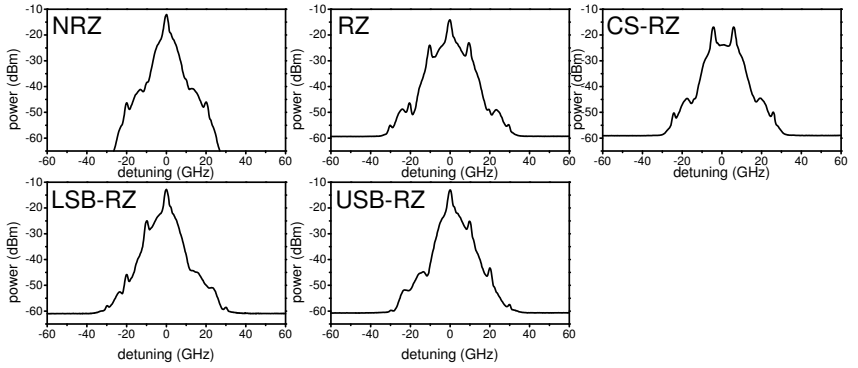

Figure C.3 Experimental spectra (in a 0.1 nm resolution bandwidth) for the various modulation formats at 10 Gbit/s.

were phase shifted by 180°. In this case, a frequency doubler was used in order to generate the 10 GHz clock signal necessary to drive the pulse pattern generator (PPG). An optical tunable delay line was inserted before MZM 2 in order to synchronise the pulse shaping to the incoming optically modulated NRZ signal. The light was then amplified using an erbium-doped fibre amplifier (EDFA) in order to compensate for the insertion loss of the modulators, before being input to the grating via a three-port optical circulator. After reflection by the grating, the signal was amplified in a second EDFA and detected in a PIN receiver (O/E). Due to the filter transfer function steepness, fast variations of the penalty are expected at the edges of the pass-band, and therefore the tunable laser wavelength was measured accurately with a wavelength meter throughout this experiment.

The spectra (in a 0.1 nm resolution bandwidth) obtained experimentally for each of the modulation formats are shown in Figure C.3. They exhibit expected features such as the reduced bandwidth of the main lobe of the spectrum of NRZ modulation compared to the RZ formats, the presence of discrete tones 10 GHz away from the carrier for RZ modulation, the suppression of the carrier and the presence of discrete tones 5 GHz away from the centre frequency of the spectrum in the case of CS-RZ modulation, as well as the reduced spectral width of the main lobe of CS-RZ compared to RZ. The single-side band spectra are asymmetric with respect to their centre frequency, one of the side-band presenting characteristics close to the ones of an NRZ spectrum, while the other side-band preserves the RZ features. We follow conventions used in radio communications and define USB as the modulation format whose spectrum exhibits suppression of the lower side-band when visualised with respect to frequency. The eye

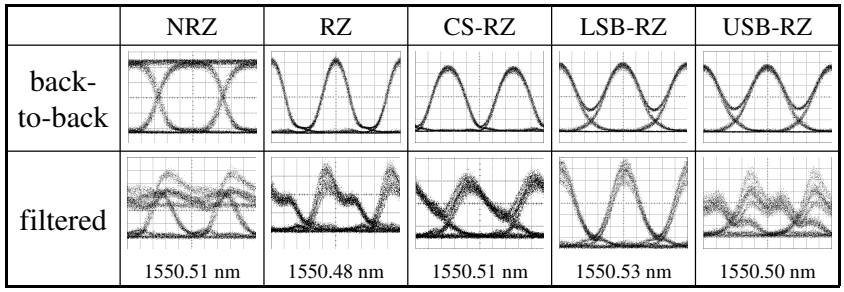

Figure C.4 Eyes diagrams at the transmitter output (top row) and after filtering (bottom row). Horizontal scale is 20 ps per division.

diagrams at the output of each of the transmitters are shown in Figure C.4 (top row) for an extinction ratio of 13 dB. The measured back-to-back sensitivities were -16.2, -17.8, -18, -17.5 and -17.5 dBm for NRZ, RZ, CS-RZ, LSB-RZ and USB-RZ, respectively.

The penalty at a bit-error-rate of 1.0×10^{-9} was measured as a function of the laser detuning with respect to the FBG centre frequency. The results are shown in Figure C.5 for the five modulation formats. It can be seen that the usable bandwidth of the device for a power penalty smaller than 1 dB depends only slightly on the modulation format. Some pulse reshaping is responsible for the negative penalty observed in the pass-band for some of the modulation formats. Filtering of amplified spontaneous emission (ASE) noise is also believed to contribute to the sensitivity improvement in the pass-band. Some penalty ripples are visible when the transmitter is tuned to the edges of the pass-band of the filter. However, the depth of those ripples is found to be dependent on the modulation format. NRZ appears to be the most affected, whereas smoother penalty curves are obtained for RZ and CS-RZ. This effect is more pronounced for negative frequency detunings, which can be correlated with the presence of a "shoulder" in the amplitude transfer function of the grating. Numerical simulations reproducing the experimental conditions of Figure C.2 and performed using the measured amplitude transfer function of the grating confirmed this observation. It is therefore believed that imperfections in the amplitude response of the FBG are responsible for the measured penalty ripples at the edges of the pass-band. It can be speculated that the broader the modulation format spectral width, the less pronounced the penalty ripples. It is therefore the relative content of the spectrum corrupted by grating imperfections that matters. For a certain frequency detuning, those imperfections will affect a larger fraction of a NRZ signal spectrum than a RZ spectrum,

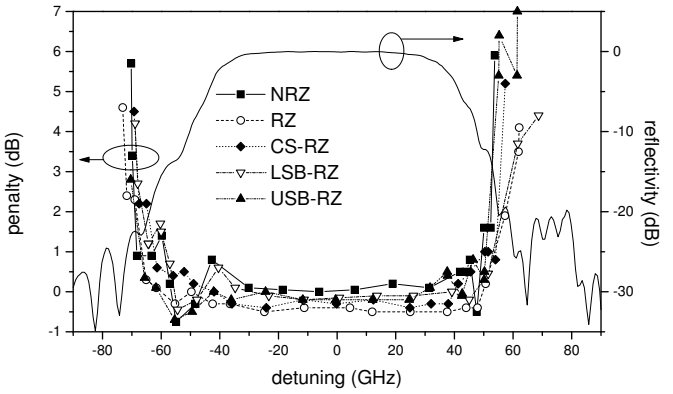

Figure C.5 Measured penalty as a function of detuning for the various modulation formats at 10 Gbit/s.

hence resulting in a larger influence on the former modulation format. In the case of LSB-RZ modulation, it is found that the penalty curve follows closely the one obtained with NRZ modulation for negative frequency detunings, while it matches the RZ penalty curve for positive detunings, in accordance with the characteristics of the signal spectrum (RZ-like for negative detuning and NRZ-like for positive detuning). The measured usable bandwidths for 1 dB power penalty for the different modulation formats are summarised in Table C.1 where they are compared to simulation results. The RZ format presents a slightly larger detuning tolerance than NRZ, due to its better resilience to the grating imperfections for negative detunings. CS-RZ and single side-band RZ exhibit intermediate performance, in accordance with their relative spectral widths. Those detuning tolerances result in bandwidth utilisations (defined as the ratio of the usable bandwidth for 1 dB power penalty to the 20 dB bandwidth of the device) of 89 to 100%, depending on the modulation format.

Eyes diagrams measured after filtering are shown in Figure C.4 (bottom row) for a wavelength of $\sim$ 1550.5 nm corresponding to a frequency detuning of $\sim$ 55 GHz. It should be noted that the eye diagrams actually correspond to slightly different wavelengths due to limitations in the repeatability of the external cavity tunable laser used in this experiment. The actual laser wavelengths, as measured using the wavelength meter, are indicated below the corresponding eye diagram. They correspond to frequency detunings of 53.9, 57.6, 53.9, 51.4 and 55.1 GHz for NRZ, RZ, CS-RZ, LSB-RZ and USB-RZ, respectively. It is confirmed that the signal gets severely degraded for lower positive detuning values in the case of NRZ

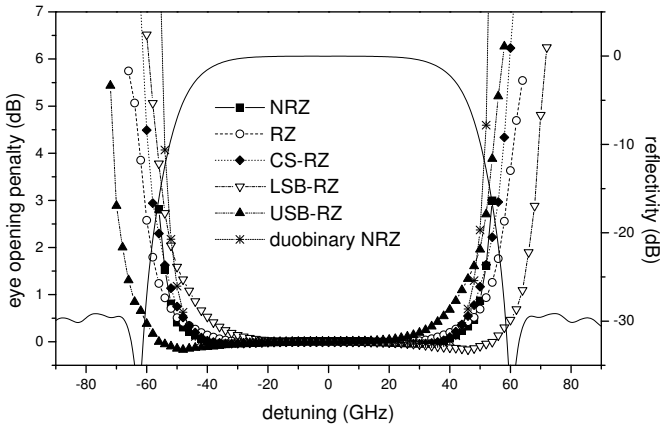

Figure C.6 Calculated EOP as a function of detuning for the various modulation formats at 10 Gbit/s.

and USB-RZ modulation. For the latter modulation format, this can be explained by the fact that most of the energy of the spectrum lies in the upper side-band, which is suppressed by low-pass filtering due to the edge of the filter transfer function for positive detunings. Although distorted, the eye diagram of RZ modulation with a frequency detuning as high as 57.6 GHz is still open, confirming the high resilience of this modulation format towards filtering by the asymmetric fibre Bragg grating. This resilience confirms the low dispersion nature of the filter, as in case dispersion were limiting the usable bandwidth of the device, it would have been expected to affect the modulation formats with the larger spectral width first.

C.4 Simulations

Numerical simulations were performed using the modelled transfer function in order to evaluate the theoretical limit for the detuning tolerance. The different RZ modulation formats were generated by considering a cascade of two Mach-Zehnder modulators with appropriate biasing and driving conditions, in analogy with the experimental set-up described in Figure C.2. Duobinary NRZ modulation was also considered. The optical duobinary signal was generated in the same way as described in Section 3.3.1, with duobinary encoding realised by low-pass filtering the electrical data signal with a 5^{th} order low-pass Bessel filter having a 3 dB bandwidth equal to 0.28 times the bit-rate. At the receiver side, the detected signal was filtered

Gbit/s	NRZ	RZ	CS-RZ	LSB	USB	Duob.
10 (e)	107	120	115	111	117	-
10 (s)	102	106	100	108	108	97
40 (s)	61	60	59	61	61	73

Table C.1 Usable bandwidth (for 1 dB penalty; in GHz) of the grating for the various modulation formats at 10 and 40 Gbit/s. (e): experiment; (s): numerical simulation.

with a 4^{th} order Bessel low-pass filter with 3 dB cut-off frequency equal to 0.7 times the bit-rate. The simulations were performed by considering the transmission of a $2^{10} - 1$ pseudo-random sequence. The eye-opening penalty (EOP) was used as the performance evaluation criterion. The results are shown in Figure C.6. As expected, the penalty curves of USB and LSB-RZ modulation are not symmetrical with respect to the grating centre frequency, due to the asymmetric nature of those signals spectra. Nevertheless, the detuning tolerance for both formats is the same. The single side-band signals being inherently chirped (the Mach-Zehnder modulator used for pulse shaping is not operated in push-pull mode), with opposite chirp for USB-RZ and LSB-RZ, one might expect two possible causes for asymmetries in the penalty curves for those modulations. First, the spectrum asymmetry will result in different penalties depending on which side-band is suppressed by the edge of the filter transfer function. Second, the chirp of the signal will interact differently with the grating dispersion depending on their relative signs. Note that in the present case the analysis is complicated by the fact that the chirp is not a linear function of time[2] and that the filter dispersion is not uniform with respect to wavelength. The pronounced asymmetry of the penalty performance of the single side-band formats cannot be observed in the experimental results of Figure C.5. This is due to the fact that the eye opening penalty metric used in the simulations only quantifies signal degradation due to pulse distortion and inter-symbol interference induced by the amplitude and phase filtering process, whereas the power penalty measured in the experiment is also affected by the signal-to-noise ratio degradation due to the excess attenuation at the edge of the filter's pass-band.

The calculated detuning tolerances for 1 dB EOP are compared to the experimental results in Table C.1. Good agreement is observed, even

[2]It can actually be shown that the chirp exhibits a sinusoidal dependence of time due to the driving conditions of the second Mach-Zehnder modulator and that its sign is the same at the leading and trailing edge of a pulse [7].

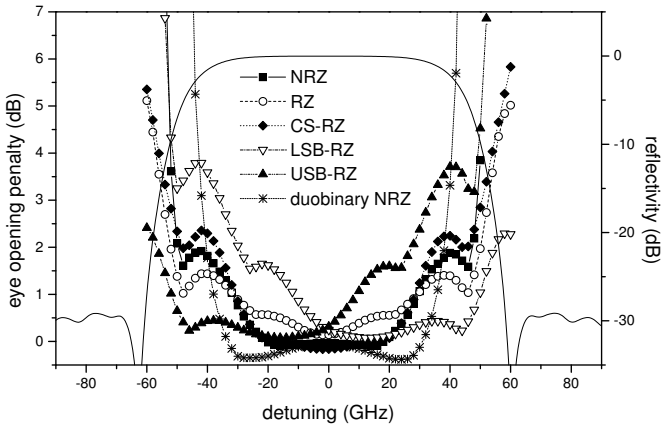

Figure C.7 Calculated EOP as a function of detuning for the various modulation formats at 40 Gbit/s.

though the evaluation criteria slightly differ. This confirms that the fabricated grating exhibits a nearly ideal response. Furthermore, running the same set of simulations by assuming that the grating was a linear phase device resulted in approximately the same detuning tolerance, confirming the reduced influence of the FBG dispersion at 10 Gbit/s. Contrarily to the case of the Gaussian apodised grating investigated in Section 3.3.2, no benefit in terms of detuning tolerance is obtained here when using duobinary modulation, which also supports the reduced influence of the filter dispersion.

Numerical simulations were also performed at 40 Gbit/s. The use of the FBG designed for 100 GHz channel spacing would result in a high spectral efficiency of 0.4 bit/s/Hz. Consequently, larger signal distortions are expected, as can be seen in Figure C.7. Nevertheless, large detuning tolerances (at least 55% of the one reached at 10 Gbit/s while the bit-rate has been multiplied by four) can still be obtained, as shown in Table C.1. This reduction of the detuning tolerance is less pronounced in the case of duobinary modulation because of its reduced bandwidth.

C.5 Conclusion

We have demonstrated a novel design for a low dispersion fibre Bragg grating and have evaluated its wavelength detuning tolerance for NRZ, RZ, CS-RZ, LSB-RZ and USB-RZ modulation. In all cases a bandwidth utilisation

factor above 89% is obtained experimentally at 10 Gbit/s, in agreement with numerical simulations. Numerical simulations also predict a detuning tolerance of at least 60 GHz when the filter is used at 40 Gbit/s, which demonstrates its applicability to WDM systems with a high spectral efficiency of 0.4 bit/s/Hz.

C.6 References

[1] G. Lenz, B. J. Eggleton, C. R. Giles, C. K. Madsen, and R. E. Slusher, "Dispersive properties of optical filters for WDM systems", *IEEE Journal of Quantum Electronics*, vol. 34, no. 8, pp. 1390–1402, 1998.

[2] M. Ibsen, R. Feced, P. Petropoulos, and M. N. Zervas, "99.9% reflectivity dispersion-less square-filter fibre Bragg gratings for high speed DWDM networks", in *Technical Digest Optical Fiber Communication Conference, OFC'00*, Baltimore, Maryland, U.S.A., post-deadline paper PD21, 2000.

[3] T. Shibata, M. Shiozaki, M. Ohmura, K. Murashima, A. Inoue, and H. Suganuma, "The dispersion-free filters for DWDM systems using 30 mm long symmetric fiber Bragg gratings", in *Technical Digest Optical Fiber Communication Conference, OFC'01*, Anaheim, California, U.S.A., paper WDD84, 2001.

[4] H.-J. Deyerl, N. Plougmann, J. B. D. Jensen, J. El-Bez, H. R. Sørensen, C. Peucheret, and M. Kristensen, "Low-dispersion fibre Bragg gratings written using the polarization control method", in *Proceedings European Conference on Optical Communication, ECOC'02*, Copenhagen, Denmark, paper 7.2.7, vol. 3, 2002.

[5] A. Hodžić, B. Konrad, and K. Petermann, "Alternative modulation formats in $N \times 40$ Gb/s WDM standard fiber RZ-transmission systems", *Journal of Lightwave Technology*, vol. 20, no. 4, pp. 598–607, 2002.

[6] J. B. Jensen, N. Plougmann, H.-J. Deyerl, P. Varming, J. Hübner, and M. Kristensen, "Polarization control method for ultraviolet writing of advanced Bragg gratings", *Optics Letters*, vol. 27, no. 12, pp. 1004–1006, 2002.

[7] B. Zsigri, "Investigation of single side band transmission in high spectral efficiency optical communication systems", Master thesis, COM, Technical University of Denmark, Kgs. Lyngby, Denmark, 2002.

Appendix D

Simulation techniques

D.1 Receiver sensitivity calculations

The design of optical communication systems relies on the estimation of performance figures of merit such as the bit-error-rate (BER) and a number of derived quantities. The most commonly used are the receiver sensitivity (defined as the average received power resulting in a given BER, typically 1.0×10^{-9}), the power penalty (defined as the difference between the sensitivity at the output of the system and the so-called back-to-back sensitivity, typically at the transmitter output) or the error free transmission distance. In order to simulate the behaviour of optical links or sub-systems, it is therefore essential to be able to compute the BER in an effective and reliable way [1].

Particularly challenging is the estimation of the BER of systems subject to non-Gaussian noise statistics or exhibiting strong patterning effects resulting in inter-symbol interference (ISI).

A common approach is to assume Gaussian probability density functions (pdf) for the input voltage to the decision circuit (at the sampling time) for both the "0" and "1" levels. The so-called Q factor can then be calculated from the mean values μ_0 and μ_1, and the standard deviations σ_0 and σ_1 of the "0" and "1" levels respectively, according to:

$$Q = \frac{\mu_1 - \mu_0}{\sigma_1 + \sigma_0} \tag{D.1}$$

The BER can then be related to the Q factor by using:

$$\mathrm{BER} = \frac{1}{2}\mathrm{erfc}\left(\frac{Q}{\sqrt{2}}\right) \tag{D.2}$$

where erfc is the complementary error function defined as:

$$\mathrm{erfc}\,(x) = \frac{2}{\sqrt{\pi}} \int_{x}^{+\infty} \exp\left(-y^2\right) dy \tag{D.3}$$

However, this technique is clearly not valid if the noise distribution is not Gaussian as well as in the presence of inter-symbol interference. In the latter case, fitting two Gaussian distributions to an eye diagram severely distorted by ISI will result in overestimated values of the standard deviations σ_0 and σ_1, leading to a pessimistic BER evaluation. The BER estimation can be improved by taking the pattern effects resulting in ISI into account. For instance, the BER can be calculated taking ISI from the two neighbouring bits into account, according to the method described in [2], which has been used throughout the simulations presented in this thesis. The transmitted pattern is divided into the eight possible combinations of three bits (000, 100, 001, 101, 111, 011, 110, 010) and Gaussian distributions are fitted to each of these combinations. A weighted averaging is then performed depending on the number of occurrences of each combination in the data stream. The method can be extended in a straightforward manner to a higher number of neighbouring bits depending on the memory of the system under investigation (see for instance [3] where a system limited by pattern effects due to saturation in semiconductor optical amplifiers was investigated and where it was shown that taking the ISI from the two neighbouring bits was not sufficient in order to provide a good estimate of the BER). Even by introducing such a method, the number of bits used in the simulation (in terms of pattern length and/or number of simulation runs) still needs to be optimised in order to provide an estimate of the BER fulfilling some kind of confidence requirement [4]. The simulated Q factor should in principle compare with values obtained experimentally, the most reliable technique being to fit BER versus decision threshold measurements obtained at high BER values for both the "0" and "1", with a curve assuming Gaussian noise statistics [5].

D.2 Validation tests

In order to ensure the reliability of the numerical simulations presented throughout this thesis, a number of validity tests have been performed. It should indeed be mentioned that quite often, the most time consuming part in the numerical analysis of an optical communication system, is not to run the simulation that will lead to results, but to ensure that it makes some sense in terms of appropriateness of the models, choice of the physical and

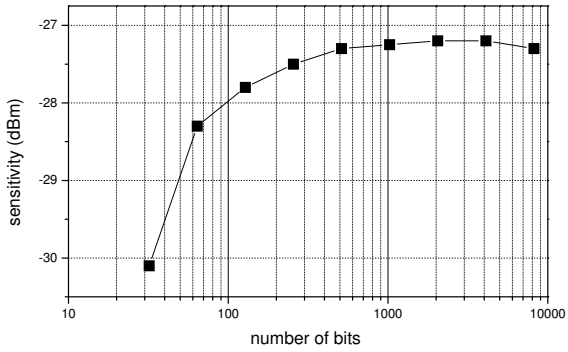

Figure D.1 Back-to-back sensitivity calculated using the Gaussian approximation as a function of the number of simulated bits for a 10 Gbit/s NRZ transmitter and receiver with 3 pA/$\sqrt{\text{Hz}}$ single-sided thermal noise density.

also, more importantly, numerical parameters such as sample rate, split-step size, number of bits, etc. Some examples of validation tests are given below.

Confronting the simulator with itself

As discussed in Section D.1 above, the numerical estimation of the bit-error-rate of a communication system remains a challenging task. This is mainly due to the fact that, contrarily to its experimental measurement, one wishes to calculate the BER without actually having to count the errors by time consuming Monte-Carlo simulations. Therefore, a trade-off often needs to be found between the reliability of the BER estimation and the number of bits used for its calculation, which will determine the execution time of the simulation. This is illustrated in Figure D.1 where the back-to-back sensitivity of a 10 Gbit/s non return-to-zero (NRZ) transmitter has been assessed numerically as a function of number of bits according to the BER evaluation method of [2]. This calculation was performed with the second generation of tools made available to us by Virtual Photonics Incorporated (PTDS for Linux), which has been used extensively for many of the simulations presented in this thesis. It can be seen that the calculated back-to-back sensitivity depends strongly on the number of bits used for its evaluation. For this particular system, the estimated sensitivity starts converging towards its final value when the number of bits is higher than 512. Consequently, the use of 1024 bits is found to constitute a good trade-off between simulation accuracy and reasonable execution time. It should be emphasised that the choice of the optimum number of bits depends on the

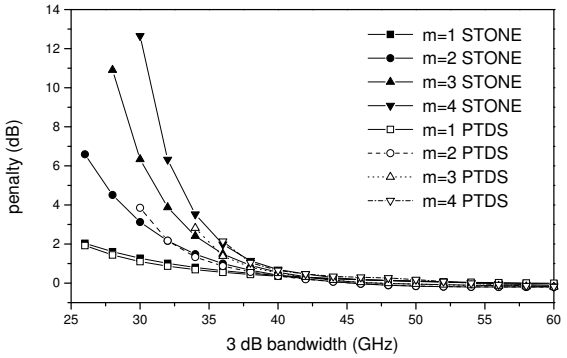

Figure D.2 Comparison of the power penalty as a function of Gaussian filter FWHM bandwidth calculated with two different simulators: PTDS from Virtual Photonics Incorporated and STONE by Christian Rasmussen. m represents the Gaussian filter order.

system being studied and the signal degradation mechanisms involved. In general, a value of 1024 bits has been found to result in a good compromise for the simulations presented in this thesis.

Confronting the simulator with others

Benchmarking different simulation tools relying on distinct models or simulation approaches also proves useful in order to define their respective range of validity and limitations. This exercise has been performed for different types of systems in order to compare results obtained with commercial products from Virtual Photonics Incorporated and with STONE (Simulation Tool for Optical NEtworks), an in-house simulator designed by Christian Rasmussen [6]. An example of such a comparison can be seen in Figure D.2 where we show the power penalty calculated as a function of Gaussian filter full-width half-maximum (FWHM) bandwidth using either STONE or PTDS. The calculation was repeated for Gaussian orders m ranging from 1 to 4. In order to enable a fair comparison of the receiver sensitivity evaluation methods, the same bit pattern was used with both simulation tools (i.e. a 1024 bit sequence was generated in PTDS and transferred to the STONE simulator). Good agreement between the two simulation tools was obtained.

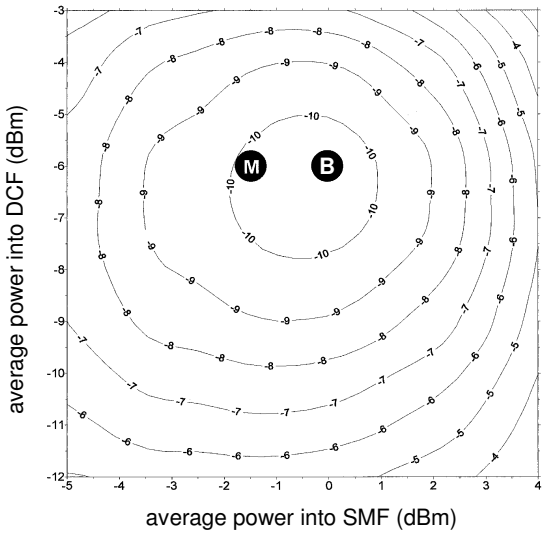

Figure D.3 Calculated log (BER) as a function of average power into the SMF and the DCF after 20×80 km 100% post-compensated SMF+DCF spans (STONE simulation). The points B and M indicate the optima calculated using BroadNed and measured in a re-circulating loop experiment, respectively.

Confronting the simulator with reality

The ultimate validity check for simulations is the comparison with measurement results obtained on the system being modelled. This task is fairly challenging since simulations of optical communication systems often require the use of simplified models for the different elements in a link (e.g. erbium doped fibre amplifiers). The reason for the use of these simplified "system" models is two-fold. First, the use of accurate physical models for individual components might be prohibitive from a time of execution point of view when one wishes to optimise a whole system. Second, such models require a detailed knowledge of many physical parameters which might not be available to the system designer. Accordingly, the present generation of optical communication systems simulators is best suited to provide a qualitative understanding of the systems being studied and their limitations. Quantitative agreement would require a high level of details in the modelling and necessitate advanced characterisation of all the elements to be found in the system.

Throughout the work reported in this thesis, it has been attempted, whenever possible, to validate simulation results with experimental data. One additional example is provided in Figure D.3 where we compare the

numerical and experimental optimisation of a dispersion map made of standard single-mode fibre (SMF) and dispersion compensating fibre (DCF). This map corresponds to one of the so-called "normalised sections" described in Chapter 5 with 80 km SMF and 100% post-compensation. The system has been optimised with respect to input power to the SMF and the DCF after 20 cascaded spans. The results of the numerical optimisation as performed using STONE are represented as a contour plot in Figure D.3. The BER at the end of the link was chosen as the performance evaluation criterion for the system. The optimum fibre input power values found using the first generation of commercial softwares from Virtual Photonics Incorporated (BroadNeD) are also represented in the graph (point B). A re-circulating loop experiment similar to the ones described in Section 5.3 was also performed on the same system, leading to the optimum point represented as M in the contour plot. Good qualitative agreement between the two simulation tools and the experimental results is obtained for the definition of the optimum parameters.

D.3 References

[1] M. C. Jeruchim, "Techniques for estimating the bit error rate in the simulation of digital communication systems", *IEEE Journal on Selected Areas in Communications*, vol. SAC-2, no. 1, pp. 153–170, 1984.

[2] C. J. Anderson and J. A. Lyle, "Technique for evaluating system performance using Q in numerical simulations exhibiting intersymbol interference", *Electronics Letters*, vol. 30, no. 1, pp. 71–72, 1994.

[3] F. Matera and M. Settembre, "Role of Q-factor and of time jitter in the performance evaluation of optically amplified transmission systems", *IEEE Journal of Selected Topics in Quantum Electronics*, vol. 6, no. 2, pp. 308–316, 2000.

[4] E. G. Shapiro, M. P. Fedoruk, and S. K. Turitsyn, "Numerical estimate of BER in optical systems with strong patterning effects", *Electronics Letters*, vol. 37, no. 19, pp. 1179–1181, 2001.

[5] N. S. Bergano, F. W. Kerfoot, and C. R. Davidson, "Margin measurements in optical amplifier systems", *IEEE Photonics Technology Letters*, vol. 5, no. 3, pp. 304–306, 1993.

[6] C. J. Rasmussen, *Transmission analysis in WDM networks*. PhD thesis, COM, Technical University of Denmark, Lyngby, Denmark, 1999.